The Dissertation Committee for Terry Glen Farmer Jr. certifies that this is the approved version of the following dissertation:

INTRAVENOUS CLOSED-LOOP GLUCOSE CONTROL IN TYPE I DIABETIC PATIENTS

Committee:

Thomas F. Edgar/supervisor

Nicholas A. Peppas/supervisor

Roger T. Bonnecaze

Krishnendu Roy

Isaac C. Sanchez

INTRAVENOUS CLOSED-LOOP GLUCOSE CONTROL IN TYPE I DIABETIC PATIENTS

by

Terry Glen Farmer Jr., B. S.

Dissertation

Presented to the Faculty of the Graduate School of

The University of Texas at Austin

in Partial Fulfillment

of the Requirements

for the Degree of

Doctor of Philosophy

The University of Texas at Austin

May 2007

ACKNOWLEDGMENTS

There are many people who have helped me get to this point, and this work would not have happened without each of their contributions. First off, I would like to thank my advisors, Thomas Edgar and Nicholas Peppas for keeping me on track and being available whenever I needed help. Chronologically, I would like to thank my math and science teachers at Lampasas High School, particularly Mark Roberts, Paul Volpe, Leslee Antilley, and Gail Wolfe, for encouraging my pursuit of chemical engineering at the undergraduate level. I would also like to thank the members of the chemical engineering faculty at the University of Texas, for all the help I was given in pursuing graduate school. Particularly, I would like to acknowledge Roger Bonnecaze and Grant Willson for allowing me to gain undergraduate research experience and for there encouragement and assistance during the graduate school application process. I would also like to thank Buddie Mullins for his mentoring and friendship during the graduate school application and selection process.

I would like to acknowledge the many people I have encountered in graduate school that have made my experience what it is. Thank you to Bryan, Tom, Dan, and Hao for all their help in collaborative homework assignments, to Ross, Mike, and Brooks for many a poker night, and to Cantor, Drew, Mikey, McLees, and Dowdle for keeping me in shape during my time here. Thank you also to Clare, Mathilde, Don, Hunter, and Steve for their friendship. Thank you also to my many lab mates in the Peppas and Edgar groups who have offered assistance over the years.

Lastly, I would to acknowledge my family. Thank you to my parents for encouraging my highest level of performance since elementary school and for their patience and understanding over the last several years. Thank you to my in-laws, for their patience and support and accepting me as one of their own during this time period. Finally, thank you most of all to my wife, Kate, and my daughter, Leah, for their support during the last nine years at the University of Texas. Thank you for being my biggest fans during the both the good times and the hard times throughout the years.

INTRAVENOUS CLOSED-LOOP GLUCOSE CONTROL

IN TYPE I DIABETIC PATIENTS

Publication No. _____

Terry Glen Farmer Jr., Ph.D.
The University of Texas at Austin, 2007

Supervisors: Thomas F. Edgar and Nicholas A. Peppas

Models describing glucose homeostasis were developed. A pharmacokinetic model describing the kinetic rates of appearance and disappearance of glucose, amino acids, fatty acids, insulin, glucagon, epinephrine, and glucagon-like peptide-1 was developed, and a physiologically-based model describing the dynamics of these species in the brain, liver, kidneys, muscle tissue, adipose tissue, gut, pancreas, and adrenal medullae was developed. Because sufficient data was not readily available, parameter estimation for the models was not performed.

Parameter estimation was investigated by using one- and two-compartment insulin models to generate test data with known parameter values and investigating the effectiveness of a nonlinear least squares algorithm with respect to estimating the actual parameter values. Parameter estimation was strongly dependent on the initial guess of the parameter set, and confidence intervals were found to be ±100% of the estimated parameter value. The use of dynamic sensitivity equations in conjunction with a stiff

differential equation solver resulted in the parameters of the one-compartment model being accurately estimated with confidence intervals less than 10%. The two-compartment parameters were not able to be accurately estimated within confidence limits, but all parameter sets from the estimation fit the test data very strongly.

Explicit closed-loop control was simulated by incorporating feedback control, feedforward control, combined feedforward/feedback control, and model predictive control into three patient models describing glucose and insulin kinetics. No controller was able to keep the minimal model glucose below 14 mmol/L in response to a 50 g oral glucose disturbance without also resulting in hypoglycemia. Sorensen model and Hovorka model simulations predicted that proportional control is able to mimic the healthy pancreas response to a 50 g oral glucose disturbance and 30 minutes of moderate exercise.

A model describing swelling and release dynamics for a pH-responsive cationic hydrogel was developed using the quasi steady-state assumption for particle swelling. The response of implicit closed-loop control system was simulated using the minimal model. Physical constraints imposed on diffusion coefficients and the collapsed particle radius results in complete insulin depletion in less than 1 minute, rendering the hydrogel system infeasible for intravenous implicit closed-loop glucose control.

TABLE OF CONTENTS

LIST OF FIGURES

LIST OF TABLES

CHAPTER 1

INTRODUCTION

As the field of bioengineering continues to grow, chemical engineers face significant challenges and have the potential to make great contributions. The ability to understand and quantify the behavior of materials in a chemical process, as well as the ability to optimize, design, and control these processes gives the chemical engineer a unique set of tools that can be applied to numerous areas associated with bioengineering. In the biological/biomedical field, chemical engineers are heavily involved in protein engineering, tissue engineering, and metabolic engineering, as well as biosensor development, the development of devices for therapeutics, and controlled drug delivery systems. The broad range of skills required to be successful in chemical engineering have proven to be equally powerful when applied to cutting edge biological and biomedical problems.

One particularly interesting area of chemical engineering that can be applied toward bioengineering is systems engineering. Because the body is constantly working to maintain homeostasis (steady state), systems engineering can be uniquely applied toward not only gaining an understanding of how the body achieves homeostasis, but also toward the development of therapeutic methods that can assist in achieving homeostasis when individuals are unable to do so themselves. Although the body is quite complex, it is highly analogous to a chemical plant, complete with multiple chemical processes working together. It is a dynamic system, consisting of multiple organ, tissue, and

cellular sites at which many chemical species are being transported, generated, and consumed.

To the systems engineer, maintaining homeostasis is analogous to controlling a chemical process. The dynamic system, in this case the body, is modeled based on the dynamics of all controlled, manipulated, and state variables. Often this modeling is based on kinetic equations for appearance (either by absorption or production) or elimination. Once these pharmacokinetic models have been developed, control systems can be developed that allow homeostasis to be maintained by controlling certain species in the body through the delivery of another species.

One of the most important new areas where systems engineering has been particularly helpful is the development of improved therapies for patients afflicted with diabetes mellitus.

Diabetes mellitus is a metabolic disease in which the body is unable to either sufficiently produce or sufficiently respond to insulin in the plasma. Insulin is the primary hormone that controls the uptake of glucose from the blood into the liver and muscle cells. Without the proper insulin response, the body will have abnormally high levels of glucose. This condition, known as ***hyperglycemia***, can result in long-term complications including kidney failure, heart failure, and can often lead to arms and legs needing to be amputated.

Although there are two distinct types of diabetes mellitus (***Type I***, in which the pancreas either does not secrete insulin or produces it in insufficient amounts, and ***Type II***, in which the pancreas has diminished insulin secretion and the response to insulin is

diminished), patients with both types are often prescribed to receive insulin therapy. In fact, while all Type I diabetic patients require insulin therapy compared to only some of the Type II patients, there are more Type II patients requiring insulin therapy than Type I patients. Insulin must be administered to the diabetic patient in order to ensure glucose levels are maintained at homeostatic levels. Thus, to the systems engineer, this is a process in which insulin is used to control glucose levels.

To provide this control for the process, three primary solutions have been proposed [1, 2]. First is the ***open-loop control method***, in which the patient, usually with the guidance of a doctor, provides insulin for his or herself. Examples of this method include the insulin injection or externally worn insulin pump. Other possibilities include the recently approved inhaled insulin, as well as the oral insulin formulations that are the focus of a great deal of research [3, 4]. While relatively easy to administer, the potential to accidentally provide more insulin than necessary is a primary disadvantage in open-loop therapies. Too much insulin can result in glucose levels that are too low, potentially resulting in death.

Of greater interest to systems engineers is the idea of ***closed-loop glucose control***. With closed-loop control, patient intervention is eliminated, allowing the individual to live a high quality life similar to that of a healthy individual. Within the closed-loop control realm there are two subtypes. The first type, ***explicit closed-loop control***, involves a glucose sensor, a control algorithm describing insulin infusion as a function of the plasma glucose levels, and an insulin pump that administers insulin based on the control algorithm. The second type, ***implicit closed-loop control***, does not require any

type of mechanical equipment. One example of implicit control is the pancreas transplant. Another is the implantation of pancreatic islets that are able to secrete insulin. The third type and the type investigated in this work is the system based on pH-responsive cationic hydrogels. These devices are able to reversibly swell and de-swell in response to a change in the pH of the environment. Because the swelling directly affects the ability of insulin to be infused from the device, the hydrogel system has the potential to act as a pH-controlled insulin release system. By tying the environmental pH to the glucose concentration, a glucose-responsive insulin release system can be developed that is able to act as the sensor and the pump.

The development of a closed-loop glucose control system requires two approaches. First, *models of the dynamics of insulin, glucose*, and all other relevant species in glucose control must be available in order to fully understand the glucose homeostatic process. Second, a *description of the control algorithm governing insulin release* must be developed and used with the model in order to simulate the controller's ability to maintain glucose homeostasis for a number of different conditions. For the implicit system, the control will be developed by the development of models describing the dynamics associated with the device behavior and then optimally designing the system in order to meet specified control requirements.

The purpose of this research was to develop in vivo simulations of closed-loop glucose control systems. This goal was achieved in three ways. First, different dynamic models of diabetic patients were investigated, and a new patient model was proposed. Second, control algorithms were developed to simulate the explicit closed-loop control

system in vivo. Finally, a model was developed describing the dynamics of the implicit closed-loop system, and simulations were performed to demonstrate the in vivo response in a diabetic patient.

As discussed by Heller [5], the training of chemical engineers in design, process control, and materials prepares them very well for the development of novel medical devices, including integrated medical systems and polymeric-based infusion devices. The use of modeling and simulation in the design step allows the chemical engineer to assess the feasibility of proposed methods, saving money that may have been used on experiments and patients and also potentially saving lives of test subjects. As such, the use of modeling and simulation toward the development of closed-loop glucose control systems is an important contribution toward medical device development.

Chapter two provides the background information necessary to understand glucose control problem, including the physiology of glucose control in healthy and diabetic patients as well as a review of the works of others providing closed-loop control solutions for the system. Chapter three will discuss the specific objectives of the research. Chapter four will describe the efforts to develop improved models for the glucose control system in diabetic patients, including physiological considerations. Chapter five will focus on system identification for patient models. Chapter six will discuss the application of explicit closed-loop control toward glucose control. Finally, chapter seven will focus on the development of a model describing the proposed implicit closed-loop control system. The dissertation will then conclude with a general discussion of the proposed methods and their efficacy.

1.1 References

1. Parker, R. S., "Insulin Delivery", in *Encyclopedia of Biomaterials and Biomedical Engineering*, G. Wnek and G. Bowlin, eds., Dekker, NY, 857-866, 2004.

2. Peppas, N. A., "Is There a Future in Glucose-Sensitive, Responsive Insulin Delivery Systems?", *J. Drug. Del. Sci. Tech.*, **14**, 247-256, 2004.

3. McMahon, G. T. and Arky, R. A., "Inhaled Insulin For Diabetes Mellitus", *N. Engl. J. Med.*, **356**, 497-502, 2007.

4. Peppas, N. A., "Devices Based on Intelligent Biopolymers for Oral Protein Delivery", *Intern. J. Pharmac.*, **277**, 11-17, 2004.

5. Heller, A., "Integrated Medical Feedback Systems For Drug Delivery", *AIChE Journ.*, **51**, 1054-1066, 2005.

CHAPTER 2

BACKGROUND

2.1 Introduction

In order to provide homeostatic control with respect to the body's plasma glucose levels, several things must first be understood. First among them is how a healthy patient is able to regulate his or her glucose levels, both throughout the day and in response to non steady-state conditions. Second, the differences between the diabetic patient and the healthy patient must be understood in order to establish which system elements need to be controlled, what constraints exist, and which manipulated variables can be used in developing a control scheme. Finally, it is important to understand the previous work performed in the area of glucose control, with respect to modeling, explicit closed-loop control, and implicit closed-loop devices. This chapter will review all of these areas in order to provide the necessary background before discussing the research completed in this dissertation.

2.2 Glucose Metabolism

In-depth discussions of glucose metabolism and complications associated with glucose control can be found in medical physiology textbooks such as [[1], endocrinology textbooks such as [2] or [3], or in clinical textbooks for diabetes mellitus such as [4]. The material is summarized here in order to provide a basic understanding of the systems and species involved in glucose control. Puckett [5] provides a more

thorough summary of glucose metabolism for a number of different conditions for both healthy and diabetic patients.

2.2.1 Glucose

Nearly every process in the body requires adenosine triphosphate (ATP) as an energy source. In order for ATP to be synthesized, the body uses glucose as its primary fuel. Therefore, glucose is the primary metabolite required for the body to function properly.

In a healthy individual, the glucose concentration is maintained at approximately 80-90 mg/dL throughout the day. This is known as the basal level. The primary source of glucose is food consumption. Although there is usually a spike associated with ingesting a meal, especially one high in carbohydrates, the plasma glucose levels of a healthy individual seldom go over about 120-140 mg/dL. If the plasma levels are higher than homeostatic levels, the excess glucose is taken into liver and muscle cells and stored as glycogen. However, there is an upper limit on the amount of glycogen that can be stored, and additional glucose is usually converted to fat.

When the glucose concentration is below the basal level, the liver will produce glucose endogenously through one of two methods. The first is glycogenolysis, in which the stored glycogen of the liver is catabolized to form glucose. The second is gluconeogenesis, in which amino acids and fatty acids stored in the liver are converted to glucose.

2.2.2 Hormones

Hormones play a major role in nearly every significant glucose metabolic process. The primary hormones, including insulin, glucagon, epinephrine, and glucagon-like peptide-1 (GLP-1) all play significant roles in allowing the healthy individual to maintain glucose at basal levels.

The primary hormone associated with glucose control is insulin. Insulin is primarily responsible for two effects. First, insulin binding to muscle and liver cells results in an order of magnitude increase in glucose uptake into those cells. Second, insulin is primarily responsible for the conversion of glucose in excess of that required for maximum glycogen storage into fat. Furthermore, insulin is responsible for the uptake of amino acids and fatty acids into the liver cells, which allows the liver cells to have enough starting materials to produce glucose via gluconeogenesis.

Insulin is produced in the beta cells of the pancreas. A basal level is secreted throughout the day in order for the body to maintain basal glucose levels. The basal insulin secretion is approximately 25 ng/min/kg body weight. A more common way to describe insulin levels is through the use of Insulin Units (U). A Unit of insulin is defined such that a milligram of pure insulin contains 22 U of biological activity [2]. As glucose ingestion causes the plasma glucose concentration to increase, the secretion rate of insulin is increased. The secretion rate usually is increased by an order magnitude with 3-5 minutes of glucose elevation.

While insulin is primarily responsible for the prevention of hyperglycemia, the hormone glucagon is primarily responsible for providing the counter-regulatory response

in glucose control. As glucose levels descend to below the basal level, usually a result of either fasting or exercise, glucagon binds to liver cells to stimulate glycogenolysis and gluconeogenesis. Furthermore, the binding of glucagon to the liver cells also increases the uptake of amino acids and fatty acids, resulting in increased glucose production via gluconeogensis. Finally, glucagon binding to adipose cells results in the endogenous production of fatty acids to be used in glucose production. Like insulin, glucagon is produced in the pancreas. Glucagon is released during exercise and during episodes of hypoglycemia [1].

Another hormone responsible for the counter-regulation of glucose is epinephrine. Like glucagon, the secretion of epinephrine results in increased gluconeogenesis. It also results in the increased mobilization of fatty acids for use in gluconeogenesis. However, unlike glucagon, epinephrine, combined with norepinephrine, constricts the size of blood vessels and dramatically decreases the flow of blood to other tissues. This results in decreasing the uptake of glucose into the other cells. The secretion of both glucagon and epinephrine/norepinephrine is increased in response to exercise. Epinephrine and norepinephrine are also secreted in high stress situations and when the plasma glucose concentration decreases well below the threshold level for glucagon release.

The final hormone that plays a relatively significant role in glucose regulation is GLP-1, the most significant hormone among the gastrointestinal hormones produced in the intestines. For reasons not completely understood, GLP-1 is released in response to a meal. The release of GLP-1 causes an increase in both pancreatic insulin production and secretion. This results in an increase in plasma insulin even before hyperglycemia is

observed. In addition, GLP-1 also plays a direct role in regulating plasma glucose levels, independent of any role it has in increasing insulin levels.

2.3 Diabetes Mellitus

As previously mentioned, diabetes mellitus is characterized by a breakdown in the glucose metabolic process. With Type I diabetes, the pancreas is unable to produce the necessary insulin to control glucose levels, while Type II diabetes is characterized by either insulin insufficiency or insufficient insulin sensitivity of the muscle and liver cells. Type II diabetes is often caused by increased intra-abdominal fat, which decreases the signal strength associated with insulin binding to liver and muscle cells. Because the secreted insulin is less effective at regulating glucose levels, the pancreas eventually begins to produce less insulin, resulting in diminished production. The current therapeutic methods for treating Type II diabetes include placing patients on a strict diet and exercise regimen, as well as the prescription of various drugs that can increase insulin sensitivity or stimulate pancreatic insulin production.

Of more interest to this research is Type I diabetes, in which the pancreas is unable to provide the necessary level of insulin to control plasma glucose levels. Type I diabetes is an autoimmune disease in which the body destroys its pancreatic beta cells. This autoimmune process normally occurs early in a person's life, with later cases normally occurring when a person is in his or her early to mid 20's. For Type I diabetic patients and a large number of Type II diabetic patients, insulin must be provided from a source other than the pancreas.

To understand the differences in glucose metabolism for a Type I diabetic patient, three scenarios will be considered, comparing the healthy patient and diabetic patient response for each. A more thorough description of the differences can be found in [1]-[5].

2.3.1 Basal Conditions

At basal conditions, glucose levels are maintained by the various hormones. It is more important to ensure that enough glucose exists in order to allow each cell in the body to perform its key metabolic processes. Of particular importance is the brain, which requires a certain amount of glucose in order to function properly. Insulin is secreted at a relatively low rate as glucose absorption is not important. Glucagon levels are relatively high to ensure that enough glucose is in circulation. Amino acids and fatty acids are readily available for gluconeogenesis.

For a Type I diabetic patient, the insulin levels will be based entirely on the quality of control that is being provided. If the amount of insulin provided is not enough, more glucose will be produced in the liver than what can be taken up into cells, resulting in hyperglycemia. If the hyperglycemic state is maintained for an extended period of time, the diabetic patient will suffer many consequences [1]. First, the increased level of glucose in the blood changes the osmotic balance of the body, resulting in the loss of water from and ultimately the dehydration of many of the body's cells. Second, as the glucose levels increase in the body beyond a threshold of approximately 200 mg/dL, glucose is no longer able to be reabsorbed in the kidneys and begins to be passed in urine.

The high levels of glucose in urine result in changes in the osmotic balance of urinary fluid, resulting in the passing of other fluids and electrolytes not normally passed. The presence of high glucose itself in the body can actually destroy tissue walls, including the walls of blood vessels, kidneys, eyes, and limbs. Diabetic patients are at higher risk for heart failure and kidney failure. In addition, it is not uncommon for diabetic patients to suffer blindness, and they often must have limbs removed because of the development of gangrene. As a final effect of frequent hyperglycemia, the inability of the body to use glucose as fuel results in the body's switching to fat metabolism and protein metabolism. This can result in the body's pH dropping to dangerous levels that can result in death from acidosis, or in the body's consuming the proteins of its tissues, also resulting in death.

While hyperglycemia could perhaps be prevented by purposely providing more insulin than required for glucose utilization, hypoglycemia would result from providing too much insulin. The amount of insulin available in the blood has a direct effect on the amount of glucose being taken into the cells of the liver and muscle cells. As the insulin availability increases, so does the uptake of glucose into the liver and muscle cells, regardless of the needs of other cells. This is problematic because glucose is the only nutrient that can be used by certain cells in sufficient quantity to allow them to sufficiently perform their metabolic processes.

The most important of these include the brain and the retina. If the brain is unable to get the necessary glucose to perform its metabolic functions, death will result. Adding to the severity of the problem is that if the pancreas is regularly increasing its glucagon

output to increase the glucose levels in response to hypoglycemia, it will eventually become insensitive to the low glucose levels, and eventually hypoglycemia will not result in the production of glucagon. Because the central nervous system is responsible for the production of epinephrine, this low level of hypoglycemia will result in the secretion of epinephrine as well. Therefore, to maintain healthy basal conditions, it is very important that a diabetic patient be able to exercise tight glucose control by using carefully determined insulin dosages.

2.3.2 Meals

When a healthy patient eats a meal, the carbohydrates are broken down into glucose, fructose, and galactose, with the fructose and galactose quickly converted into glucose. Fats are converted to triglycerides, phospholipids, and cholesterol, and proteins are converted to amino acids. During this period the body naturally increases its insulin levels to facilitate glucose uptake. This increase in insulin results in a decrease in glucagon levels and increased glucose uptake into the liver and peripheral cells. As previously mentioned, the release of insulin is in conjunction with GI hormones released, allowing the body to maintain near normal levels of plasma glucose. A healthy patient will rarely go over 140 mg/dL, even during a meal.

When a diabetic patient eats a meal, the outcome again strongly depends on the quality of insulin therapy. Specifically, the patient's glucose levels will depend on both the amount of insulin administered and the time of administration. If insulin levels are too low, two dramatic effects will result in extreme hyperglycemia. First, there will not

be enough insulin to allow the glucose to be taken into the liver and peripheral cells. Second, the low insulin levels will result in relatively high glucagon levels, which will actually result in even higher levels of glucose in the blood.

In addition to the amount of insulin administered for a meal, the time of administration plays a major role in maintaining normoglycemic conditions. This time usually corresponds with the production of the GI hormones associated with the meal. If the administration is too early, the result will be the onset of hypoglycemia before the meal is absorbed and hyperglycemia near the end of the meal, as there will not be sufficient insulin to allow the glucose infusion from the end of the meal to be utilized. If the insulin is administered too late, hyperglycemia will result at the beginning of the meal and hypoglycemia will result at the end of the meal or shortly after.

2.3.3 Exercise

The primary hormone influenced during exercise is epinephrine. Even before a person is actually exercising, his or her epinephrine levels will increase in preparation for the exercise that is about to take place. This epinephrine increase results in the metabolism of most cells increasing by an order of magnitude. To provide this energy, the increased epinephrine levels act to increase glucose and fatty acid production while simultaneously decreasing glucose uptake into liver or muscle cells. Insulin levels naturally decrease in response to higher levels of epinephrine, decreasing the uptake. While glucagon is mainly unaffected during exercise shorter than 90 minutes in duration,

an increase in the hormone occurs after approximately 90 minutes, further increasing the level of glucose available for utilization.

As with both meal consumption and in maintaining basal conditions, glucose metabolism for a diabetic patient is strongly dependent on the quality of insulin therapy received. If too much insulin is present in the body prior to exercise, the result will be an increase in glucose uptake in the liver and periphery and the inhibition of both glucose and fatty acid production. Because fatty acid levels do not increase, the glucose utilization by the cells increases. The consequence of all of these effects is the onset of hypoglycemia, a common occurrence during exercise for diabetic patients.

When too little insulin is present during exercise, the result will be hyperglycemia. This is not a problem during exercise, as the increased glucose levels provide additional fuel that can be used. However, once exercise has been completed, the patient now has higher glucose levels than normal, and there is no effort by the body to restore the levels to normal.

As the previous sections showed, diabetes can result in very serious consequences for both hyper- and hypoglycemia. The ability to live a life of nearly the same quality as a healthy patient largely depends on the ability of the patient to provide the right amount of insulin at the right time. In order to achieve this optimal type of administration, several insulin delivery methods have been proposed and developed.

2.4 Review of Insulin Delivery Techniques

To effectively control glucose in Type I and some Type II diabetic patients, insulin must be administered in such a way that neither hyper- nor hypoglycemic episodes are regularly experienced. Several different insulin administration techniques have been studied. Several other methods have been proposed and are the focus of current research. Each method can be classified by the type of control provided and by the site at which insulin is delivered. Each will be discussed below.

2.4.1 Open Loop Methods

Open loop methods of insulin delivery focus on a patient administering insulin to his or herself at different times of the day. The purpose here is to briefly describe open loop methods of control. Any interested reader is directed to reference [6] for a more thorough review of the open loop route.

The most common method of open loop insulin delivery is the subcutaneous insulin injection. Patients will often inject a slow acting insulin formulation in the morning to provide the basal insulin requirement throughout the day. This analog, known as insulin glargine, is developed by modifying certain amino acids on the different insulin chains [6]. Once altered, it is able to provide a steady release of insulin all day. In addition to the basal requirement, patients will inject insulin into subcutaneous tissue prior to meals. The amount of insulin to inject will depend on both a measurement of glucose and on an estimate of the amount of food that is about to be eaten. To provide rapid insulin during this situation, a fast acting insulin formulation such as insulin aspart

or insulin lispro is used. This method suffers from the requirement of three or more daily injections into a layer of subcutaneous tissue. In addition, because the injected insulin must diffuse through the subcutaneous tissue in order to be absorbed into the bloodstream, and because some of this insulin may be degraded in the subcutaneous tissue during this diffusion, not all of the injected insulin will be available for in the body. Also, the diffusion across the subcutaneous layer will create an additional time delay in addition to the delay associated with insulin binding to mediate glucose uptake. Finally, because the insulin will go straight from the subcutaneous layer to the bloodstream, the first pass effect, in which approximately 40% of insulin secreted from the pancreas is degraded in the liver before reaching the bloodstream, will not occur. This will result in increased uptake into the muscle cells and decreased uptake into the liver relative to a healthy patient.

An improvement to the insulin injection is the externally worn insulin pump. The pump is always attached to the diabetic patient, and a basal amount of insulin is provided throughout the day. When the patient is going to modify his or her insulin delivery because of a meal or exercise, the insulin infusion rate can be modified. Pumps have recently been developed to determine the bolus size for a given situation [7]. The patient must input his or her blood glucose levels and an estimate of the size of the load (meal size or exercise load) and the change in infusion will be determined. This type of administration has two primary advantages over injections. First, because the pump has a catheter that is always in contact with the patient, multiple insertions will not be required, increasing the quality of life for the patient. The exception for this is when the catheter is

periodically changed, but his is still a significant improvement to the three or more injections usually required. The second advantage is ease in which a change in the insulin infusion can be made. If a patient is was to eat a different amount of food than projected, or were to exercise for a different duration, the insulin rate can be adjusted to account for this. However, the disadvantages associated with subcutaneous delivery still exist. Furthermore, the patient is required to wear a bulky device at the abdominal area. Such a device would definitely be noticeable and would have a definite impact on the quality of life for the patient.

In addition to subcutaneous delivery, other open loop methods have been proposed that take advantage of other administration sites. Recently, the Food and Drug Administration has approved the use of Exubera, an inhaled form of insulin, to be used by insulin dependent diabetic patients [8]. The biggest advantage of such a technique is the increase in patient compliance, as a result of no longer having to receive injections or having to wear an external pump. However, several disadvantages exist. First, the bioavailability of inhaled insulin is less than that of a subcutaneous infusion. In addition, a slow releasing insulin analog has not been developed in an inhaled form, so basal administration is still necessary. Finally, because the absorption rate of insulin via the lungs can vary significantly for circumstances such as if a patient smokes or develops a cold, the dose must be carefully determined. Over-absorption of insulin can easily result in severe hypoglycemia [6].

In addition to inhalation, NIH funding is currently being applied toward the development of oral insulin delivery. Like the inhalation route, the oral route would in

theory prevent the patient from having to receive multiple daily injections. However, there do exist a few drawbacks to oral delivery. The first disadvantage of the oral route is the difficulty in maintaining the integrity of insulin in the harsh environment of the stomach. Insulin must be able to pass through the stomach and into the intestines for absorption into the bloodstream. However, the acidic gastric environment will degrade insulin, requiring a protective vehicle to allow the insulin to pass safely to the small intestine. Peppas [9] has developed a biomaterial for oral delivery of proteins that protects them in the harsh stomach environment and releases them in the higher pH environment of the small intestine. While protein degradation is one main cause of low bioavailability for protein delivery, another disadvantage of oral delivery is the low bioavailability associated with poor absorption from the intestine into bloodstream [10]. Ongoing research in many labs, including the Peppas laboratory, is currently focused on improving the transport of insulin across the intestinal epithelium.

In addition to oral and inhaled insulin delivery, other proposed methods include delivery via the eyes, skin, and nasal passages [6]. All open loop delivery systems require some level of patient or doctor involvement in the insulin administration. This will require a blood glucose measurement, an estimate of the meal to be consumed, and a calculation in order determine an empirical estimate of the insulin requirement. With the exception of the insulin pump, the open loop method requires a patient to live a predictable lifestyle, one in which his or her meal is prepared specifically for the given insulin bolus and exercise must be performed only in accordance with the insulin received.

2.4.2 Closed-Loop Delivery

An effective alternative to open loop insulin delivery is closed-loop delivery, in which the involvement of the patient in maintaining glucose control is minimal. Such a system would be able to determine the insulin requirement in real time, regardless of the situation, and deliver the proper insulin dosage. It would be able to change the infusion as the patient's activity changes and, ideally, would exist internally, eliminating the requirement of wearing external equipment. Such a system would also aim to significantly reduce the number of injections required or to eliminate them altogether.

The ideal method of closed loop delivery would be to repair the body's natural ability to infuse insulin. One method to achieve this would be the pancreas transplant. Ideally, the transplantation of a healthy pancreas would enable a diabetic patient to produce insulin as a healthy patient. However, there are many shortcomings associated with this approach. First, this method depends strongly on the availability of a healthy pancreas for transplantation. Second, the body of a pancreas recipient often undergoes an immune response that ultimately rejects the foreign organ [6].

Another natural method would be to restore to the patient's pancreas the ability to naturally secrete insulin as a healthy patient [11]. While such a method has promise, a great deal of research must be performed before this type of therapy can be useful to humans. A third method involves implanting encapsulated islet cells from a healthy pancreas, in the hopes that the immune response associated with the foreign pancreas can be avoided. At the same time, the islet beta cells will be able to produce insulin as a healthy pancreas would. This method is the subject of much ongoing research [6].

While natural pancreatic restoration methods are ideal, research must still be completed in order to determine the feasibility of these methods becoming reality. Perhaps a more realistic method of closed-loop control involves engineered solutions. First is the idea of explicit closed-loop control, in which a glucose sensor, an insulin infusion algorithm, and an insulin pump are used to form an artificial pancreas. Second is the idea of implicit-closed loop control, in which polymeric material is able to act as the sensor, control algorithm, and infusion system. To test the validity of such methods, simulations are performed by first developing a model of the infusion and then implementing the infusion model with a model of glucose dynamics within a diabetic patient. Patient modeling, explicit closed-loop control, and implicit closed-loop control will now be discussed.

2.4.3 Diabetic Patient Models

Models describing the important metabolite and hormone dynamics in diabetic patients have been developed since 1960 in order to gain understanding of the glucose homeostasis system and to simulate what effect certain therapies would have on the patient. This review covers different models developed during the last few decades. Others have written reviews on the models and described their various advantages and shortcomings. The interested reader is directed to Sorensen [12], Puckett [5], Parker and Doyle [13], and Steil [14] for more insight.

Patient models can be broken down into two main groups. On one side is the pharmacokinetic model, in which elimination and absorption kinetics are described for

each species, and a theoretical number of compartments is determined based on elimination and absorption data [15]. The second type is the physiologically explanatory model, in which organ system is considered to be a compartment, and mass balances are written for each organ system by considering convection resulting from blood flow, diffusion from blood to within organ cells, and metabolic processes [16, 17]. Both types have been developed in the past. While the pharmacokinetic (PK) models have the advantage of being easier to identify from experimental data, Doyle [18] has shown that more complex models may be needed to provide the necessary accuracy for effective control studies.

The first known PK model for glucose regulation was developed by Bolie [19]. The model consisted of one linear equation for insulin and one for glucose. Elimination and absorption kinetics were described by first order rate equations. While developed for a healthy patient, assuming that insulin secretion was simply proportional to glucose, the diabetic patient can be described by setting the first order insulin secretion rate constant to zero. Ackerman et al. [20] modified the model by tying insulin and all other hormones involved in glucose regulation together as a single variable. The model form remained the same however. The main criticisms of these models are that they represent a clear oversimplification of the glucose regulatory system. Besides the fact that insulin or hormone secretion is more complex than a simple first order process, the use of a single insulin or hormone compartment has been criticized by multiple reviewers, including Sorensen [12], and Parker and Doyle [13].

Frost et al. [21] developed a two-compartment PK model for insulin in healthy and diabetic patients. For healthy patients, the insulin secretion rate is given as an exponential function of glucose. For diabetics the secretion is taken to zero. Insulin elimination was taken to be a nonlinear saturation function of insulin for healthy patients and a first order process for diabetic patients. Frost himself admits that this also is an oversimplification, but notes a strong fit to patient data. His two compartment model with nonlinear sinks is also an improvement over the earlier developed models.

Sherwin et al. [22] and Cerasi et al. [23] simultaneously developed a three-compartment PK model in which a central compartment is continuously exchanging insulin with two side compartments. While more complex with respect to the number of insulin compartments, insulin appearance and elimination from each compartment is modeled as first order elimination kinetics. The model of Cerasi also has six linear ordinary differential equations (ODE's) to describe physiological insulin secretion. While the three insulin compartments are said to provide more physiological accuracy than the one compartment models previously used, the one compartment glucose model of Cerasi is likely inaccurate. Insel et al. [24] developed a three-compartment glucose model that included nonlinear terms to account for insulin effects on glucose uptake. However, the nonlinear term is effectively zero order with respect to insulin, and thus does not really effectively show accurate insulin effects in glucose consumption.

The majority of PK models developed since then have been modifications of the original PK models previously developed. Tranberg and Dencker [25] developed a two-compartment insulin model very much like that of Frost. Home et al. [26] and Kobayashi

et al. [27] both used a one-compartment model to fit kinetic parameters from patient data. Hipszer et al. [28] recently used the one-, two-, and three-compartment insulin models to fit insulin data from diabetic patients, concluding that a single insulin compartment is all that is needed to describe insulin kinetics. Salszieder et al. [29] developed a one-compartment model for both insulin and glucose, but increased model complexity in two ways. First, they assumed that glucose production and uptake were best expressed as differential equations. Second, they assumed that insulin accumulation was a function both of the glucose concentration and the derivative of the glucose concentration, an assumption which, as discussed later, forms the basis of many of the control systems designed for glucose control. Parker and Doyle [13] indicated that this model was not able to accurately describe faster dynamic processes associated with glucose regulation.

Perhaps the most widely used PK model to describe glucose and insulin kinetics is the minimal model developed by Bergman and Cobelli [30]. The authors chose from seven different PK model structures, including some of the previously developed models, to select the model structure displaying both a strong representation of intravenous glucose tolerance test (IVGTT) data and physiological relevance. The minimal model, which is derived in Appendix A, consists of a single glucose department and two insulin compartments. The pharmacokinetic diagram is given in Figure 2-1. Glucose elimination is considered to be a nonlinear function of both glucose and a term representing insulin that is bound to liver and peripheral cells. While originally developed based on animal studies, the model was later applied to human studies [31,32], to an oral glucose tolerance test (OGTT) [33], and to a mixed meal test [34].

There have been several published studies displaying the shortcomings of the minimal model, including the work of Quon et al. [35] and Finegood and Tzur [36]. Both groups found that the minimal model does not accurately quantify the relative contributions of insulin and glucose with respect to glucose uptake. Quon et al., including Cobelli [37] later determined that the problem stemmed from the use of a single glucose compartment. This lead to efforts to develop an improved minimal model, beginning with a two-compartment glucose model by Cobelli et al. [38,39], and ultimately leading to the recently developed hot IVGTT two-compartment minimal model [40]. The model continues to be improved today [41].

More recently, control engineers have gained an interest in the PK model developed by Hovorka et al. [42, 43]. In a similar manner to Bergman and Cobelli with the minimal model, Hovorka et al. proposed a number of different models before deciding on the one that both best fit the data as well as corresponded to physiology. The model diagram is given in Figure 2-2, and the model equations and parameter values are given in Appendix B. It uses two glucose compartments and three insulin-action compartments, describing the appearance and elimination of each species as a first order process. While there is only a single actual insulin compartment, three different types of insulin action are described and assumed to different with respect to their ability to affect glucose metabolism. This coincides well with the original claims of minimal model critics, which may have a lot to do with its rapid acceptance among control engineers. Hovorka et al. [44] recently improved upon the model to more accurately describe the kinetics associated with subcutaneous insulin delivery.

The second major type of patient model are those that describe biochemical species dynamics at each significant organ site. These models are developed by selecting as the main compartments only those organs in which significant species appearance or disappearance occur, and writing mass balances accordingly [16]. The first model of this type was developed by Foster et al. [45] in 1973. This model assumed a glucose compartment for blood, muscle, and the liver, while assuming a single compartment each for insulin, glucagon, and fatty acids. Guyton et al., including Foster [46] increased the complexity of Foster's model. A central organs compartment was added to the glucose model, insulin secretion from the pancreas was made more complex, and diffusion was included in the transport equations. Sorensen [12] improved Guyton's work by dividing the central organs compartment into the brain and gut compartments and by including the counter-regulatory effects of glucagon. A model diagram of Sorensen's glucose model is given in Figure 2-3, and the full model equations are given in Appendix C. The model of Foster et al. is the only one to include fatty acid metabolism.

Other physiologically relevant models include the models of glucose [47] and insulin [48] of Tiran et al., the model of Cobelli et al. [49], and the model of Puckett [5]. The many parameters of Tiran's models were estimated using dog data. The models also did not include the affects of glucagon. The models are also given in transfer function form, meaning that they represent linear representations of the systems. The model of Cobelli considers glucose to be a single subsystem, and contradicts his own minimal model improvements made years later. Puckett developed a model very similar to Sorensen's, but did not include glucagon effects, and removed all transport terms besides

the metabolic sources and sinks. In this way, her model represents a multi-compartment PK model. As such, any dynamics associated with other transport will not be captured by this model.

While Sorensen's model has been the most widely used physiological model with respect to glucose control, it has been criticized for not accurately representing observed glucose behaviors in diabetic patients. Steil [14] has pointed out that the model underpredicts the threshold glucose concentration at which insulin action becomes saturated. He also mentions that the model poorly represents the glucose concentration of a patient with zero insulin and that the sharp drop in glucose that is experienced by patients whose insulin levels rise quickly is also not predicted. However, despite these shortcomings, it remains the most accurate physiologically accurate model developed to date.

In addition to the development of a model, the model parameters must be accurately estimated in order to ensure reasonable simulation results. While the assumed accuracy of physiological models relative to PK models makes them enticing for control simulations, they suffer from the drawback of having tens to hundreds of parameters that must be identified. Because specific patient metabolic rates cannot usually be measured, many different techniques have had to be used in order to estimate model parameters. Some authors, such as Bolie [19], Guyton et al. [46], Tiran [47, 48], and Sorensen [12], used average reported parameters, such as compartment volumes and blood flows. Sorensen and Bolie chose to extrapolate human parameters from reported dog and rat parameters, assuming a linear relationship based only on bodyweight. In other instances,

specific data were acquired that allowed specific model parameters to be determined, such as most of the kinetic parameters of Sorensen's mode and the diffusion terms of Tiran's models. Most often, however, the model parameters were estimated by comparing model responses to glucose and insulin data, and selecting the parameter set that minimizing the sum of the squared residuals. It would appear that the lower order models have an advantage in that they can be estimated with a single set of glucose or insulin data, whereas the larger models will have to either assume average parameters values from literature or be able to use experimental data for a specific biochemical species in a specific tissue compartment. Finally, it should be noted that most average patient parameter values are given for a 70 kg adult male, independent of age, and that values for a human not matching this description would still have to be determined, either through experiment or approximation.

2.4.4 Explicit Closed-Loop Control

By utilizing the principles of process control, the body can be treated as a chemical process. Glucose metabolism can be simplified to the control of a single variable, glucose, through the use of a single manipulated variable, insulin. The effectiveness of such methods depends on the effective development of glucose sensors, insulin pumps, and control algorithms relating the insulin infusion to past, present, and predicted glucose values.

The development of improved glucose sensing methods is probably the most active component of research being applied toward the development of an explicit closed-

loop system. Even without the pump and algorithm, the use of a glucose sensor that is able to give frequent blood glucose measurements in real time is a dramatic improvement to drawing blood via a fingerstick and measuring glucose directly. Joseph and Torjman [50] summarized the different types of sensors being developed, including sensor design and biological issues associated with each. Among the sensors discussed are those implanted in either the subcutaneous tissue or the bloodstream. Most invasive sensors are based on enzyme catalyzed glucose oxidation. One issue associated with implanted sensors is the immune response of the body to foreign species. This can reduce the life of the sensor and can also interfere with its ability to give accurate readings. Another issue is the frequency of measurements. Medtronic-Minimed (Minnapolis, MN) has developed external sensors capable of giving measurements less than five minutes apart [51]. However, the device is not implantable. Devices implanted in the subcutaneous tissue also have the issue of not reading the actual glucose values of blood. The diffusion of glucose from blood to the subcutaneous tissue can result in time delays of around 30 minutes. Schmidtke et al. [52] and Freeland and Bonnecaze [53] have worked on developing dynamic models so that blood glucose values can be inferred from subcutaneous values. Much research is still needed, however, in order to develop implantable devices that can frequently report accurate glucose values for long periods of time [54, 55]. In addition, the lack of developed sensor technology for the other biochemical species to be determined in real time severely limits the possibilities of control to be based on glucose measurements only.

The second mechanical component of the system is the insulin infusion pump. Insulin pumps currently developed by Medtronic-Minimed are able to provide rapid-acting insulin throughout the day either as a basal pulse or as a bolus for a meal [56]. With the patented "Bolus Wizard" the insulin bolus will be calculated based on the size of the meal and the current glucose measurement. However, implantation of such a device is still a work in progress. Many issues must be resolved, including the immune response of the body, the location of the device, and how often the pump's insulin must be replaced. While Renard [57] argues that the pump should be placed within the peritoneum, a device planted under the skin may be easier to refill. However, such a device would likely be supplying insulin to the subcutaneous tissue, and delivery would not be like that of a healthy patient.

Parker and co-workers [58] reviewed many of the algorithms developed for glucose control prior to 2000. Bequette [59] also reviewed many of the older developments while also reviewing algorithms developed through 2005. The aim of this work is to summarize those reviews and to review algorithms developed since 2005.

The first algorithm of real significance with respect to the development of the artificial pancreas was proposed by Albisser [60]. This algorithm provided insulin when glucose was higher than the desired level and dextrose when glucose was lower than desired. The dextrose infusion rate was proportional to glucose infusion, and the insulin infusion rate was based on a nonlinear proportional plus derivative (PD) algorithm. The "Biostator" algorithms [61] improved upon Albisser's work to try to improve the response of blood glucose to a meal. This algorithm suffered from many problems. First,

the control algorithm consisted of many patient-dependent parameters, meaning the algorithm would have to be developed for a specific patient [58]. If patient parameters changed over time, the algorithm may also have to be reprogrammed. The second major problem is that the derivative was calculated using finite difference for the previous four measurements [59]. Because each measurement was one minute apart, the rate immediately after the beginning or end of a meal will inevitably suffer from a time lag before it is properly adjusted. In addition, measurement noise associated with any of the four points could also dramatically affect the infusion rate. Many authors [58] tried to create improvements to the Albisser's algorithm, but no controllers were found to outperform the original nonlinear PD algorithm.

As validation that the PD algorithm is indeed the best representation, Nomura et al. [62] studied the response of beta cells of healthy rats to a step disturbance of glucose. Glucose was infused at a constant rate, and the insulin concentration was noted with time. A biphasic response was observed, and the time constants associated with each phase were estimated. The biphasic response of the pancreas is shown in Figure 2-4. Steil et al. [63] investigated Albisser's algorithm and the algorithms of "Biostator" while also proposing a PID algorithm for insulin infusion. Controller effectiveness was studied by performing simulations using the model of Cobelli et al. [49]. For the simulation, the model was initially in the hyperglycemic state, and the ability of the controller to return glucose levels to normal was investigated. The algorithm has been implemented in the implantable pumps of Medtronic Minimed, and the ability to return glucose levels to normal in hyperglycemic diabetic dogs was observed. The pump was also implanted into

human subjects, and the control algorithm was demonstrated to result both hyperglycemia after the consumption of a meal and hypoglycemia after the meal. An argument against the use of PID controllers to mimic the biphasic insulin profile is provided in reference [59]. The author argues that such a response can be the result of any control system in which integral action is present, and that internal model controllers can also have the same response. He also argues that integral control can result in hypoglycemia as a result of infusing too much insulin.

Many authors have studied control algorithms by performing simulations using the well known patient models. Furler et al. [64] investigated the use of a semiclosed-loop algorithm based only on current glucose levels by performing simulations with the minimal model. The ability to return glucose levels from hyperglycemia to normal was observed, but no attempt was made to prevent glucose levels from approaching hyperglycemia after consumption of a meal. Sorensen [12] developed on internal model controller, and simulations were performed using his developed patient model. The controller is able to keep glucose levels under 140 mg/dL during a 100 g oral glucose tolerance test (OGTT). Parker et al. argue in reference [58] that the effectiveness of the controller is highly parameter dependent and that changing the model parameters results in the controller no longer being able to reject the disturbance.

Recent efforts in algorithm development have focused on advanced control methods. Among the first advanced control systems were the optimal controllers developed by Ollerton [65] and Fisher [65]. Ollerton used optimal control to minimize the integral of the squares of the differences between a glucose measurement and the

glucose set point. The minimal model was discretized with a 10 minute sampling interval, and the insulin infusion profile minimizing the objective function was chosen as the optimal profile. A 180 minute sampling time is also used, but such a long sampling time would be unable to correct for a meal disturbance that was present in between the samples. The author shows that the algorithm is able to return an initially hyperglycemic patient to normal levels, even in the present of a 100 g/day infusion of glucose. However, the algorithm is unconstrained with respect to the states, inputs, and outputs, and the optimal solution results in insulin levels below zero mU/L, which are not physically attainable. Even with negative insulin levels, the control system is unable to prevent the onset of hypoglycemia. Fisher also used the integral squared error objective function to apply optimal control to the minimal model, but chose three different semiclosed-loop insulin delivery systems to investigate. The first system was comprised of a basal infusion and injections when necessary, the second consisted of an infusion pump only that was optimized every hour, and the third system consisted of the optimal hourly infusion and the injection when needed. The optimal injection and pump infusion, where applicable, were determined using the objective function. Fisher shows that the best controllers consist of the optimal insulin injection, and that the optimal infusion alone will not be able to reject a meal disturbance without the onset of hypoglycemia.

Other methods of advanced control that have been applied include the application of H_∞ control by Parker et al. [67]. The authors applied H_∞ control to a modified version of Sorensen's model in which model parameter uncertainty is considered. The control

was applied after the model was reduced. Simulations showed that neither hyper- nor hypoglycemia are approached.

The most recent developments in closed-loop control focus on model predictive control (MPC) to provide the optimal control profile while considering constraints. Given measured outputs, model parameters are estimated using state estimation, and an objective function is solved based on the model prediction of the future glucose trajectory resulting from that particular insulin profile. Parker et al. [68] developed a model-based algorithm employing a linearized version of the Sorensen model, a Kalman filter, and a linear quadratic objective function. Like other methods applied to Sorensen's model, neither hyper- nor hypoglycemia were approached. Bequette and Lynch [69] applied linear MPC to the Sorensen model by using the minimal model to determine the insulin infusion profile. The authors later applied MPC directly to the minimal model, showing that neither hyper- nor hypoglycemia are approached during a meal [70]. Hovorka et al. [43] applied nonlinear MPC to Hovorka's original model. While the authors were able to show that NMPC used along with an injection at mealtime is able to reduce hyperglycemia and prevent hypoglycemia, no work was presented in which only the MPC controller was used.

Diaz et al. [71] applied predictive functional control Carson's model. While able to simulate the reduction of hyperglycemia during a meal and the prevention of hypoglycemia, the results were achieved by utilizing insulin infusion rates that lead to hyperinsulinism [1]. Finally, Cinar et al. [72] developed an online simulation tool employing MPC to control a patient using Puckett's model as both model and patient.

2.4.5 Implicit Closed-Loop Control

The development of an effective explicit closed-loop control system depends on the ability of engineers to develop an effective sensor for each output, an effect control algorithm that allows the controlled variables to be maintained at normal levels during many different conditions, and an effective infusion pump. The pump and the sensor must be able to be implanted and they must be able to respond quickly to the changing environment.

An alternative that removes the necessity of developed equipment is the implicit-closed loop control system, in which a chemical system is acting as all three components of the control system. The system, which contains insulin, is able to modify its insulin release profile in response to a change in the local environment. By mechanically changing in response to its environment, the system acts as a sensor. By releasing insulin through natural transport processes, the device acts as the infusion system. By being optimally designed to release the right amount of insulin for each condition, the device development is the control algorithm.

Because the required stimulus is the state of the local environment, a logical candidate to serve as such a device is the environmentally responsive hydrogel. Hydrogels are cross-linked hydrophilic polymer networks that are able to absorb large amounts of water [73]. The functional groups of the polymer backbone can be modified to allow the hydrogel to swell or deswell in response to many different stimuli, including pH and temperature.

To be used as glucose sensors, Albin et al. [74], as well as Peppas et al. [75-77], have incorporated enzyme-catalyzed glucose oxidation into the hydrogels by immobilizing glucose oxidase into the gel network. Because one of the reaction products is gluconic acid, it is logical to develop the gels to be pH-responsive. Because the release of insulin should increase in response to increased glucose, it is also natural that the hydrogel system be designed to swell in response to an increase in acid concentration, or a pH decrease.

Hydrogel systems that are responsive to pH changes can be divided into two groups. The first are the anionic hydrogels the swell in response to a high pH. These gels contain acid groups that deprotonate at a high pH. This ionization results in repulsions among functional groups within the chains. Examples of anionic hydrogels include the poly(methacrylic acid-graft-ethylene glycol) gels developed by Peppas et al. [9] for oral delivery, and the poly(N-isopropylacrylamide-co-methacrylic acid) gels developed Siegel et al. to serve as a chemomechanical oscillator [78, 79].

Cationic hydrogels are hydrogels that swell in response to a decrease in pH. These gels contain basic functional groups, such as methacrylates. Below the pK of the functional group, the functional groups become protonated, which results in a change in hydrophilicity of the network, causing an increase in water uptake into the gel [76]. This results in increased swelling at the pH below the pK of the functional groups.

Many people have studied the swelling and release characteristics of pH-sensitive cationic hydrogels. Firestone and Siegel [80] investigated the swelling kinetics of copolymer gels of methacrylic acid and dimethylaminoethyl methacrylate, poly(MMA-

co-DMAEM) as a function of pH, ionic strength, and temperature, showing that these systems can take in as much as 8 times their collapsed weight in water. Siegel et al. [81] showed that the pK of the buffer solution has a strong effect on the swelling of these gel systems. Firestone and Siegel [82] showed that these systems are able to demonstrate oscillatory swelling and deswelling and that successive pH increases with time resulted in successive deswelling to a specific swelling ratio. Cornejo-Bravo and Siegel [83] studied water sorption for copolymers of diethylaminoethyl methacrylate and methyl methacrylate (poly(DEAEM-co-MMA)), but no dynamic swelling or release results were given. Finally, Siegel et al. [84] investigated the release of caffeine from a hydrogel disk approximately 13 mm in diameter and 0.33 mm thick, and the effects of buffers on release [85]. At a pH of 3, the loaded disk no longer released caffeine at approximately 100 minutes from the start of the experiment. The completion time had increased to 200 minutes for pHs of 5 and 7. All of Siegel's swelling studies showed the gels reaching their equilibrium swelling ratios on the order of hours.

Many people in the Peppas laboratory at UT-Austin have investigated the swelling and release of pH-sensitive cationic hydrogels as well. Peppas and Hariharan [86] studied both dynamic and equilibrium swelling for a poly(diethylaminoethyl methacrylate-co-hydroxyethyl methacrylate) (poly(DEAEM-co-HEMA)), poly(diethylaminoethyl acrylate-co-hydroxyethyl methacrylate) (poly(DEAEA-co-HEMA), and poly(methacrylaminopropyl ammonium chloride-co-hydroxyethyl methacrylate) (poly(MAPTAC-co-HEMA)). They were able to demonstrate that poly(DEAEA-co-HEMA) showed no water sorption at a pH of 8, while water the gels

were able to uptake more than 10 times weight of the collapsed gel at a pH of 3. Using poly(DEAEM-co-HEMA) they demonstrated that 1mm thick disks would reach equilibrium swelling in approximately 3 hours, displaying weight swelling ratios ranging from 1.5 to 2.5 times the original weight of the gel. Peppas, Hariharan, and am Ende [90] performed release studies of oxprendol HCl from poly(DEAEA-co-HEMA) and poly(DEAEM-co-HEMA). Maximum drug release was observed to occur from 1 mm disks within 12 hours for poly(DEAEA-co-HEMA) and on the order of one day for poly(DEAEM-co-HEMA), with rapid release occurring in the first 5 hours, followed by slower release until the device no longer releases.

Because increasing the number of functional groups results in a lower transition pH for swelling, cationic hydrogels of poly(diethylaminoethyl methacrylate-co-ethylene glycol monomethyl ether monomethacrylate) (poly(DEAEM-g-EGMMA)) were developed by Podual, Doyle, and Peppas [76-77, 88-89], and Podual, Peppas, and Schwarte [75]. A small amount of PEGMMA was added to the gels to impart stealth capabilities in the body, preventing a rapid immune response from occurring. The gels displayed a transition pH of around 7.1, and displayed volume swelling ratios ranging from 8 for highly cross-linked gels to over 40 for lightly cross-linked devices. Dynamic studies showed that disks measuring 1 cm in diameter and 1 mm in thickness would reach equilibrium swelling in response to a pH change below the transition pH in approximately 5-6 hours. Microparticles of poly(DEAEM-g-EGMMA) were developed, and results showed that the gels reached equilibrium swelling nearly instantaneously to a decrease in pH below the transition pH [77]. The gels were also shown to be glucose

sensitive by observing their swelling in solutions of different glucose concentrations [88]. Finally, insulin release was demonstrated in response to change in glucose. Insulin was shown to be completely released from the system within 20 minutes [89].

Based on the currently developed formulations of poly(DEAEM-g-EGMMA), the hydrogel system would function as an implicit closed-loop system by way of the following mechanism, as shown in Figure 2-5. Small hydrogel particles would be injected directly into the bloodstream, where they would be protected from the body's immune response by the ethylene glycol grafts. As the glucose concentration of the blood increases, there will be increased diffusion of glucose to within the gel system. Within the gel, the presence of immobilized glucose oxidase will result in the enzyme catalyzed oxidation of glucose, forming gluconic acid. This acid formation will result in a slight pH change. The pH change will not be large because of the presence of buffers in the bloodstream, most importantly the bicarbonate buffer system [1]. When the pH decreases below the transition pH of the gel, swelling will occur, resulting in an increase in the diffusivity of species from the gel by up to a factor of ten. This results in an order of magnitude increase in insulin infusion from the gel, which results in increased glucose uptake. As the glucose concentration decreases, oxidation will decrease, and as hydrogen ions naturally diffuse out of the gel, the pH will increase again, resulting in a collapse of the particle.

There have been a number of modeling efforts associated with hydrogels. These can be grouped according to the various steps in the swelling and release process. A review of the different models assuming different transports mechanisms and different

methods of viscoelastic chain relaxation can be found in reference [90]. With respect the development of control relevant transport models, Lustig and Peppas [91] developed scaling laws to describe the diffusion of solutes in hydrogels that do not exhibit swelling behavior. Peppas, Harland, et al. [92] modeled the combined dissolution and diffusion of a drug that is released from the non-swelling system. Peppas and Hariharan [93] and Albin et al. [74] both developed models describing swelling and release from pH responsive hydrogel films, and Podual et al. [94, 95] developed a model describing swelling and release from poly(DEAEM-g-EGMMA) spherical particles. To the knowledge of the authors, there have been no previous attempts to simulate the response of pH-responsive hydrogels in vivo.

2.5 Conclusions

This chapter explained the major details regarding glucose metabolism, diabetes, and current and proposed therapeutic methods for treating diabetes. Included in the discussion was a review of all pertinent patient models, control algorithms, and efforts toward developing an implicit closed-loop control system. From the discussion, several observations can be made. First, there is no model in existence that accurately describes each species in the glucose metabolism process. A fatty acid PK has recently been proposed [96], but the majority of models and control configurations continue to focus solely on glucose and insulin, while a few include glucagon. Second, with the exception of a few MPC algorithms applied to Sorensen's model, no control algorithm appears to be able to prevent hyperglycemia without an additional injection at meal time. And

finally, there exists a need to study the in vivo effectiveness of implicit closed-loop control systems. This will be investigated in a later chapter. Through simulations of the in vivo effectiveness, the hydrogel design characteristics can be optimized so that effective implicit-closed loop control can be provided.

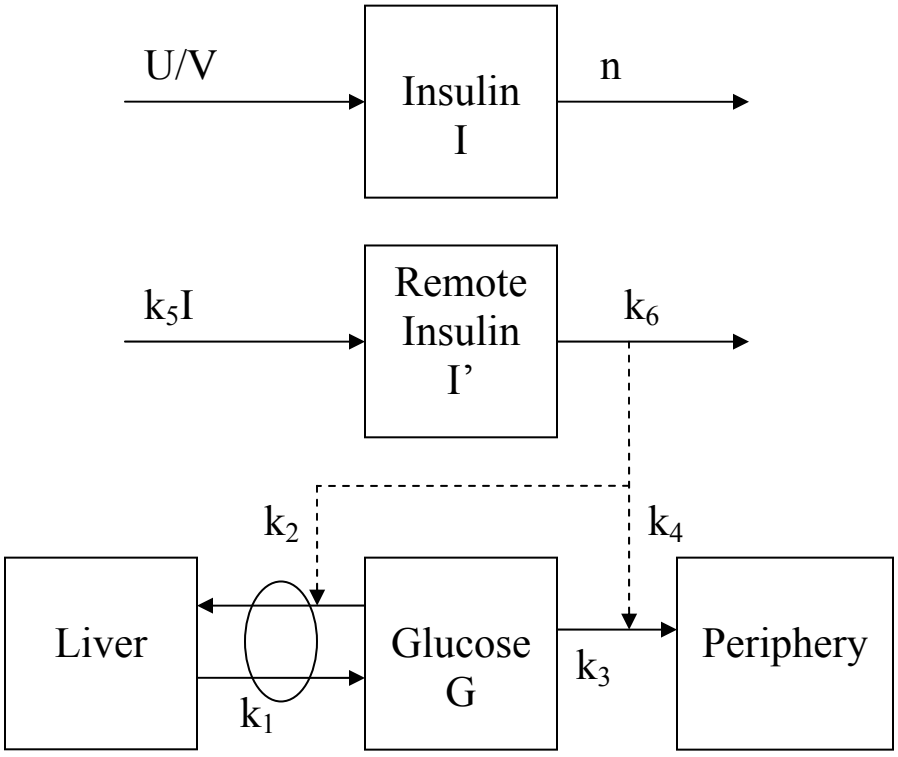

Figure 2-1: Pharmacokinetic diagram of the minimal model. Solid lines represent material appearance or disappearance, and dashed lines represent contributions toward the kinetic appearance or disappearance. The k_i's represent the rate coefficients for each term with respect to the kinetic process.

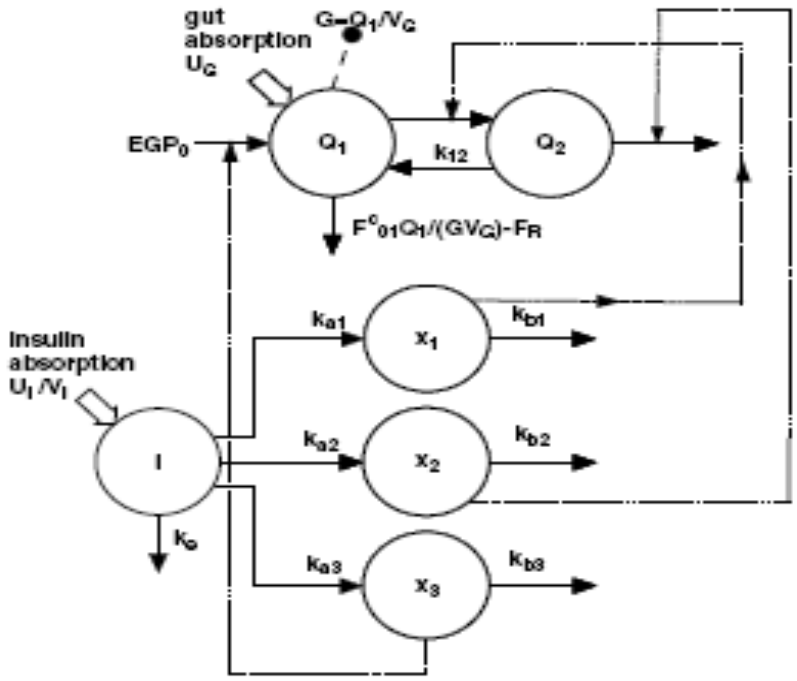

Figure 2-2: Pharmacokinetic diagram from Hovorka model [43]. Q_1 and Q_2 represent the mass of glucose in compartments 1 and 2, respectively. I represents plasma insulin, and x_1, x_2, and x_3 represent insulin action toward glucose uptake, production, and exchange between the two compartments. Solid lines represent kinetic appearance or disappearance. Dashed lines represent action by insulin. Large solid arrows represent a single non-continuous source of either glucose or insulin.

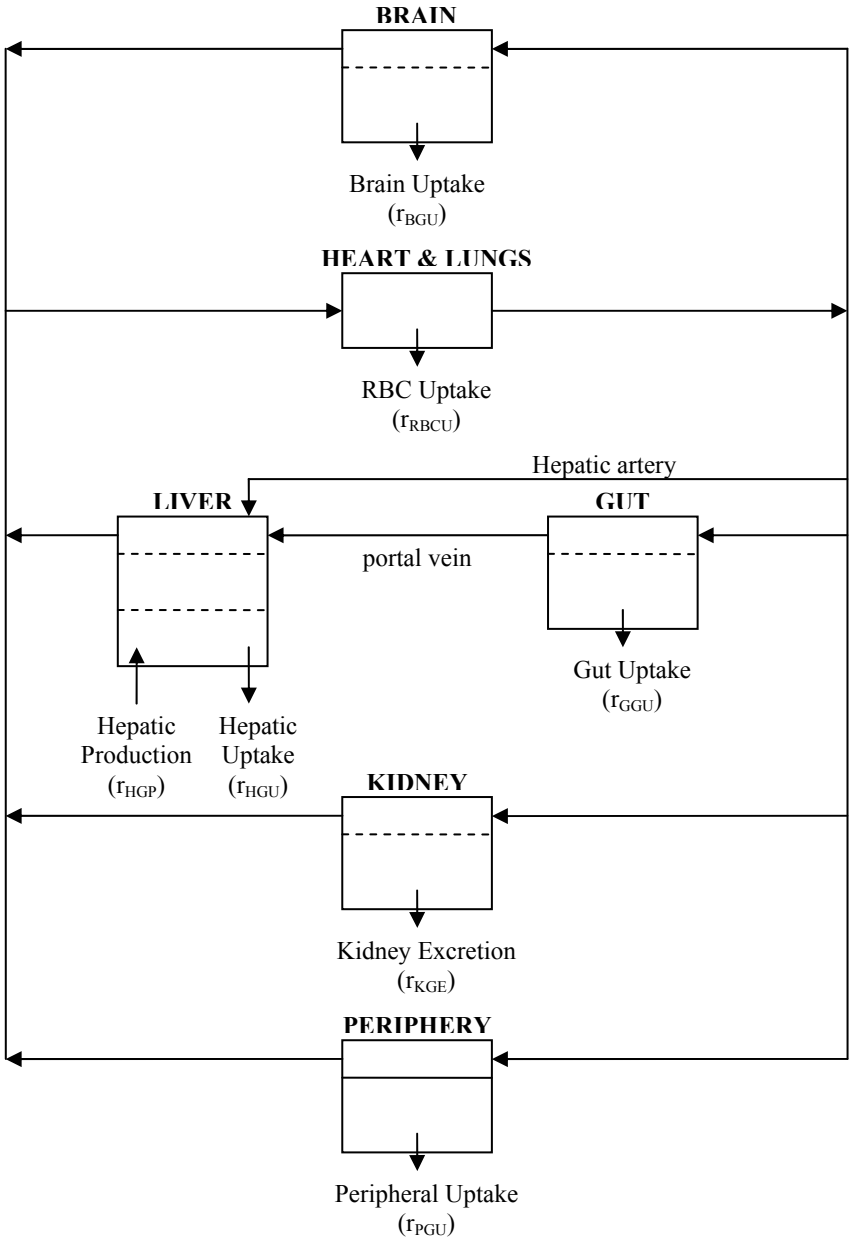

Figure 2-3: Flow diagram of the Sorensen glucose model [12].

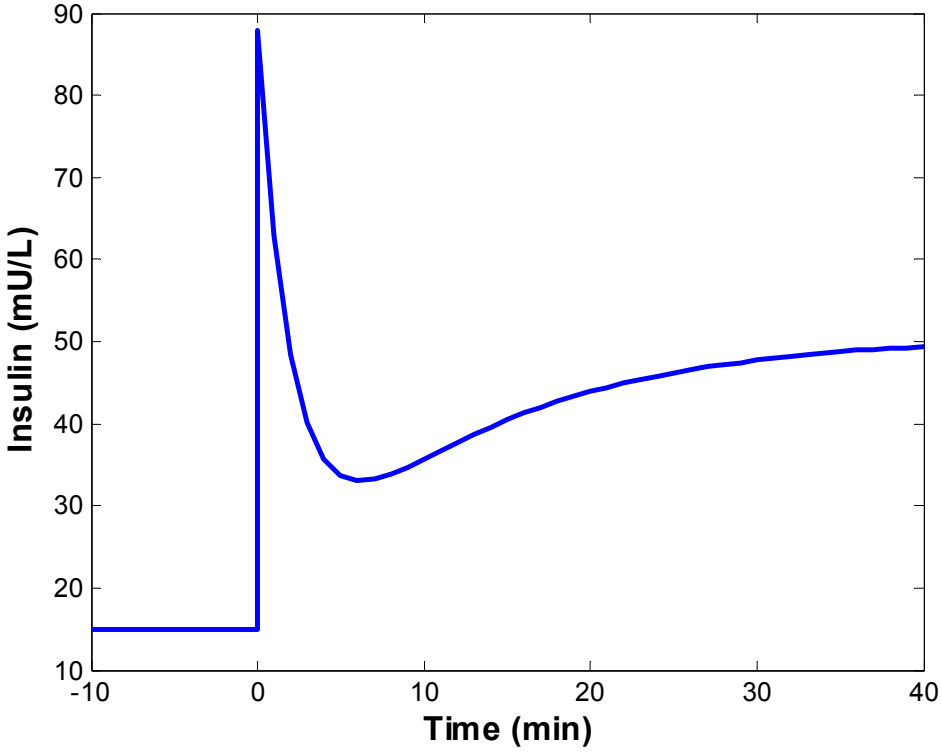

Figure 2-4: Biphasic insulin response to step increase in glucose, as modeled by Nomura et al. [62]. At time zero the glucose concentration is increased from 80 mg/dL to 160 mg/dL and maintained at the new level. A basal insulin concentration of 15 mU/L was assumed, as the results of the model simulation are given as insulin levels above basal. At the time of the glucose change, a sharp spike in insulin occurs, known as first phase release. This response falls off rapidly, followed by a second delayed release phase that gradually increases to the steady state insulin value.

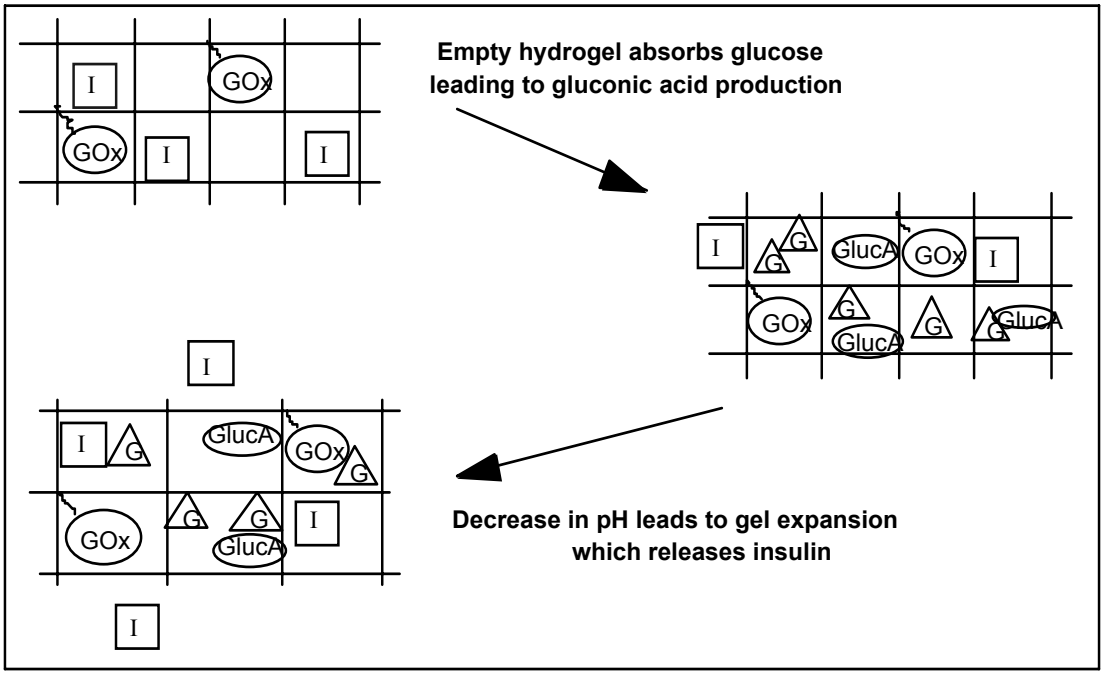

Figure 2-5: Schematic of mechanics of pH-responsive cationic hydrogels with glucose oxidase, based on the work of Podual [93]. Glucose appearance results in the production of gluconic acid, which decreases the system pH. pH-induced swelling results in increased diffusion of insulin from within the gel. As glucose is utilized, the mechanism is reversed.

2.6 References

1. Guyton, A. and Hall, J., *Textbook of Medical Physiology*, 11th ed., Elsevier Saunders, Philadelphia, PA, 2006.

2. Larsen, P.R., Kronenberg, H.M., Melmed,S., and Kenneth S. Polonsky, eds., *Williams Textbook of Endocrinology*, 10th ed., Saunders, Philadelphia, PA, 2003.

3. Greenspan, F. S., and David G. Gardner, eds., *Basic and Clinical Endocrinology*, 7th ed., McGraw-Hill, United States, 2004.

4. LeRoith, D., Taylor, S. I., and Jerrold M. Olefsky, eds., *Diabetes Mellitus: A Fundamental and Clinical Text*, 2nd ed., Lippincott, Williams, and Wilkins, Philadelphia, PA, 2000.

5. Puckett, W.R., *Dynamic Modelling of Diabetes Mellitus*, PhD Dissertation, Department of Chemical Engineering, The University of Wisconsin-Madision, 1992.

6. Parker, R. S., "Insulin Delivery", in *Encyclopedia of Biomaterials and Biomedical Engineering*, G. Wnek and G. Bowlin, eds., Dekker, NY, 857-866, 2004.

7. Medtronic Minimed, "Bolus Wizard Calculator," available http://www.minimed.com/products/insulinpumps/features/boluswizard.html, March 2007.

8. McMahon, G. T. and Arky, R. A., "Inhaled Insulin For Diabetes Mellitus", *New Engl. J. Med.*, **356**, 497-502, 2007.

9. Peppas, N. A., "Devices Based on Intelligent Biopolymers for Oral Protein Delivery", *Int.. J. Pharm..*, **277**, 11-17, 2004.

10. Morishita, M., and Peppas, N. A., "Is The Oral Route Possible For Peptide and Protein Drug Delivery," *Drug Discov. Today*, **11**, 905-910, 2006.

11. Bouwens, L., and Rooman, I., "Regulation of Pancreatic Beta Cell Mass," *Physiol. Rev.*, **85**, 1255-1270, 2005.

12. Sorensen, J. T., "A Physiologic Model of Glucose Metabolism in Man and Its Use to Design and Assess Improved Insulin Therapies For Diabetes", Ph.D. thesis, Dept. Chem. Eng., Massachusetts Institute of Technology, Cambridge, 1985.

13. Parker, R. S., and Doyle, F. J. III, "Control-Relevant Modeling in Drug Delivery," *Adv. Drug Deliver. Rev.*, **48**, 211-228, 2001.

14. Steil, G. M., Clark, B., Kanderian, S., and Rebrin, K., "Modeling Insulin Action For Development of a Closed-Loop Artificial Pancreas," *Diabetes Technology & Therapeutics*, **7**, 94-108, 2005.

15. Holz, M., and Fahr, A., "Compartmental Modeling," *Adv. Drug Deliver. Rev.*, **48**, 249-264, 2001.

16. Himmelstein, K. J., and Lutz, R. J., "A Review of the Applications of Physiologically Based Pharmacokinetic Modeling," *J. Pharmacokinet. Biopharm.*, **7**, 127-145, 1979.

17. Bischoff, K. B., "Physiologically Based Pharmacokinetic Modeling," in *Pharmacokinetics in Risk Assessment: Drinking Water and Health, Volume 8*, NAS Press, Washington, 36-61, 1987.

18. Doyle, F. J. III, Dorski, C., Harting, J. E., and Peppas, N. A., "Control and Modeling of Drug Delivery Devices For the Treatment of Diabetes," in *Proc. American Control Conf.*, Seattle, Washington, 776-780, 1995.

19. Bolie, V. W., "Coefficients of Normal Blood Glucose Regulation," *J. Clin. Invest.*, **39**, 783-788, 1960.

20. Ackerman, E., Gatewood, L. C., Rosevear, J. W., and Molnar, G. D., "Model Studies of Blood-Glucose Regulation," *B. Math. Biophys.*, **27**, 21-37, 1965.

21. Frost, D. P., Srivastava, M. C., Jones, R. H., Nabarro, J. D. N., and Sonksen, P. H., "The Kinetics of Insulin Metabolism In Diabetes Mellitus," *Postgrad. Med. J.*, **49**, 949-954, 1973.

22. Sherwin, R. S., Kramer, K. J., Tobin, J. D., Insel, P. A., Liljenquist, J. E., Berman, M., and Andres, R., "A Model of the Kinetics of Insulin In Man," *J. Clin. Invest.*, **53**, 1481-1492, 1974.

23. Cerasi, E., Fick, G., and Rudemo, M., "A Mathematical Model For the Glucose Induced Insulin Release In Man," *Europ. J. Clin. Invest.*, **4**, 267-278, 1974.

24. Insel, P. A., Liljenquist, J. E., Tobin, J. D., Sherwin, R. S., Watkins, P., Andres, R., and Berman, M., "Insulin Control of Glucose Metabolism In Man," *J. Clin. Invest.*, **55**, 1057-1066, 1975.

25. Tranberg, K. G., and Dencker, H., "Modeling of Plasma Disappearance of Unlabeled Insulin In Man," *Am. J. Physiol.*, **235**, E577-E585, 1978.

26. Home, P. D., Massi-Benedetti, M., Shepard, G. A., Hanning, I., Alberti, K. G., and Owens, D. R., "A Comparison of the Activity and Disposal of Semi-Synthetic Human Insulin and Porcine Insulin In Normal Man By the Glucose Clamp Technique," *Diabetologia*, **22**, 41-45, 1982.

27. Kobayashi, T., Sawano, S., Itoh, T., Kosaka, K., Hirayama, H., and Kasuya, Y., "The Pharmacokinetics of Insulin After Continuous Subcutaneous Infusion or Bolus Subcutaneous Injection In Diabetic Patients," *Diabetes*, **32**, 331-336, 1983.

28. Hipszer, B., Joseph, J., and Kam, M., "Pharmacokinetics of Intravenous Insulin Delivery in Humans With Type I Diabetes," *Diabetes Technology & Therapeutics*, **7**, 83-93, 2005.

29. Salzsieder, E., Albrecht, G., Fischer, U., and Freyse, E. J., "Kinetic Modeling of the Glucoregulatory System to Improve Insulin Therapy," *IEEE T. Bio.-Med. Eng.*, **32**, 846-855, 1985.

30. Bergman, R. N., Ider, Y. Z., Bowden, C. R., and Cobelli, C., "Quantitative Estimation of Insulin Sensitivity," *Am. J. Physiol.*, **236**, E667-E677, 1979.

31. Bergman, R. N., Bowden, C. R., and Cobelli, C., "The Minimal Model Approach to Quantification of Factors Controlling Glucose in Man," in *Carbohydrate Metabolism*, C. Cobelli and R. N. Bergman, Eds., Wylie, London, 269-296, 1981.

32. Bergman, R. N., Phillips, L. S., and Cobelli, C., "Physiologic Evaluation of Factors Controlling Glucose Tolerance in Man," *J. Clin. Invest.*, **68**, 1456-1467, 1981.

33. Dalla Man, C., Campioni, M., Polonsky, K. S., Basu, R., Rizza, R. A., Toffolo, G., and Cobelli, C., "Two-Hour Seven-Sample Oral Glucose Tolerance Test and Meal Protocol: Minimal Model Assessment of β-Cell Responsitivity and Insulin Sensitivity In Nondiabetic Individuals," *Diabetes*, **54**, 3265-3273, 2005.

34. Caumo, A., Bergman, R. N., and Cobelli, C., "Insulin Sensitivity From Meal Tolerance Tests In Normal Subjects: A Minimal Model Index," *J. Clin. Endocr. Metab.*, **85**, 4396-4402, 2000.

35. Quon, M. J., Cochran, C., Taylor, S. I., and Eastman, R. C., "Non-Insulin-Mediated Glucose Disappearance In Subjects With IDDM. Discordance Between Experimental Results and Minimal Model Analysis," *Diabetes*, **43**, 890-896, 1994.

36. Finegood, D. T., and Tzur, D., "Reduced Glucose Effectiveness Associated With Reduced Insulin Release: An Artifact of the Minimal-Model Method," *Am. J. Physiol.*, **271**, E485-E495, 1996.

37. Cobelli, C., Bettini, F., Caumo, A., and Quon, M. J., "Overestimation of Minimal Model Glucose Effectiveness In Presence of Insulin Response Is Due to Undermodeling," *Am. J. Physiol.*, **277**, E1031-E1036, 1998.

38. Caumo. A, Vicini, P., Zachwieja, J., Avogaro, A., Yarasheski, K., Bier, D., M., and Cobelli, C., "Undermodeling Affects Minimal Model Indexes: Insights From a Two-Compartment Model," *Am. J. Physiol.*, **276**, E1171-E1193, 1999.

39. Cobelli, C., Caumo, A., and Omenetto, M., "Minimal Model S_G Overestimation and S_I Underestimation: Improved Accuracy By a Bayesian Two-Compartment Model," *Am. J. Physiol.*, **277**, E481-E488, 1999.

40. Toffolo, G., and Cobelli, C., "The Hot IVGTT Two-Compartment Minimal Model: An Improved Version," *Am. J. Physiol.*, **284**, E317-E321, 2003.

41. Krudys, K. M., Dodds, M. G., Nissan, S. M., and Vicini, P., "Integrated Model of Hepatic and Peripheral Glucose Regulation For Estimation of Endogenous Glucose Production During the Hot IVGTT," *Am. J. Physiol.*, **288**, E1038-E1046, 2005.

42. Hovorka, R, Shojaee-Moradie, F., Carroll, P. V., Chassin, L. J., Gowrie, I. J., Jackson, N. C., Tudor, R. S., Umpleby, A. M., and Jones, R. H., "Partitioning Glucose Distribution/Transport, Disposal, and Endogenous Production During IVGTT", *Amer. J. Physiol.,* **282,** E992–1007, 2002.

43. Hovorka, R., Canonico, V., Chassin, L. J., Haueter, U., Massi-Benedetti, M., Federici, M. O., Pieber, T. R., Schaller, H. C., Schaupp, L., Vering, T., and Wilinska, M. E., "Nonlinear Model Predictive Control of Glucose Concentration In Subjects With Type I Diabetes", *Physiol. Meas.*, **25**, 905-920, 2004.

44. Wilinska, M. E., Chassin, L. J., Schaller, H. C., Schaupp, L., Pieber, T. R., and Hovorka, R., "Insulin Kinetics In Type-1 Diabetes: Continuous and Bolus Delivery of Rapid Acting Insulin," *IEEE Trans. Biomed. Eng.*, **52**, 3-12, 2005.

45. Foster, R. O., Soeldner, J. S., Tan, M. H., and Guyton, J. R., "Short Term Glucose Homeostasis In Man: A System's Dynamics Model," *J. Dyn. Syst. Meas. Control,* **95**, 308-314, 1973.

46. Guyton, J. R., Foster, R. O., Soeldner, J. S., Tan, M. H., Kahn, C. B., Koncz, L., and Gleason, R. E., "Model of Glucose-Insulin Homeostasis In Man That

Incorporates the Heterogeneous Fast Pool Theory of Pancreatic Insulin Release," *Diabetes*, **27**, 1027-1042, 1978.

47. Tiran, J. and Galle K. R., "A Simulation Model of Extracellular Glucose Distribution In the Human Body," *Ann. Biomed. Eng.*, **3**, 34-46, 1975.

48. Tiran, J., Avruch, L. I., and Albisser, A. M., "A Circulation and Organs Model For Insulin Dynamics," *Am. J. Physiol.*, **237**, E331-E339, 1979.

49. Cobelli, C., Federspil, G., Pacini, G., Salvan, A., and Scandellari, C., "An Integrated Mathematical Model of the Dynamics of Blood Glucose and Its Hormonal Control," *Math. Biosci.*, **58**, 27-60, 1981.

50. Joseph, J. I., and Torjman, M. J., "Glucose Sensors," in *Encyclopedia of Biomaterials and Biomedical Engineering*, G. Wnek and G. Bowlin, eds., Dekker, NY, 683-692, 2004.

51. Medtronic Minimed, "REAL-Time Glucose Monitoring," available http://www.minimed.com/products/insulinpumps/components/cgm.html, March 2007.

52. Schmidtke, D. W., Freeland, A. C., Heller, A., and Bonnecaze, R. T., "Measurement and Modeling of the Transient Difference Between Blood and Subcutaneous Glucose Concentrations In the Rat After Injection of Insulin," *Proc. Natl. Acad. Sci.*, **95**, 294-299, 1998.

53. Freeland, A. C. and Bonnecaze, R. T., "Inference of Blood Glucose Concentrations From Subcutaneous Glucose Concentrations: Applications to Glucose Biosensors," *Ann. Biomed. Eng.*, **27**, 525-537, 1999.

54. Ginsberg, B. H., "How Accurate Are Accuracy Measurements of Continuous Glucose Sensing," *Diabetes Technology & Therapeutics*, **7**, 673-674, 2005.

55. Colberg, S. R., "Glucose Monitoring and Physical Activity: The Present and Future Challenges," Diabetes Technology & Therapeutics, 7, 681-683, 2005.

56. Medtronic Minimed, "Minimed Paradigm 522 or 722 Insulin Pump," available http://www.minimed.com/products/insulinpumps/components/insulinpump.html, March 2007.

57. Renard, E., "Implantable Closed-Loop Glucose-Sensing and Insulin Delivery: The Future of Insulin Pump Therapy," *Curr. Opin. Pharmacol.*, **2**, 708-716, 2002.

58. Parker, R. S., Doyle, F. J. III, and Peppas, N. A., "The Intravenous Route To Blood Glucose Control," IEEE Eng. Med. Biol., **20**, 65-73, 2001.

59. Bequette, B. W., "A Critical Assessment of Algorithms and Challenges In the Development of a Closed-Loop Artificial Pancreas," *Diabetes Technology and Therapeutics*, **7**, 28-47, 2005.

60. Albisser, A. M., Leibel, B. S., Ewart, T. G., Davidovac, Z., Botz, C. K., and Zingg, W., "An Artificial Endocrine Pancreas," *Diabetes*, **23**, 389-396, 1974.

61. Clemens, A. H., "Feedback Control Dynamics For Glucose Controlled Insulin Infusion Systems," *Med. Prog. Technol.*, **6**, 91-98, 1979.

62. Nomura, M., Shichiri, M., Kawamori, R., Yamasaki, Y., Iwama, N., and Abe, H., "A Mathematical Insulin-Secretion Model and Its Validation In Isolated Rat Pancreatic Islets Perfusion," *Comput. Biomed. Res.*, **17**, 570-579, 1984.

63. Steil, G. M., Panteleon, A. E., and Rebrin, K., "Closed-Loop Insulin Delivery—the Path to Physiological Glucose Control," *Adv. Drug Deliver Rev.*, **56**, 125-144, 2004.

64. Furler, S. M., Kraegen, E.W., Smallwood, R.H, and Chisolm, D.J., "Blood Glucose Control by Intermittent Loop Closure in the Basal Mode: Computer Simulation Studies with a Diabetic Model", *Diabetes Care*, **8**, 553-561, 1985.

65. Ollerton, R. L., "Application of Optimal Control Theory to Diabetes Mellitus," *Int. J. Control*, **50**, 2503-2522, 1989.

66. Fisher, M. E., "A Semiclosed-Loop Algorithm For the Control of Blood Glucose Levels In Diabetics," *IEEE Trans. Biomed. Eng.*, **38**, 57-61, 1991.

67. Parker, R. S., Doyle, F. J. III, Ward, J. H., and Peppas, N. A., "Robust H_∞ Glucose Control In Diabetes Using a Physiological Model," *AIChE J.*, **46**, 2537-2549, 2000.

68. Parker, R. S., Doyle, F. J., III, and Peppas, N. A., "A Model-Based Algorithm For Blood Glucose Control In Type I Diabetic Patients," *IEEE Trans. Biomed. Eng.*, **46**, 148-157, 1999.

69. Lynch, S. M., and Bequette, B. W., "Estimation-Based Model Predictive Control of Blood Glucose In Type I Diabetics: A Simulation Study," in *Proceedings of the IEEE 27th Annual Northeastern Bioengineering Conference,* Storrs, CT, 79-80, 2001.

70. Lynch, S. M., and Bequette, B. W., "Model Predictive Control of Blood Glucose In Type I Diabetics Using Subcutaneous Glucose Measurements," in *Proceedings of the 2002 American Control Conference*, Anchorage, AK, 4039-4043, 2002.

71. Diaz, R. G., Roldan, G., and Basualdo, M., "A Decision Support System Based On a Closed Loop PFC Applied For Type I Diabetes," in *Proceedings of the 16th IFAC World Congress*, Prague, Czech Republic, 2005.

72. Agar, B., Birol, G., and Cinar, A., "Virtual Experiments For Controlling Blood Gulcose Level In Type I Diabetes," in *Proc. 2nd Joint EMBS-BMES Conference*, Houston, TX, 2002.

73. Peppas, N. A., "Hydrogels," in *Biomaterials Science*, B. D. Ratner, A. S. Hoffman, F. J., Schoen, and J. E. Lemons, Eds., Academic Press, NY, 100-107, 2004.

74. Albin, G. W., Horbett, T. A., Miller, S. R., and Ricker, N. L., "Theoretical and Experimental Studies of Glucose Sensitive Membranes," *J. Control. Release*, **6**, 267-291, 1987.

75. Schwarte, L. M., Podual, K., and Peppas, N. A., "Cationic Hydrogels For Controlled Release of Proteins and Other Macromolecules," in I. McCullogh and S. W. Shalaby, Eds., *Tailored Polymeric Materials For Controlled Drug Delivery Systems*, ACS Symposium Series, Vol. 709, 56-66, 1998.

76. Podual, K., Doyle, F. J., III, and Peppas, N. A., "Preparation and Dynamic Response of Cationic Copolymer Hydrogels Containing Glucose Oxidase," *Polymer*, **41**, 3975-3983, 2000.

77. Podual, K., Doyle, F. J., III, and Peppas, N. A., "Dynamic Behavior of Glucose Oxidase-Containing Microparticles of Poly(Ethylene Glycol)-Grafted Cationic Hydrogels In an Environment of Changing pH," *Biomaterials*, **21**, 1439-1450, 2000.

78. Leroux, J. and Siegel, R. A., "Autonomous Gel/Enzyme Oscillator Fueled By Glucose: Preliminary Evidence For Oscillations," *Chaos*, **9**, 267-275, 1999.

79. Dhanarajan, A. P., Misra, G. P., and Siegel, R. A., "Autonomous Chemomechanical Oscillations In a Hydrogel/Enzyme System Driven By Glucose," *J. Phys. Chem. A*, **106**, 8835-8838, 2002.

80. Firestone, B. A., and Siegel, R. A., "Kinetics and Mechanisms of Water Sorption In Hydrophobic, Ionizable Copolymer Networks," *J. Appl. Polymer Sci.*, **43**, 901-914, 1991.

81. Siegel, R. A., Johannes, I., Hunt, C. A., and Firestone, B. A., "Buffer Effects On Swelling Kinetics In Polybasic Gels," *Pharm. Res.*, **9**, 76-81, 1992.

82. Firestone, B. A. and Siegel, R. A., "Dynamic pH-Dependent Swelling Properties of a Hydrophobic Polyelectrolyte Gel," *Polym. Commun.,* **29**, 204-208, 1988.

83. Cornejo-Bravo, J. M. and Siegel, R. A., "Water Vapor Sorption Behavior of Copolymers of N,N-Diethylaminoethyl Methacrylate and Methyl Methacrylate," *Biomaterials*, **17**, 1187-1196, 1993.

84. Siegel, R. A., Falamarzian, M., Firestone, B. A., and Moxley, B. C., "pH-Controlled Release From Hydrophobic/Polyelectrolyte Copolymer Hydrogels," *J. Control. Release*, **8**, 179-182, 1988.

85. Cornejo-Bravo, J. M. and Siegel, R. A., "Kinetics of Drug Release From Hydrophobic Polybasic Gels: Effect of Buffer Acidity," *J. Control. Release*, **33**, 223-229, 1995.

86. Hariharan, D. and Peppas, N. A., "Characterization, Dynamic Swelling Behavior and Solute Transport In Cationic Networks With Applications To the Development of Swelling-Controlled Release Systems," *Polymer*, **37**, 149-161, 1996.

87. Ende, M. T., Hariharan, D., and Peppas, N. A., "Factors Influencing Drug and Protein Transport and Release From Ionic Hydrogels," *React. Polym.*, **25**, 127-137, 1995.

88. Podual, K., Doyle, F. J. III, and Peppas, N. A., "Glucose-Sensitivity of Glucose Oxidase-Containing Cationic Polymer Hydrogels Having Poly(Ethylene Glycol) Grafts," *J. Control. Release*, **67**, 9-17, 2000.

89. Podual, K., Doyle, F. J. III, and Peppas, N. A., "Insulin Release From pH-Sensitive Cationic Hydrogels," *Proceed. Intern. Symp. Control. Rel. Bioact. Mater.*, **25**, 56-57, 1998.

90. Podual, K., "Glucose-Sensitive Cationic Hydrogels For Insulin Release," PhD Dissertation, Department of Chemical Engineering, Purdue University, West Lafayette, IN, 1998.

91. Lustig, S. R., and Peppas, N. A., "Solute Diffusion in Swollen Membranes. IX. Scaling Laws For Solute Diffusion In Gels," *J. App. Polymer Sc.*, **36**, 735-747, 1988.

92. Harland, R. S., Dubernet, C., Benoit, J., and Peppas, N. A., "A Model of Dissolution-Controlled, Diffusional Drug Release From Non-Swellable Polymeric Microspheres," *J. Control. Release*, **7**, 207-215, 1988.

93. Hariharan, D. and Peppas, N. A., "Modelling of Water Transport and Solute Release In Physiologically Sensitive Gels," *J. Contr. Rel.*, **23**, 123-136, 1993.

94. Podual, K., Doyle, F. III, and Peppas, N. A., "Modeling of Water Transport In and Release From Glucose-Sensitive Swelling-Controlled Release Systems Based On Poly(Diethylaminoethyl Methacrylate-g-Ethylene Glycol)," *Ind. Eng. Chem. Res.*, **43**, 7500-7512, 2004.

95. Podual, K. and Peppas, N. A., "Relaxational Behavior and Swelling-pH Master Curves of Poly[(Diethylaminoethyl Methacrylate)-Graft-(Ethylene Glycol)] Hydrogels," *Polym. Int.*, **54**, 581-593, 2005.

96. Roy, A., and Parker, R. S., "Dynamic Modeling of Free Fatty Acid, Glucose, and Insulin: An Extended 'Minimal Model'," *Diabetes Technology & Therapeutics*, **8**, 617-626, 2006.

CHAPTER 3

RESEARCH OBJECTIVES

The primary focus of this research was to develop simulations of the in vivo efficacy of different types of closed-loop control systems in patients with diabetes mellitus. This research had three primary research objectives. The first was to develop an improved model of metabolite and hormone dynamics for both healthy and diabetic patients. The second was to apply principles of process control toward the development of explicit closed-loop control systems employing an insulin infusion pump with an algorithm to determine the insulin infusion rate. The final objective was to develop mathematical relations describing the implicit closed-loop control system and simulate its response. With each individual objective achieved, the in vivo response of the control systems to both basal and non-basal conditions could be observed in order to assess the potential effectiveness of such systems within actual patients.

3.1 Patient Model Development

In order to simulate how insulin and other hormones affect plasma glucose, patient models with sufficiently detailed biological information are required. While the glucoregulatory system involves multiple metabolites and hormones, most existing models focus only on the dynamics of glucose and insulin. Mathematical models describing the dynamics of all metabolic species and hormones that are involved in the minute-to-minute control of glucose were developed in order to fully understand the

system as one involving more species than simply glucose and insulin. The models were developed by first determining the primary biochemical species (given in Chapter 2).

Next, the specific tissue sites of the important metabolic dynamics for each species were determined, and mass balances were developed around each site. For this objective, both simple pharmacokinetic and complex physiologic models were developed.

3.2 Model Parameter Estimation

With the models developed, the next objective in completing the modeling efforts was to identify the model parameter values. However, as data were not attainable for this, the ability to identify even simple models was investigated. Using both patient data and test data, with and without noise, the ability to determine model parameters for a low order insulin pharmacokinetic model was investigated. We carried out this investigation by assessing the ability of pre-developed optimization solvers to successfully re-estimate the model parameters using data generated by a model with a specified set of parameter values. This investigation was performed for varying levels of model complexity and includes an investigation of confidence intervals, output sensitivity to each parameter, and numerical effects in the estimation process.

3.3 Explicit Closed-Loop Control

Because the developed patient dynamic models were unable to be successfully identified, explicit closed-loop control systems have been developed by a number of

researchers for three specific models, namely the minimal model [1], the Sorensen model [2], and the Hovorka model [3]. For each model, the effectiveness of proportional-integral-derivative (PID) control, feedforward control, and optimal control was investigated in this thesis for different conditions and different model parameter sets. Each control system uses a different algorithm, based on glucose levels, to determine the insulin infusion rate, assuming release is provided by an implanted pump that allows release directly into the bloodstream. Specifically, the effectiveness of each control system was assessed for basal conditions, after a meal, or during exercise. Finally, a controller developed based on Sorensen's representation of pancreatic insulin secretion was developed, and its effectiveness in controlling glucose was assessed.

3.4 Implicit Closed-Loop Control System Development

The feasibility of using injectible micro- or nanosphere particles of pH-responsive cationic hydrogels was also assessed by investigating the ability of the system to provide insulin for basal and non-basal glucose levels. To achieve this assessment, a model was developed describing the dynamics of glucose, insulin, and gluconic acid within the gel. The effect of gluconic acid on insulin release was also modeled by considering how the system's pH would change, how this pH would affect swelling, and how swelling would affect insulin release.

With the model developed, simulations were performed with the minimal model in order to determine the effectiveness of the hydrogel system at controlling glucose within a diabetic patient. A number of simulations were performed in order to determine

the effect of each model parameter, and ultimately, each system design specification, on the system's response. Next the system was optimized in order to find the parameter set that allows for two characteristic conditions to be satisfied: (1) glucose was to be maintained at a normoglycemic range during basal conditions; (2) the injectible system was to remain active in the body for an extended period of time. Both the constrained and unconstrained optimization problems were considered. For the unconstrained problem, it was assumed that each parameter can take on any physically realistic value. For the constrained problem, it was assumed that each parameter may have a physical limitation, such as the size of a particle or the number of particles that can exist in the body. Based on the simulations, the effectiveness of the hydrogel system to provide intravenous insulin release were determined, and the system's feasibility is discussed.

3.5 References

1. Bergman, R.N., Bowden, C. R., and Cobelli, C., "The Minimal Model Approach to Quantification of Factors Controlling Glucose Disposal in Man", in C. Cobelli and R.N. Bergman, eds., *Carbohydrate Metabolism*, 269-293, Wiley, Chichester, UK, 1981 .

2. Sorensen, J.T., "A Physiologic Model of Glucose Metabolism in Man and Its Use to Design and Assess Improved Insulin Therapies For Diabetes", Ph.D. thesis, Dept. Chem. Eng., Massachusetts Institute of Technology, Cambridge, 1985.

3. Hovorka, R, Shojaee-Moradie, F., Carroll, P. V., Chassin, L. J., Gowrie, I. J., Jackson, N. C., Tudor, R. S., Umpleby, A. M., and Jones, R. H., "Partitioning Glucose Distribution/Transport, Disposal, and Endogenous Production During IVGTT", *Amer. J. Physiol.,* **282,** E992–1007, 2002.

4. Hovorka, R., Canonico, V., Chassin, L. J., Haueter, U., Massi-Benedetti, M., Federici, M. O., Pieber, T. R., Schaller, H. C., Schaupp, L., Vering, T., and Wilinska, M. E., "Nonlinear Model Predictive Control of Glucose Concentration In Subjects With Type I Diabetes", *Physiol. Meas.*, **25**, 905-920, 2004.

CHAPTER 4

PATIENT DYNAMIC MODELING

4.1 Introduction

The use of models in the development of novel medical therapeutic systems can greatly improve the development process. By being able to perform an accurate simulation of the behavior of patients treated by the therapeutic methods, two important advantages are realized relative to development without simulation. First, the use of simulation is a significantly cheaper alternative to testing in patients and animals, both in terms of dollars spent and time spent in gaining approval for such experiments, the development of experimental protocols, and experimental setup and performance. Second, a simulation can quickly reveal device design characteristics that will not be effective, preventing any catastrophic results from occurring, including the loss of lives. In addition to these two primary advantages, the ability of simulations to show the system response for a large number of design configurations and scenarios in a relatively short amount of time demonstrates that, at the very least, the use of simulations as a precursor to experiments is a highly effective way to improve the design process.

Two different types of patient models can be developed. The first type, the pharmacokinetic model [1], simply describes the kinetics of absorption and elimination of a species for a certain number of theoretical compartments. Often a single compartment, representing the circulation is chosen. Elimination and absorption kinetics are most often described by first order kinetics. When the model does not match data, the model

structure is changed by either increasing the number of compartments used or by changing the mathematical description of the kinetic rates.

The second type of model developed is the physiologically-based model [2], in which the most significant organ tissues are chosen as well-mixed compartments, and the concentration of species is assumed to be uniform within that compartment. Mass balances describing blood flow convection, mass transfer within each compartmental space, and the metabolic processes are written for each species at each compartment. The result is a large, multi-compartment model based on physiology.

Both the pharmacokinetic and the physiologically-based model have their advantages and disadvantages. The physiologically-based model has the potential to be a better model for both simulation and for use in model-based control methods, as a result of its thorough description of each species in the body. However, because there are so many parameters to be identified with such a large model, the pharmacokinetic models have the advantage that, while perhaps not describing metabolism as accurately as the explanatory models, an estimate of the model parameters is easier to obtain, thus making them easier to use.

Previous work has focused mostly on insulin and glucose modeling, while some models do exist that describe glucagon [2], [3], [4], and fatty acids [4], [5]. The purpose of this chapter is to develop a model framework to describe all the biochemical species associated with glucose metabolism, as given in Chapter 2. Both the pharmacokinetic and the explanatory model framework will be developed. This is done by first noting the relevant tissues and metabolic sources and sinks for each species. Next, the basic

differential equations will be developed for each species and each compartment. Finally, each metabolic source and sink term will be described as a general function of the biochemical species involved. The chapter concludes with a discussion of the potential forms of the metabolic equations and parameter identification of the developed frameworks.

4.2 Methods

Model development with respect to the different model frameworks was fairly systematic. To develop the pharmacokinetic model, the methods described in reference [1] are employed. For the development of the physiological models, the methods described by Bischoff and co-authors [6-9] were employed. For both models, the biochemical species and each of their metabolic sources and sinks must be known in order to develop an accurate model. For the physiological models, the locations of each metabolic source and sink must also be known in order determine the specific compartments to be modeled. To gather this information, physiology textbooks, such as [10] and [11], and previously developed explanatory models such as [2] and [12], were used.

To develop the pharmacokinetic framework, each species was initially assumed to be best described as existing in a single compartment. Each species was determined to be a function of its metabolic processes. Based on the physiology studies, the metabolic process equations were described as general functions of the species that are known to

affect that particular metabolic process. Because data were not readily available, the models were left in their general form.

To develop the physiological models, each organ at which a specific metabolic process occurs was assumed to be a well mixed compartment of uniform concentration throughout a particular space within the compartment. As shown in Figure 4-1, each compartment is assumed to have three different spatial regions. First is the vascular space, which is in constant contact with blood flow. The middle space is the interstitial space, an area within the capillaries and containing the organ cells. The inner most region is the intracellular space, where the metabolic processes are assumed to occur. The volume of each compartment space is considered constant.

For each physiological compartment, transient mass balances are written according to [9]. For the vascular space, mass transfer is assumed to occur via convection from blood flow and from diffusion to the interstitial space. For the interstitial space, mass transfer occurs via diffusion from the vascular space and to the intracellular space. For the intracellular space, mass transfer occurs via diffusion from the interstitial space and via the cellular metabolic processes either consuming or producing a specific species. Finally, because the kinetic equations cannot be identified without data, a list of possible representations is provided in order to complete as much of the framework development as possible in the absence of data.

4.3 Results

4.3.1 Pharmacokinetic Modeling

A description of the various model variables and parameters, including units, is provided in Table 4-1. To develop pharmacokinetic models of each species, the significant metabolic processes associated with each species was investigated, and summarized in the compartment diagrams given in Figures 4-2 through 4-8. For each species, the dynamic change of species concentration within the constant volume compartment was assumed to be a function of both endogenous and exogenous inputs and uptake or elimination. A single compartment was assumed, as no data was used to determine the number of compartments best representing the actual kinetics of the species.

Physiologically, glucose appears endogenously, through gluconeogenesis or glycogenolysis, or exogenously, either orally or via an injection. Glucose disappears by being taken into cells and either stored as glycogen, converted to fat, or used in the formation of ATP. The pharmacokinetic description of glucose dynamics is shown in Figure 4-2 and represented mathematically by Equations (4.1)-(4.4).

$$\frac{dS}{dt} = r_{S,end} + r_{S,ex} - r_{S,elim} \tag{4.1}$$

$$r_{S,end} = f\left(t, S, I, G, E, F, A, K_{S,end}\right) \tag{4.2}$$

$$r_{S,ex} = g\left(t, M_S\right) \tag{4.3}$$

$$r_{S,elim} = h\left(t, S, I, E, K_{S,elim}\right) \tag{4.4}$$

As both Hovorka et al. [13] and Cobelli et al. [14] have shown, glucose is probably more accurately represented as having two compartments. Given the recent praise of the Hovorka model, (4.1) is likely best represented as two different equations , each representing a different compartment. Endogenous production and most cellular uptake would likely occur in a second compartment, and exogenous production, and transport to and from cells would be represented in the central compartment.

Endogenous glucose production and uptake would be functions of glucose, insulin, glucagon, and epinephrine, as well as amino acids, fatty acids, and glycogen. Insulin and glucose both act to decrease production, while glucagon and epinephrine act to increase production. Also included in this function would be the glycogen levels, which allow for glycogenolysis, and the fatty acid and amino acid levels, which allows for gluconeogenesis. Therefore, these kinetic rates are assumed to be function of the other species and metabolites, as well as any kinetic parameters associated with the process. Exogenous glucose would be considered a function of the source, including the amount given and the particular absorption kinetics associated with the source.

Amino acids play many different roles in glucose metabolism. Many are important for gluconeogenesis. Some amino acids, especially, lysine and arginine, are able to cause an increase in insulin secretion. Others, including alanine, cause an increase in glucagon secretion. These effects show the importance in including amino acids in the overall glucose metabolism process. Like glucose, amino acids appear as a result of both endogenous production and from external sources of proteins. They are taken up into various cells to form proteins or are converted to glucose. Amino acid

pharmacokinetics are shown in the PK diagram of Figure 4-3. The amino acid mass balances are given in Equations (4.5)-(4.8).

$$\frac{dA}{dt} = r_{A,endogenous} + r_{A,exogenous} - r_{A,uptake/elimination} \tag{4.5}$$

$$r_{A,endogenous} = f\left(t, S, I, G, E, F, A, K_{A,End}\right) \tag{4.6}$$

$$r_{A,exogenous} = g\left(t, M\right) \tag{4.7}$$

$$r_{A,uptake/elimination} = h\left(t, A, I, K_{A,uptake/elim}\right) \tag{4.8}$$

The amino acid model is very similar to the glucose model. Given both circulation and intracellular amino acids, two compartments may be appropriate for amino acid kinetics. Endogenous production occurs by breaking down proteins. This occurs primarily for gluconeogenesis, making endogenous production a strong function of glucose, epinephrine, and glucagon levels. Insulin is also known to promote protein formation, meaning that increased insulin would be expected to decrease production. Finally, during starvation, once glucose and fatty acid levels are diminished, amino acids become the primary source of fuel, resulting in increased production. Amino acid uptake will depend on the acid levels, and insulin has been shown to increase uptake promote protein formation. Finally, an exogenous source will be a function of the method of administration, including absorption kinetics associated with the administration technique and the volume administered.

Like glucose and amino acids, fatty acids are produced endogenously and supplied exogenously, in the form of a meal. Fatty acids combine with amino acids to form glucose via gluconeogenesis. In addition, when glucose levels are low, fatty acids become the primary source of fuel for the body. The fatty acid PK diagram is given in Figure 4-4, and Equations (4.9)-(4.12) show the fatty acid PK model.

$$\frac{dF}{dt} = r_{F,endogenous} + r_{F,exogenous} - r_{F,uptake/elimination} \tag{4.9}$$

$$r_{F,endogenous} = f\left(t, S, I, G, E, F, K_{F,End}\right) \tag{4.10}$$

$$r_{F,exogenous} = g\left(t, M\right) \tag{4.11}$$

$$r_{F,uptake/elimination} = h\left(t, S, I, E, F, K_{F,uptake/elim}\right) \tag{4.12}$$

A recent paper by Roy and Parker [5] shows a developed fatty acid PK model. It treats fatty acids as existing in a single compartment, while also including additional remote compartments, to describe the effects of fatty acids on glucose metabolism. Given the uptake and production of fatty acids in certain cells in the body, it may be appropriate to represent fatty acids as existing in two circulating compartments in addition to any compartments describing action. However, as fatty acid binding does not affect glucose uptake, it may be inappropriate to use remote compartments in the model description.

Fatty acid production is considered to be a function of glucose, insulin, glucagon, and epinephrine. The existence of the glucose-fatty acid cycle results in a direct

dependence on glucose. Low glucose levels result in low insulin and high glucagon levels. Glucagon is known to increase fatty acid production while also decreasing fatty acid conversion to lipids. Epinephrine is also known to result in increased fatty acid production. However, both glucagon and epinephrine are also responsible for increasing the rate of gluconeogenesis, which would result in increased fatty acid elimination. Thus, both fatty acid production and elimination are functions of glucose and the regulatory and counter-regulatory hormones of glucose metabolism. Like glucose and amino acids, the exogenous source of fatty acids is assumed to depend on the source type and the amount of fatty acid delivered.

Insulin is assumed to appear either through endogenous production from the pancreas or from an external source. It is assumed to be degraded primarily at the binding sites and at the kidneys. Figure 4-5 shows the insulin PK diagram. Insulin pharmacokinetics are represented by Equations (4.13)-(4.16).

$$\frac{dI}{dt} = r_{I,endogenous} + r_{I,exogenous} - r_{degradation/elimination} \tag{4.13}$$

$$r_{I,endogenous} = f_I\left(t, I, S, A, E, G1, K_{I,endogenous}\right) \tag{4.14}$$

$$r_{I,exogenous} = g_I\left(t, M\right) \tag{4.15}$$

$$r_{I,degradation} = h_I\left(t, I, K_{I,degradation}\right) \tag{4.16}$$

Insulin is considered by most to also best be represented as existing in multiple compartments. While Hovorka's representation of a single insulin compartment being

responsible for three different type of insulin action, which vary dynamically, the addition of its action on glucagon production and fatty acid and amino acid levels may result in the full scale model consisting of many insulin action compartments.

Insulin secretion is considered to be a function of many variables besides simply glucose. It is considered to be a function of its own values, meaning that insulin would be expected to continue to supply insulin at high insulin levels. Insulin production is also increased by an increase in gastrointestinal hormones, including glucagon like peptide-1 (GLP-1), and amino acids are known to have a potentiating effect on insulin secretion [10]. Finally, epinephrine, when produced at levels to restore falling glucose levels, is able to inhibit insulin secretion [15]. An exogenous source will be a function only of the amount given, and any absorption kinetics associated with the method of delivery. Uptake is assumed to occur only as a function of the insulin concentration and the kinetic rates.

Glucagon is assumed to appear only endogenously, although the idea of exogenous glucagon infusion is gaining acceptance [16]. Glucagon elimination is assumed to occur at the liver cell binding sites and the kidneys. Glucagon dynamics are described by Equations (4.17)-(4.19), and its pharmacokinetic diagram is shown in Figure 4-6.

$$\frac{dG}{dt} = r_{G,endogenous} - r_{G,degradation/elimination} \tag{4.17}$$

$$r_{G,endogenous} = f_G\left(t, S, I, A, E, K_{G,endogenous}\right) \tag{4.18}$$

$$r_{G,degradation/elimination} = g_G\left(t, G, K_{G,degradation/elimination}\right) \tag{4.19}$$

Glucagon is assumed to exist in only a single compartment. However, given that it also binds to various cells, it may also be best represented as having a central compartment, and two different action compartments. One of these compartments could represent the activation of the glucose production, and the other could represent fatty acid production. Perhaps a third action compartment could represent the inhibition of fatty acid uptake in some cells.

Endogenous glucagon production is a function of glucose, insulin, amino acids, and epinephrine. As the counter-regulatory hormone, glucagon secretion is inhibited by high glucose levels. Because the glucagon-producing alpha cells are downstream of the insulin-producing beta cells, the presence of insulin is also able to inhibit glucagon secretion [15]. Amino acids are known to increase glucagon secretion, and exercise is also known to result in an increase in glucagon levels. Because most of the effects of exercise result from the increased epinephrine production, a functional relationship may exist between the two hormones. Glucagon elimination is assumed to occur as a function only of glucagon levels.

While epinephrine is present in the body at normal glucose levels, the effects of epinephrine on glucose regulation are not usually observed unless the person is exercising or if a person is experiencing hypoglycemia and his or her glucagon response is insufficient to return glucose levels to normal. It should be mentioned that the sympathetic hormones naturally exist as both epinephrine and norepinephrine. However,

because most norepinephrine is converted to epinephrine, and because most of the effects mentioned are in response to the sympathetic nervous system responses to low glucose, the epinephrine/norepinephrine complex is simply being lumped together as a single hormone. The appearance of epinephrine in these circumstances is assumed to occur endogenously only, and disappearance is assumed to occur via degradation. The epinephrine model diagram is shown in Figure 4-7, and the model equations are given by Equations (4.20)-(4.22).

$$\frac{dE}{dt} = r_{E,endogenous} - r_{E,degradation/elimination} \tag{4.20}$$

$$r_{E,endogenous} = f_E\left(t, S, G, K_{E,endogenous}\right) \tag{4.21}$$

$$r_{E,degradation/elimination} = g_E\left(t, E, K_{E,degradation/elimination}\right) \tag{4.22}$$

Given that epinephrine increases glucose levels by either increasing production, decreasing uptake, and decreasing insulin secretion, a total of four compartments may be appropriate to represent all of the dynamics associated with epinephrine. Epinephrine secretion for the purpose of glucose regulation is a function of both glucose and glucagon levels, as previously mentioned. An additional term, perhaps best represented in the kinetic rate parameter, is the increased epinephrine secretion in response to exercise. Like the other hormones previously mentioned, epinephrine elimination is assumed to be a function only of the epinephrine levels.

GLP-1 is secreted only response to a meal, and as such it is assumed that is appearance only occurs endogenously. To be more accurate, GLP-1 is actually a part of many gastrointestinal hormones responsible for what it known as the incretin effect of increasing insulin secretion [17]. GLP-1 accounts for more than 70% of the total incretin effect, with the remaining effect caused by gastric inhibitory polypeptide (GIP) and a minimal effect from other hormones. For simplicity the two have been lumped together, as both are generated in response to a meal and both act to increase insulin production. Its disappearance occurs through general degradation at the liver and kidneys. Figure 4-8 shows the hormone's pharmacokinetic diagram, and the PK model equations are given by (4.23)-(4.25).

$$\frac{dG1}{dt} = r_{G1,endogenous} - r_{G1,degradation/elimination} \tag{4.23}$$

$$r_{G1,endogenous} = f_{G1}\left(t, S, K_{G1,endogenous}\right) \tag{4.24}$$

$$r_{G1,degradation/elimination} = g_{G1}\left(t, G1, K_{G1,degradation/elimination}\right) \tag{4.25}$$

As previously mentioned, the production of GLP-1 occurs as result of the digestion process. As a gastrointestinal hormone, GLP-1 would be a function of the glucose levels in a compartment associated with a meal, such as Hovorka's meal description, as shown in the Appendix. As the hormone is known to increase insulin secretion, a two-compartment representation, in which one describes its circulation

levels, and the other describes its activation with respect to insulin secretion potentiation, may be appropriate. Elimination is assumed to be a function only of GLP-1.

4.3.2 Physiological Modeling

For physiological modeling, the same general sources and sinks are used that were used in the pharmacokinetic modeling efforts. However, all production and elimination must be specified according to the tissue region at which the metabolic process occurs. Table 4-2 describes each of the variables of the model, while Table 4-3 describes each subscript and superscript. The physiologic diagrams of each metabolic species are shown in Figures 4-9 through 4-15. The initial physiologic equations will likely be eliminated upon simplification and identification with data. Initially, the total concentration of each species is assumed to be divided among the ionized version of each species, the form of the species bound to receptors, and the unbound form. Most physiologic models developed [2], [9], [12] have assumed that the different species exist only in free form. For completeness, all three terms will be left unless noted. In addition, mass transfer between compartment spaces is left in its general flux form. Simplifications such as those used by Sorensen [2] and others developing physiologic models can be easily applied to further simplify the expressions.

Glucose has previously been described as having appearance in the form of endogenous production and disappearance in the form of cellular uptake for fuel or storage. Specifically, endogenous glucose production occurs in the liver primarily. Uptake occurs in the liver, the brain, the muscle and fat cells, the gut, and the red blood

cells in circulation. Glucose also diffuses into the pancreas to promote insulin secretion. The overall glucose model is shown in Figure 4-9. To describe this process, Equation (4.26) describes the overall glucose balance in circulation.

$$
\begin{aligned}
&w_S^B V_S^B \frac{dS_B}{dt} + w_S^B V_S^B \frac{dS_B^*}{dt} + p_S^B V_S^B \frac{dx_S^B}{dt} = \\
&-Q_S^H \left(w_S^B S_B + w_S^B S_B^* + p_S^B x_S^B \right) + Q_S^{Br} \left(w_S^{B_{Br}} S_B^{Br} + w_S^{B_{Br}} S_B^{Br^*} + p_S^{B_{Br}} x_S^{B_{Br}} \right) \\
&+ Q_S^L \left(w_S^{B_L} S_B^L + w_S^{B_L} S_B^{L^*} + p_S^{B_L} x_S^{B_L} \right) + Q_S^K \left(w_S^{B_K} S_B^K + w_S^{B_K} S_B^{K^*} + p_S^{B_K} x_S^{B_K} \right) \\
&+ Q_S^A \left(w_S^{B_A} S_B^A + w_S^{B_A} S_B^{A^*} + p_S^{B_A} x_S^{B_A} \right) + Q_S^M \left(w_S^{B_M} S_B^M + w_S^{B_M} S_B^{M^*} + p_S^{B_M} x_S^{B_M} \right) \\
&+ Q_S^G \left(w_S^{B_G} S_B^G + w_S^{B_G} S_B^{G^*} + p_S^{B_G} x_S^{B_G} \right) + Q_S^P \left(w_S^{B_P} S_B^P + w_S^{B_P} S_B^{P^*} + p_S^{B_P} x_S^{B_P} \right)
\end{aligned}
\tag{4.26}
$$

Each tissue compartment is assumed to have three separated compartmental spaces, each with its own uniform concentration of the species, and each able to transport materials to and from adjacent spaces. The glucose equations for the brain compartment spaces are given by Equations (4.27) through (4.29). The brain is known to have a specific daily glucose requirement, and as such, the brain utilization rate of glucose can be assumed to be a constant.

$$
\begin{aligned}
&V_S^{B_{Br}} \left(w_S^B \frac{dS_B^{Br}}{dt} + w_S^B \frac{dS_B^{Br^*}}{dt} + p_S^B \frac{dx_S^{B_{Br}}}{dt} \right) = \\
&Q_S^{Br} \left(w_S^B S_B + w_S^B S_B^* + p_S^B x_S^B - w_S^{B_{Br}} S_B^{Br} - w_S^{B_{Br}} S_B^{Br^*} - p_S^{B_{Br}} x_S^{B_{Br}} \right) - (jA)_{BI,Br}
\end{aligned}
\tag{4.27}
$$

$$
V_S^{I_{Br}} \left(w_S^I \frac{dS_I^{Br}}{dt} + w_S^I \frac{dS_I^{Br^*}}{dt} + p_S^I \frac{dx_S^{I_{Br}}}{dt} \right) = (jA)_{BI,Br} - (jA)_{IC,Br} \tag{4.28}
$$

$$V_S^{C_{Br}}\left(w_S^C\frac{dS_C^{Br}}{dt}+w_S^C\frac{dS_C^{Br^*}}{dt}+p_S^C\frac{dx_S^{C_{Br}}}{dt}\right)=(jA)_{IC,Br}-r_{BSU} \tag{4.29}$$

The liver is the site of glucose production, and is a primary site of insulin-dependent glucose uptake. These rates are also dependent on the glucagon and epinephrine levels. The glucose balances for the insulin compartment spaces are given by Equations (4.30) -(4.32).

$$V_S^{B_L}\left(w_S^B\frac{dS_B^L}{dt}+w_S^B\frac{dS_B^{L^*}}{dt}+p_S^B\frac{dx_S^{B_L}}{dt}\right)= \tag{4.30}$$
$$Q_S^L\left(w_S^BS_B+w_S^BS_B^*+p_S^Bx_S^B-w_S^{B_L}S_B^L-w_S^{B_L}S_B^{L^*}-p_S^{B_L}x_S^{B_L}\right)-(jA)_S^{BI,L}$$

$$V_S^{I_L}\left(w_S^I\frac{dS_I^L}{dt}+w_S^I\frac{dS_I^{L^*}}{dt}+p_S^I\frac{dx_S^{I_L}}{dt}\right)=(jA)_S^{BI,L}-(jA)_S^{IC,L} \tag{4.31}$$

$$V_S^{C_L}\left(w_S^C\frac{dS_C^L}{dt}+w_S^C\frac{dS_C^{L^*}}{dt}+p_S^C\frac{dx_S^{C_L}}{dt}\right)=(jA)_S^{IC,L}+r_{LSP}-r_{LSU} \tag{4.32}$$

The kidneys are able to utilize glucose without hormone mediation. However, as glucose levels increase above a threshold value, kidney excretion of glucose become an important metabolic sink. The kidney glucose mass balances are given by Equations (4.33)-(4.35).

$$V_S^{B_K}\left(w_S^B\frac{dS_B^K}{dt}+w_S^B\frac{dS_B^{K^*}}{dt}+p_S^B\frac{dx_S^{B_K}}{dt}\right)= \tag{4.33}$$
$$Q_S^K\left(w_S^BS_B+w_S^BS_B^*+p_S^Bx_S^B-w_S^{B_K}S_B^K-w_S^{B_K}S_B^{K^*}-p_S^{B_K}x_S^{B_K}\right)-(jA)_S^{BI,K}$$

$$V_S^{I_K}\left(w_S^I\frac{dS_I^K}{dt}+w_S^I\frac{dS_I^{K^*}}{dt}+p_S^I\frac{dx_S^{I_K}}{dt}\right)=(jA)_S^{BI,K}-(jA)_S^{IC,K} \tag{4.34}$$

$$V_S^{C_K}\left(w_S^C\frac{dS_C^K}{dt}+w_S^C\frac{dS_C^{K^*}}{dt}+p_S^C\frac{dx_S^{C_K}}{dt}\right)=(jA)_S^{IC,K}-r_{KSE} \tag{4.35}$$

When glucose levels are in excess, beyond what the body needs for cellular processes and beyond the maximum that can be used for glycogen synthesis and storage, the additional glucose is taken into the adipose tissue and converted to fat. When fuel is needed, the fat will then be converted to fatty acids. The adipose tissue glucose balances are given by Equations (4.36)-(4.38).

$$V_S^{B_A}\left(w_S^B\frac{dS_B^A}{dt}+w_S^B\frac{dS_B^{A^*}}{dt}+p_S^B\frac{dx_S^{B_A}}{dt}\right)= \tag{4.38}$$
$$Q_S^A\left(w_S^BS_B+w_S^BS_B^*+p_S^Bx_S^B-w_S^{B_A}S_B^A-w_S^{B_A}S_B^{A^*}-p_S^{B_A}x_S^{B_A}\right)-(jA)_S^{BI,A}$$

$$V_S^{I_A}\left(w_S^I\frac{dS_I^A}{dt}+w_S^I\frac{dS_I^{A^*}}{dt}+p_S^I\frac{dx_S^{I_A}}{dt}\right)=(jA)_S^{BI,A}-(jA)_S^{IC,A} \tag{4.39}$$

$$V_S^{C_A}\left(w_S^C\frac{dS_C^A}{dt}+w_S^C\frac{dS_C^{A^*}}{dt}+p_S^C\frac{dx_S^{C_A}}{dt}\right)=(jA)_S^{IC,A}-r_{ASU} \tag{4.40}$$

As was previously mentioned, muscle is one of the two primary locations for glycogen storage. Muscle, along with the liver, is a site at which glucose uptake must be insulin mediated. Epinephrine also affects the rate of glucose uptake into the muscle cells. The glucose mass balances for muscle tissue are described by Equations (4.41)-(4.43).

$$V_S^{B_M}\left(w_S^B\frac{dS_B^M}{dt}+w_S^B\frac{dS_B^{M^*}}{dt}+p_S^B\frac{dx_S^{B_M}}{dt}\right)= \tag{4.41}$$
$$Q_S^M\left(w_S^BS_B+w_S^BS_B^*+p_S^Bx_S^B-w_S^{B_M}S_B^M-w_S^{B_M}S_B^{M^*}-p_S^{B_M}x_S^{B_M}\right)-(jA)_S^{BI,M}$$

$$V_S^{I_M}\left(w_S^I\frac{dS_I^M}{dt}+w_S^I\frac{dS_I^{M^*}}{dt}+p_S^I\frac{dx_S^{I_M}}{dt}\right)=(jA)_S^{BI,M}-(jA)_S^{IC,M} \tag{4.42}$$

$$V_S^{C_M}\left(w_S^C\frac{dS_C^M}{dt}+w_S^C\frac{dS_C^{M^*}}{dt}+p_S^C\frac{dx_S^{C_M}}{dt}\right)=(jA)_S^{IC,M}-r_{MSU} \tag{4.43}$$

The gut is the primary location of glucose absorption from a meal. In addition, Sorensen [2] has concluded that the gut itself has a constant glucose requirement, further increasing the necessity that it be included as a physiologic compartment of interest. The gut glucose mass balances are given by Equations (4.44)-(4.46).

$$V_S^{B_G}\left(w_S^B\frac{dS_B^G}{dt}+w_S^B\frac{dS_B^{G^*}}{dt}+p_S^B\frac{dx_S^{B_G}}{dt}\right)= \tag{4.44}$$
$$Q_S^G\left(w_S^BS_B+w_S^BS_B^*+p_S^Bx_S^B-w_S^{B_G}S_B^G-w_S^{B_G}S_B^{G^*}-p_S^{B_G}x_S^{B_G}\right)-(jA)_S^{BI,G}$$

$$V_S^{I_G}\left(w_S^I\frac{dS_I^G}{dt}+w_S^I\frac{dS_I^{G^*}}{dt}+p_S^I\frac{dx_S^{I_G}}{dt}\right)=(jA)_S^{BI,G}-(jA)_S^{IC,G} \tag{4.45}$$

$$V_S^{C_G}\left(w_S^C\frac{dS_C^G}{dt}+w_S^C\frac{dS_C^{G^*}}{dt}+p_S^C\frac{dx_S^{C_G}}{dt}\right)=(jA)_S^{IC,G}+r_{GSA}-r_{GSU} \tag{4.46}$$

Lastly, with respect to glucose, the natural insulin response of the pancreas regarding glucose control is initiated by glucose uptake into the pancreatic cells. Therefore, the pancreas will be considered a tissue of interest for a healthy patient. Although no insulin secretion is expected to occur, the uptake of glucose into pancreatic cells would still be expected in a Type I diabetic patient. The pancreas glucose mass balances are given by Equations (4.47)-(4.49).

$$V_S^{B_P}\left(w_S^B\frac{dS_B^P}{dt}+w_S^B\frac{dS_B^{P^*}}{dt}+p_S^B\frac{dx_S^{B_P}}{dt}\right)= \tag{4.47}$$
$$Q_S^P\left(w_S^BS_B+w_S^BS_B^*+p_S^Bx_S^B-w_S^{B_P}S_B^P-w_S^{B_P}S_B^{P^*}-p_S^{B_P}x_S^{B_P}\right)-(jA)_S^{BI,P}$$

$$V_S^{I_P}\left(w_S^I\frac{dS_I^P}{dt}+w_S^I\frac{dS_I^{P^*}}{dt}+p_S^I\frac{dx_S^{I_P}}{dt}\right)=(jA)_S^{BI,P}-(jA)_S^{IC,P} \tag{4.48}$$

$$V_S^{C_P}\left(w_S^C\frac{dS_C^P}{dt}+w_S^C\frac{dS_C^{P^*}}{dt}+p_S^C\frac{dx_S^{C_P}}{dt}\right)=(jA)_S^{IC,P}-r_{PSU} \tag{4.49}$$

The glucose model consists of 24 dynamic mass balance equations. This number is considerably greater than the number in the Sorensen model [2] for three reasons. First, Sorensen was able to reduce the number of compartmental space equations by

investigating the mass transfer between adjacent compartments. When mass transfer was determined to be extremely fast relative to the other rates in the process, the two compartments were assumed to be in equilibrium and were considered to be a single compartment. Second, Sorensen considered the pancreas to be a part of the liver, and as such did not develop balances for it. Finally, Sorensen lumped adipose and muscle tissue together, designating it as the periphery. Because this model takes into account fatty acid dynamics, this lumping has not been performed.

Fatty acids appear in the body as a result of either ingesting a fatty meal or from the endogenous production from the breakdown of triglycerides. They are eliminated by utilization by cells when glucose is low, or by being consumed for gluconeogenesis. Physiologically, fatty acid metabolism occurs in the blood, the adipose tissue, the liver, the gut, and perhaps the kidneys and the pancreas. Figure 4-10 shows the fatty acid compartmental diagram. The overall blood fatty acid balance is given by Equation (4.50).

$$
\begin{aligned}
&w_F^B V_F^B \frac{dF_B}{dt} + w_F^B V_F^B \frac{dF_B^*}{dt} + p_F^B V_F^B \frac{dx_F^B}{dt} = \\
&-Q_F^H \left(w_F^B F_B + w_F^B F_B^* + p_F^B x_F^B \right) + Q_F^L \left(w_F^{B_L} F_B^L + w_F^{B_L} F_B^{L^*} + p_F^{B_L} x_F^{B_L} \right) \\
&+Q_F^K \left(w_F^{B_K} F_B^K + w_F^{B_K} F_B^{K^*} + p_F^{B_K} x_F^{B_K} \right) + Q_F^A \left(w_F^{B_A} F_B^A + w_F^{B_A} F_B^{A^*} + p_F^{B_A} x_F^{B_A} \right) \\
&+Q_F^M \left(w_F^{B_M} F_B^M + w_F^{B_M} F_B^{M^*} + p_F^{B_M} x_F^{B_M} \right) + Q_F^G \left(w_F^{B_G} F_B^G + w_F^{B_G} F_B^{G^*} + p_F^{B_G} x_F^{B_G} \right) \\
&+Q_F^P \left(w_F^{B_P} F_B^P + w_F^{B_P} F_B^{P^*} + p_F^{B_P} x_F^{B_P} \right)
\end{aligned}
\tag{4.50}
$$

The liver is a primary site of importance for fatty acid metabolism. It is one of the two locations of fat storage in the body. It is also the primary site of gluconeogenesis.

Metabolically, this means the both fatty acid uptake and fatty acid production occur in the liver. The liver fatty acid mass balances are given by Equations (4.51)-(4.53).

$$V_F^{B_L}\left(w_F^B \frac{dF_B^L}{dt} + w_F^B \frac{dF_B^{L^*}}{dt} + p_F^B \frac{dx_F^{B_L}}{dt} \right) = \tag{4.51}$$
$$Q_F^L\left(w_F^B F_B + w_F^B F_B^* + p_F^B x_F^B - w_F^{B_L} F_B^L - w_F^{B_L} F_B^{L^*} - p_F^{B_L} x_F^{B_L}\right) - \left(jA\right)_F^{BI,L}$$

$$V_F^{I_L}\left(w_F^I \frac{dF_I^L}{dt} + w_F^I \frac{dF_I^{L^*}}{dt} + p_F^I \frac{dx_F^{I_L}}{dt} \right) = \left(jA\right)_F^{BI,L} - \left(jA\right)_F^{IC,L} \tag{4.52}$$

$$V_F^{C_L}\left(w_F^C \frac{dF_C^L}{dt} + w_F^C \frac{dF_C^{L^*}}{dt} + p_F^C \frac{dx_F^{C_L}}{dt} \right) = \left(jA\right)_F^{IC,L} + r_{LFP} - r_{LFU} \tag{4.53}$$

The kidneys are assumed to be a site of significance because of the general filtration and reabsorption that occurs with all blood substances. While it is likely that most or all fatty acids would be reabsorbed into the blood upon filtration, the equations are still included for completeness, and a decision to eliminate them should be based on experimental data in which kidney fatty acid filtration and reabsorption have been measured. In addition, at low glucose concentrations, fatty acids would be the primary fuel source for kidney function to continue. The kidney fatty acid mass balances are given by Equations (4.54)-(4.56).

$$V_F^{B_K}\left(w_F^B \frac{dF_B^K}{dt} + w_F^B \frac{dF_B^{K^*}}{dt} + p_F^B \frac{dx_F^{B_K}}{dt} \right) = \tag{4.54}$$
$$Q_F^K\left(w_F^B F_B + w_F^B F_B^* + p_F^B x_F^B - w_F^{B_K} F_B^K - w_F^{B_K} F_B^{K^*} - p_F^{B_K} x_F^{B_K}\right) - \left(jA\right)_F^{BI,K}$$

$$V_F^{I_K}\left(w_F^I\frac{dF_I^K}{dt}+w_F^I\frac{dF_I^{K^*}}{dt}+p_F^I\frac{dx_F^{I_K}}{dt}\right)=(jA)_F^{BI,K}-(jA)_F^{IC,K} \tag{4.55}$$

$$V_F^{C_K}\left(w_F^C\frac{dF_C^K}{dt}+w_F^C\frac{dF_C^{K^*}}{dt}+p_F^C\frac{dx_F^{C_K}}{dt}\right)=(jA)_F^{IC,K}+r_{KFR}-r_{KFU} \tag{4.56}$$

The adipose tissue is the second primary site of importance for fatty acid kinetics. Like the liver, fatty acids are stored as triglycerides in the adipose tissue. When glucose levels are low, the triglycerides are converted back to fatty acids and released to be used both the body's cells as fuel and by the liver for gluconeogenesis. The adipose tissue fatty acid balance is given by Equations (4.57)-(4.59).

$$V_F^{B_A}\left(w_F^B\frac{dF_B^A}{dt}+w_F^B\frac{dF_B^{A^*}}{dt}+p_F^B\frac{dx_F^{BA}}{dt}\right)= \tag{4.57}$$
$$Q_F^L\left(w_F^BF_B+w_F^BF_B^*+p_F^Bx_F^B-w_F^{B_A}F_B^A-w_F^{B_A}F_B^{A^*}-p_F^{B_A}x_F^{B_A}\right)-(jA)_F^{BI,A}$$

$$V_F^{I_A}\left(w_F^I\frac{dF_I^A}{dt}+w_F^I\frac{dF_I^{A^*}}{dt}+p_F^I\frac{dx_F^{I_A}}{dt}\right)=(jA)_F^{BI,A}-(jA)_F^{IC,A} \tag{4.58}$$

$$V_F^{C_A}\left(w_F^C\frac{dF_C^A}{dt}+w_F^C\frac{dF_C^{A^*}}{dt}+p_F^C\frac{dx_F^{C_A}}{dt}\right)=(jA)_F^{IC,A}+r_{AFP}-r_{AFU} \tag{4.59}$$

Like glucose, exogenous fatty acid appearance will likely occur as a result of a meal. During digestion, the fats of the meal will be broken down to form fatty acids. While the gut likely does not utilize fatty acids during normal conditions, they are the

primary fuel source at hypoglycemic conditions. The gut fatty acid mass balances are described in Equations (4.60)-(4.62).

$$V_F^{B_G}\left(w_F^B\frac{dF_B^G}{dt}+w_F^B\frac{dF_B^{G^*}}{dt}+p_F^B\frac{dx_F^{B_G}}{dt}\right)= \tag{4.60}$$
$$Q_F^G\left(w_F^BF_B+w_F^BF_B^*+p_F^Bx_F^B-w_F^{B_G}F_B^G-w_F^{B_G}F_B^{G^*}-p_F^{B_G}x_F^{B_G}\right)-\left(jA\right)_F^{BI,G}$$

$$V_F^{I_G}\left(w_F^I\frac{dF_I^G}{dt}+w_F^I\frac{dF_I^{G^*}}{dt}+p_F^I\frac{dx_F^{I_G}}{dt}\right)=\left(jA\right)_F^{BI,G}-\left(jA\right)_F^{IC,G} \tag{4.61}$$

$$V_F^{C_G}\left(w_F^C\frac{dF_C^G}{dt}+w_F^C\frac{dF_C^{G^*}}{dt}+p_F^C\frac{dx_F^{C_G}}{dt}\right)=\left(jA\right)_F^{IC,G}+r_{GFA}-r_{GFU} \tag{4.62}$$

To pump blood throughout the body, the heart derives its energy primarily from fatty acids. Therefore, the heart represents a significant source of fatty acid utilization. The heart fatty acid balance is given by Equations (4.63)-(4.65).

$$V_F^{B_H}\left(w_F^B\frac{dF_B^H}{dt}+w_F^B\frac{dF_B^{H^*}}{dt}+p_F^B\frac{dx_F^{B_H}}{dt}\right)= \tag{4.63}$$
$$Q_F^H\left(w_F^BF_B+w_F^BF_B^*+p_F^Bx_F^B-w_F^{B_H}F_B^H-w_F^{B_H}F_B^{H^*}-p_F^{B_H}x_F^{B_H}\right)-\left(jA\right)_F^{BI,H}$$

$$V_F^{I_H}\left(w_F^I\frac{dF_I^H}{dt}+w_F^I\frac{dF_I^{H^*}}{dt}+p_F^I\frac{dx_F^{I_H}}{dt}\right)=\left(jA\right)_F^{BI,H}-\left(jA\right)_F^{IC,H} \tag{4.64}$$

$$V_F^{C_H}\left(w_F^C\frac{dF_C^H}{dt}+w_F^C\frac{dF_C^{H^*}}{dt}+p_F^C\frac{dx_F^{C_H}}{dt}\right)=\left(jA\right)_F^{IC,H}-r_{HFU} \tag{4.65}$$

The resulting fatty acid physiologic model consists of 16 transient mass balances. Although the primary sites of importance regarding fatty acid metabolism have been listed, other tissues could be included during hypoglycemia conditions. While the brain and the red blood cells cannot use fatty acids as fuel for ATP generation, nearly every other cell can. Therefore, balances for the pancreas and for muscle tissue are included in order to model fatty acid metabolism during hypoglycemia and exercise. Pancreatic fatty acid is described in Equations (4.66)-(4.68), and the muscle tissue fatty acid balance is described by Equations (4.69)-(4.72).

$$V_F^{B_P}\left(w_F^B\frac{dF_B^P}{dt}+w_F^B\frac{dF_B^{P^*}}{dt}+p_F^B\frac{dx_F^{B_P}}{dt}\right)= \tag{4.66}$$
$$Q_F^P\left(w_F^BF_B+w_F^BF_B^*+p_F^Bx_F^B-w_F^{B_P}F_B^P-w_F^{B_P}F_B^{P^*}-p_F^{B_P}x_F^{B_P}\right)-(jA)_F^{BI,P}$$

$$V_F^{I_P}\left(w_F^I\frac{dF_I^P}{dt}+w_F^I\frac{dF_I^{P^*}}{dt}+p_F^I\frac{dx_F^{I_P}}{dt}\right)=(jA)_F^{BI,P}-(jA)_F^{IC,P} \tag{4.67}$$

$$V_F^{C_P}\left(w_F^C\frac{dF_C^P}{dt}+w_F^C\frac{dF_C^{P^*}}{dt}+p_F^C\frac{dx_F^{C_P}}{dt}\right)=(jA)_F^{IC,P}-r_{PFU} \tag{4.68}$$

$$V_F^{B_M}\left(w_F^B\frac{dF_B^M}{dt}+w_F^B\frac{dF_B^{M^*}}{dt}+p_F^B\frac{dx_F^{B_M}}{dt}\right)= \tag{4.69}$$
$$Q_F^M\left(w_F^BF_B+w_F^BF_B^*+p_F^Bx_F^B-w_F^{B_P}F_B^M-w_F^{B_M}F_B^{P^*}-p_F^{B_M}x_F^{B_M}\right)-(jA)_F^{BI,M}$$

$$V_F^{I_M}\left(w_F^I\frac{dF_I^M}{dt}+w_F^I\frac{dF_I^{M^*}}{dt}+p_F^I\frac{dx_F^{I_M}}{dt}\right)=(jA)_F^{BI,M}-(jA)_F^{IC,M} \tag{4.70}$$

$$V_F^{C_M}\left(w_F^C\frac{dF_C^M}{dt}+w_F^C\frac{dF_C^{M^*}}{dt}+p_F^C\frac{dx_F^{C_M}}{dt}\right)=(jA)_F^{IC,M}-r_{MFU} \tag{4.71}$$

The overall fatty acid model consists of 22 differential equations, excluding any differential equations associated with the metabolic sources or sinks. Nearly all the sources and sinks are likely considered constant, with the exception of those involved with the liver and adipose tissue. Both of those are likely functions of glucose, fatty acids, and glucagon, which is known to increase fatty acid production and inhibit liver fatty acid uptake. Uptake is also a function of insulin, as high insulin values are known to also promote fat storage in adipose and liver cells.

Amino acids are known to appear as a result of ingesting proteins in food. They are also produced endogenously by the breakdown of proteins in various cells. They are taken into the body primarily for protein storage but also for the purpose of gluconeogenesis. During starvation, when glucose and fatty acids are not available, amino acids become the primary source of fuel. However, given that such a condition requires days of starving, amino acids as fuel will not be considered. The primary sites of importance for amino acid metabolism are the blood, the liver and kidneys, the gut, and the pancreas. The physiologic diagram of amino acids is given in Figure 4-11. Equation (4.72) describes the overall amino acid balance in blood.

$$
\begin{aligned}
&w_A^{B} V_A^{B} \frac{dA_B}{dt} + w_A^{B} V_A^{B} \frac{dA_B^{*}}{dt} + p_A^{B} V_A^{B} \frac{dx_A^{B}}{dt} = \\
&-Q_A^{H}\left(w_A^{B} A_B + w_A^{B} A_B^{*} + p_A^{B} x_A^{B}\right) + Q_A^{L}\left(w_A^{B_L} A_B^{L} + w_A^{B_L} A_B^{L^*} + p_A^{B_L} x_A^{B_L}\right) \\
&+Q_A^{K}\left(w_A^{B_K} A_B^{K} + w_A^{B_K} A_B^{K^*} + p_A^{B_K} x_A^{B_K}\right) + Q_A^{G}\left(w_A^{B_G} A_B^{G} + w_A^{B_G} A_B^{G^*} + p_A^{B_G} x_A^{B_G}\right) \\
&+Q_A^{P}\left(w_A^{B_P} A_B^{P} + w_A^{B_P} A_B^{P^*} + p_A^{B_P} x_A^{B_P}\right)
\end{aligned}
\tag{4.72}
$$

Certain amino acids are known to affect pancreatic hormone secretion. Arginine and lysine are known to potentiate the glucose stimulus for insulin secretion. Arginine and alanine are known to stimulate glucagon secretion directly. Because of these effects, it is assumed that amino acids are being taken into the pancreas in order to produce the observed responses. Amino acid kinetics at the pancreas are described by Equations (4.73)-(4.75).

$$V_A^{B_P}\left(w_A^B\frac{dA_B^P}{dt}+w_A^B\frac{dA_B^{P^*}}{dt}+p_A^B\frac{dx_A^{B_P}}{dt}\right)= \tag{4.73}$$
$$Q_A^P\left(w_A^BA_B+w_A^BA_B^*+p_A^Bx_A^B-w_A^{B_P}A_B^P-w_A^{B_P}A_B^{P^*}-p_A^{B_P}x_A^{B_P}\right)-\left(jA\right)_A^{BI,P}$$

$$V_A^{I_P}\left(w_A^I\frac{dA_I^P}{dt}+w_A^I\frac{dA_I^{P^*}}{dt}+p_A^I\frac{dx_A^{I_P}}{dt}\right)=\left(jA\right)_A^{BI,P}-\left(jA\right)_A^{IC,P} \tag{4.74}$$

$$V_A^{C_P}\left(w_A^C\frac{dA_C^P}{dt}+w_A^C\frac{dA_C^{P^*}}{dt}+p_A^C\frac{dx_A^{C_P}}{dt}\right)=\left(jA\right)_A^{IC,P}-r_{PAU} \tag{4.75}$$

Amino acids do not exist in large quantities in the body. Instead, they are primarily stored as proteins throughout body's many cells and tissues. There also exist plasma proteins that are used for various metabolic functions. When there is a deficiency in a particular plasma protein, it is quickly synthesized. Proteins of various tissue cells are converted to amino acids. These are then released to the blood and taken up by the liver, where the protein is synthesized and released to the plasma. Because of this, the primary site of amino acid activity is the liver. The liver is able to take in large amounts

of amino acids and store them as proteins. The liver is also the site of gluconeogenesis. The mass balances for amino acids in the liver are given by Equations (4.76)-(4.78).

$$V_A^{B_L}\left(w_A^B\frac{dA_B^L}{dt}+w_A^B\frac{dA_B^{L^*}}{dt}+p_A^B\frac{dx_A^{B_L}}{dt}\right)= \tag{4.76}$$
$$Q_A^L\left(w_A^BA_B+w_A^BA_B^*+p_A^Bx_A^B-w_A^{B_L}A_B^L-w_A^{B_L}A_B^{L^*}-p_A^{B_L}x_A^{B_L}\right)-(jA)_A^{BI,L}$$

$$V_A^{I_L}\left(w_A^I\frac{dA_I^L}{dt}+w_A^I\frac{dA_I^{L^*}}{dt}+p_A^I\frac{dx_A^{I_L}}{dt}\right)=(jA)_A^{BI,L}-(jA)_A^{IC,L} \tag{4.77}$$

$$V_A^{C_L}\left(w_A^C\frac{dA_C^L}{dt}+w_A^C\frac{dA_C^{L^*}}{dt}+p_A^C\frac{dx_A^{C_L}}{dt}\right)=(jA)_A^{IC,L}+r_{LAP}-r_{LAU} \tag{4.78}$$

The kidneys are also able to store large amounts of proteins that can be easily converted to amino acids when needed, although to a lesser extent than the liver. In addition, the kidney is routinely filtering and reabsorbing amino acids. Like glucose, excess amino acids are lost in the urine. The amino acid balances of the kidneys are given by Equations (4.79)-(4.81).

$$V_A^{B_K}\left(w_A^B\frac{dA_B^K}{dt}+w_A^B\frac{dA_B^{K^*}}{dt}+p_A^B\frac{dx_A^{B_K}}{dt}\right)= \tag{4.79}$$
$$Q_A^K\left(w_A^BA_B+w_A^BA_B^*+p_A^Bx_A^B-w_A^{B_K}A_B^K-w_A^{B_K}A_B^{K^*}-p_A^{B_K}x_A^{B_K}\right)-(jA)_A^{BI,K}$$

$$V_A^{I_K}\left(w_A^I\frac{dA_I^K}{dt}+w_A^I\frac{dA_I^{K^*}}{dt}+p_A^I\frac{dx_A^{I_K}}{dt}\right)=(jA)_A^{BI,K}-(jA)_A^{IC,K} \tag{4.80}$$

$$V_A^{C_K}\left(w_A^C \frac{dA_C^K}{dt} + w_A^C \frac{dA_C^{K^*}}{dt} + p_A^C \frac{dx_A^{C_K}}{dt} \right) = \left(jA\right)_A^{IC,K} + r_{KAR} - r_{KAU} - r_{KAE} \tag{4.81}$$

The gut is a region of significance because of the appearance of amino acids from a meal. In addition, there will also be a small amount of protein storage resulting from amino acid uptake. The gut amino acid kinetics are described by Equations (4.82)-(4.84).

$$V_A^{B_G}\left(w_A^B \frac{dA_B^G}{dt} + w_A^B \frac{dA_B^{G^*}}{dt} + p_A^B \frac{dx_A^{B_G}}{dt} \right) = \tag{4.82}$$
$$Q_A^G\left(w_A^B A_B + w_A^B A_B^* + p_A^B x_A^B - w_A^{B_G} A_B^G - w_A^{B_G} A_B^{G^*} - p_A^{B_G} x_A^{B_G}\right) - \left(jA\right)_A^{BI,G}$$

$$V_A^{I_G}\left(w_A^I \frac{dA_I^G}{dt} + w_A^I \frac{dA_I^{G^*}}{dt} + p_A^I \frac{dx_A^{I_G}}{dt} \right) = \left(jA\right)_A^{BI,G} - \left(jA\right)_A^{IC,G} \tag{4.83}$$

$$V_A^{C_G}\left(w_A^C \frac{dA_C^G}{dt} + w_A^C \frac{dA_C^{G^*}}{dt} + p_A^C \frac{dx_A^{C_G}}{dt} \right) = \left(jA\right)_A^{IC,G} + r_{GAA} - r_{GAU} \tag{4.84}$$

The overall amino acid model has thirteen dynamic equations. Most of the metabolic terms will be functions of insulin and glucagon. Insulin decreases endogenous production and gluconeogenesis, while glucagon promotes gluconeogenesis. Insulin must also be present for protein formation to occur, meaning that its presence results in increased amino acid uptake. Finally, gluconeogenesis will only occur at low glucose levels, meaning that glucose levels will also play a role in amino acid metabolism.

The given physiologic equations up to now describe the kinetics of the three metabolic species glucose, amino acids, and fatty acids. Also of importance are the

different hormones regulating these species. Insulin appears endogenously via the pancreas or exogenously from a delivery system. It is degraded at its primary action sites, the muscle and liver cells, and is also cleared at the kidneys. These are the regions of significance for insulin, as shown in Figure 4-12. The overall insulin balance in blood is given by Equation (4.85). Insulin is known to circulate in an unbound form [10], so the bound terms have been eliminated from this model.

$$\begin{aligned} &w_I^B V_I^B \frac{dI_B}{dt} + w_I^B V_I^B \frac{dI_B^*}{dt} = -Q_I^H \left(w_I^B I_B + w_I^B I_B^* \right) + Q_I^L \left(w_I^{B_L} I_B^L + w_I^{B_L} I_B^{L^*} \right) \\ &+ Q_I^K \left(w_I^{B_K} I_B^K + w_I^{B_K} I_B^{K^*} \right) + Q_I^M \left(w_I^{B_M} I_B^M + w_I^{B_M} I_B^{M^*} \right) + Q_I^P \left(w_I^{B_P} I_B^P + w_I^{B_P} I_B^{P^*} \right) \end{aligned} \tag{4.85}$$

The pancreas is the site of insulin secretion. The secretion is known to be a function of glucose, amino acids, and GLP-1. All cells at which insulin action does not occur are assumed to degrade insulin by the enzyme insulinase. Therefore, insulin degradation is also included at the pancreas. The pancreas mass balances for insulin are given by Equations (4.86)-(4.88).

$$\begin{aligned} &V_I^{B_P} \left(w_I^B \frac{dI_B^P}{dt} + w_I^B \frac{dI_B^{P^*}}{dt} \right) = \\ &Q_I^P \left(w_I^B I_B + w_I^B I_B^* - w_I^{B_P} I_B^P - w_I^{B_P} I_B^{P^*} \right) - \left(jA \right)_I^{BI,P} \end{aligned} \tag{4.86}$$

$$V_I^{I_P} \left(w_I^I \frac{dI_I^P}{dt} + w_I^I \frac{dI_I^{P^*}}{dt} \right) = \left(jA \right)_I^{BI,P} - \left(jA \right)_I^{IC,P} \tag{4.87}$$

$$V_I^{C_P}\left(w_I^C \frac{dI_C^P}{dt} + w_I^C \frac{dI_C^{P^*}}{dt} \right) = \left(jA\right)_I^{IC,P} + r_{PIS} - r_{PID} \tag{4.88}$$

Insulin action primarily occurs at the liver, where the metabolic processes of glucose, amino acids, and fatty acids take place. It is here that nearly 40% of the insulin produced is eliminated via degradation upon binding to liver cells. The liver insulin balances are shown in Equations (4.89)-(4.91).

$$V_I^{B_L}\left(w_I^B \frac{dI_B^L}{dt} + w_I^B \frac{dI_B^{L^*}}{dt} \right) = \tag{4.89}$$
$$Q_I^L\left(w_I^B I_B + w_I^B I_B^* - w_I^{B_L} I_B^L - w_I^{B_L} I_B^{L^*}\right) - \left(jA\right)_I^{BI,L}$$

$$V_I^{I_L}\left(w_I^I \frac{dI_I^L}{dt} + w_I^I \frac{dI_I^{L^*}}{dt} \right) = \left(jA\right)_I^{BI,L} - \left(jA\right)_I^{IC,L} \tag{4.90}$$

$$V_I^{C_L}\left(w_I^C \frac{dI_C^L}{dt} + w_I^C \frac{dI_C^{L^*}}{dt} \right) = \left(jA\right)_I^{IC,L} - r_{LID} \tag{4.91}$$

Insulin action also occurs at the muscle cells, where glucose uptake is facilitated by insulin binding. Like the liver, muscle cells degrade insulin upon the completion of the action. The muscle insulin balances are given in Equations (4.92)-(4.94).

$$V_I^{B_M}\left(w_I^B \frac{dI_B^M}{dt} + w_I^B \frac{dI_B^{M^*}}{dt} \right) = \tag{4.92}$$
$$Q_I^M\left(w_I^B I_B + w_I^B I_B^* - w_I^{B_M} I_B^P - w_I^{B_M} I_B^{M^*}\right) - \left(jA\right)_I^{BI,M}$$

$$V_I^{I_M}\left(w_I^I \frac{dI_I^M}{dt} + w_I^I \frac{dI_I^{M^*}}{dt} \right) = \left(jA\right)_I^{BI,M} - \left(jA\right)_I^{IC,M} \tag{4.93}$$

$$V_I^{C_P}\left(w_I^C \frac{dI_C^M}{dt} + w_I^C \frac{dI_C^{M^*}}{dt} + p_I^C \frac{dx_I^{C_M}}{dt} \right) = \left(jA\right)_I^{IC,M} - r_{MID} \tag{4.94}$$

In addition to the action sites, insulin is degraded at a slight level in nearly all tissues, including the heart, the gut, and the adipose tissue. For simplicity, these slight levels of degradation will be assumed to be lumped into kidney, where the majority of insulin degradation occurs via the enzyme insulinase. For completeness, these regions could be modeled, and are shown on the physiologic diagram. The insulin balances for the kidneys are given by Equations (4.95)-(4.97).

$$V_I^{BK}\left(w_I^B \frac{dI_B^K}{dt} + w_I^B \frac{dI_B^{K^*}}{dt} \right) = \tag{4.95}$$
$$Q_I^K\left(w_I^B I_B + w_I^B I_B^* - w_I^{B_K} I_B^K - w_I^{B_K} I_B^{K^*}\right) - \left(jA\right)_I^{BI,K}$$

$$V_I^{I_K}\left(w_I^I \frac{dI_I^K}{dt} + w_I^I \frac{dI_I^{K^*}}{dt} \right) = \left(jA\right)_I^{BI,K} - \left(jA\right)_I^{IC,K} \tag{4.96}$$

$$V_I^{C_K}\left(w_I^C \frac{dI_C^K}{dt} + w_I^C \frac{dI_C^{K^*}}{dt} \right) = \left(jA\right)_I^{IC,K} - r_{KID} \tag{4.97}$$

The overall insulin balance consists of thirteen equations as a result of reducing the insignificant effects of the gut, heart and adipose tissue. To simulate the effects of

oral insulin formulations, the gut could be included. To account for Type I diabetes, the pancreatic insulin release term can be eliminated, and an exogenous source term could be added.

Glucagon has physiologic kinetics very similar to insulin. It is produced in the pancreas, in response to glucose and amino acids. It also is affected by insulin secretion from the pancreas. It is degraded primarily at the action sites of glucagon, including the liver and adipose tissue. It is also degraded at the kidneys. The physiologic diagram of glucagon is shown in Figure 4-13. The overall balance of glucagon in the blood is given by Equation (4.98).

$$\begin{aligned} &w_G^B V_G^B \frac{dG_B}{dt} + w_G^B V_G^B \frac{dG_B^*}{dt} + p_G^B V_G^B \frac{dx_G^B}{dt} = \\ &-Q_G^H \left(w_G^B G_B + w_G^B G_B^* + p_G^B x_G^B \right) + Q_G^L \left(w_G^{B_L} G_B^L + w_G^{B_L} G_B^{L^*} + p_G^{B_L} x_G^{B_L} \right) \\ &+Q_G^K \left(w_G^{B_K} G_B^K + w_G^{B_K} G_B^{K^*} + p_G^{B_K} x_G^{B_K} \right) + Q_G^P \left(w_G^{B_P} G_B^P + w_G^{B_P} G_B^{P^*} + p_G^{B_P} x_G^{B_P} \right) \\ &+Q_G^A \left(w_G^{B_A} G_B^A + w_G^{B_A} G_B^{A^*} + p_G^{B_A} x_G^{B_A} \right) \end{aligned} \tag{4.98}$$

The pancreas is the site of glucagon production. As previously mentioned, this is a function of pancreatic insulin, glucose, and amino acids. The pancreas glucagon mass balance is described by Equations (4.99)-(4.101).

$$\begin{aligned} &V_G^{B_P} \left(w_G^B \frac{dG_B^P}{dt} + w_G^B \frac{dG_B^{P^*}}{dt} + p_G^B \frac{dx_G^{B_P}}{dt} \right) = \\ &Q_G^P \left(w_G^B G_B + w_G^B G_B^* + p_G^B x_G^B - w_G^{B_P} G_B^P - w_G^{B_P} G_B^{P^*} - p_G^{B_P} x_G^{B_P} \right) - \left(jA \right)_G^{BI,P} \end{aligned} \tag{4.99}$$

$$V_G^{I_P}\left(w_G^I\frac{dG_I^P}{dt}+w_G^I\frac{dG_I^{P^*}}{dt}+p_G^I\frac{dx_G^{I_P}}{dt}\right)=\left(jA\right)_G^{BI,P}-\left(jA\right)_G^{IC,P} \tag{4.100}$$

$$V_G^{C_P}\left(w_G^C\frac{dG_C^P}{dt}+w_G^C\frac{dG_C^{P^*}}{dt}+p_G^C\frac{dx_G^{C_P}}{dt}\right)=\left(jA\right)_G^{IC,P}+r_{PGS} \tag{4.101}$$

The liver is one of the primary action sites for glucagon. Glucagon causes the liver to increase the rate of gluconeogenesis. It also suppresses the rate of fatty acid uptake to form triglycerides. Upon action, glucagon is degraded. The glucagon balance in the liver is given by Equations (4.102)-(4.104).

$$V_G^{B_L}\left(w_G^B\frac{dG_B^L}{dt}+w_G^B\frac{dG_B^{L^*}}{dt}+p_G^B\frac{dx_G^{B_L}}{dt}\right)= \tag{4.102}$$
$$Q_G^L\left(w_G^BG_B+w_G^BG_B^*+p_G^Bx_G^B-w_G^{B_L}G_B^L-w_G^{B_L}G_B^{L^*}-p_G^{B_L}x_G^{B_L}\right)-\left(jA\right)_G^{BI,L}$$

$$V_G^{I_L}\left(w_G^I\frac{dG_I^L}{dt}+w_G^I\frac{dG_I^{L^*}}{dt}+p_G^I\frac{dx_G^{I_L}}{dt}\right)=\left(jA\right)_G^{BI,L}-\left(jA\right)_G^{IC,L} \tag{4.103}$$

$$V_G^{C_L}\left(w_G^C\frac{dG_C^L}{dt}+w_G^C\frac{dG_C^{L^*}}{dt}+p_G^C\frac{dx_G^{C_L}}{dt}\right)=\left(jA\right)_G^{IC,L}-r_{LGD} \tag{4.104}$$

The second primary site for glucagon action is the adipose tissue, where glucagon acts to increase the production of fatty acids from stored fat. Upon the completion of its action, the glucagon is degraded at the cells. The adipose tissue glucagon balance is given by Equations (4.105)-(4.107).

$$V_A^{B_A}\left(w_G^B\frac{dG_B^A}{dt}+w_G^B\frac{dG_B^{A^*}}{dt}+p_G^B\frac{dx_G^{B_A}}{dt}\right)= \tag{4.105}$$
$$Q_G^A\left(w_G^BG_B+w_G^BG_B^*+p_G^Bx_G^B-w_G^{B_A}G_B^A-w_G^{B_A}G_B^{A^*}-p_G^{B_A}x_G^{B_A}\right)-\left(jA\right)_G^{BI,A}$$

$$V_G^{I_A}\left(w_G^I\frac{dG_I^A}{dt}+w_G^I\frac{dG_I^{A^*}}{dt}+p_G^I\frac{dx_G^{I_A}}{dt}\right)=\left(jA\right)_G^{BI,A}-\left(jA\right)_G^{IC,A} \tag{4.106}$$

$$V_G^{C_A}\left(w_G^C\frac{dG_C^A}{dt}+w_G^C\frac{dG_C^{A^*}}{dt}+p_G^C\frac{dx_G^{C_A}}{dt}\right)=\left(jA\right)_G^{IC,A}-r_{AGD} \tag{4.107}$$

Like insulin, nearly all glucagon that is not used by binding to cells to affect a metabolic process will be degraded at the kidneys. This degradation should be considered a function only of the glucagon levels. The mass balances for glucagon at the kidneys is given by Equations (4.108)-(4.110).

$$V_G^{B_K}\left(w_G^B\frac{dG_B^K}{dt}+w_G^B\frac{dG_B^{K^*}}{dt}+p_G^B\frac{dx_G^{B_K}}{dt}\right)= \tag{4.108}$$
$$Q_G^K\left(w_G^BG_B+w_G^BG_B^*+p_G^Bx_G^B-w_G^{B_K}G_B^K-w_G^{B_K}G_B^{K^*}-p_G^{B_K}x_G^{B_K}\right)-\left(jA\right)_G^{BI,K}$$

$$V_G^{I_K}\left(w_G^I\frac{dG_I^K}{dt}+w_G^I\frac{dG_I^{K^*}}{dt}+p_G^I\frac{dx_G^{I_K}}{dt}\right)=\left(jA\right)_G^{BI,K}-\left(jA\right)_G^{IC,K} \tag{4.109}$$

$$V_G^{C_K}\left(w_G^C\frac{dG_C^K}{dt}+w_G^C\frac{dG_C^{K^*}}{dt}+p_G^C\frac{dx_G^{C_K}}{dt}\right)=\left(jA\right)_G^{IC,K}-r_{KGD} \tag{4.110}$$

The resulting glucagon model has 13 dynamic mass balance equations. This adds considerable complexity relative to previous efforts to model glucagon dynamics, notably

the one compartment glucagon model of Sorensen. Given the ability to estimate the metabolic processes associated with glucagon, as well as the model parameters, this model should represent a significant advancement from previous models.

Epinephrine becomes a hormone of significance when glucagon levels are insufficient to increase glucose levels to normal. It is secreted primarily from the adrenal medullae, and acts directly on liver cells to increase gluconeogenesis and inhibit uptake [11]. It is also able to act at the pancreas to inhibit insulin secretion and increase glucagon secretion. To allow the body to perform properly, fatty acid production is increased in the liver and adipose cells. Finally, during exercise epinephrine acts on the heart to increase the flow of blood. Epinephrine is assumed to be degraded at the target cells. This is represented in the physiologic diagram for epinephrine, shown in Figure 4-14. Equation (4.111) shows the overall epinephrine balance in the blood.

$$
\begin{aligned}
&w_E^B V_E^B \frac{dE_B}{dt} + w_E^B V_E^B \frac{dE_B^*}{dt} + p_E^B V_E^B \frac{dx_E^B}{dt} = \\
&-Q_E^H \left(w_E^B E_B + w_E^B E_B^* + p_E^B x_E^B \right) + Q_E^{Br} \left(w_E^{B_{Br}} E_E^{Br} + w_E^{B_{Br}} E_B^{Br^*} + p_E^{B_{Br}} x_E^{B_{Br}} \right) \\
&+ Q_E^L \left(w_E^{B_L} E_B^L + w_E^{B_L} E_B^{L^*} + p_E^{B_L} x_E^{B_L} \right) + Q_E^K \left(w_E^{B_K} E_B^K + w_E^{B_K} E_B^{K^*} + p_E^{B_K} x_E^{B_K} \right) \\
&+ Q_E^A \left(w_E^{B_A} E_B^A + w_E^{B_A} E_B^{A^*} + p_E^{B_A} x_E^{B_A} \right) + Q_E^M \left(w_E^{B_M} E_B^M + w_E^{B_M} E_B^{M^*} + p_E^{B_M} x_E^{B_M} \right) \\
&+ Q_E^G \left(w_E^{B_G} E_B^G + w_E^{B_G} E_B^{G^*} + p_E^{B_G} x_E^{B_G} \right) + Q_E^P \left(w_E^{B_P} E_B^P + w_E^{B_P} E_B^{P^*} + p_E^{B_P} x_E^{B_P} \right)
\end{aligned}
\tag{4.111}
$$

For simplicity, the adrenal medullae, which is part of the sympathetic nervous system, has been lumped with the brain only for labeling purposes. Thus, the superscript, Br, as shown in Table 4-3, represents the brain and adrenal medullae. This is the site of

epinephrine secretion. The adrenal medullae epinephrine balance is given Equations (4.112)-(4.114).

$$V_E^{B_{Br}}\left(w_E^B\frac{dE_B^{Br}}{dt}+w_E^B\frac{dE_B^{Br^*}}{dt}+p_E^B\frac{dx_E^{B_{Br}}}{dt}\right)= \tag{4.112}$$
$$Q_E^{Br}\left(w_E^B E_B+w_E^B E_B^*+p_E^B x_E^B-w_E^{B_{Br}}E_B^{Br}-w_E^{B_{Br}}E_B^{Br^*}-p_E^{B_{Br}}x_E^{B_{Br}}\right)-\left(jA\right)_E^{BI,Br}$$

$$V_E^{I_{Br}}\left(w_E^I\frac{dE_I^{Br}}{dt}+w_E^I\frac{dE_I^{Br^*}}{dt}+p_E^I\frac{dx_E^{I_{Br}}}{dt}\right)=\left(jA\right)_E^{BI,Br}-\left(jA\right)_E^{IC,Br} \tag{4.113}$$

$$V_E^{C_{Br}}\left(w_E^C\frac{dE_C^{Br}}{dt}+w_E^C\frac{dE_C^{Br^*}}{dt}+p_E^C\frac{dx_E^{C_{Br}}}{dt}\right)=\left(jA\right)_E^{IC,Br}+r_{BES} \tag{4.114}$$

All tissues affected by epinephrine are assumed to be a site of epinephrine degradation. These tissues include the liver, muscle and adipose tissue, the pancreas, and finally the kidneys. The balances for muscle tissue are given by Equations (4.118)-(4.120) and the balances for adipose tissue are given by Equations (4.121)-(4.123). The balances for the pancreas are given by Equations (4.124)-(4.126), and finally, the balances for the kidney are shown in Equations (4.127)-(4.129).

$$V_E^{B_L}\left(w_E^B\frac{dE_B^{L}}{dt}+w_E^B\frac{dE_B^{L^*}}{dt}+p_E^B\frac{dx_E^{B_L}}{dt}\right)= \tag{4.115}$$
$$Q_E^{L}\left(w_E^B E_B+w_E^B E_B^*+p_E^B x_E^B-w_E^{B_L}E_B^{L}-w_E^{B_L}E_B^{L^*}-p_E^{B_L}x_E^{B_L}\right)-\left(jA\right)_E^{BI,L}$$

$$V_E^{I_L}\left(w_E^I\frac{dE_I^{L}}{dt}+w_E^I\frac{dE_I^{L^*}}{dt}+p_E^I\frac{dx_E^{I_L}}{dt}\right)=\left(jA\right)_E^{BI,L}-\left(jA\right)_E^{IC,L} \tag{4.116}$$

$$V_E^{C_L}\left(w_E^C\frac{dE_C^L}{dt}+w_E^C\frac{dE_C^{L^*}}{dt}+p_E^C\frac{dx_E^{C_L}}{dt}\right)=(jA)_E^{IC,L}-r_{LED} \tag{4.117}$$

$$V_E^{B_M}\left(w_E^B\frac{dE_B^M}{dt}+w_E^B\frac{dE_B^{M^*}}{dt}+p_E^B\frac{dx_E^{B_M}}{dt}\right)= \tag{4.118}$$
$$Q_E^M\left(w_E^BE_B+w_E^BE_B^*+p_E^Bx_E^B-w_E^{B_M}E_B^M-w_E^{B_M}E_B^{M^*}-p_E^{B_M}x_E^{B_M}\right)-(jA)_E^{BI,M}$$

$$V_E^{I_M}\left(w_E^I\frac{dE_I^M}{dt}+w_E^I\frac{dE_I^{M^*}}{dt}+p_E^I\frac{dx_E^{I_M}}{dt}\right)=(jA)_E^{BI,M}-(jA)_E^{IC,M} \tag{4.119}$$

$$V_E^{C_M}\left(w_E^C\frac{dE_C^M}{dt}+w_E^C\frac{dE_C^{M^*}}{dt}+p_E^C\frac{dx_E^{C_M}}{dt}\right)=(jA)_E^{IC,M}-r_{MED} \tag{4.120}$$

$$V_E^{B_A}\left(w_E^B\frac{dE_B^A}{dt}+w_E^B\frac{dE_B^{A^*}}{dt}+p_E^B\frac{dx_E^{B_A}}{dt}\right)= \tag{4.121}$$
$$Q_E^A\left(w_E^BE_B+w_E^BE_B^*+p_E^Bx_E^B-w_E^{B_A}E_B^A-w_E^{B_A}E_B^{A^*}-p_E^{B_A}x_E^{B_A}\right)-(jA)_E^{BI,A}$$

$$V_E^{I_A}\left(w_E^I\frac{dE_I^A}{dt}+w_E^I\frac{dE_I^{A^*}}{dt}+p_E^I\frac{dx_E^{I_A}}{dt}\right)=(jA)_E^{BI,A}-(jA)_E^{IC,A} \tag{4.122}$$

$$V_E^{C_A}\left(w_E^C\frac{dE_C^A}{dt}+w_E^C\frac{dE_C^{A^*}}{dt}+p_E^C\frac{dx_E^{C_A}}{dt}\right)=(jA)_E^{IC,A}-r_{AED} \tag{4.123}$$

$$V_E^{B_P}\left(w_E^B\frac{dE_B^P}{dt}+w_E^B\frac{dE_B^{P^*}}{dt}+p_E^B\frac{dx_E^{B_P}}{dt}\right)= \tag{4.124}$$
$$Q_E^P\left(w_E^BE_B+w_E^BE_B^*+p_E^Bx_E^B-w_E^{B_P}E_B^P-w_E^{B_P}E_B^{P^*}-p_E^{B_P}x_E^{B_P}\right)-(jA)_E^{BI,P}$$

$$V_E^{I_P}\left(w_E^I\frac{dE_I^P}{dt}+w_E^I\frac{dE_I^{P^*}}{dt}+p_E^I\frac{dx_E^{I_P}}{dt}\right)=(jA)_E^{BI,P}-(jA)_E^{IC,P} \tag{4.125}$$

$$V_E^{C_P}\left(w_E^C\frac{dE_C^P}{dt}+w_E^C\frac{dE_C^{P^*}}{dt}+p_E^C\frac{dx_E^{C_P}}{dt}\right)=(jA)_E^{IC,P}-r_{PED} \tag{4.126}$$

$$V_E^{B_K}\left(w_E^B\frac{dE_B^K}{dt}+w_E^B\frac{dE_B^{K^*}}{dt}+p_E^B\frac{dx_E^{B_K}}{dt}\right)= \tag{4.127}$$
$$Q_E^K\left(w_E^BE_B+w_E^BE_B^*+p_E^Bx_E^B-w_E^{B_K}E_B^K-w_E^{B_K}E_B^{K^*}-p_E^{B_K}x_E^{B_K}\right)-(jA)_E^{BI,K}$$

$$V_E^{I_K}\left(w_E^I\frac{dE_I^K}{dt}+w_E^I\frac{dE_I^{K^*}}{dt}+p_E^I\frac{dx_E^{I_K}}{dt}\right)=(jA)_E^{BI,K}-(jA)_E^{IC,K} \tag{4.128}$$

$$V_E^{C_K}\left(w_E^C\frac{dE_C^K}{dt}+w_E^C\frac{dE_C^{K^*}}{dt}+p_E^C\frac{dx_E^{C_K}}{dt}\right)=(jA)_E^{IC,K}-r_{KED} \tag{4.129}$$

The resulting epinephrine model consists of 19 differential equations. The metabolic processes affected by epinephrine are assumed to be affected by the blood levels of the hormone. Secretion is assumed to be a function of glucose, glucagon, and the exercise level of the individual. High levels will result in increased secretion. Finally, while blood flow rates will likely have to be estimated from literature values, they can be modeled as a function of the epinephrine levels, to account for the fact that epinephrine causes the heart to increase blood flow.

The final hormone to model is GLP-1. It is produced in the gut region and acts to increase insulin secretion by binding to the pancreatic beta cells directly [16]. Elimination occurs at the target cells, and blood GLP-1 is eliminated primarily through degradation via the kidneys. The hormone also plays a role in glucose production in the liver and fatty acid production in the adipose tissue. These regions are therefore considered the compartments of significance. Figure 4-15 shows the physiologic diagram for GLP-1. The overall balance in blood is given by Equation (4.130).

$$
\begin{aligned}
&w_{G1}^{B}V_{G1}^{B}\frac{d(G1)_{B}}{dt}+w_{G1}^{B}V_{G1}^{B}\frac{d(G1)_{B}^{*}}{dt}+p_{G1}^{B}V_{G1}^{B}\frac{dx_{G1}^{B}}{dt}= \\
&-Q_{G1}^{H}\left(w_{G1}^{B}(G1)_{B}+w_{G1}^{B}(G1)_{B}^{*}+p_{G1}^{B}x_{G1}^{B}\right)+Q_{G1}^{L}\left(w_{G1}^{B_L}(G1)_{B}^{L}+w_{G1}^{B_L}(G1)_{B}^{L^*}+p_{G1}^{B_L}x_{G1}^{B_L}\right) \\
&+Q_{G1}^{K}\left(w_{G1}^{B_K}(G1)_{B}^{K}+w_{G1}^{B_K}(G1)_{B}^{K^*}+p_{G1}^{B_K}x_{G1}^{B_K}\right)+Q_{G1}^{G}\left(w_{G1}^{B_G}(G1)_{B}^{G}+w_{G1}^{B_G}(G1)_{B}^{G^*}+p_{G1}^{B_G}x_{G1}^{B_G}\right) \\
&+Q_{G1}^{P}\left(w_{G1}^{B_P}(G1)_{B}^{P}+w_{G1}^{B_P}(G1)_{B}^{P^*}+p_{G1}^{B_P}x_{G1}^{B_P}\right)+Q_{G1}^{A}\left(w_{G1}^{B_A}(G1)_{B}^{A}+w_{G1}^{B_A}(G1)_{B}^{A^*}+p_{G1}^{B_A}x_{G1}^{B_A}\right)
\end{aligned}
\tag{4.130}
$$

The primary degradation site of GLP-1 is the kidneys. It is assumed that the degradation rate is a function of GLP-1 concentration only. Equations (4.131)-(4.133) show the kidney GLP-1 mass balances.

$$
\begin{aligned}
&V_{G1}^{B_K}\left(w_{G1}^{B}\frac{d(G1)_{B}^{K}}{dt}+w_{G1}^{B}\frac{d(G1)_{B}^{K^*}}{dt}+p_{G1}^{B}\frac{dx_{G1}^{B_K}}{dt}\right)= \\
&Q_{G1}^{K}\left(w_{G1}^{B}(G1)_{B}+w_{E}^{B}(G1)_{B}^{*}+p_{G1}^{B}x_{G1}^{B}-w_{G1}^{B_K}(G1)_{B}^{K}-w_{G1}^{B_K}(G1)_{B}^{K^*}-p_{G1}^{B_K}x_{G1}^{B_K}\right)-(jA)_{G1}^{BI,K}
\end{aligned}
\tag{4.131}
$$

$$
V_{G1}^{I_K}\left(w_{G1}^{I}\frac{d(G1)_{I}^{K}}{dt}+w_{G1}^{I}\frac{d(G1)_{I}^{K^*}}{dt}+p_{G1}^{I}\frac{dx_{G1}^{I_K}}{dt}\right)=(jA)_{G1}^{BI,K}-(jA)_{G1}^{IC,K} \tag{4.132}
$$

$$
V_{G1}^{C_K}\left(w_{G1}^{C}\frac{d(G1)_{C}^{K}}{dt}+w_{G1}^{C}\frac{d(G1)_{C}^{K^*}}{dt}+p_{G1}^{C}\frac{dx_{G1}^{C_K}}{dt}\right)=(jA)_{G1}^{IC,K}-r_{K(G1)D} \tag{4.133}
$$

The gut region is where GLP-1 is secreted in response to a meal. This secretion is assumed to be a function of the meal eaten, such as the size and composition of the meal. The balance equations for gut GLP-1 are given by Equations (4.134)-(4.136)

$$V_{G1}^{B_G}\left(w_{G1}^{B}\frac{d(G1)_B^G}{dt}+w_{G1}^{B}\frac{d(G1)_B^{G^*}}{dt}+p_{G1}^{B}\frac{dx_{G1}^{B_G}}{dt}\right)= \tag{4.134}$$
$$Q_{G1}^{G}\left(w_{G1}^{B}(G1)_B+w_E^B(G1)_B^*+p_{G1}^{B}x_{G1}^{B}-w_{G1}^{B_G}(G1)_B^G-w_{G1}^{B_G}(G1)_B^{G^*}-p_{G1}^{B_G}x_{G1}^{B_G}\right)-(jA)_{G1}^{BI,G}$$

$$V_{G1}^{I_G}\left(w_{G1}^{I}\frac{d(G1)_I^G}{dt}+w_{G1}^{I}\frac{d(G1)_I^{G^*}}{dt}+p_{G1}^{I}\frac{dx_{G1}^{I_G}}{dt}\right)=(jA)_{G1}^{BI,G}-(jA)_{G1}^{IC,G} \tag{4.135}$$

$$V_{G1}^{C_G}\left(w_{G1}^{C}\frac{d(G1)_C^G}{dt}+w_{G1}^{C}\frac{d(G1)_C^{G^*}}{dt}+p_{G1}^{C}\frac{dx_{G1}^{C_G}}{dt}\right)=(jA)_{G1}^{IC,G}+r_{G(G1)S} \tag{4.136}$$

The remaining sites, including the pancreas, adipose tissue, and liver, are considered important because of the actions performed by GLP-1 at these sites. It is assumed that each intracellular space is a site of degradation for the hormone, and the balances have been written to reflect this. Equations (4.137)-(4.139) show the GLP-1 balance in the pancreas, followed by the liver with Equations (4.140)-(4.142). Finally, the adipose tissue GLP-1 balances are given by Equations (4.143)-(4.145).

$$V_{G1}^{B_P}\left(w_{G1}^{B}\frac{d(G1)_B^P}{dt}+w_{G1}^{B}\frac{d(G1)_B^{P^*}}{dt}+p_{G1}^{B}\frac{dx_{G1}^{B_P}}{dt}\right)= \tag{4.137}$$
$$Q_{G1}^{P}\left(w_{G1}^{B}(G1)_B+w_E^B(G1)_B^*+p_{G1}^{B}x_{G1}^{B}-w_{G1}^{B_K}(G1)_B^P-w_{G1}^{B_K}(G1)_B^{P^*}-p_{G1}^{B_P}x_{G1}^{B_P}\right)-(jA)_{G1}^{BI,P}$$

$$V_{G1}^{I_P}\left(w_{G1}^{I}\frac{d(G1)_I^P}{dt}+w_{G1}^{I}\frac{d(G1)_I^{P^*}}{dt}+p_{G1}^{I}\frac{dx_{G1}^{I_P}}{dt}\right)=(jA)_{G1}^{BI,P}-(jA)_{G1}^{IC,P} \tag{4.138}$$

$$V_{G1}^{C_P}\left(w_{G1}^{C}\frac{d(G1)_C^P}{dt}+w_{G1}^{C}\frac{d(G1)_C^{P^*}}{dt}+p_{G1}^{C}\frac{dx_{G1}^{C_P}}{dt}\right)=(jA)_{G1}^{IC,P}-r_{P(G1)U} \tag{4.139}$$

$$V_{G1}^{B_L}\left(w_{G1}^{B}\frac{d(G1)_B^L}{dt}+w_{G1}^{B}\frac{d(G1)_B^{L^*}}{dt}+p_{G1}^{B}\frac{dx_{G1}^{B_L}}{dt}\right)= \tag{4.140}$$
$$Q_{G1}^{L}\left(w_{G1}^{B}(G1)_B+w_E^B(G1)_B^*+p_{G1}^{B}x_{G1}^{B}-w_{G1}^{B_K}(G1)_B^L-w_{G1}^{B_L}(G1)_B^{L^*}-p_{G1}^{B_L}x_{G1}^{B_L}\right)-(jA)_{G1}^{BI,L}$$

$$V_{G1}^{I_L}\left(w_{G1}^{I}\frac{d(G1)_I^L}{dt}+w_{G1}^{I}\frac{d(G1)_I^{L^*}}{dt}+p_{G1}^{I}\frac{dx_{G1}^{I_L}}{dt}\right)=(jA)_{G1}^{BI,L}-(jA)_{G1}^{IC,L} \tag{4.141}$$

$$V_{G1}^{C_L}\left(w_{G1}^{C}\frac{d(G1)_C^L}{dt}+w_{G1}^{C}\frac{d(G1)_C^{L^*}}{dt}+p_{G1}^{C}\frac{dx_{G1}^{C_L}}{dt}\right)=(jA)_{G1}^{IC,L}-r_{L(G1)D} \tag{4.142}$$

$$V_{G1}^{B_A}\left(w_{G1}^{B}\frac{d(G1)_B^A}{dt}+w_{G1}^{B}\frac{d(G1)_B^{A^*}}{dt}+p_{G1}^{B}\frac{dx_{G1}^{B_A}}{dt}\right)= \tag{4.143}$$
$$Q_{G1}^{A}\left(w_{G1}^{B}(G1)_B+w_E^B(G1)_B^*+p_{G1}^{B}x_{G1}^{B}-w_{G1}^{B_K}(G1)_B^A-w_{G1}^{B_A}(G1)_B^{A^*}-p_{G1}^{B_A}x_{G1}^{B_A}\right)-(jA)_{G1}^{BI,A}$$

$$V_{G1}^{I_A}\left(w_{G1}^{I}\frac{d(G1)_I^A}{dt}+w_{G1}^{I}\frac{d(G1)_I^{A^*}}{dt}+p_{G1}^{I}\frac{dx_{G1}^{I_A}}{dt}\right)=(jA)_{G1}^{BI,A}-(jA)_{G1}^{IC,A} \tag{4.144}$$

$$V_{G1}^{C_A}\left(w_{G1}^{C}\frac{d(G1)_C^A}{dt}+w_{G1}^{C}\frac{d(G1)_C^{A^*}}{dt}+p_{G1}^{C}\frac{dx_{G1}^{C_A}}{dt}\right)=(jA)_{G1}^{IC,A}-r_{A(G1)D} \tag{4.145}$$

The overall model consists of 120 mass balance equations. In addition, there will be differential or algebraic relationships for each metabolic source or sink term. This system, if fully developed through parameter identification and simplifications, will be the most complete description of glucose homeostasis that has been developed.

4.3.3 Metabolic Sources and Sinks

The metabolic source and sink terms have been left in a general form. Without data, the exact form of the terms cannot be determined. However, the representation of

the metabolic processes of previous models provides a foundation of possible representations that will be discussed here for use with data when it becomes available.

Perhaps the simplest representation of each source or sink is a simple rate law that is a particular order with respect to each species known to affect the process. Most commonly, kinetic rates are assumed to be first order with respect to each species involved. The general representation is shown by Equation (4.146).

$$r_i = k(t)G^a(t)I^b(t)S^c(t)F^d(t)A^e(t)E^f(t)G1^g(t) \tag{4.146}$$

Other types of kinetic relationships, including Michaelis-Menten and additive relationships have also been used to describe the rate, and could be considered as possible descriptions. Others have made use of a nonlinear equation in which the basal rate is multiplied by dimensionless multiplicative terms described by each influencing species.

$$r_i = r_{i,basal}M_{i,S}M_{i,I}M_{i,G}M_{i,F}M_{i,A}M_{i,E}M_{i,G1} \tag{4.147}$$

Where M_i is the multiplicative function in each variable for metabolic process i. Each M will have associated parameters that must be estimated. It may also be necessary to describe the nonlinear functions as differential equations describing the binding a hormone to a receptor, in which case the rate is a function of the receptor-bound species, which is a function of the circulation species concentrations.

In order to capture parameter variability, either among patients, or within a specific patient (from exercising, circadian rhythms, etc.), the parameters in each set, k_i, will likely be functions of time themselves.

Of notable exception to the above description are the descriptions for exogenous glucose and insulin inputs. The exogenous glucose input will be in the form of a meal, and the term will be used to describe glucose absorption from a meal. Similarly, the insulin infusion rate will be input by either the user in the case of an infusion pump, or by the release mechanism of the device. However, for both types, the parameters will still be time varying to account for parameter variability.

4.4 Conclusions

Two different systems of equations have been developed to describe glucose homeostasis. A pharmacokinetic model was provided, with recommendations on the number of compartments to develop based on the metabolic processes of each species. A detailed physiological model was developed to more fully describe the process at each tissue region. Finally, several possible equation forms were proposed as possible descriptions of the metabolism kinetics.

The next step in the process would be to identify the model, based on simplifications, a literature search for parameter values, and finally, fitting model responses to data in order to estimate certain parameter values. The desired data would show recorded observations of the all metabolites and hormones in the different tissue regions as a function of time. If such data were available and parameters were estimated,

the developed models would have the potential to be an improvement over existing models in their ability to describe the glucoregulatory process. This could lead to multivariable control algorithms, in which multiple metabolites are controlled by the precise infusion of multiple hormones.

It is quite possible that the physiologic model will consist of over one thousand model parameters, and identifying these parameters could take years by itself. It has been suggested that a large number of the model parameters may be constant within specific classes of patients. Such classes could be based on age, gender, ethnicity, and bodyweight. If parameter values are indeed constant within patient classes, the number of parameters to be estimated for an individual patient could be dramatically reduced. However, given the size of the models, with respect to equations and model parameters, and the lack of appropriate data, it was decided that model identification and validation was outside the scope of this work. As the focus of this work is the development of improved methods of glucose control, simulations will be performed on existing models while noting possible shortcomings of the simulation results.

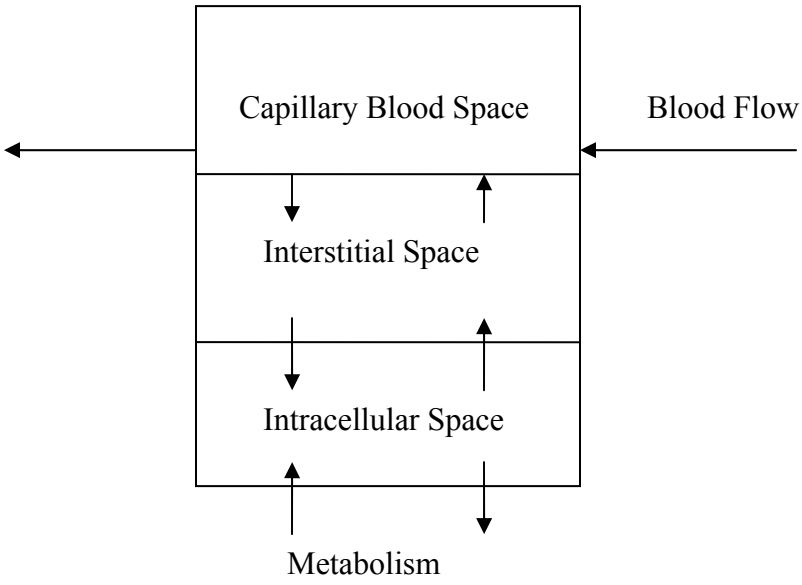

Figure 4-1: Spatial diagram of a physiologic compartment. Each compartment has a blood space, where blood flows through capillaries at the region. Species then diffuse into the interstitial space and then into the intracellular space, where metabolic processes occur. The arrows represent mass transfer.

Table 4-1: Pharmacokinetic Model Variables and Parameters		
Variable	**Definition**	**Units**
S	Plasma Glucose Concentration	mmol/L
A	Plasma Amino Acid Concentration	mg/L
F	Plasma Fatty Acid Concentration	nmol/L
I	Plasma Insulin Concentration	mU/L
G	Plasma Glucagon Concentration	ng/L
E	Plasma Epinephrine Concentration	nmol/L
$G1$	Plasma Glucagon-Like Peptide-1 Concentration	nmol/L
$r_{i,endogenous}$	Rate of endogenous production	species dependent
$r_{i,exogenous}$	Rate of exogenous input	species dependent
M_i	Quantity of exogenous input	species dependent
$K_{i,endogenous}$	Kinetic rate coefficients for endogenous input	species, coefficient dependent
$r_{i,uptake/elimination}$	rate of species disappearance	species dependent
$K_{i,uptake/elimination}$	Kinetic rate coefficients for species disappearance	species, coefficient dependent

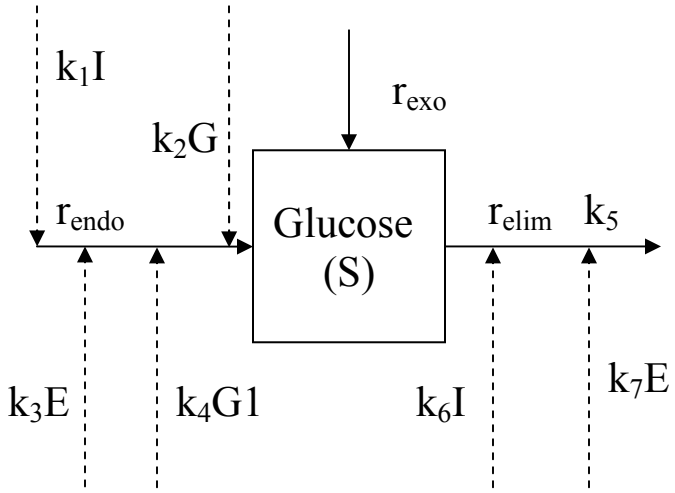

Figure 4-2: Pharmacokinetic model diagram for glucose. The solid lines represent metabolic sources and sinks. The dashed lines represent actions by the species on the metabolic source or sink. For simplicity, each contribution toward a metabolic action is represented as first order kinetics in the contributing species.

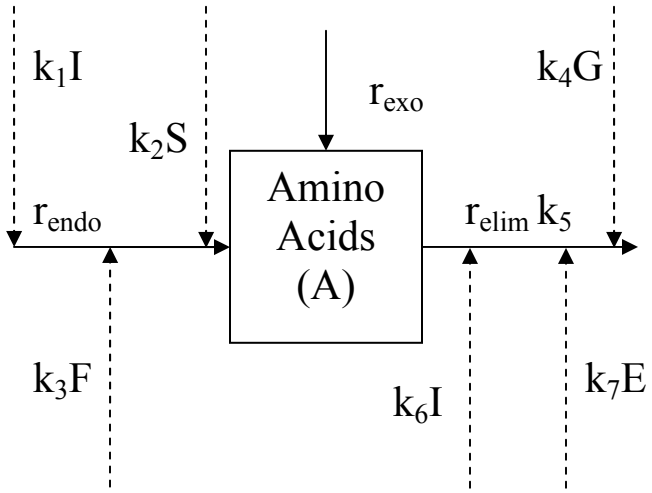

Figure 4-3: Pharmacokinetic model diagram for amino acids. The solid lines represent metabolic sources and sinks. The dashed lines represent actions by the species on the metabolic source or sink. For simplicity, each contribution toward a metabolic action is represented as first order kinetics in the contributing species.

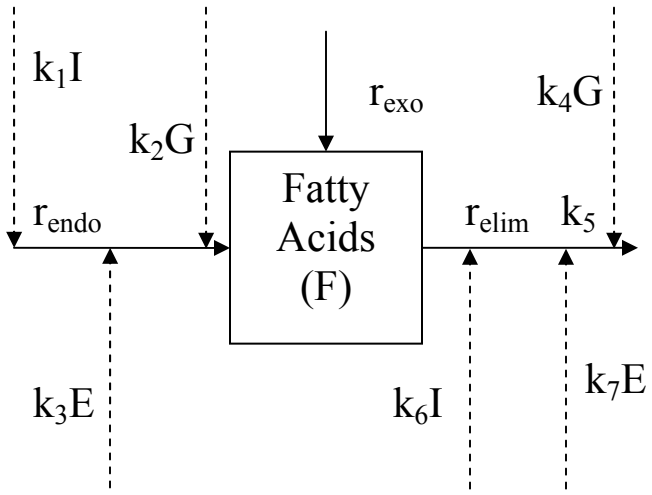

Figure 4-4: Pharmacokinetic model diagram for fatty acids. The solid lines represent metabolic sources and sinks. The dashed lines represent actions by the species on the metabolic source or sink. For simplicity, each contribution toward a metabolic action is represented as first order kinetics in the contributing species.

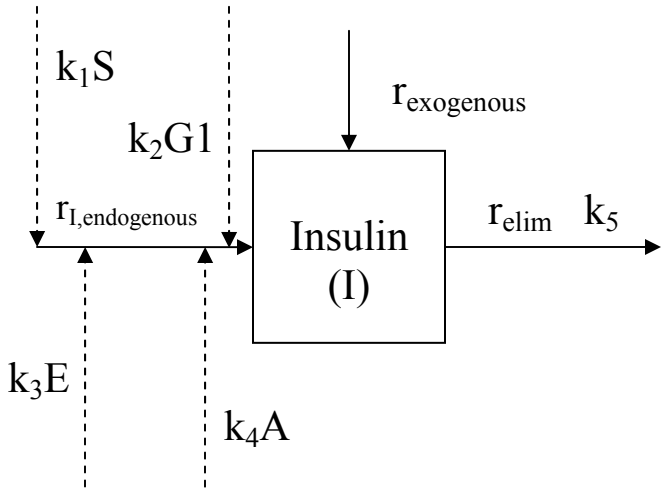

Figure 4-5: Pharmacokinetic model diagram for insulin. The solid lines represent metabolic sources and sinks. The dashed lines represent actions by the species on the metabolic source or sink. For simplicity, each contribution toward a metabolic action is represented as first order kinetics in the contributing species. Note that for a Type I diabetic patient, $r_{I,endogenous}$ is approximately zero, and thus all actions associated with endogenous release are eliminated.

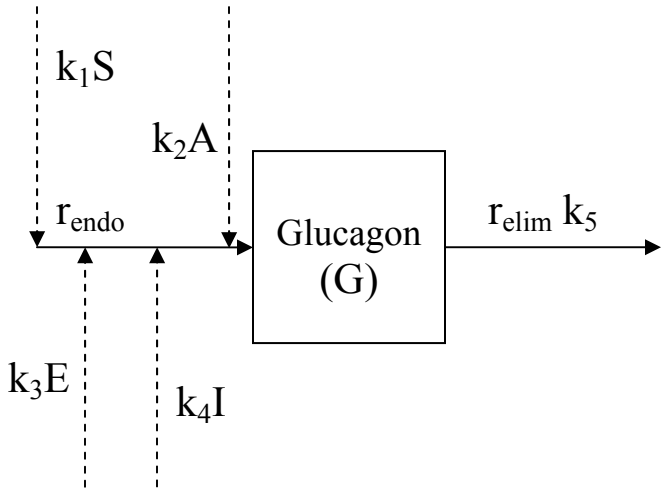

Figure 4-6: Pharmacokinetic model diagram for glucagon. The solid lines represent metabolic sources and sinks. The dashed lines represent actions by the species on the metabolic source or sink. For simplicity, each contribution toward a metabolic action is represented as first order kinetics in the contributing species.

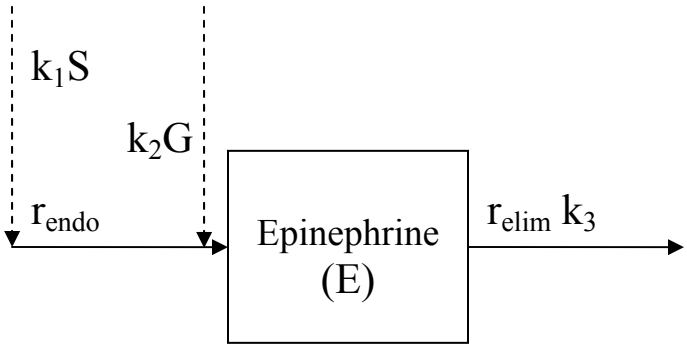

Figure 4-7: Pharmacokinetic model diagram for epinephrine. The solid lines represent metabolic sources and sinks. The dashed lines represent actions by the species on the metabolic source or sink. For simplicity, each contribution toward a metabolic action is represented as first order kinetics in the contributing species.

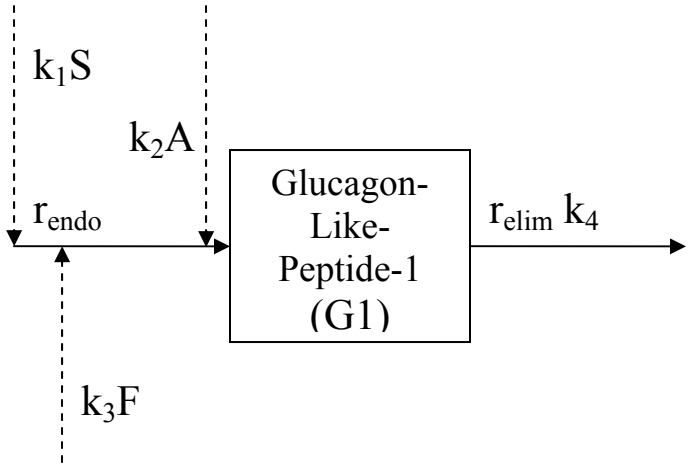

Figure 4-8: Pharmacokinetic model diagram for glucagon-like peptide-1. The solid lines represent metabolic sources and sinks. The dashed lines represent actions by the species on the metabolic source or sink. For simplicity, each contribution toward a metabolic action is represented as first order kinetics in the contributing species.

Table 4-2: Physiologic Model Variables and Parameters		
Variable/Parameter	**Definition**	**Units**
S	Glucose	mmol/L
F	Fatty acids	nmol/L
A	Amino Acids	mg/L
I	Insulin	mU/L
G	Glucagon	ng/L
E	Epinephrine	nmol/L
GI	Glucagon-Like Peptide-1	nmol/L
x_i	Bound form of species i	dimensionless
$(i)^*$	Ionized form of species i	species dependent
r_{ijk}	Metabolic source or sink k, of species j in compartment i	species dependent
Q_i	Blow rate of species i in blood	L/min
w_i	Weight fraction of species i	dimensionless
$(jA)_i$	Mass transfer rate of species i	species dependent
V_i	Compartment volume of species i	L
p_i	Plasma protein concentration that can bind species i	species dependent

Table 4-3: Summary of Superscripts and Subscripts For Physiologic Model	
Abbreviation	**Definition**
A	Adipose Tissue
A *(metabolic rate subscript)*	Absorption
B	Blood Space
Br	Brain and Adrenal Medullae
C	Intracellular Space
D	Degradation
G	GI Tract
I	Interstitial Space
K	Kidneys
M	Muscle Tissue
P	Pancreas
P *(metabolic rate subscript)*	Production (Endogenous)
U	Uptake

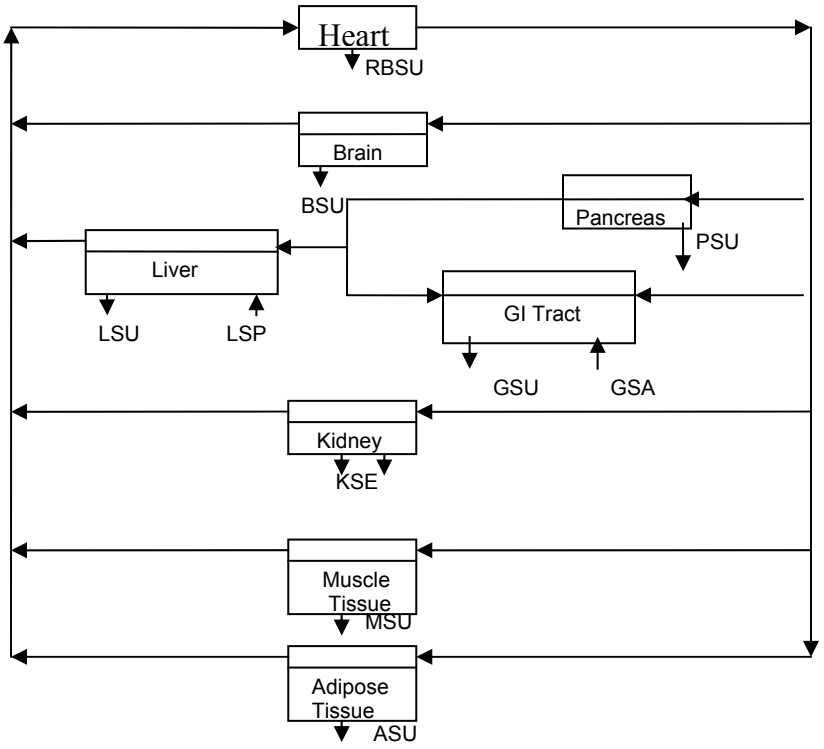

Figure 4-9: Physiologic diagram of glucose metabolism. Each compartment is divided into the blood space, where blood flows, and the interstitial/intracellular space below the blood space. Inlet arrows at each compartment represent species appearance, while outlet arrows represent disappearance.

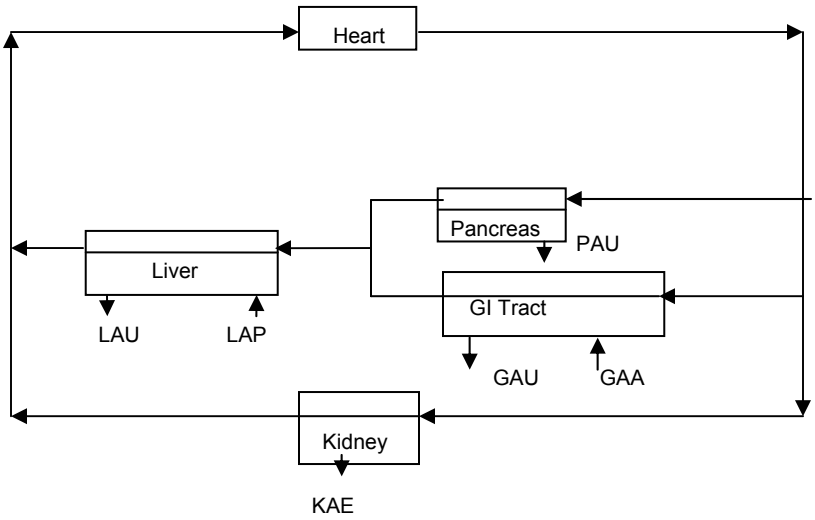

Figure 4-10: Physiologic diagram of amino acid metabolism. Each compartment is divided into the blood space, where blood flows, and the interstitial/intracellular space below the blood space. Inlet arrows at each compartment represent species appearance, while outlet arrows represent disappearance.

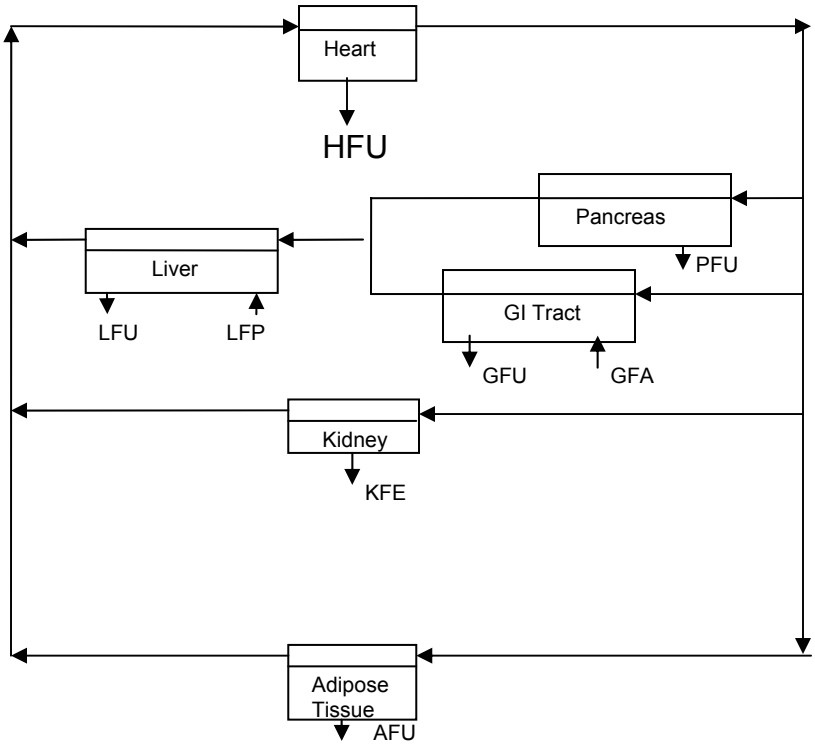

Figure 4-11: Physiologic diagram of fatty acid metabolism. Each compartment is divided into the blood space, where blood flows, and the interstitial/intracellular space below the blood space. Inlet arrows at each compartment represent species appearance, while outlet arrows represent disappearance.

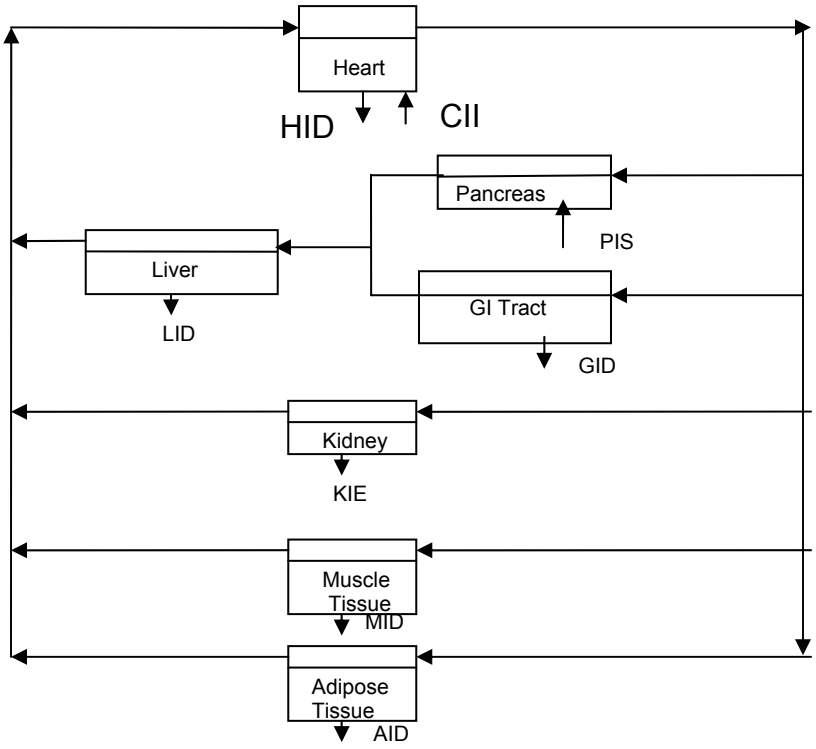

Figure 4-12: Physiologic diagram of insulin metabolism. Each compartment is divided into the blood space, where blood flows, and the interstitial/intracellular space below the blood space. Inlet arrows at each compartment represent species appearance, while outlet arrows represent disappearance.

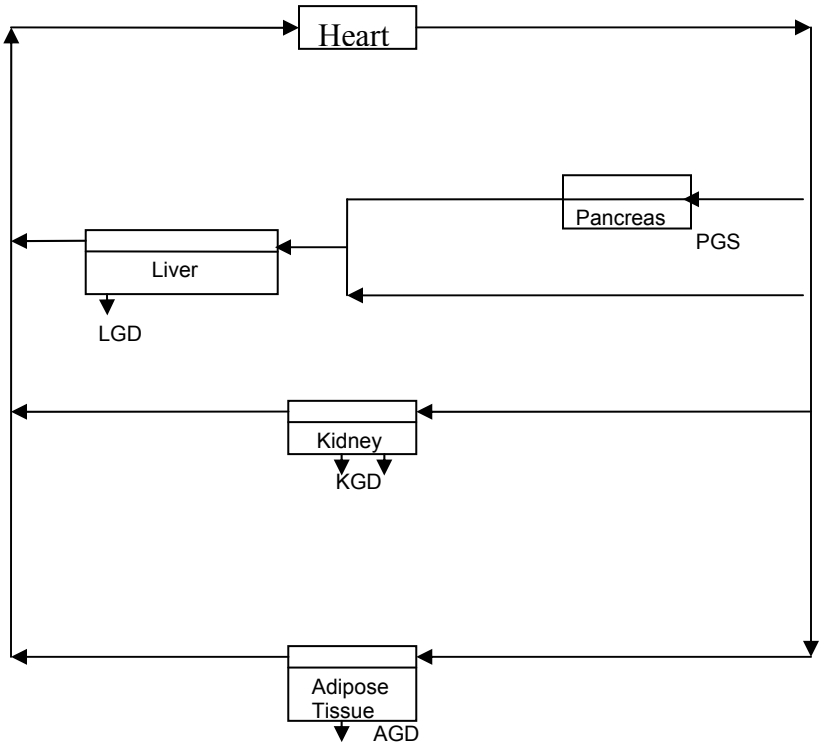

Figure 4-13: Physiologic diagram of glucagon metabolism. Each compartment is divided into the blood space, where blood flows, and the interstitial/intracellular space below the blood space. Inlet arrows at each compartment represent species appearance, while outlet arrows represent disappearance.

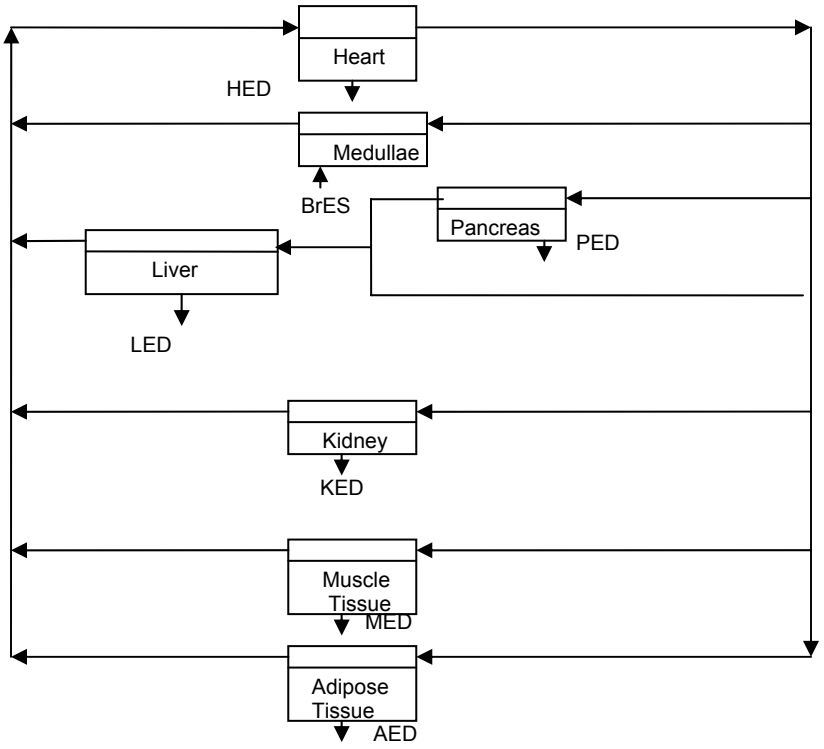

Figure 4-14: Physiologic diagram of epinephrine metabolism. Each compartment is divided into the blood space, where blood flows, and the interstitial/intracellular space below the blood space. Inlet arrows at each compartment represent species appearance, while outlet arrows represent disappearance.

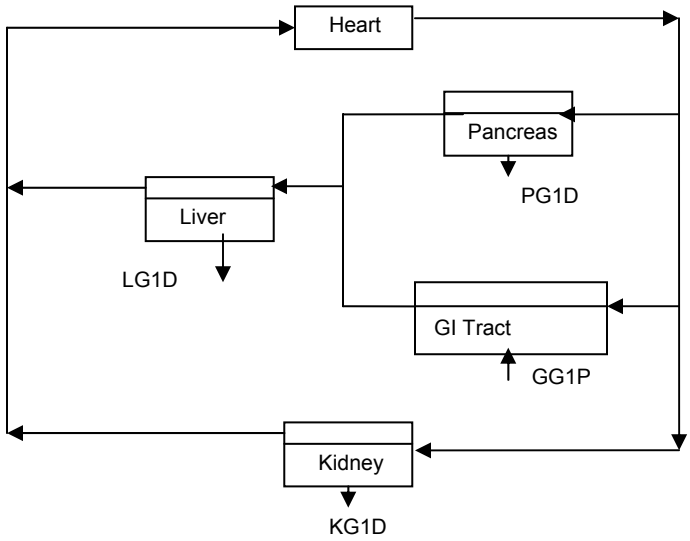

Figure 4-15: Physiologic diagram of glucagon-like peptide-1 metabolism. Each compartment is divided into the blood space, where blood flows, and the interstitial/intracellular space below the blood space. Inlet arrows at each compartment represent species appearance, while outlet arrows represent disappearance.

4.5 References

1. Holz, M., and Fahr, A., "Compartmental Modeling," *Adv. Drug Deliver. Rev.*, **48**, 249-264, 2001.

2. Sorensen, J. T., "A Physiologic Model of Glucose Metabolism in Man and Its Use to Design and Assess Improved Insulin Therapies For Diabetes", Ph.D. thesis, Dept. Chem. Eng., Massachusetts Institute of Technology, Cambridge, 1985.

3. Foster, R. O., Soeldner, J. S., Tan, M. H., and Guyton, J. R., "Short Term Glucose Homeostasis In Man: A System's Dynamics Model," *J. Dyn. Syst. Meas. Control,* **95**, 308-314, 1973.

4. Guyton, J. R., Foster, R. O., Soeldner, J. S., Tan, M. H., Kahn, C. B., Koncz, L., and Gleason, R. E., "Model of Glucose-Insulin Homeostasis In Man That Incorporates the Heterogeneous Fast Pool Theory of Pancreatic Insulin Release," *Diabetes*, **27**, 1027-1042, 1978.

5. Roy, A., and Parker, R. S., "Dynamic Modeling of Free Fatty Acid, Glucose, and Insulin: An Extended 'Minimal Model'," *Diabetes Technology & Therapeutics*, **8**, 617-626, 2006.

6. Bischoff, K. B., "Applications of a Mathematical Model For Drug Distribution in Mammals," in *Chemical Engineering in Medicine and Biology*, D. Hershey, Ed., Plenum, NY, 417-446, 1967.

7. Bischoff, K. B., "Some Fundamental Considerations of the Applications of Pharmacokinetics to Cancer Chemotherapy," *Cancer Chemoth. Rep. 1*, **59**, 777-793, 1975.

8. Bischoff, K. B., and Brown, R. G., "Drug Distribution in Mammals," *Chem. Eng. Prog. Symp. Ser.*, **66**, 33-45, 1966.

9. Bischoff, K. B., "Physiologically Based Pharmacokinetic Modeling," in *Pharmacokinetics in Risk Assessment: Drinking Water and Health, Volume 8*, NAS Press, Washington, 36-61, 1987.

10. Guyton, A. and Hall, J., *Textbook of Medical Physiology*, 11th ed., Elsevier Saunders, Philadelphia, PA, 2006.

11. Larsen, P.R., Kronenberg, H.M., Melmed,S., and Kenneth S. Polonsky, eds., *Williams Textbook of Endocrinology*, 10th ed., Saunders, Philadelphia, PA, 2003.

12. Puckett, W.R., *Dynamic Modelling of Diabetes Mellitus*, PhD Dissertation, Department of Chemical Engineering, The University of Wisconsin-Madision, 1992.

13. Hovorka, R, Shojaee-Moradie, F., Carroll, P. V., Chassin, L. J., Gowrie, I. J., Jackson, N. C., Tudor, R. S., Umpleby, A. M., and Jones, R. H., "Partitioning Glucose Distribution/Transport, Disposal, and Endogenous Production During IVGTT", *Amer. J. Physiol.,* **282,** E992–1007, 2002.

14. Cobelli, C., Bettini, F., Caumo, A., and Quon, M. J., "Overestimation of Minimal Model Glucose Effectiveness In Presence of Insulin Response Is Due to Undermodeling," *Am. J. Physiol.*, **277**, E1031-E1036, 1998.

15. Cryer, P. E., "Glucose Homeostasis and Hypoglycemia," in Larsen, P.R., Kronenberg, H.M., Melmed,S., and Kenneth S. Polonsky, eds., *Williams Textbook of Endocrinology*, 10th ed., Saunders, Philadelphia, PA, 1585-1618, 2003.

16. El-Khatib, F. H., Jiang, J., and Damiano, E. R., "Adaptive Closed-Loop Control Provides Blood-Glucose Regulation Using Dual Subcutaneous Insulin and Glucagon Infusion In Diabetic Swine," *J. Diabetes Sci. Tech.*, **1**, 181-192, 2007.

17. Habener, J. F., "Insulinotropic Glucagon-Like Peptides," in LeRoith, D., Taylor, S. I., and Jerrold M. Olefsky, Eds., *Diabetes Mellitus: A Fundamental and Clinical Text*, 2nd ed., Lippincott, Williams, and Wilkins, Philadelphia, PA, 94-105, 2000.

CHAPTER 5

PARAMETER IDENTIFICATION OF PATIENT MODELS

5.1 Introduction

While the development of model equations to be used for prediction, data interpretation, and simulation is important, the model will not be able to give meaningful predictions unless its parameters are accurately determined. For patient modeling, this can often mean finding average parameter values in literature, such as the dog kinetic parameters used by Bolie [1], or the organ volumes and blood flow rates of dogs used by Tiran [2,3] or humans, as used by Sorensen [4]. More often, however, patient parameters will have to be identified by fitting the model to patient data and selecting reasonable parameter values that give the closest fit to the data.

In the previous chapter, two different model frameworks were developed to describe the dynamics of the different biochemical species throughout the body. The first was a pharmacokinetic model, in which each species, with the exception of insulin, was assumed to be uniform in a single circulatory compartment. The second was a physiological-based model, in which the significant organ tissues were determined to be compartments needed for each species. Elimination and appearance within each compartment was to be described by either first order kinetics of the different species, by the dimensionless multiplicative factors of Sorensen's model, or by use of system identification techniques.

Unfortunately, the lack of patient data makes it impossible to identify a) the number of compartments of the different species for the pharmacokinetic models, and b)

the best representation of appearance and elimination kinetics. While literature data may have been acquired to try to determine certain parameters, it was decided that the task of searching for literally hundreds of values of volumes and flows for the physiological model would be a chore that at worst may end up incomplete and at best may end up describing a model that is still not able to be validated without patient data. Because patient data was not able to be acquired in this research, the developed model frameworks cannot be taken any further.

There are, however, other aspects of model identification that can be explored. Parameter identification is in effect a parameter optimization. Parameters are normally chosen to minimize an objective function the data to the model prediction, often while satisfying physical constraints. Most often, the objective function chosen is the sum of the squares of errors in the model fit relative to the data, as given by Equation (5.1).

$$\Phi = \sum_i \left(y_i - \hat{y}(x_i)\right)^2 \tag{5.1}$$

In Equation (5.1), y_i is the actual dependent variable value when the independent variable is at x_i. The term $\hat{y}(x_i)$ is the model prediction for the same independent variable value. As an optimization problem, an initial guess is required in order to search for the optimal set of parameters. Often when optimal parameter sets are given, they are given without a discussion of the initial guess used and without a discussion of the uncertainty of the parameters. Rawlings [5] provided a review of parameter estimation of crystallization models and found that not only were confidence intervals not being reported, but those

intervals, once determined, were often so large that there was no real certainty associated with the reported parameter values.

In this chapter, identification of kinetic parameters from a simple pharmacokinetic insulin model is investigated. Using a set of generated test data, the ability of a least squares optimization routine to estimate the model parameters is explored. The effect of different choices of initial guesses is studied, as well as confidence limits associated with the optimal parameter values. To improve parameter estimation, the use of stiff vs. non-stiff solvers is investigated, and the improvement in model identification as a result of including parameter sensitivities in the optimization routine is studied.

5.2 Methods

5.2.1 Model Selection and Test Data Generation

To show the estimation methods for a specific set of data, the pharmacokinetic insulin model of Hipszer, Joseph, and Kam will be used [6]. The authors proposed a compartmental model for insulin dynamics as shown in Figure 5-1. Compartments two and three are additional compartments that were proposed. The model equations are given by Equations (5.2)-(5.5) below.

$$\frac{dx_1}{dt} = -(A_{01} + A_{21} + A_{31})x_1(t) + A_{12}x_2(t) + A_{13}x_3(t) + U(t) \tag{5.2}$$

$$\frac{dx_2}{dt} = A_{21}x_1(t) - A_{12}x_2(t) \tag{5.3}$$

$$\frac{dx_3}{dt} = A_{31}x_1(t) - A_{13}x_3(t) \tag{5.4}$$

$$y = \frac{x_1}{V} \tag{5.5}$$

For the model, A_{ij} represents the fractional kinetic elimination rate of insulin from the j^{th} compartment to the i^{th} compartment. Compartment zero represents degradation. The model, as defined, consists of three compartments. To decrease the number of compartments, the kinetic rates associated with compartments two, three, or both, are set to zero. The state variable x_i represents the mass of insulin in the i^{th} compartment. The variable V represents the insulin distribution volume in the central compartment. Finally, U represents the insulin infusion rate as a function of time.

Given the dynamic model for insulin in one-, two-, or three-compartments within the body, a test set of data was generated. The initial condition of all states was set at zero mU. At time zero, an insulin pump was turned on, and a step in the insulin infusion rate from 0 to 20 mU/min was performed. At 150 minutes, a second step change occurs, with the insulin infusion rate increasing from 20 mU/min to 40 mU/min. The model parameters used for the test data generation were A_{01} = 0.12 min^{-1} and V = 15 L. All parameters associated with the two- or three-compartment model were set to zero, resulting in a set of data for a one-compartment model. The resulting profile of the test data is given in Figure 5-2. All sets of test data used for the estimations are given in Appendix D.

5.2.2 Parameter Estimation and Sensitivity Calculations

Once the test data were generated, an optimization solver was used to determine the optimal values of the parameters for each model, given the test data and a set of initial guesses for each parameter set. Based on the test data and the given initial guess, the optimization solver was used to minimize the objective function given by Equation (5.1).

To further improve the estimation, the sensitivities of each parameter as a function of time and the given parameter set were determined. The sensitivity of any state variable with respect to a model parameter is defined according to Equation (5.6).

$$S_{ij} = \left(\frac{\partial x_i}{\partial \theta_j} \right)_{\theta_{k \neq j}} \tag{5.6}$$

The sensitivity of the output y with respect to each parameter was determined as a function of time for a particular set of model parameters by incorporating the differential equation given in Equation (5.7) into the solver used to solve the model.

$$\frac{dS}{dt} = f_x S + f_\theta \tag{5.7}$$

In Equation (5.7), S is the $n_d x n_p$ sensitivity matrix in which n_d is the number of observations of the output variable y, and n_p is the number of model parameters. The matrix f_x is the mxn matrix of the derivatives of the model system with respect to the

individual states. The matrix f_θ is the mxn$_p$ matrix of the derivative of the model system with respect to the model parameters [7]. The result of the simulation was the predicted model response of the state variables as well as the time profile of the sensitivities. This served three purposes. First, the sensitivities give a strong indication of which parameters are most significantly affecting the output measured in the data, which allows us to determine the utility of higher order models. Second, the sensitivity is used to calculate the gradient and Hessian of the system, which is used to determine the (1-α)% confidence limits associated with each parameter estimate. Finally, incorporating a value of the gradient and Hessian into the optimization solver dramatically improves the precision of the parameter estimation, as will be shown later. For various sets of parameter values, sensitivities as a function of time were simulated and plotted for each of the compartmental models.

5.2.3 Confidence Limit Determination

Once the sensitivities for each parameter were determined, the 95% confidence interval was determined for each parameter in order to determine a) how narrow the range of potential values of the model parameters is, and b) whether or not the actual parameter values associated with the test data fall within the interval. The (1-α)% confidence interval was calculated using Equation (5.8).

$$\left(\theta-\hat{\theta}\right)^T H\big|_{\theta=\hat{\theta}}\left(\theta-\hat{\theta}\right)\le 2s^2 n_p F\left(n_p, n_d-n_p, \alpha\right) \tag{5.8}$$

In Equation (5.8), θ is the actual set of system parameters, $\hat{\theta}$ is the estimated parameter set, and α corresponds to the (1-α)% confidence limit. F represents the F probability function, which can found in statistics textbooks [8] or computed with computational software. H is the Hessian matrix, which is the matrix of second derivatives of the objective function with respect to the model parameters, as shown in Equation (5.9).

$$H_{kj} = \frac{\partial^2 \Phi}{\partial \theta_k \partial \theta_j} = 2\sum_i \left[\frac{\partial x_i}{\partial \theta_k} \frac{\partial x_i}{\partial \theta_j} - \left(\tilde{x}_i - x_i\right) \frac{\partial^2 x_i}{\partial \theta_k \partial \theta_j} \right] \tag{5.9}$$

Clearly, the Hessian is a $n_p x n_p$ matrix. To simplify this calculation the Gauss-Newton approximation was used, in which the second term of Equation (5.9) is neglected. This approximation usually holds very well when the model fits the data very well or when the second derivatives are smaller than the first derivatives [7]. Expressed in matrix notation, the Gauss-Newton approximation of the Hessian is then expressed by Equation (5.10).

$$H = 2S^T S \tag{5.10}$$

The final term from Equation (5.8) is s^2, the sample variance. It is determined by Equation (5.11).

$$s^2 = \frac{\Phi\left(\hat{\theta}\right)}{n_d - n_p} \tag{5.11}$$

The estimations from the first part were performed again, this time also reporting the 95% confidence limits and whether or not each parameter was within the range of its estimate.

5.2.4 Estimation with Sensitivity Calculations Included

The next improvement to the estimation procedure was to incorporate the calculation of the gradient and Hessian matrix into the optimization solver. This required incorporating the relationship between the sensitivity matrix and Hessian, as well as the relationship between the sensitivity matrix and the gradient, as shown in Equation (5.12).

$$\nabla\Phi = -2S^T e \tag{5.12}$$

In Equation (5.12), Φ is the scalar value of the objective function. The vector e is a vector of length n_d, where each element is the difference between the measured output and the model prediction for each time. The estimations were again repeated for the different sets of initial parameter guesses for the different model frameworks. Estimations were also performed in which direct model correspondence was used to note any difficulties in estimating parameters for a higher order model when a low order model is used to generate test data. For this, a new set of test data was generated, using the literature parameter values of the two-compartment model for the simulated test data [9].

In order to observe how successful the estimation is with a real system, noise was added to the generated test data. First, a constant noise of 5% was added. Second, a random noise vector was added in order to simulate a real unknown process. Estimation using the previously mentioned initial guess sets was performed a final time.

Finally, in order to determine the validity of the estimations, simulations were performed for a different set of conditions. Using six estimated parameter sets for the two-compartment model, using the test data of the one-compartment model, each model was subjected to a series of five step changes. At time zero, the insulin infusion rate is increased to 15 mU/min. At 150 min, the rate is increased to 25 mU/min. At 300 min, the rate is increased to 35 mU/min. At 450 min, the rate is increased to 45 mU/min. Finally, at 600 min, the rate is increased to 55 mU/min. Each simulated was plotted on the same graph in order to compare the responses of the different parameter sets to the same input set.

5.2.5 Computational Methods

To solve the systems of ordinary differential equations, the MATLAB solvers ode45 and ode23s were used [10]. The solver ode45 is a nonstiff solver implementing the 5^{th} order Runge-Kutta Dormand-Prince pair to solve the system for each specified time. The solver ode23s is a stiff solver implementing a modified Rosenbrock formula of order 2. Both solvers were used for each initial parameter value set in order to compare the effectiveness of stiff vs. nonstiff solvers.

To perform the optimization, the MATLAB function "fmincon" was used to perform the minimization of a constrained optimization problem. The function "fmincon" can be tailored to fit the desired optimization. For our problem, a line-search method was incorporated into the solver as the means to search for the minimum. Initially the Levenberg-Marquartd [11] method is selected as the search method, but MATLAB switches to a line search method [12] because the solver "fmincon" is not able to handle constraints with the Levenberg-Marquardt method. The MATLAB source code used for parameter estimation is provided in Appendix E.

5.3. Results

5.3.1 Initial Parameter Estimation

Initially, the model parameters were estimated for the one- and two-compartment insulin pharmacokinetic models by an initial guess of the parameters that was within ±200% of the determined model parameters of similar models from literature [13], [9]. Table 5-1 shows the estimation results for the one-compartment model. The different parameter sets used as initial guesses for the two-compartment model are given in Table 5-2, and the parameter estimation results for the two-compartment model are given in Table 5-3.

Tables 5-1 and 5-3 show that the estimation of only two model parameters strongly depends on the initial starting values assigned to each parameter and that the task of estimating four model parameters is even more difficult. Both tables show that when the actual parameter set is chosen as the initial guess, the routine converges quickly on

the actual parameters, demonstrating the effectiveness of the routine. It is not included here, but similar work performed for the three-compartment models resulted in the same observations. The estimations for the higher order models often resulted in solutions that violated constraints, and given that no constraint was defined for the volume, V, in the model, the extremely large values associated with the optimal V show that it also is violating physical constraints. Comparing the different solvers, neither solver appears to do an effective job of estimating the model parameters to be the actual values used for the test data.

5.3.2 Sensitivity Studies

The sensitivity of the output with respect to each parameter for each model was then determined, using the same sets of initial guesses. For the one-compartmental model, the parameters of importance were A_{01}, V, and y_0. Each was made either very large or very small, and the timed sensitivity profile was determined for that particular parameter set. From the sensitivity profile, the relative sensitivity profile was determined using Equation (5.13).

$$\overline{S}_{ij} = S_{ij}\left(\frac{\theta_j}{y_i}\right) \tag{5.13}$$

The relative sensitivities are scaled to an order of magnitude of 1. Figure 5-3 shows the relative sensitivity profile for the parameters when A_{01} is 0.12 min^{-1}, V is 15 L,

and y_0 is 15 mU/L. As can be seen, the model output is highly sensitive to the two parameters of the one-compartment model. The spikes can be attributed to the step changes causing a reduction in the relative sensitivity for a brief instant before the sensitivities rapidly approach -1 once again.

Figures 5-4 and 5-5 show the effects of increasing the model parameters on the sensitivity profile. Figure 5-4 was generated by setting A_{01} to 0.6 min^{-1}, and Figure 5-5 was generated by setting V to 100 L. Two observations can be made here. First, the increase of the model parameters to high levels results in overshoot before the relative sensitivity with respect to A_{01} reaches the steady state value of -1. Second, a high value of A_{01} results in a very rapid approach to the steady state sensitivity, while the large V value appears to slow down the approaching of the steady state. One thing that is clear in all three figures, however, is that the output is highly sensitive to the two model parameters for both medium and high values of the parameters.

Sensitivity calculations were also performed for the two- and three-compartment models. Figure 5-6 shows the relative sensitivity profile for the two-compartment model. For this simulation, the parameters were set approximately to those reported in literature [9]. A_{01} was set to 0.25 min^{-1}, A_{12} to 0.05 min^{-1}, A_{21} to 0.06 min^{-1}, and V to 5 L. As can be seen in the figure, the additional parameters associated with the two-compartment model reach a steady state value of 0, while the one-compartment model parameters continue to approach a value of -1. This implies that the system output is relatively insensitive to the additional parameters encountered by increasing the complexity of the model.

Figure 5-7 shows the relative sensitivity profile for the three compartment model. Again, the parameters selected were similar to those reported in literature for a three-compartment insulin model [14]. As expected, the output is insensitive to the additional parameters introduced by the third compartment, A_{13} and A_{31}, as the sensitivities of both parameters stay very near zero for the entire duration of the simulation. The only time any sensitivity profile showed results counter to those showed in Figures 5-6 and 5-7 for the multicompartment models was when A_{01} was considerably smaller than A_{21} and A_{31}. This is not typically expected, as it implies that the majority of the insulin from the central compartment would be going to the side compartments instead of being eliminated from the body. Such a system would result in the accumulation of insulin in the side compartments to very high levels. Thus, it is concluded that such parameter sets are unreasonable, and that reasonable parameter sets show that the output of plasma insulin levels appear to be relatively insensitive to additional parameters beyond those used for a one-compartment model.

5.3.3 Confidence Limit Determination

Using the different sets of initial parameter guesses for each model, the 95% confidence limits were determined. They are shown in Tables 5-4 and 5-5 for the one- and two- compartment models respectively. The interval is expressed as a percentage of the optimal parameter. The parameter set number corresponds to the same set of initial parameters used in Tables 5-1 and 5-2.

Table 5-4 shows that estimation using the one-compartment model and test data from the one-compartment model will have fairly low confidence limits, typically lower than 10% of the estimated parameter value. However, the low values also mean that in many instances, the actual parameter value is not within the 95% confidence limit of the estimated parameter value. Such an observation casts doubt on the ability to use least squares to estimate parameters of dynamic systems. Table 5-5 shows that the limits are much larger for the higher order model. Parameters for the two-compartment model were observed to have 95% confidence limits greater than 200%, meaning that there is no real way to know what the parameter value is with any certainty. Ideally, the estimation should produce confidence limits that are fairly narrow but that still contain the actual parameter value within the interval. The values in Tables 5-4 and 5-5 show that using only the system of equations and the optimization routine does not result in an estimate of parameters that can be considered accurate with any real level of certainty.

5.3.4 Parameter Estimation With Sensitivities

Table 5-6 shows the estimated parameter values for the one-compartment insulin model when sensitivities are included in the optimization routine, and Table 5-7 shows the confidence limits associated with the estimated parameters. There are several observations that can be made. First, the estimated model parameters are much closer to the actual model parameters when sensitivity calculations have been included in the routine. Second, the use of ode23s, the stiff-solver, results in a nearly exact estimate of the model parameters, demonstrating a considerable improvement to estimation routines

employing a non-stiff solver. Finally, the calculated 95% confidence limits are very small, with the largest confidence interval being within ±2% of the estimated parameter value. For the one-compartment model, parameter estimation that employs both the parameter sensitivity dynamics and a stiff differential equation has demonstrated superiority over solvers that do not have both features.

To further test the effectiveness of the estimation of the one-compartment model parameters, different types of noise were added to the data. The first type of noise assumed that each point was 5% larger or 5% smaller in value than the actual test data point. The second type was random noise added to the process. The estimation results for the one-compartment model are given by Table 5-8, and the associated confidence limits are given in Table 5-9. The parameters were estimated very close to the actual parameter values in spite of the appearance of noise. The model fits for the noisy data are shown in Figure 5-8 and 5-9. Even with noise, the parameter estimation routine employing both a stiff solver and the parameter sensitivities is able to accurately determine the parameter values with low confidence intervals, regardless of the initial guess.

Table 5-10 shows the parameter estimation results for the one-compartment generated test data with the two-compartment model, again employing the parameter sensitivity equations in the optimization routine Table 5-11 shows the confidence limits of the estimated parameter values. There appears to be minimal improvement to the parameter estimation of the higher order model. The optimal parameters are still highly dependent upon the initial guess of the parameter set. While there is an improvement in

the size of the confidence intervals, the actual parameter values routinely fall out of this 95% confidence range, demonstrating the inability of the routine to be able to effectively estimate model parameters with any sort of certainty.

While estimation of higher order model parameters appears to not be improved by the use of sensitivities with respect to converging to the actual parameters with small confidence limits, Figure 5-10 shows that the actual model fit is fairly good. Figure 5-10 shows the fit of the two-compartment parameters resulting in the highest Φ value to the test data generated. The model appears to fit the data very well, implying that multiple parameter sets will be able to fit the data reasonably well.

One reason that the two-compartment model may fit the one-compartment model well with multiple parameter sets is because of the general differences in the responses between the two models to the same input. To investigate this hypothesis, a set of test data from the two-compartment model was generated using parameter set one of Table 5-8, and the two-compartment model was used to estimate the parameters. The different parameter sets used as initial guesses are given by Table 5-12. The results of the estimation are given in Table 5-13, with the confidence limits for each estimation reported in Table 5-14. For the case of data generated with the two-compartment model, like the case with the one-compartment model, the estimated parameter set is highly dependent on the choice of initial guess for the parameter set. Figure 5-11 demonstrates that the estimated parameter set with the worst Φ value is still able to fit the data particularly well.

An interesting observation from Table 5-9 is that the estimation routine appears to work very well as long as the one-compartment model parameters A_{01} and V are initially chosen to be at or near the exact values. Having an accurate estimate of these parameters enables the entire parameter set to be estimated effectively, but the presence of the additional parameters prevents the accurate estimation of the parameter set when the one-compartment parameters are not known accurately. The significance of the one-compartment parameters is not great enough, however, to estimate the one-compartment parameters from the one-compartment model.

Given the ability of the estimated parameters, whether the actual parameters or not, to fit the data reasonably well, the ability of the estimated parameter sets to make accurate predictions was investigated by subjecting the model patients to a series of five step changes, including changes outside the range of the test data. Figure 5-12 shows the results. While the parameter sets differ considerably in some cases, the predictions are basically exactly the same for all the different model parameter sets. This gives a stronger argument for the presence of multiple optimal parameter sets.

5.4 Conclusions

Given a published insulin pharmacokinetic model, test data has been generated, and the ability of an optimization routine to effectively estimate the actual parameter set used for data generation was evaluated. Parameter sets can easily be estimated for algebraic relations, but parameter estimation of differential equations without analytical solutions is not a trivial matter. While parameter sets can easily be estimated when there

is no input associated with the system, the optimal parameter set of a dynamic model consisting of an insulin input is highly dependent on the initial guess of the parameter values. The estimated parameter sets may also not be known with any degree of certainty, as 95% confidence limit calculations have shown.

Estimation can be improved for a one-compartment model by including the sensitivity of the output for each parameter in the estimation, and by using a stiff solver with the optimization routine. This improved routine has demonstrated the ability determine the parameter set in different types of noise as well. For higher order models, the parameter estimate is still highly dependent on the initial guess of the parameter set, but models generated using the estimated parameters are able to both fit the data and make predictions nearly equal to those of the actual parameter set, demonstrating the possibility of multiple parameter sets that accurately reflect data.

For patient models with a large number of parameters such as the physiological models developed in Chapter 4, model identification is best performed by using as many data sets as possible to identify as few parameters at a time as possible. Clearly blood values of each species would not be sufficient to accurately estimate hundreds of parameters, as it was not sufficient to estimate even 4 parameters in a two-compartment model. Literature values of parameters can effectively be used, but sensitivity studies of the outputs with respect to a specific parameter should be used in order to determine how important that value is with respect to prediction and response. For the two-compartment model, plasma insulin was fairly insensitive to the two-compartment parameters, and estimation depended nearly entirely on the initial guess of the one compartment

parameters. Given literature values of parameters that are insignificant with respect to output sensitivity, low order estimation problems should be formulated using as few unknown sensitive parameters at a time. Finally, given literature values of parameter with a high degree of sensitivity, the possibility of the existence of multiple optimal parameter sets should give the user confidence that the value is likely reasonable enough to make effective predictions. Of course the model should still be validated using a different set of output data.

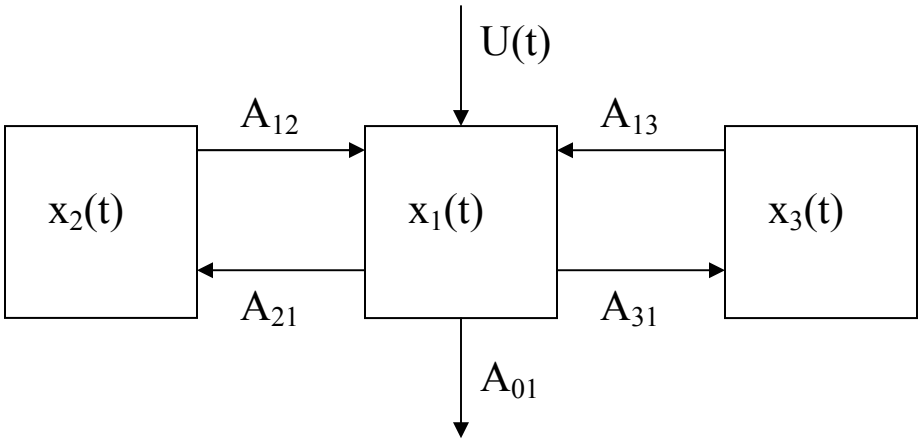

Figure 5-1: Diagram of the intravenous insulin pharmacokinetic model as proposed by Hipszer, Joseph, and Kam [6]. The central compartment represents the plasma. This compartment is assumed to be constantly in exchange with two other compartments that do not take in or lose insulin through any means other than exchange with the central compartment. The model order can be reduced by eliminating the side compartments. One or both can be eliminated to give a one-, two-, or three-compartment model.

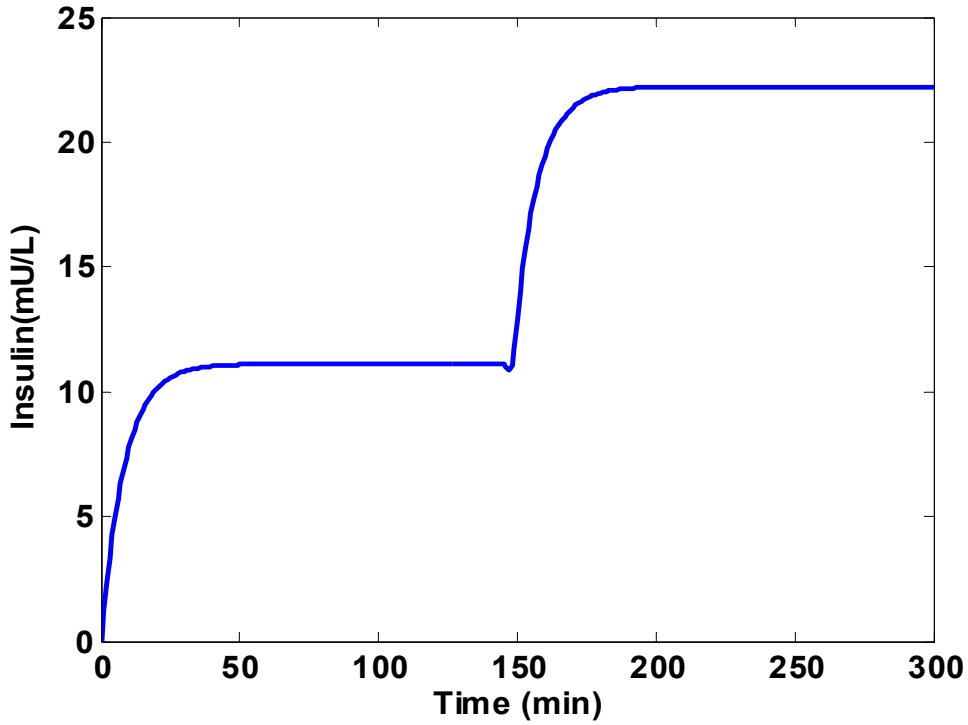

Figure 5-2: Graph of test data for insulin as a function of time in response to two step changes in the infusion rate of insulin from a pump. At time zero, the patient of known one-compartment model parameters is subjected to step change in insulin infusion from zero to 20 mU/min. At 150 minutes, the patient is again subjected to an insulin infusion step change from 20 to 40 mU/min.

Table 5-1: Initial Parameter Estimation For One-Compartment Model						
Solver	**Parameter Set**	**Initial A_{01} (min^{-1})**	**Initial V (L)**	**SSE (mU^2/L^2)**	**Optimal A_{01} (min^{-1})**	**Optimal V (L)**
Ode45	1	0.12	15	0	0.12	15
Ode23s	1	0.12	15	0	0.12	15
Ode45	2	0.1333	10.1	38.5	0.165	10.98
Ode23s	2	0.1333	10.1	$1.5x10^{-10}$	0.12	15
Ode45	3	0.06	15	284	0.0597	29.5
Ode23s	3	0.06	15	323	0.0521	33.8
Ode45	4	0.12	22.5	560	0.0505	35.6
Ode23s	4	0.12	22.5	6.2	0.1058	16.98

Table 5-2: Initial Two-Compartment Parameter Sets Used For Estimation				
Parameter Set	**A_{01} (min^{-1})**	**V (L)**	**A_{12} (min^{-1})**	**A_{21} (min^{-1})**
1	0.12	15	0	0
2	0.2	6	0.2	0.2
3	0.1	6	0.2	0.2
4	0.2	6	0.1	0.2
5	0.2	6	0.2	0.1
6	0.2	3	0.2	0.2

Table 5-3: Initial Parameter Estimation For Two-Compartment Model						
Solver	**Parameter Set**	**A_{01} (min^{-1})**	**V (L)**	**A_{12} (min^{-1})**	**A_{21} (min^{-1})**	**Φ (mU^2/L^2)**
Ode23s	1	0.12	15	0	0	0
Ode23s	2	0.229	6.7	0.0463	0.462	1060
Ode23s	3	0.6	1.1772	0	0.4694	$2.00x10^4$
Ode23s	4	0.318	5.67	0.273	0.433	21.1
Ode23s	5	0.106	16.1697	0.4079	0.35	303
Ode23s	6	0	$2.12x10^5$	0.6	$4.17x10^{-4}$	$8.76x10^4$
Ode45	1	0.12	15	0	0	0
Ode45	2	0.19	9.47	0.6.00	0.323	3.74
Ode45	3	0	$1.60x10^5$	0	0	$8.73x10^4$
Ode45	4	0.219	8.22	0.599	0.523	3.01
Ode45	5	0.153	11.8	0.6	0.1886	1.0256
Ode45	6	0	$3.46x10^4$	0	0	$8.74x10^4$

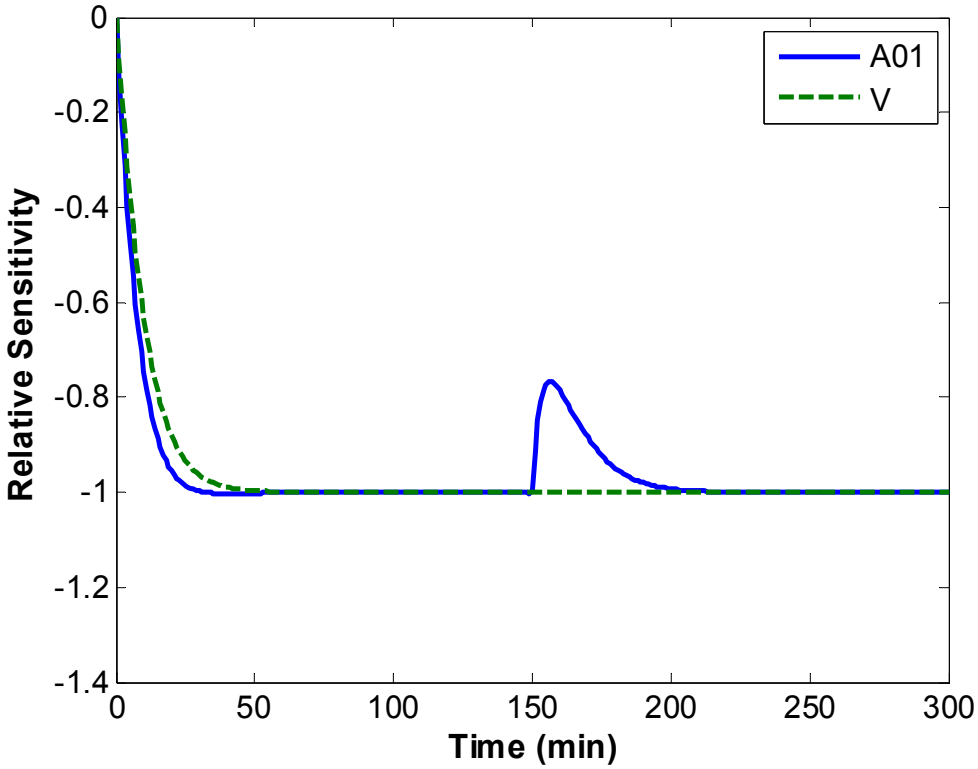

Figure 5-3: Relative sensitivity profile for one-compartment model, with A_{01}=0.12 min^{-1}, V=15 L, and y_0=15 mU/L. Plasma insulin is highly sensitive to both parameters. At time 0 and 150 min, a change in the sensitivity is observed as a result of the step change in insulin infusion at those times. The steady sensitivity is quickly re-established in both cases.

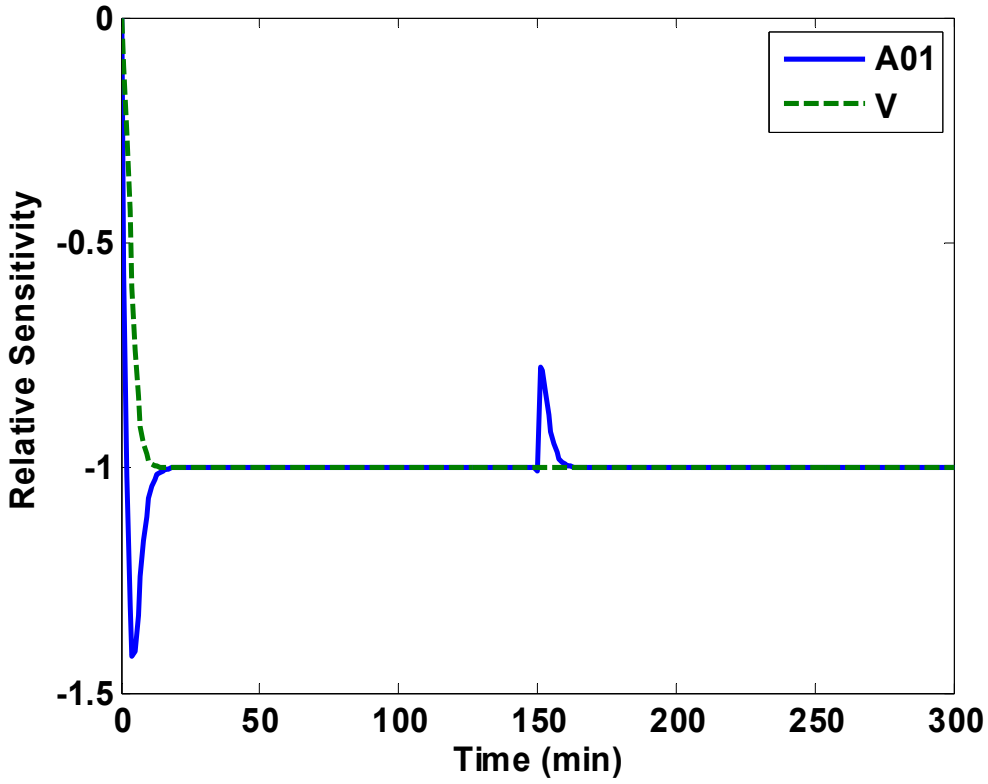

Figure 5-4: Relative sensitivity profile for one-compartment model, with A_{01} = 0.6 min^{-1}, V = 15 L, and y_0 = 15 mU/L. The output insulin is highly sensitive to both one-compartment model parameters. A change in sensitivity is observed at time 0 and 150 min, in response to the insulin infusion step changes. The large elimination value causes the sensitivity to approach its steady state level very rapidly.

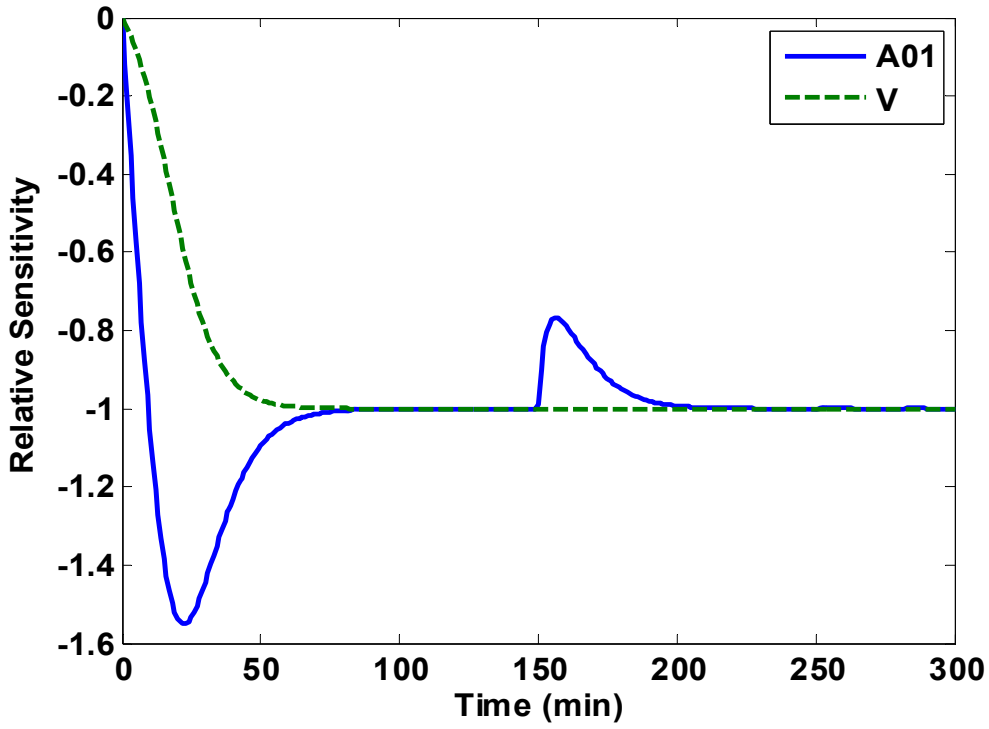

Figure 5-5: Relative sensitivity profile for one-compartment model, with A_{01} = 0.12 min^{-1}, V = 100 L, and y_0 = 15 mU/L. Sensitivity dynamics are observed at time 0 and 150 min in response to the insulin infusion step changes. At high volumes, both sensitivities return to their steady state values very slowly.

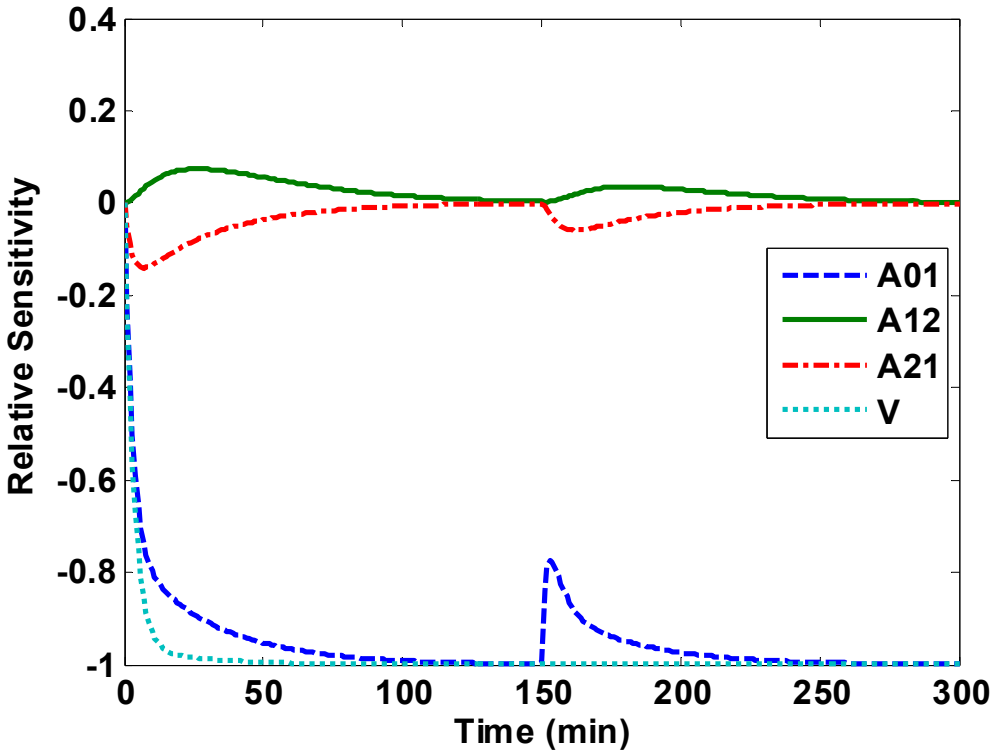

Figure 5-6: Relative sensitivity profile for two-compartment model, with A_{01}= 0.25 min^{-1}, A_{12}=0.05 min^{-1}, A_{21}=0.06 min^{-1}, and V = 5 L. The output response is highly sensitive to the one-compartment parameters, V and A_{01}, while the parameters added as a result of increasing the model order have steady state values of zero. The output appears to be insensitive to the two-compartment parameters.

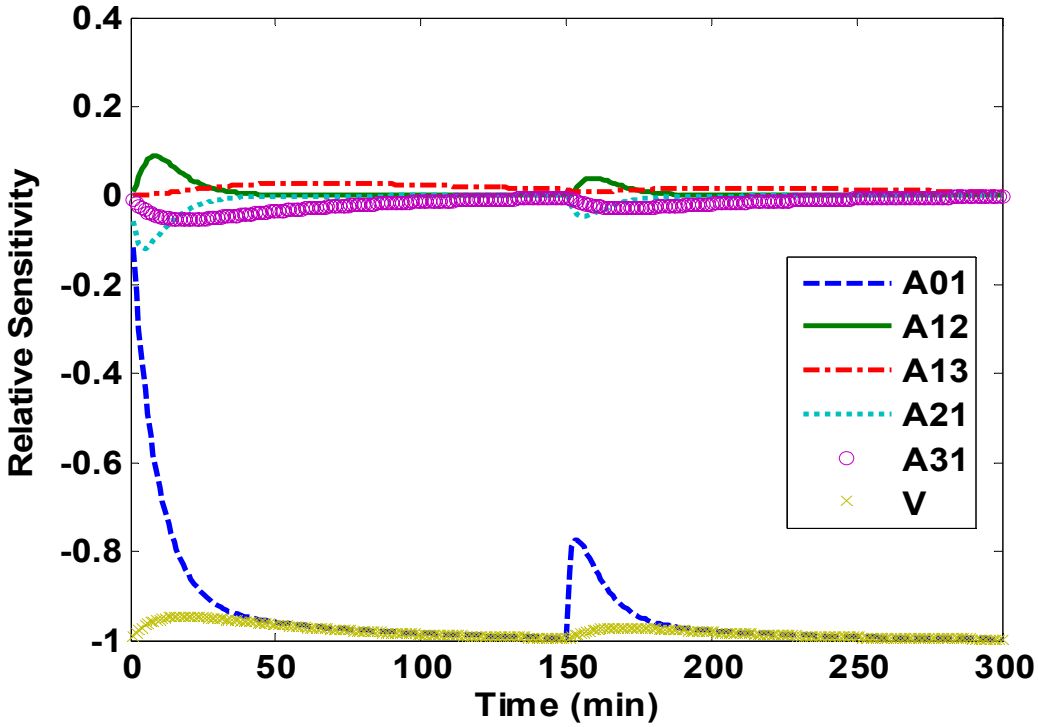

Figure 5-7: Relative sensitivity profile for three-compartment model, with A_{01} = 0.25 min^{-1}, A_{12} = 0.4 min^{-1}, A_{13} = 0.02 min^{-1}, A_{21} = 0.14 min^{-1}, A_{31} = 0.04 min^{-1}, V = 3.5 L. The output is highly sensitive to the one-compartment model parameters, A_{01} and V. It appears to be insensitive to the higher order model parameters, which all have a steady state value of zero.

Table 5-4: Confidence Intervals For One-CompartmentModel			
Solver	**Parameter Set**	**A_{01} (min^{-1})**	**V (L)**
Ode45	1	0%	0%
Ode23s	1	0%	0%
Ode45	2	2%	2%
Ode23s	2	6%	6%
Ode45	3	11%	10%
Ode23s	3	12%	12%
Ode45	4	2%	2%
Ode23s	4	1%	1%

Table 5-5: Confidence Intervals For Two-Compartment Model					
Solver	**Parameter Set**	**A_{01} (%)**	**A_{12} (%)**	**A_{21} (%)**	**V (%)**
Ode23s	1	Exact	Exact	Exact	Exact
Ode23s	2	92	166	308	92
Ode23s	3	1.6×10^9	2.2×10^9	4×10^9	1.6×10^9
Ode23s	4	244	134	442	244
Ode23s	5	70	134	213	70
Ode23s	6	66	80	202	66
Ode45	1	Exact	Exact	Exact	Exact
Ode45	2	605	670	1834	605
Ode45	3	Inf	Inf	Inf	Inf
Ode45	4	189	222	588	189
Ode45	5	58.1	69	178	58
Ode45	6	Inf	Inf	Inf	Inf

Table 5-6: Parameter Estimation For One-Compartment Model, Using Sensitivity Calculations				
Solver	**Parameter Set**	**A_{01} (min^{-1})**	**V (L)**	**Φ (mU^2/L^2)**
Ode45	1	0.12	15	0
Ode23s	1	0.12	15	0
Ode45	2	0.113	15.8	11.1
Ode23s	2	0.12	14.995	$3.89x10^{-5}$
Ode45	3	.1212	14.8184	9.37
Ode23s	3	0.1201	14.9882	$2.69x10^{-4}$
Ode45	4	0.125	14.4	11.8
Ode23s	4	0.12	14.9953	$5.5x10^{-5}$

Table 5-7: Parameter Confidence Intervals For One-Compartment Model Using Sensitivity Calculations			
Solver	**Parameter Set**	**A_{01} Interval (%)**	**V Interval (%)**
Ode45	1	0	0
Ode23s	1	0	0
Ode45	2	2	2
Ode23s	2	<1	<1
Ode45	3	2	2
Ode23s	3	<1	<1
Ode45	4	2	2
Ode23s	4	<1	<1

Table 5-8: Noisy Data Parameter Estimation For One-Compartment Model, Using Sensitivity Calculations				
Noise Type	**Parameter Set**	**A_{01} (min^{-1})**	**V (L)**	**Φ (mU^2/L^2)**
5%	1	0.1199	15.0137	219
Random	1	0.1236	14.2	35
5%	2	0.12	15	219
Random	2	0.1234	14.2	33
5%	3	0.1199	15.0128	219
Random	3	0.1266	13.85	35
5%	4	0.12	15	219
Random	4	0.1241	14.15	36

Table 5-9: Noisy Data Confidence Limits For One-Compartment Model, Using Sensitivity Calculations			
Noise Type	**Parameter Set**	**A_{01} (%)**	**V (%)**
5%	1	10	10
Random	1	4	4
5%	2	10	10
Random	2	4	4
5%	3	10	10
Random	3		4
5%	4	10	10
Random	4	4	4

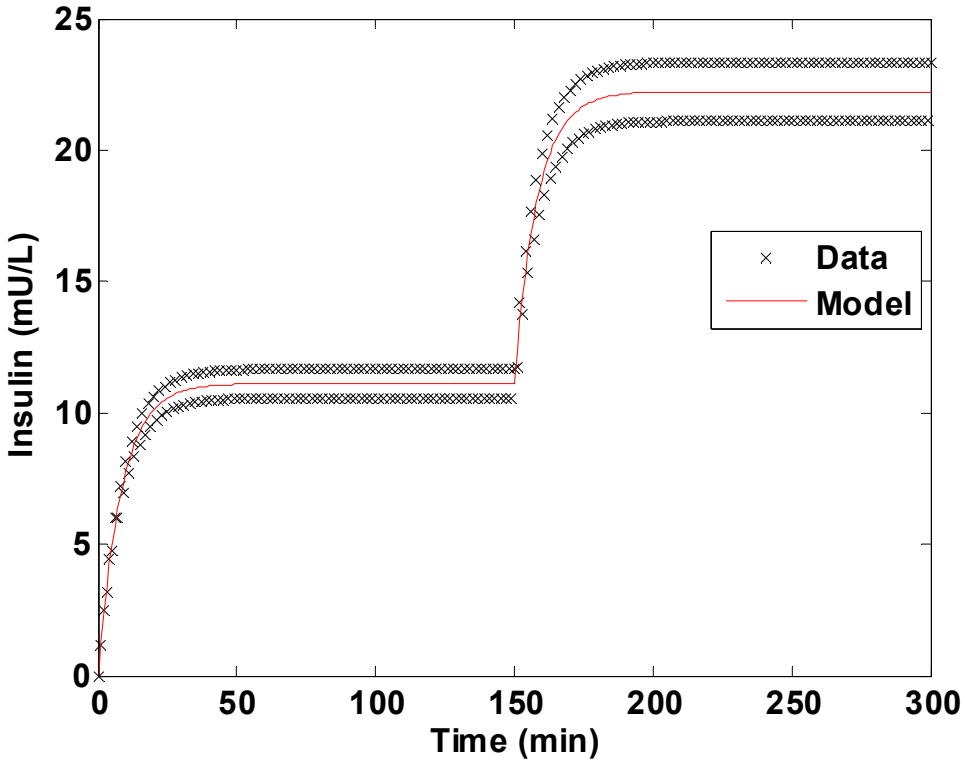

Figure 5-8: Model fit for test data generated with one-compartment model and 5% bias for each measurement. Model parameters are A_{01} = 0.119 min^{-1} and V = 15.01 L. The model fits exactly within the data, and the estimated parameter set is nearly identical to the actual parameter set of the generated data without the addition of noise.

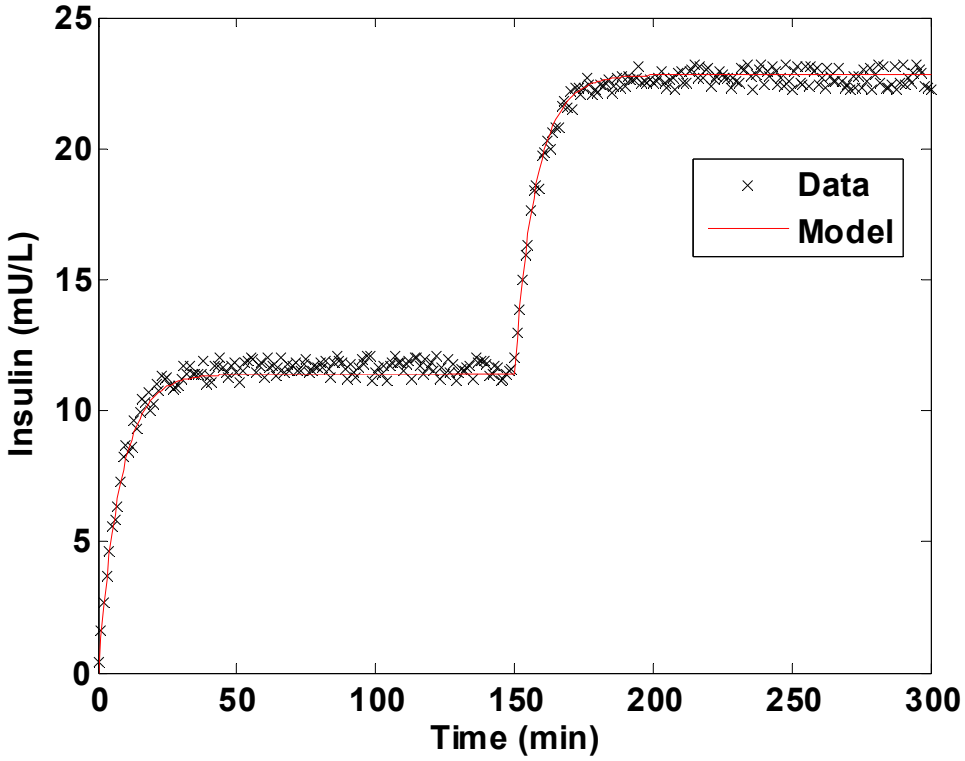

Figure 5-9: Model fit for random noise added to test data. Model fit is for A_{01} = 0.1262 min^{-1} and V = 13.9 L. This parameter set represents the worst fit to the noisy data. The model fits into the data very well.

Table 5-10:Parameter Estimation for Two-Compartment Model, Using Sensitivity Calculations						
Solver	**Parameter Set**	**A_{01} (min^{-1})**	**V (L)**	**A_{12} (min^{-1})**	**A_{21} (min^{-1})**	**Φ (mU^2/L^2)**
Ode23s	1	0.12	15	0	0	0
Ode23s	2	0.246	7.32	0.578	0.6	4.23
Ode23s	3	0.2401	7.49	0.5993	0.5999	3.78
Ode23s	4	0.264	6.82	0.507	0.6	6.04
Ode23s	5	0.269	6.6815	0.492	0.6	6.6191
Ode23s	6	0.3399	5.29	0.338	0.6	16.8
Ode45	1	0.12	15	0	0	0
Ode45	2	0.231	7.78	0.558	0.439	9.88
Ode45	3	0.2407	7.47	0.5548	0.4778	9.92
Ode45	4	0.263	6.84	0.543	0.558	10.1
Ode45	5	0.281	6.40	0.5052	0.5867	10.48
Ode45	6	0.3744	4.80	0.32	0.6	17

Table 5-11: Confidence Limits For Two-Compartment Model, Using Sensitivity Calculations					
Solver	**Parameter Set**	**A_{01} (%)**	**A_{12} (%)**	**A_{21} (%)**	**V (%)**
Ode23s	1	Exact	Exact	Exact	Exact
Ode23s	2	37	42	110	37
Ode23s	3	36	43	111	36
Ode23s	4	39	40	106	39
Ode23s	5	39	40	105	39
Ode23s	6	44	36	97	44
Ode45	1	Exact	Exact	Exact	Exact
Ode45	2	47	71	169	47
Ode45	3	48	62	163	48
Ode45	4	50	59	150	50
Ode45	5	48	51	134	48
Ode45	6	41	33	88	41

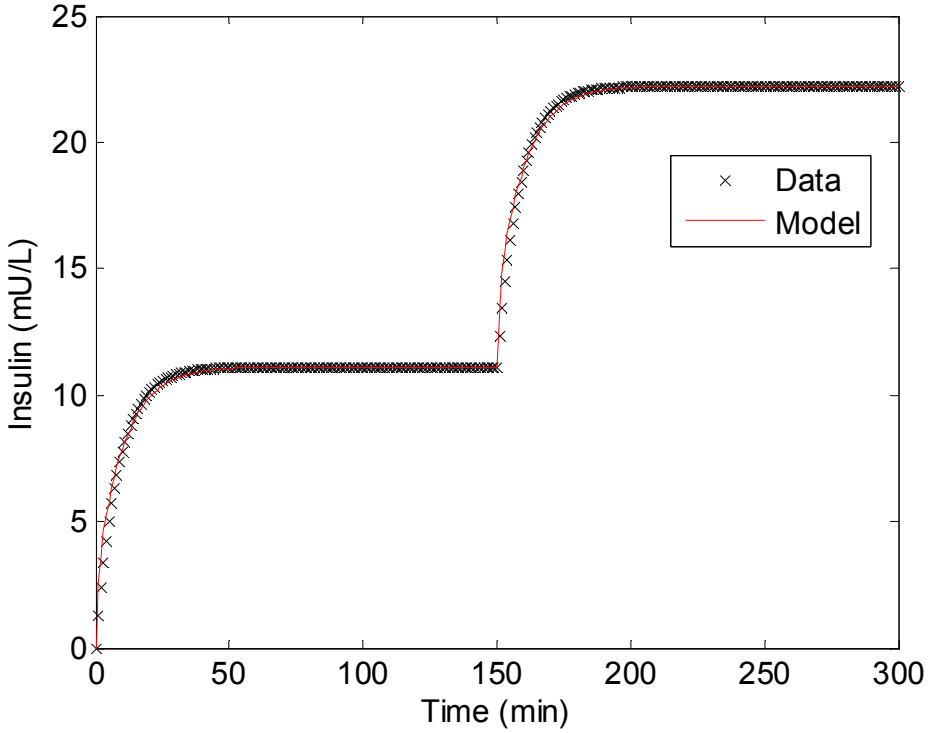

Figure 5-10: Model fitting of two-compartment model to one-compartment test data. A_{01} = 0.34 min^{-1}, A_{12} = 0.338 min^{-1}, A_{21} = 0.6 min^{-1}, and V = 5.29 L. The model fit appears to be nearly on top of the plot.

Table 5-12: Parameter Sets For Two Compartment Estimation				
Parameter Set	**A_{01} (min^{-1})**	**V(L)**	**A_{12} (min^{-1})**	**A_{21} (min^{-1})**
1	0.2	6	0.05	0.06
2	0.3	6	0.05	0.06
3	0.1	6	0.05	0.06
4	0.2	9	0.05	0.06
5	0.2	3	0.05	0.06
6	0.2	6	0.08	0.06

Table 5-13: Two-Compartment Model Parameter Estimation Using Two-Compartment Model Test Data						
Solver	**Parameter Set**	**A_{01} (min^{-1})**	**V (L)**	**A_{12} (min^{-1})**	**A_{21} (min^{-1})**	**Φ (mU^2/L^2)**
Ode23s	1	0.2	6.00	0.05	0.06	0
Ode23s	2	0.2384	5.05	0.0648	0.0937	3.89
Ode23s	3	0.191	6.27	0.0481	0.0541	0.332
Ode23s	4	0.157	7.6	0.031	0.034	11.2
Ode23s	5	0.2922	4.12	0.085	0.16	14
Ode23s	6	0.2003	5.99	0.05	0.06	0.011
Ode45	1	0.2	6.00	0.05	0.06	0
Ode45	2	0.239	5.03	0.0655	0.0967	3.03
Ode45	3	0.192	6.26	0.047	0.054	0.241
Ode45	4	0.158	7.57	0.0299	0.0288	9.44
Ode45	5	0.2946	4.09	0.086	0.162	15
Ode45	6	0.2005	5.99	0.0504	0.0606	0.002

Table 5-14: Two-Compartment Model Confidence Limits Using Two-Compartment Model Test Data					
Solver	**Parameter Set**	**A_{01} (%)**	**A_{12} (%)**	**A_{21} (%)**	**V (%)**
Ode23s	1	0	0	0	0
Ode23s	2	3	7	9	3
Ode23s	3	1	3	3	1
Ode23s	4	4	17	15	4
Ode23s	5	8	12	19	8
Ode23s	6	<1	<1	<1	<1
Ode45	1	0	0	0	0
Ode45	2	3	7	9	3
Ode45	3	7	2	2	7
Ode45	4	3	17	13	3
Ode45	5	9	12	19	9
Ode45	6	<1	<1	<1	<1

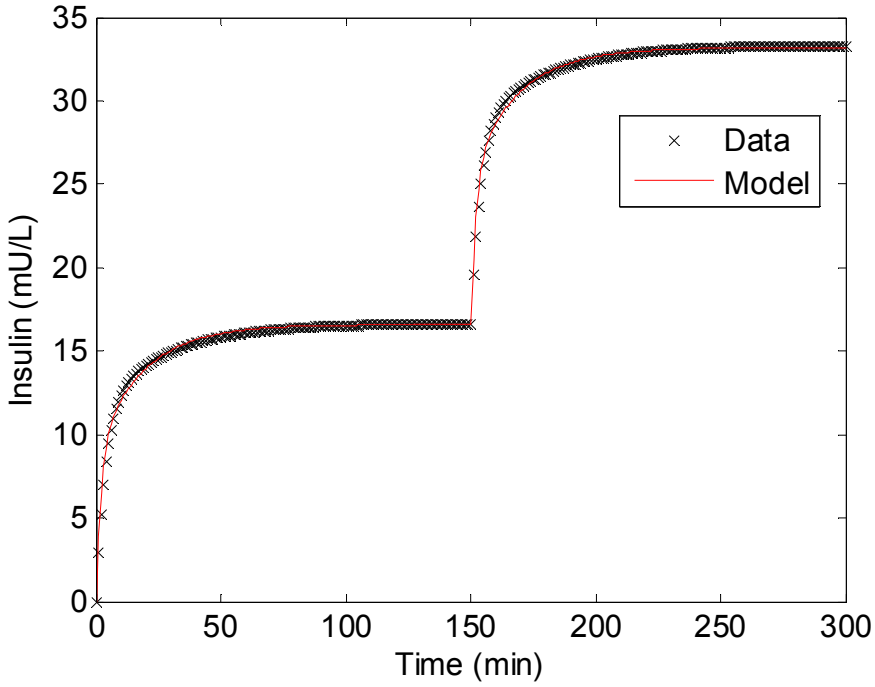

Figure 5-11: Two-compartment model fit for test data generated by two-compartment model. Data parameters are A_{01} = 0.2 min^{-1}, A_{12} = 0.05 min^{-1}, A_{21} = 0.06 min^{-1}, and V = 6 L. Model parameters are A_{01} = 0.2922 min^{-1}, A_{12} = 0.085 min^{-1}, A_{21} = 0.16 min^{-1}, and V = 4.12 L. The model fit appears to be directly on top of the data plot.

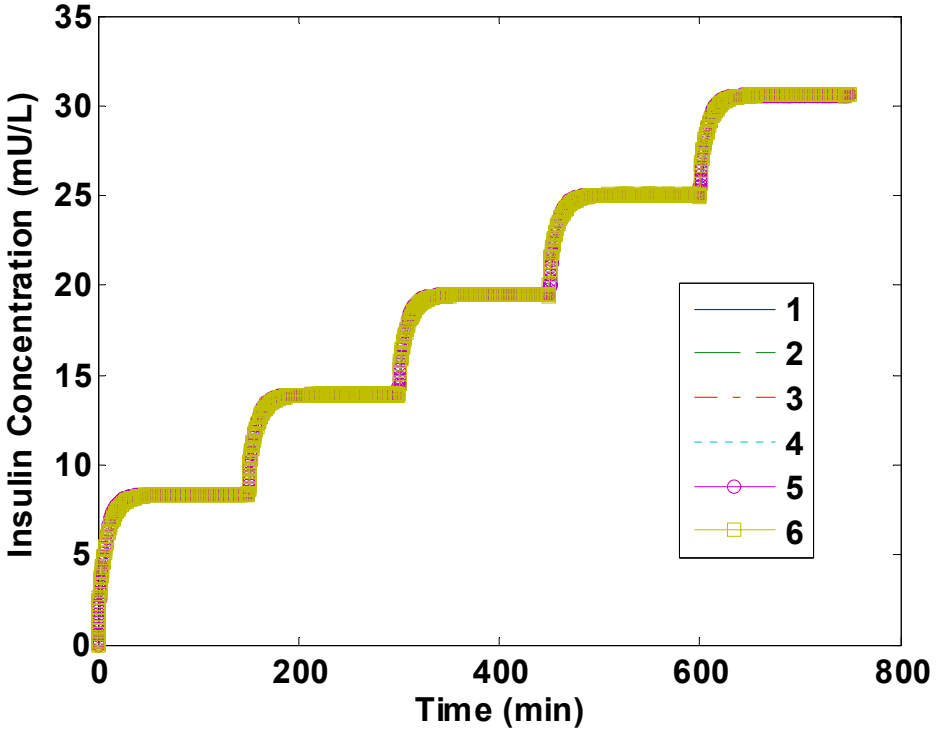

Figure 5-12: Generation of data for different parameter sets of two-compartment model. Model parameters based on estimation of two-compartment parameters using one-compartment test data. All parameter sets fit on the same trajectory, with very little difference among the predicted profiles. Each legend entry represents the optimal parameter set from that particular initial guess parameter set.

5.5 References

1. Bolie, V. W., "Coefficients of Normal Blood Glucose Regulation," *J. Clin. Invest.*, **39**, 783-788, 1960.

2. Tiran, J. and Galle K. R., "A Simulation Model of Extracellular Glucose Distribution In the Human Body," *Ann. Biomed. Eng.*, **3**, 34-46, 1975.

3. Tiran, J., Avruch, L. I., and Albisser, A. M., "A Circulation and Organs Model For Insulin Dynamics," *Am. J. Physiol.*, **237**, E331-E339, 1979.

4. Sorensen, J. T., "A Physiologic Model of Glucose Metabolism in Man and Its Use to Design and Assess Improved Insulin Therapies For Diabetes", Ph.D. thesis, Dept. Chem. Eng., Massachusetts Institute of Technology, Cambridge, 1985.

5. Rawlings, J. B., Miller, S. M., and Witkowski, W. R., "Model Identification and Control of Solution Crystallization Processes: A Review," *Ind. Eng. Chem. Res.*, **32**, 1275-1296, 1993.

6. Hipszer, B., Joseph, J., and Kam, M., "Pharmacokinetics of Intravenous Insulin Delivery in Humans With Type I Diabetes," *Diabetes Technology & Therapeutics*, **7**, 83-93, 2005.

7. Rawlings, J. B. and Ekerdt, J. G., *Chemical Reactor Analysis and Design Fundamentals*, Nob Hill, Madison, WI, 2002.

8. Johnson, R. A., Ed., *Miller & Freund's Probability and Statistics For Engineers, Sixth Edition*, Prentice Hall, Upper Saddle River, NJ, 2000.

9. Frost, D. P., Srivastava, M. C., Jones, R. H., Nabarro, J. D. N., and Sonksen, P. H., "The Kinetics of Insulin Metabolism In Diabetes Mellitus," *Postgrad. Med. J.*, **49**, 949-954, 1973.

10. Shampine, L. F. and Reichelt, M. W., "The MATLAB ODE Suite," *SIAM J. Sci. Comput.*, **18**, 1-22, 1997.

11. Constantinides, A. and Mostoufi N., *Numerical Methods For Chemical Engineers With MATLAB Applications*, Prentice Hall, Upper Saddle River, NJ, 1999.

12. Edgar, T. F. and Himmelblau, D. M., *Optimization of Chemical Processes*, McGraw-Hill, NY, 1988.

13. Home, P. D., Massi-Benedetti, M., Shepard, G. A., Hanning, I., Alberti, K. G., and Owens, D. R., "A Comparison of the Activity and Disposal of Semi-Synthetic

Human Insulin and Porcine Insulin In Normal Man By the Glucose Clamp Technique," *Diabetologia*, **22**, 41-45, 1982.

14. Sherwin, R. S., Kramer, K. J., Tobin, J. D., Insel, P. A., Liljenquist, J. E., Berman, M., and Andres, R., "A Model of the Kinetics of Insulin In Man," *J. Clin. Invest.*, **53**, 1481-1492, 1974.

CHAPTER 6

EXPLICIT CLOSED-LOOP CONTROL SIMULATIONS

6.1 Introduction

As previously discussed, Type I diabetes is a medical affliction associated with the body's inability to provide the necessary insulin to maintain normal glucose levels. While the metabolic pathways associated with glucose homeostasis are complex, it was shown in previous chapters that the system can be treated as a chemical process. Through either pharmacokinetic or physiologic modeling, the system's states, inputs, outputs, and parameters can be formulated and identified with patient data. By treating glucose metabolism as a chemical process, chemical engineering principles such as process control can be applied to maintain normal glucose levels.

An important part of the control process is the definition of all controlled, manipulated, and state variables. A simple system could be one in which only one variable is controlled with only one output. Specifically for glucose regulation, glucose would be the lone controlled variable and insulin would be the single manipulated variable. A more complex system could involve maintaining all the metabolites at certain levels. As discussed in previous chapters, the concentrations of other metabolites can affect glucose levels as well. This multi-output control could be designed such that all the hormones of significance could be used as manipulated variables.

Effective explicit closed-loop control can only be realized when the necessary sensors, control algorithms, and actuators (delivery systems) are developed. For an

intravenous delivery system, both the sensors and the pumps should be implantable. Sensors should be in place to give the values of all controlled variables at sample times on the order of minutes to provide minute-to-minute control of the variable. The implanted pumps should be able to supply all the manipulated variables for multiple days in order to prevent having to refill the reservoirs too frequently.

The control algorithm developed will depend on the availability of measurements for each species as well as the ability to effectively infuse the manipulated variable species. To date, most developed control methods focus on controlling glucose using insulin. The lack of effective fatty acid or amino acid sensors to be implanted makes the use of these species for feedback measurements in multivariable control infeasible at present. While recent research efforts have focused on the implementation of a control system utilizing glucagon, such work is relatively recent, and the large majority of glucose control still focuses on insulin as the single manipulated variable.

As discussed in Chapter 4, the use of models facilitates the investigation of control system effectiveness by allowing simulations to be performed that capture the glucose response to various conditions, including meal consumption and exercise. By implementing the control algorithm as the source of insulin secretion, the effectiveness of the control system with respect to maintaining normal glucose levels can be investigated without the use of experiments.

This chapter investigates the effectiveness of explicit closed-loop control through simulations with existing patient models. Various methods of single input-single output control are applied to study the effectiveness of insulin infusion algorithms with respect

to maintaining acceptable glucose levels in different situations encountered by diabetic patients.

6.2 Methods

To study the effectiveness of different control algorithms, the control algorithms are used to determine the infusion rate for various patient models. The ability of the each controller to maintain normal glucose levels in response to meal and exercise is investigated by noting the glucose response and the insulin infusion profile as a function of time for each situation, using each model.

6.2.1 Patient models

Three different patient models have been used to assess closed-loop controller performance. The first is the minimal model of Bergman and Cobelli [1]. The modified form by Furler et al. [2] to describe dynamics without pancreatic insulin release is described by equations (6.1)-(6.3).

$$\frac{dG(t)}{dt} = -P_1\left(G(t) - G_b\right) - G(t)X(t) + D(t) \tag{6.1}$$

$$\frac{dX(t)}{dt} = -P_2\left(X(t) - X_b\right) + P_3\left(I(t) - I_b\right) \tag{6.2}$$

$$\frac{dI(t)}{dt} = -nI(t) + \frac{U(t)}{V} \tag{6.3}$$

G is the plasma glucose concentration, X is a term proportional to the insulin concentration in the "remote compartment", which represents the compartment of insulin action (i.e., insulin bound to liver and peripheral cells), and I represents plasma insulin levels. D represents an external glucose source, such as a meal or an oral or injected glucose dose. U represents an exogenous insulin source. The parameters P_1, P_2, P_3, and n represent first order kinetic elimination rates for each state variable, and V represents the insulin circulation volume. The model equations are derived from the pharmacokinetic diagram of Figure 2-1, as shown in Appendix A. The average parameter values for a Type I diabetic patient are given in Table 6-1.

To simulate control using an explanatory model, the Sorensen model [3] is used. Originally developed as a healthy patient model, it includes 3 additional ordinary differential equations (ODEs) to describe pancreatic insulin release as a function of glucose. To simulate a diabetic patient, the pancreatic insulin release term is set to zero, and the three ODEs of the secretion are eliminated. The resulting model consists of 19 ODEs describing glucose, insulin, and glucagon dynamics throughout the different organ systems of the body, including the gut, brain, blood, periphery, liver, and kidneys. The compartmental diagrams of the model are given in Figures 6-1 through 6-3. The model parameters and their literature values are given in the appendix.

Finally, because of its recent gain of acceptance among control engineers, Hovorka's model [4] will be used. The model equations are given in Appendix B, and the pharmacokinetic diagram of the model is given in Figure 2-3. The model's two glucose compartments and three insulin action compartments correspond to what most

reviewers say are the most accurate pharmacokinetic descriptions of glucose and insulin, including Sorensen [3] and Cobelli et al. [5].

6.2.2 Meal Models

To describe the absorption of a meal, the description of used by Fisher [6] is chosen, as given in Equation (6.4).

$$D(t) = A\,exp(-b(t - t_{meal})) \tag{6.4}$$

The parameter b represents the absorption rate of the meal. The parameter A represents the size of the meal. Because the integral of the equation from t_0 to infinity gives the total size of the meal, A can be determined to be the following quantity:

$$A = M_{meal} b \tag{6.5}$$

The parameter t_{meal} represents the time at which the meal begins digestion. Bequette [7] adds a 20 minute time constant to the meal to account for the physiological process of digestion before the glucose begins to appear in the blood. This time constant, interpreted as the inverse of the parameter b, is equal to 0.05 min^{-1}. When t is less than t_{meal}, the variable D is zero.

For Sorensen's model, Equation (6.4) is substituted into the gut glucose equation as a source of oral glucose. Hovorka's model [4] has its own meal model, described by Equation (6.6).

$$D(t) = \frac{M_{meal} A_{meal} t \, exp\left(-\frac{t}{t_{max}}\right)}{t_{max}^2} \tag{6.6}$$

The model is derived in Appendix F. The variable A_{meal} represents the percent availability of the meal consumed. The variable t_{max} represents the time, from the beginning of the meal consumption, for the absorption rate to reach its maximum. This model represents a meal as a two compartment chain. Each compartment has a kinetic elimination rate coefficient of $1/t_{max}$. Compartment one has no input, and is initially described as the amount of total available glucose. Compartment two has the output of compartment one as its input, and the absorption of glucose into the blood as its output. The meal absorption rate is described as the concentration in compartment two multiplied by its rate coefficient.

6.2.3 Exercise Models

Roy and Parker [8] and Lenart and Parker [9] proposed two different exercise models. Both models assumed that exercise increases metabolism, and that the increase in metabolic rates is best described as a function of the exercise levels, which are described by the current oxygen consumption levels as a percentage of maximum oxygen

consumption level, PVO_2^{max}. The first description is used with the minimal model to match published exercise data. It is combined with Equations (6.1) through (6.3) to give the total description of the patient, as shown in Equations (6.7) through (6.13)

$$\frac{dG(t)}{dt} = -P_1(G(t) - G_b) - X(t)G(t) + D(t) + G_{prod}(t) - G_{up}(t) \tag{6.7}$$

$$\frac{dX(t)}{dt} = -P_2(X(t) - X_b) + P_3(I(t) - I_b) \tag{6.8}$$

$$\frac{dI(t)}{dt} = -nI(t) + \frac{U(t)}{V} - I_e(t) \tag{6.9}$$

$$\frac{dG_{prod}(t)}{dt} = a_1 PVO_2^{max}(t) - a_2 G_{prod}(t) \tag{6.10}$$

$$\frac{dG_{up}(t)}{dt} = \left(a_3 PVO_2^{max}(t) + a_4\right) PVO_2^{max}(t) - a_5 G_{up}(t) \tag{6.11}$$

$$\frac{dI_e(t)}{dt} = a_6 PVO_2^{max}(t) - a_7 I_e(t) \tag{6.12}$$

$$\frac{dPVO_2^{max}(t)}{dt} = \left(\frac{1}{\tau_{ex}}\right)\left(-PVO_2^{max}(t) + PVO_{2,ultimate}^{max}\right) \tag{6.13}$$

The new state variables G_{prod}, G_{up}, I_e, and PVO_2^{max} represent the glucose production rate, glucose uptake rate, insulin removal rate, and exercise intensity, respectively. Each parameter a_i represents the kinetic rate coefficient for the increase or decrease in metabolic rate for each type of exercise enhanced process. The parameter τ_{ex} is the time constant for changing from one exercise level to another. The final parameter

of Equation (6.13) represents the maximum exercise level that will be achieved. The model is simple, basing rate increases on first or second order kinetics. Given the pharmacokinetic-type description of the exercise model in [8], this model is also applied to Hovorka's model.

The model in reference [9] was developed for use with the Sorensen model. It is similar to the model in reference [8] in that it is based on PVO_2^{max}, which is also described by Equation (6.13) in this model. However, there are some key differences that need to be mentioned. First, the reported blood flow rates had to be modified according to literature of reported blood flow for different exercise levels. Second, by the very nature of differences between the two model types, specifically their equations describing metabolism, the metabolic effects of exercise with respect to glucose production and uptake and insulin elimination had to be developed to fit the Sorensen model form. To do this, specific dimensionless multiplicative factors representing exercise contributions had to be developed. For glucose uptake, the multiplicative factor is described by Equation (6.14).

$$M_{PGU}^{E} = 1 + \frac{PGU_E(m_{EM})}{PGU_b} \tag{6.14}$$

The parameter m_{EM} represents the mass of exercise muscle and PGU_E represents the exercising muscle glucose uptake rate. It is described by Equation (6.15)

$$\frac{dPGU_E(t)}{dt} = \left(\frac{1}{\tau_{EGU}}\right)\left(-PGU_E(t) + ePGU_E\right) \tag{6.15}$$

The variable τ_{EGU} is the time constant associated with increasing glucose uptake from one exercise level to another level. The variable $ePGU_E$ represents the maximum uptake rate for a particular level of exercise. The effect of exercise on glucose production is found the same way, using the basal production rate and the mass of exercising muscle. The primary difference is that the production rate of exercising muscle is set equal to the uptake rate of exercising muscle, assuming glucagon is able to produce enough glucose to supply the amount needed in increased uptake. This is shown in Equation (6.16).

$$M_{HGP}^{E} = 1 + \frac{PGU_E m_{EM}}{HGP_b} \tag{6.16}$$

Finally, regarding insulin removal, insulin peripheral uptake was modified to account for the observation that uptake increases by a factor of 3.4 when 100% of a person's muscle is active [9]. This is shown Equation (6.17).

$$PIU = \frac{I_P\left(1 + 2.4\left(\frac{m_{EM}}{m_{TM}}\right)\right)}{\left[\frac{1-F}{FQ_P^I} - \frac{\tau_P^I}{V_{PI}}\right]} \tag{6.17}$$

The parameter m_{TM} represents the total mass of muscle of the individual. The remaining model parameters are defined in Appendix C. The authors [9] modified the parameter *F* in order to maintain constant insulin uptake rates in response to increased blood flow rates. All exercise parameters for the models in references [8] and [9] are given in Table 6-2.

6.2.4 Control Algorithms

To investigate the effectiveness of control in response to meals and exercise in diabetic patients, several control algorithms were employed. The algorithms are used to determine the infusion parameter *U(t)* for each model. Each algorithm will now be described.

The first method studied was a simple feedback control system utilizing the proportional plus integral plus derivative (PID) control algorithm. The feedback process control diagram is shown in Figure 6-4. The PID algorithm is described by Equation (6.18).

$$U(t) = U_{basal} + Kc\left[\left(y(t) - y_{setpoint}\right) + \frac{1}{\tau_I}\int_0^t \left(y(t) - y_{setpoint}\right)dt + \tau_D \frac{d\left(y(t) - y_{setpoint}\right)}{dt}\right] \tag{6.18}$$

The parameter K_c is the proportional gain, τ_I is the integral time, and τ_D is the derivative time. The variable *y* corresponds to the system outputs. In this case *y* corresponds to the system's glucose concentration. The controller is based on the error in

y relative to its set point. To maintain basal conditions, $y_{setpoint}$ is set to be the basal glucose concentration. The controller was designed for each model by subjecting the model to a step change in the insulin infusion rate, and then fitting the data by a first order plus time delay (FOPTD) model, as shown by Equation (6.19).

$$y = \begin{cases} 0 & (t \le \theta) \\ KM\left(1 - exp\left(-\frac{t-\theta}{\tau}\right)\right) & (t > \theta) \end{cases} \tag{6.19}$$

K is the process gain, defined as the change in the output variable in response to a unit change in the manipulated variable. M is the magnitude of the step change, τ is the time constant, defined as the time for the output to reach approximately 63% of its steady state value, and θ is the time delay in the process. Given the step response data, a FOPTD model can be regressed. Once the FOPTD model was determined, the controller tuning parameters K_c, τ_I, and τ_D were calculated using the Internal Model Control (IMC) PID tuning guidelines given in reference [10]. The controller tuning equations are shown in Equations (6.20) through (6.22).

$$K_c = \left(\frac{1}{K}\right)\frac{\tau + \frac{\theta}{2}}{\tau_c + \frac{\theta}{2}} \tag{6.20}$$

$$\tau_I = \tau + \frac{\theta}{2} \tag{6.21}$$

$$\tau_D = \frac{\tau\theta}{2\tau + \theta} \tag{6.22}$$

The parameter τ_c is the desired closed-loop process time constant. Increasing the value of τ_c results in increasingly conservative control. For parameter tuning, τ_c was taken to be equal to the process time delay. Once the PID tuning parameters were initially determined, they were tuned by increasing and decreasing the different actions in order meet the desired control objectives. These objectives are discussed in the next section.

The second type of algorithm used employs feedforward control. Feedforward control is based on the idea that, given a known value of the disturbance, a controller can be designed such that corrective action is taken before the disturbance enters the process. Ideally, the disturbance never affects the process. While this is not the case in reality, feedforward control is able to significantly reduce the effects of measured disturbances on a process. Figure 6-5 shows a schematic of feedforward control, and Figure 6-6 shows a feedforward control scheme combined with a feedback scheme.

The feedforward control algorithm is defined by converting the patient model into transfer functions for the manipulated variable and the disturbance variable. For low order models this can usually be performed manually. For higher order models, such as the Sorensen model, it is best to develop FOPTD models for the different input variables, and developing the control law based on the simplified models. Once the transfer functions for each input is determined, the feedforward controller is determined from Equation (6.23).

$$G_{ff} = -\frac{G_D}{G_U} \tag{6.23}$$

In Equation (6.23) the variable G_D represents the disturbance transfer function, and G_U represents the manipulated variable transfer function. As previously mentioned, this control setup is usually used in combination with a feedback controller. The combined feedback/feedforward method was also employed as a potential control system.

The third type of control system employed model predictive control (MPC). MPC uses measurements of the system outputs and a model of the system to predict future state and output values. The model predictive control block diagram is given in Figure 6-7. Based on the predictions, a control scheme is given in which the value for the manipulated variable is determined for the next M time steps in order to bring the system to a desirable level. The control scheme is determined by minimizing an objective function of the outputs and inputs. Constraints can also be incorporated into the MPC problem in order to produce a control scheme that keeps the system within necessary operating conditions. The typical setup for MPC implementation of a linear model is given in Equations (6.24)-(6.27) [11].

$$\min_{u^N} \Phi_k = x_{k+N}^T H x_{k+N} + \Delta u_{k+N}^T S \Delta u_{k+N} +$$

$$\sum_{j=0}^{N-1} \left(x_{k+j}^T C^T Q C x_{k+j} + u_{k+j}^T R u_{k+j} + \Delta u_{k+j}^T S \Delta u_{k+j} \right) \tag{6.24}$$

$$u_{min} \le u_{k+j} \le u_{max}, j = 0, 1, \ldots, N\text{-}1 \tag{6.25}$$

$$y_{min} \leq y_{k+j} \leq y_{max}, j = j_1, j_1 + 1, \ldots, j_2 \quad (6.26)$$

$$\Delta u_{min} \leq \Delta u_{k+j} \leq \Delta u_{max}, j = 0, 1, \ldots, N \quad (6.27)$$

Equation (6.24) represents the linear model and quadratic objective function. *C, H, Q, R,* and *S* are weighting matrices, specified by the designer. Equations (6.25) through (6.26) represent the system constraints. Once the optimization problem is solved, the first control move is executed, and the problem is resolved at the next step.

As a final method of control, a physiological pancreatic secretion model was used to determine the body's natural response to glucose. For this controller, Sorensen's pancreas model [3] was used. The equations and model parameters for pancreatic insulin release for a healthy patient are given in the Appendix.

6.2.5 Control Objectives

The overall objective of control with respect to insulin dependent diabetes is to mimic a healthy pancreas as much as possible. In this regard, the controller should be able to keep glucose levels at the patient's basal level during normal fasting conditions. Ideally, the patient should remain in the normal range after meal consumption and during exercise as well.

These objectives were considered when designing different controllers for different patient models, using average parameters. First, the basal insulin infusion rate allowing glucose levels to remain at their steady-state, basal values was determined. Then, beginning with a simple feedback algorithm, a controller was developed to try to

satisfy the objectives with respect to a meal disturbance. If the controller type was not successful, a different type of controller was tested. If the controller was successful, it was then used to maintain glucose levels for exercise.

After the performance of the control strategies was determined, the model was investigated in order to determine why a given control strategy was or was not successful. With these investigations in place, different conclusions can be drawn regarding the ability to apply explicit process control to a diabetic patient.

6.2.6 Computational Methods

To perform the control simulations, three different computational steps needed to be performed. First, each dynamic model was programmed in order to simulate its behavior when no controller is present. Second, each control system was designed. Finally, the control system was implemented with each patient model in order for closed-loop simulations to be performed.

MATLAB was used to perform all simulations. The MATLAB function ode45 [12], which is based on the 5^{th} order Runge-Kutta Dormand-Prince Pair, was used to solve the sets of differential equations,. To determine the steady state insulin infusion rates, each state variable was set to zero, and the equations were algebraically solved to determine the basal state values. Given the basal state values, the basal infusion rate could easily be calculated from state equations involving insulin infusion.

For the Sorensen model, because of the nature of the equations, initialization required an iterative process. The insulin basal values of the diabetic patient are assumed

to depend on the steady state infusion rate. The nature of the glucose equations are such that a plasma glucose value is needed to determine the glucose value of the other states. Thus, the iteration is performed for a specific infusion rate by guessing a plasma glucose value, using it to determine the initial values of glucose concentrations in the various tissues (liver, periphery, gut, etc.), and then using those values to determine if the plasma glucose values match. The MATLAB source code for this initialization is provided in Appendix G, and Sorensen [3] discusses it more fully, including iteration diagrams.

To design the PID controllers, FOPTD models were developed using the Microsoft Excel Solver to minimize the sum of squared residuals. Sorensen provided the FOPTD models for his diabetic patient model in reference [3]. As previously mentioned, the PID parameters were determined using reference [10]. PID control was implemented in MATLAB by treating U(t) as the manipulated variable. Feedforward control and feedforward-feedback control were implemented using MATLAB Simulink. MPC was implemented using the Model Predictive Control Toolbox in MATLAB. To simulate the healthy patient response, the healthy patient Sorensen model was used.

6.3. Results

6.3.1 Generation of Healthy Patient Response

The healthy glucose and insulin responses for a 50 g oral glucose disturbance and an exercise session are given in Figures 6-8 and 6-9. The healthy model glucose response shows a maximum spike to slightly under 12 mmol/L. While this is high for a meal, it is a reasonable expectation for a glucose load of this size, as shown by oral glucose

tolerance test (OGTT) data in references [3] and [13]. As glucose levels fall, they fall slightly below 4 mmol/L before leveling off at the basal rate. All of this occurs within two hours of the ingested oral glucose load. The healthy patient exercise model shows a 30 minute exercise period at a moderate intensity of 60 % VO_2^{max}. As the figure shows, the glucose level stays above 4 mmol/L during and after exercise. Glucose levels fall slightly initially as the blood flow rates change. This is followed by a sharp rise in glucose resulting from the rapid increase in glucose production relative to uptake. After exercise, a short spike is observed as the blood flows return to normal. This is followed by a sharp drop resulting from total glucose production decreasing much faster than total uptake. As uptake rates return to normal, the steady state condition is approached.

6.3.2 Control of Glucose Using the Minimal Model

Using the model parameters of Table 6-1, the steady state insulin infusion rate to maintain glucose levels at 4.5 mmol/L was determined to be approximately 16.667 mU/min. Note that for $P_1 = 0$ min^{-1}, the model assumes that only insulin-dependent uptake occurs. As such, any glucose in excess of what the current insulin infusion can act on will simply remain in the circulation. In this way, the glucose compartment of a Type I diabetic patient can be considered similar to a storage tank.

Figure 6-10 shows the simulation of a diabetic patient ingesting 50 g of glucose orally with only the basal infusion of insulin to enhance glucose uptake. Upon ingestion, the glucose concentration approaches a new steady state at approximately 28 mmol/L. When insufficient insulin is available to enhance glucose uptake, nothing beyond the

basal glucose uptake will occur. Because glucose-dependent uptake is assumed to be non-existent, the additional glucose is simply added to the circulation, as in the situation in which more of a substance is added to a storage tank.

Figure 6-11 shows the glucose response to a step change in the insulin infusion rate. The model clearly demonstrates the behavior of an integrating system, as the step change causes a continuous decline in the glucose level. The parameters of the FOPTD model are given in Table 6-3, as are the PID control parameters. The glucose response to the 50 g glucose ingestion with the tuned PID controller is shown in Figure 6-12. The two lines included in the glucose plot represent the upper and lower limits observed by a healthy patient in response to the same glucose input. The controller gain and derivative time were maximized to decrease the glucose excursion to as small in magnitude as possible. The integral time of 3300 minutes essentially eliminates integral action. The addition of integral action results in heavy oscillations in the glucose response that often results in severe hypoglycemia being realized, as well as steady state offset. At the optimal control configuration, the glucose excursion still rises above the specified upper limit. The insulin infusion rate had no upper limit, and the resulting infusion rate of nearly 600 mU/min is not sufficient to prevent the excursion. The infusion rate is clearly above the rate of the healthy patient and my be infeasible as an upper limit for an infusion pump.

Given the relatively poor performance of PID control to effectively control the glucose response, at even high infusion rates, feedforward control was employed in order to provide control before the glucose excursion is realized. Because the feedforward

controller design equation is based on process and disturbance variable transfer functions, the minimal model was subjected to a step increase in the disturbance variable, and a first order plus time model was estimated from the response. The model parameters are given Table 6-3. Because there is no time delay in the disturbance model, the resulting feedforward equation would be physically unrealizable, as the negative delay implies the controller responds in anticipation of a disturbance that has yet to be measured. The controller is approximated by adding the 30 minute process delay to the time constant to get the following feedforward controller, which is physically realizable.

$$G_{ff} = \frac{1.08 \times 10^5 (3331s + 1)}{6.44(1.08 \times 10^5 s + 1)} \tag{6.28}$$

Figure 6-13 shows the glucose response with feedforward control only, and Figure 6-14 shows the response when feedforward control is implemented with a PID controller to provide control of both the excursion and the glucose levels. As Figure 6-13 shows, because the controller is based only on the disturbance, there is no counter-regulation as glucose is falling to prevent hypoglycemia. In addition, the gain is still not large enough to prevent the excursion, and it appears that infusing insulin in response to the oral glucose at the time of appearance does not offer any advantages to PID control. Figure 6-15 shows that as PID control is implemented with feedforward-control, a tradeoff exists between the approach of hypoglycemia vs. hyperglycemia. The originally developed feedforward controller, when used in conjunction with PID control, prevents

the hyperglycemia excursion, but at the cost of severe hypoglycemia. Because this can lead to coma or death, such an occurrence is not an option in design. To prevent this from happening, the feedforward controller gain was reduced by two orders of magnitude, and the results are nearly identical to those of PID control alone. Therefore, feedforward control appears to offer no advantages to PID control.

For the MPC controller to be developed, the minimal model first had to be linearized by performing a Taylor series expansion at the steady-state basal condition. Given the state-space model, the MPC controller is designed by selecting values for the weights, *H, S, Q* and *R*, the constraints on glucose and insulin infusion, and the control and prediction horizons. For MPC design, *Q* was set to 1 and *R, H,* and *S* were set to zero. The only constraint established was that the insulin infusion rate could not go below zero. Finally, both horizons were set to 14 discrete time steps, assuming a sample time of 5 minutes. Figure 6-15 shows the linearized minimal model MPC-controlled glucose response to the 50 g glucose sample. By adjusting the control and prediction horizons, the controller can be adjusted to minimize the excursion or prevent hypoglycemia, but the minimum excursion that prevents hypoglycemia is still 20 mmol/L. To be consistent, the control profile was used on the non-linearized minimal model, and the results are shown in Figure 6-16. From the figure it can be seen that the actual model and the linearized model give quite different responses. The actual glucose excursion is consistent with those previously shown for this model. The figure also shows that control based on the linear model would result in severe hypoglycemia. It is conceivable, however, that a nonlinear MPC controller would likely be better able to handle the hypoglycemia, as the

linear controller applied was not adjusting in real time as a nonlinear controller would. The linear controller could be adjusted in real time for the linear model, but only the data record of the linear profile was used for the nonlinear model. Regardless, both controllers were still unable to prevent hyperglycemia while using perhaps infeasible insulin rates, meaning that MPC controlled glucose poorly.

Finally, the nonlinear pancreas model of Sorensen [3] was used to simulate a controller that emulates human behavior. It should be noted, however, that an investigation of the pancreas model reveals that pancreatic insulin release is simply being modeled as a nonlinear proportional-plus-derivative (PD). Nonetheless, given its success in predicting OGTT responses in healthy patients, it was employed in its exact form, as shown in Figure 6-17. Both hyperglycemia and severe hypoglycemia are predicted, meaning that either the Sorensen pancreas is not an accurate portrayal of the healthy pancreas, or that certain shortcomings of the minimal model prevent it from being controlled, even by natural means.

While it is possible that neither model is adequate, there are shortcomings to the minimal model that may render control impossible. First is the assumption that P_1 is zero for a Type I diabetic patient. This parameter set was given by Furler et al. [2] and has been used by other control engineers, including Fisher [6], Ollerton [14], and Bequette [7]. As previously mentioned, this implies that glucose can neither be produced nor taken up independently of insulin. Both Sorensen and Hovorka assume that glucose can contribute to uptake and production in the absence of insulin, and both models are preferred to the minimal model today. Allowing P_1 to be nonzero would naturally lead to

increased glucose uptake at high insulin, as well as increased production at low insulin. Also problematic with the minimal model is that the single kinetic rate coefficient for all insulin binding, P_3, is consistently on the order of 10^{-4} min^{-1}, a full two orders of magnitude slower than other processes. This leads to the 30 minute time delay as seen by the FOPTD regression. Sorensen and Hovorka improve upon this by including multiple action terms, which allow certain processes to occur much quicker than others, as binding is not considered slow for each process. From a control standpoint, this could be overcome by being able to adjust the manipulated variable before the disturbance is encountered, such as through the priming bolus that nearly every successful control implementation with the minimal model has used. This could also be used to provide feedforward control if the controller was able to measure the disturbance in real time, but the disturbance was subject to some time delay that prevented it from affecting glucose immediately. Physiologically, this may be what the incretins, especially glucagon-like peptide-1, are actually doing. Perhaps by being released in response to glucose in the gut, and then causing insulin release, insulin is being released into the blood before the glucose has been passed from the GI tract.

6.3.3 Control of Glucose Using the Sorensen Model

The Sorensen model for a diabetic patient is unique in that the steady state conditions are a function of the steady state infusion rate. This is in contrast to the minimal model, in which a specific rate is given for a specific basal set of conditions, and the integrating behavior of the model results in the rapid increase or decrease in glucose

concentration. To remain consistent, the basal condition of 4.5 mmol/L and 15 mU/L were chosen for glucose and insulin respectively. Trial and error was then used to determine which steady infusion rate yielded this basal condition. The basal insulin infusion was found to be approximately 21.45 mU/min.

Figure 6-18 shows the Sorensen model glucose response to a 50 g glucose source. By inspection of the figure, two things are evident. First, there is no integrating behavior, as the glucose level is restored to normal in spite of only the basal insulin. This shows that glucose is able to mediate uptake independently of insulin. Second, the excursion is minimal, already lower than any controller was able to achieve for the minimal model. Given the relatively low magnitude of the excursion, the first type of control attempted was simply proportional control, without any integral or derivative action. The response with this controller is shown in Figure 6-19 with a controller gain of 13 (mU/min)/(mmol/L). The Sorensen model is easily controlled using the simplest control algorithm that can be developed. Neither hyper- nor hypoglycemia are ever approached, and the maximum insulin infusion is less than even the maximum of the pancreas model used to describe a healthy patient.

The ease at which the Sorensen model is controlled can be explained by an investigation of the model glucose response at steady state with no insulin infusion, as shown in Figure 6-20. Given no insulin, the Sorensen model predicts a glucose concentration below 10 mmol/L. In reality, untreated Type I diabetic patients typically achieve glucose levels between 20 and 70 mmol/L [15]. Given this discrepancy, the Sorensen model appears to overestimate the effect of glucose levels on the body's

glucose uptake rates into liver and muscle cells, as less insulin is required to bring glucose to a certain level than is expected in a patient.

Mathematically, these shortcomings appear in the liver glucose uptake equations and curve fitting of Sorensen's development work [3]. First, an investigation of the Sorensen model plots of the effect of glucose on uptake shows that the data does not fit the mathematical representation, with the model predicting nearly twice the glucose uptake than what was observed in data for high glucose values. Second, data were not used to fit the insulin contribution to uptake. Assumptions based on canine studies were used to develop the equation specifying that tripling the insulin concentration results in a doubling of the uptake rate over time. Finally, a plot of the predicted uptake vs. actual uptake shows a poor fit, in which the predicted uptake is usually greater than the actual uptake observed. Given the ease of control and the physiological shortcomings, the Sorensen model was not used in further studies in this work.

6.3.4 Control of Glucose Using the Hovorka Model

The steady state initial condition was determined by defining the basal glucose level, and then setting each dynamic equation to zero. The basal insulin infusion was found to be 7.3 mU/min. Given the basal condition, the model glucose response to the 50 g glucose ingestion with a basal amount of insulin being provided is shown in Figure 6-21. Like the Sorensen model, glucose mediated uptake does appear to play a role in naturally decreasing glucose levels in response to the input. However, the process is

more gradual than that shown by the Sorensen model, implying that role of glucose in uptake is not emphasized as strongly as it is by the Sorensen model.

Given the small magnitude of the glucose excursion, proportional control was initially employed to try to control the process. The results are shown in Figure 6-22. Simple control based only on a proportionality of the glucose residuals is shown to be all that is needed for tight glucose control. Neither hyper- nor hypoglycemia are approached, and glucose values are brought to normal very rapidly. Figure 6-24 show the controller's ability to regulate glucose during 30 minutes of moderate (PVO_2^{max} = 60) exercise. Two observations can be made regarding the figure. First, it appears that a new steady state is reached after exercise. Mathematically, this results from the glucose uptake rate being modeled much slower than the rate used in the exercise model used with the Sorensen model. If the model parameters were modified to match the physiological considerations used in Parker's other exercise model, this offset would not occur, as the glucose levels would return to normal much faster. Second, even with the offset, the change in glucose from the basal level is minimal, showing that the controller is able to maintain normal levels during both meals and exercise.

The ease of control with the Hovorka model brings into question the validity of the model. If the model is indeed accurate, then how inaccurate can the Sorensen model actually be when very similar simulation results were produced? One major difference between the models is that when insulin is removed, the glucose concentration becomes steady at 22.4 mU/L, a quantity that is consistent with physiological observations. So

whether the model is inaccurate or not, the Sorensen model still has fundamental issues that should be resolved before its use is acceptable.

One noticeable characteristic of the Hovorka model is the use of relatively low insulin values to achieve a certain glucose level. The basal insulin level calculated for this Hovorka model is considerably smaller than the values determined for the minimal and Sorensen models, as well as the reported average values of basal secretion from the pancreas [14]. In addition, the amount of insulin used to reject the glucose disturbance was less than a third of the insulin secretion of the healthy pancreas model used by Sorensen. Based on these findings, the Hovorka model may have a problem with overpredicting the effects of insulin on metabolism. One difference between the model of Hovorka and the model used in this work is that Hovorka's model is based on subcutaneous infusion, whereas the control simulations assume intravenous infusion. This difference was accounted for by eliminating time constants associated with insulin transport from the subcutaneous tissue to the blood. It may be possible that the over prediction of insulin loss during the subcutaneous infusion may cancel the over-prediction of action from the actual plasma insulin.

6.4 Conclusions

Control of glucose during an ingestion of an oral glucose load was simulated using the minimal model, the Sorensen model, and the Hovorka model. Using the minimal model, no method of closed-loop control proved effective at keeping glucose levels below a hyperglycemic limit without also experiencing severe hypoglycemia.

These results may be a result of assuming no glucose-dependent uptake or production of glucose. The assumption of a single insulin action that is characterized by very slow kinetic rates results in long time delays for the model. With the Sorensen model, control can easily achieved by simply using proportional control. However, given the relatively low glucose values at zero insulin, as well as the poor agreement between liver glucose uptake data and the Sorensen uptake model, the Sorensen model has physiological shortcomings that prevent the simulation results from being considered accurate. Using the increasingly popular Hovorka model for control simulations resulted in proportional control being highly effective at maintaining normal glucose levels in response to both a meal and exercise. However, the ability of low insulin levels relative to pancreatic secretion to effectively control glucose brings up the possibility that the Hovorka may overestimate the role of insulin in glucose metabolism.

Assuming that Hovorka's model is indeed accurate, explicit-closed loop control appears to be a feasible method of use in the treatment of insulin dependent diabetes mellitus. However, such control will depend on other factors, including the development of effective implantable sensors and an implantable infusion pump. In addition, the ability of the controller to handle measurement noise, sensor time delays, and delays in the changing the pump flow rate will also have to be investigated. Such considerations do not have to be made with implicit closed-loop control, the focus of the next chapter.

Table 6-1: Minimal Model Patient Parameters For Type I Diabetic Patients [2]		
Parameter	**Value**	**Units**
P_1	0	min^{-1}
P_2	0.025	min^{-1}
P_3	0.000013	$L\ mU^{-1}\ min^{-2}$
n	5/54	min^{-1}
V	12.0	L

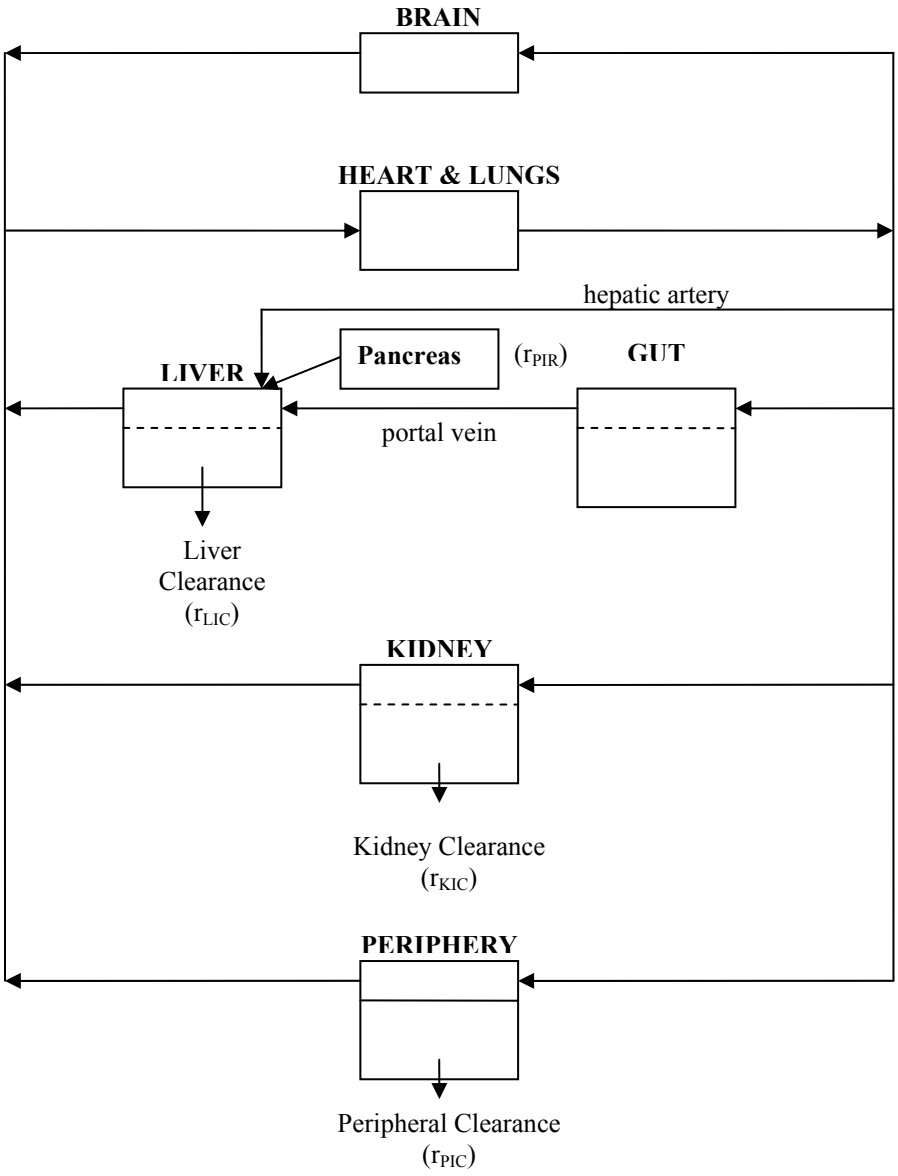

Figure 6-1: Flow diagram of the Sorensen insulin model [3]. Material flow is represented by the arrows. The dotted lines represent an interface at which mass transfer between intercompartmental spaces can occur. The solid line within a compartment represents a barrier that prevents intercompartmental mass transfer.

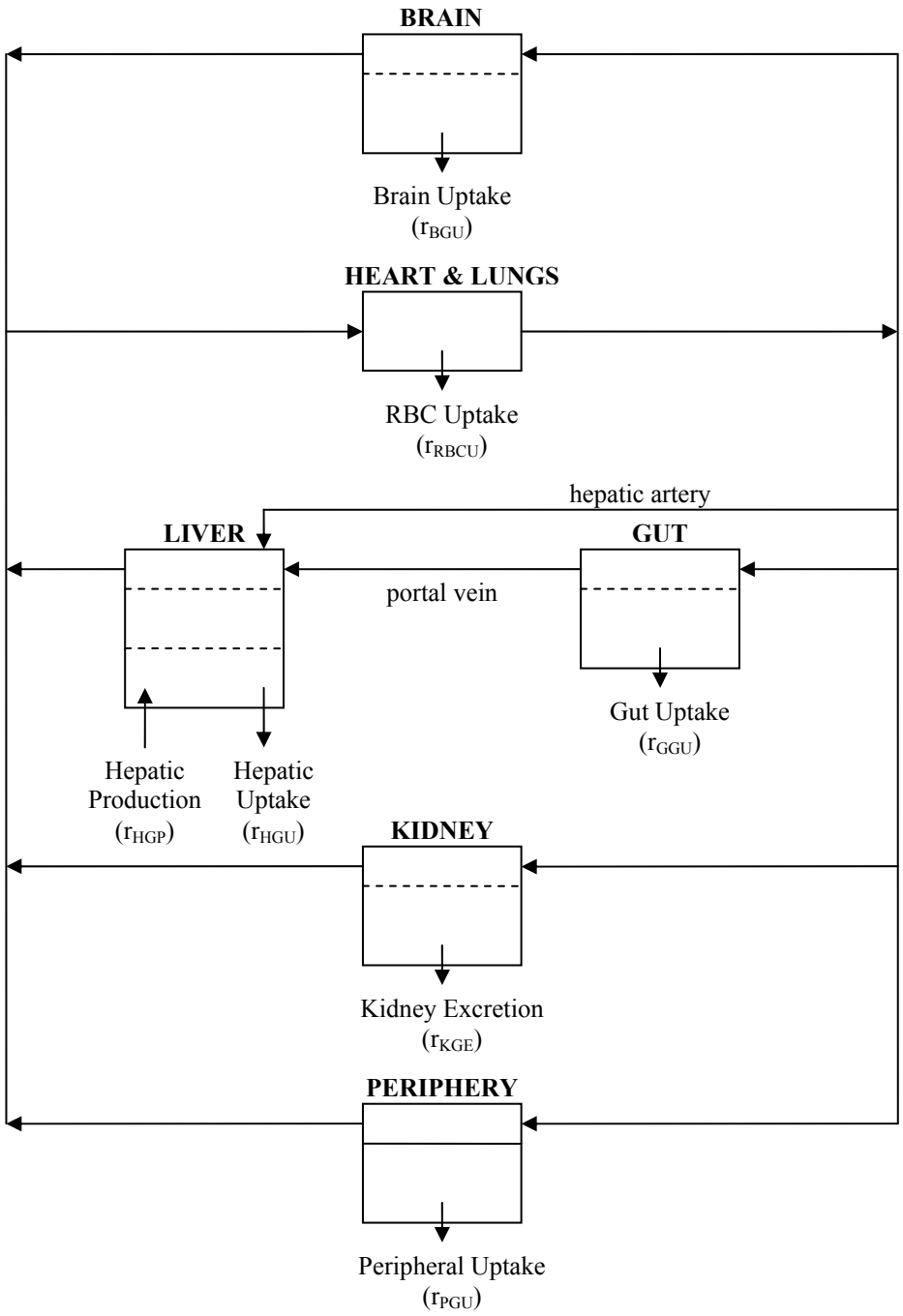

Figure 6-2: Flow diagram of the Sorensen glucose model [3].

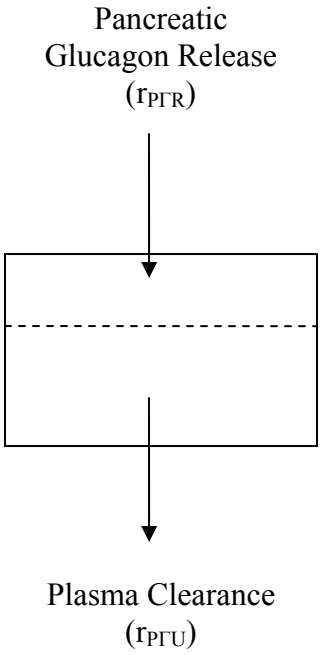

Figure 6-3: Flow diagram of the Sorensen glucagon model [3]. Arrows represent inflow and outflow of material through a compartment. The dotted line represent an interface for mass transfer for the two compartmental spaces of the glucagon compartment.

Table 6-2: Model Parameters For the Exercise Models For Minimal Model [8] and Sorensen Model [9]			
Parameter	**Model**	**Value**	**Units**
a_1	Minimal	6.11×10^{-4}	mmol L^{-1} min^{-1}
a_2	Minimal	0.9	min^{-1}
a_3	Minimal	5.56×10^{-8}	mmol L^{-1} min^{-1}
a_4	Minimal	7.22×10^{-6}	mmol L^{-1} min^{-1}
a_5	Minimal	0.00002	min^{-1}
a_6	Minimal	0.00025	mU L^{-1} min^{-1}
a_7	Minimal	0.009	min^{-1}
τ_{EX}	Minimal	5/3	min
τ_{EX}	Sorensen	5/4	min
τ_{EGU}	Sorensen	30	min
$ePGU_a$ ($PVO_2^{max} = 8$)	Sorensen	0	mg min^{-1} kg^{-1}
$ePGU_a$ ($PVO_2^{max} = 30$)	Sorensen	32	mg min^{-1} kg^{-1}
$ePGU_a$ ($PVO_2^{max} = 60$)	Sorensen	85	mg min^{-1} kg^{-1}
Q_G^L ($PVO_2^{max} = 30$)	Sorensen	9.8	dL min^{-1}
Q_G^L ($PVO_2^{max} = 60$)	Sorensen	6.1	dL min^{-1}
Q_G^K ($PVO_2^{max} = 30$)	Sorensen	8.1	dL min^{-1}
Q_G^K ($PVO_2^{max} = 60$)	Sorensen	5.3	dL min^{-1}
Q_G^P ($PVO_2^{max} = 30$)	Sorensen	50.6	dL min^{-1}
Q_G^P ($PVO_2^{max} = 30$)	Sorensen	99.1	dL min^{-1}

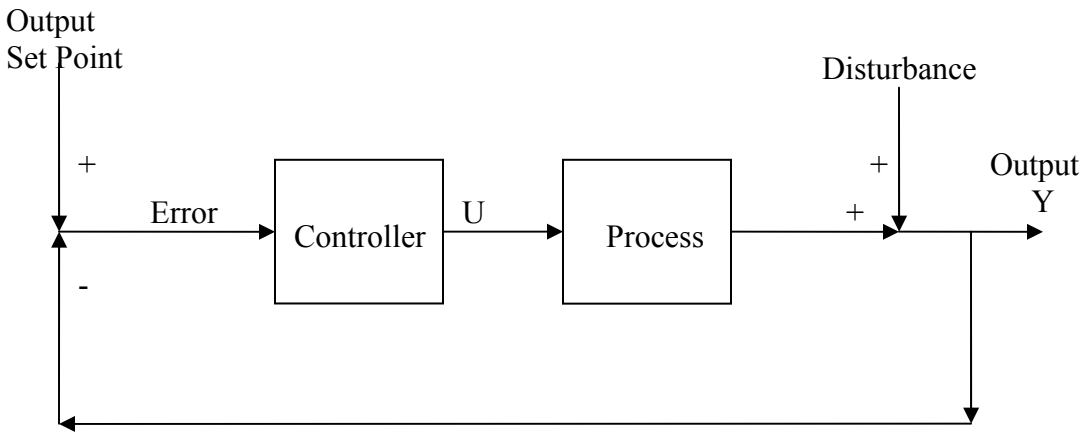

Figure 6-4: Schematic diagram of a PID feedback control process. At a point where two arrows intersect, the plus or minus indicates that the particular signal is being added or subtracted at the junction. The output signal is compared to the setpoint, and a PID control action is taken based on this measurement to produce U. U and the disturbance both interact with the process to result in the new output value.

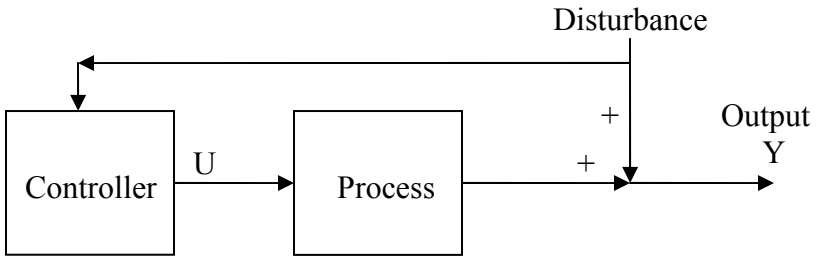

Figure 6-5: Schematic of a feedforward control process. The plus signs at the intersection of arrows means the two signals are added. The controller output, U, is determined by the disturbance. The process then interacts with both the disturbance and the output variable to produce the system output.

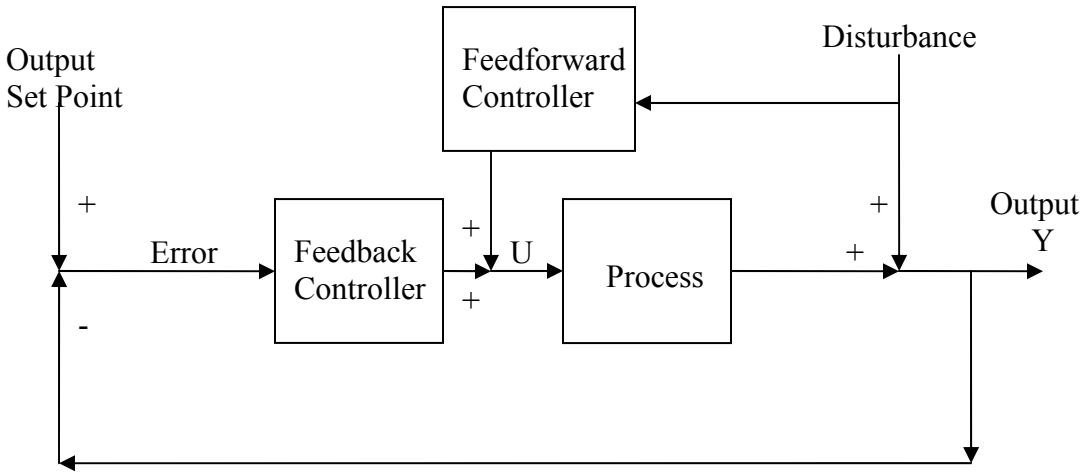

Figure 6-6: Schematic of combined feedforward and feedback control. The feedforward control signal is determined for a measurement of the disturbance, and the feedback control signal is based on output signal error relative to the set point. The two signals are combined to give U(t), the process input. The process interacts with the input and the disturbance to produce the output signal, Y.

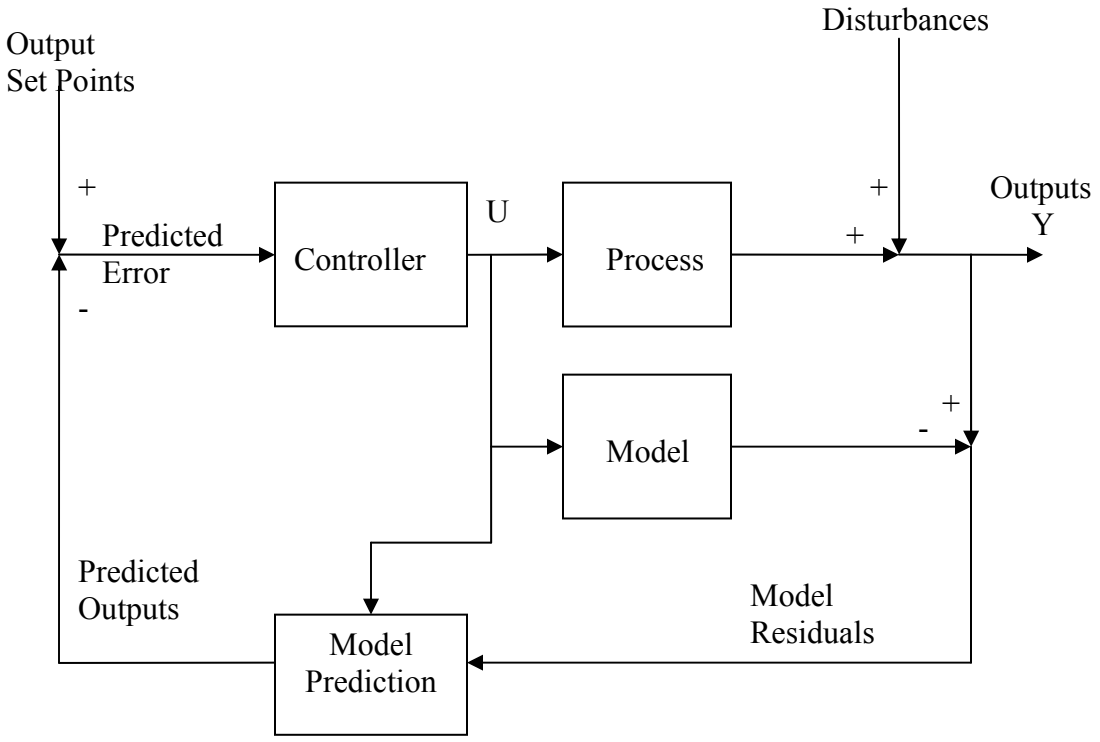

Figure 6-7: Schematic diagram of model predicted control. Based on the current input, a model is used to predict the value of the output. The actual measured output is used to determine the model residual. The residual is used to more accurately predict future outputs, based on the current process input U. Given the output setpoints and output predictions, the controller determines the optimal U profile to minimize a specified objective function. If the disturbance can be measured, it can be used with the predictor to develop a feedforward-feedback controller. If the setpoints change, the optimal determination of setpoints can also be tied to the MPC schematic.

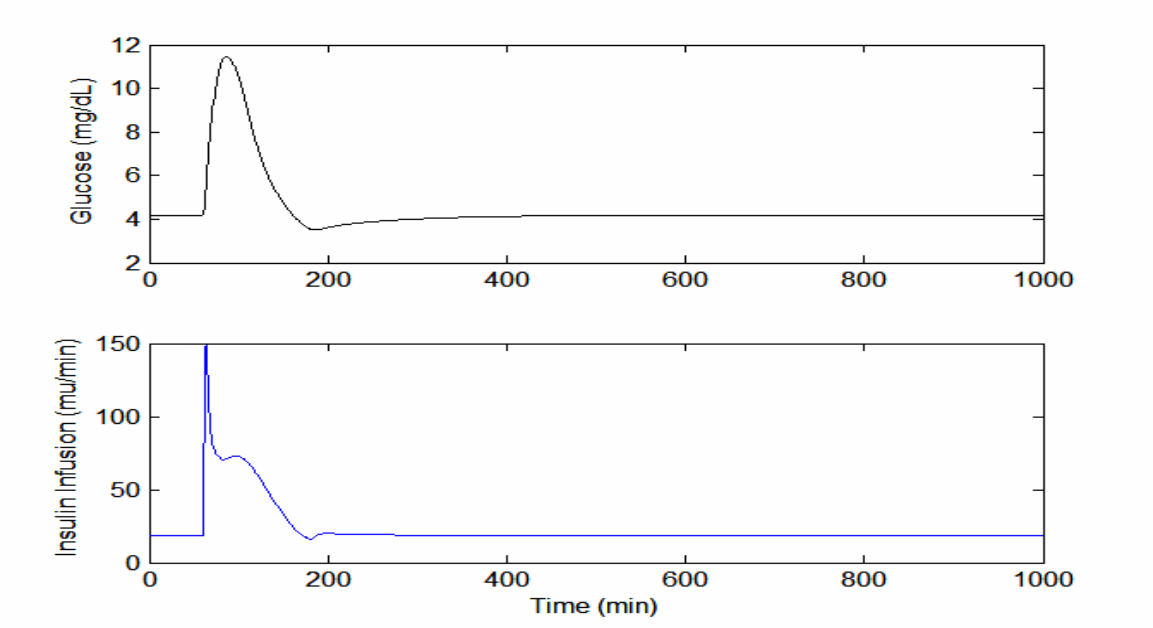

Figure 6-8: Sorensen model simulated response of a healthy patient to a 50 g oral glucose load ingested at t = 60 min. Glucose is expected to rise to nearly 12 mmol/L, fall to slightly below 4 mmol/L, and return to basal rate within 2 hours of ingesting the load. The insulin infusion rate rises sharply to 150 mU/min before sharply falling and giving a proportional 2nd phase response.

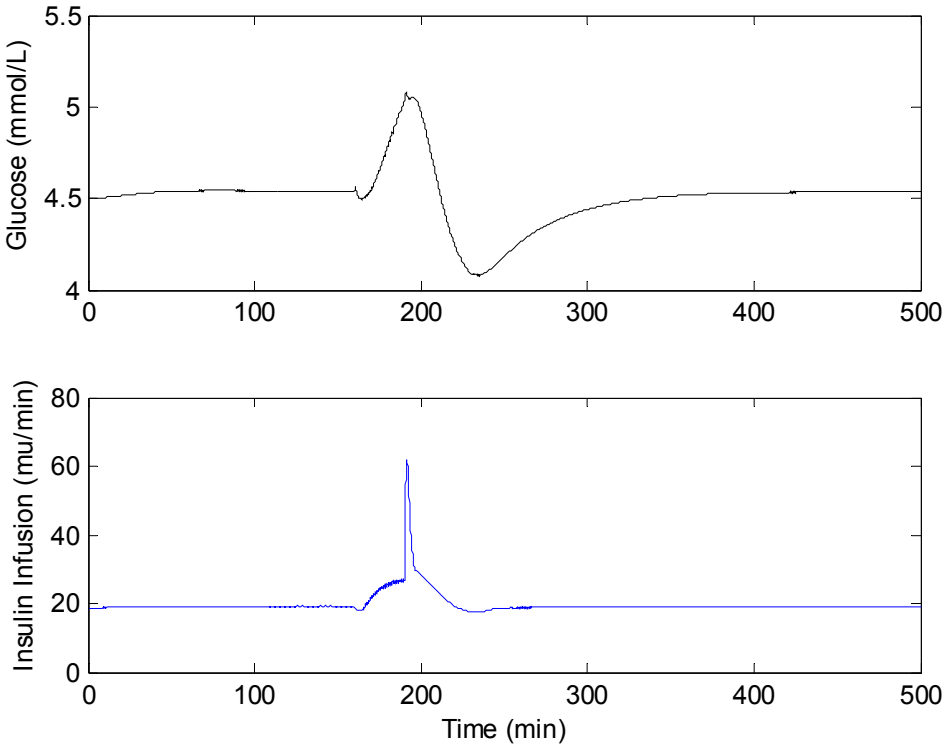

Figure 6-9: Simulation of healthy patient glucose and insulin responses to a thirty-minute session of moderate (60% VO_2^{max}) exercise. Exercise begins at 160 minutes and stops at time 190 min. Maximum glucose rise is between 5 and 5.2 mmol/L, while lowest point on the profile is greater than 4 mmol/L, so hypoglycemia is never observed. Insulin peaks at 60 mU/min, in response to increased hepatic production and higher peripheral blood flow.

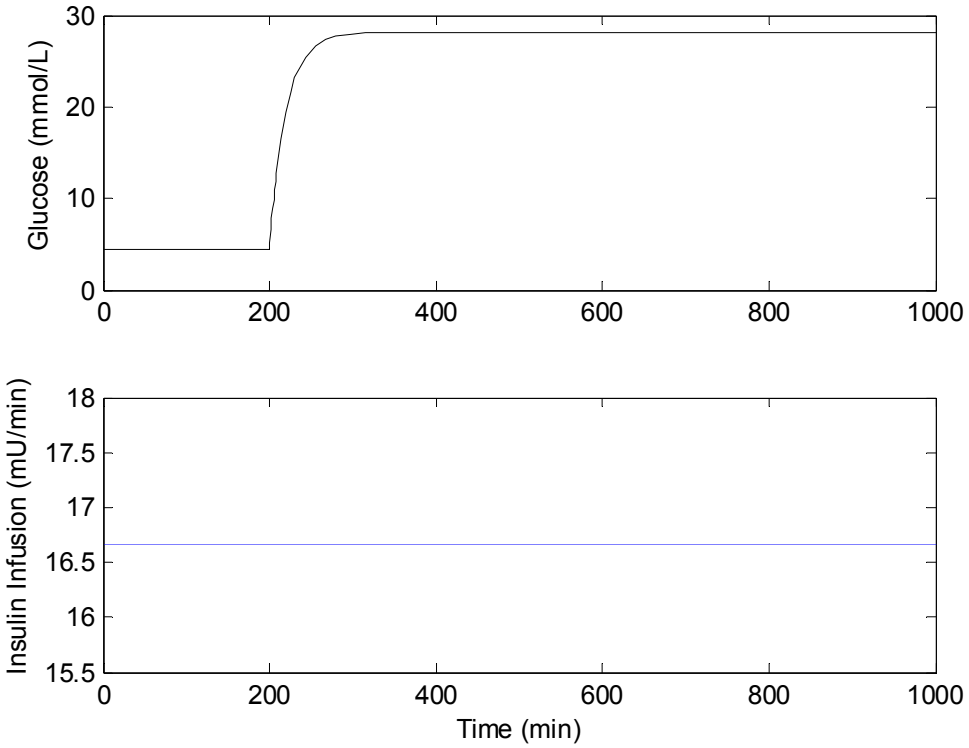

Figure 6-10: Minimal model glucose profile of a Type I diabetic patient ingesting a 50 g glucose sample. Ingestion begins at 200 minutes. In the presence of no additional insulin beyond the basal infusion, the patient approaches a new steady state glucose concentration in the hyperglycemic realm.

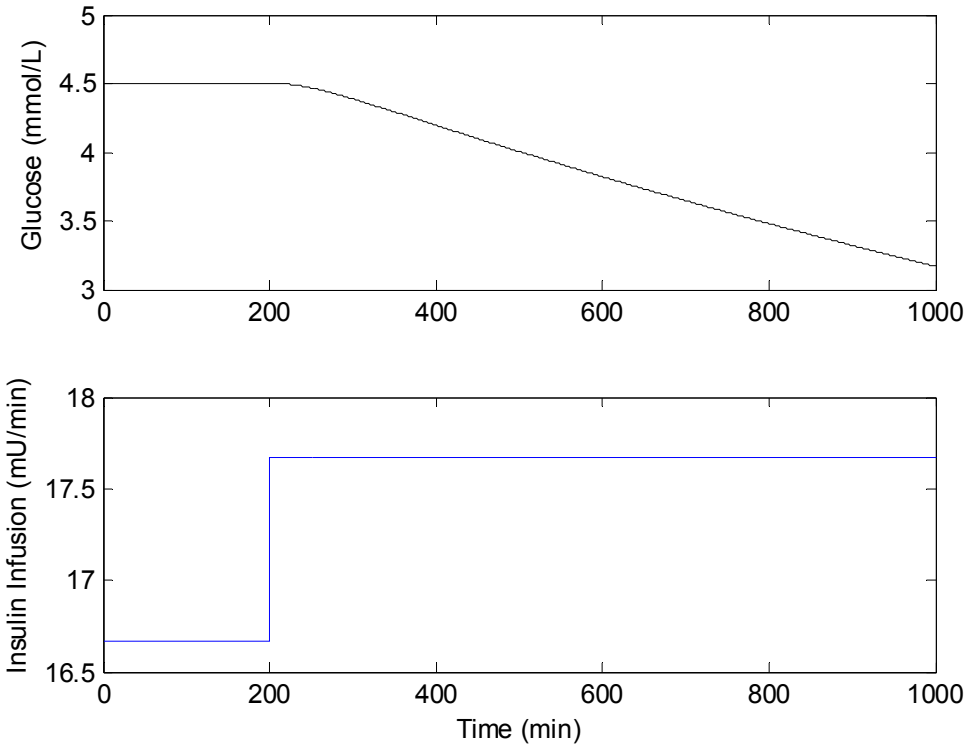

Figure 6-11: Glucose response of the minimal model to a unit step increase in the insulin infusion rate at time 200 min.

Table 6-3: First Order Plus Time Delay (FOPTD) and PID Tuning Parameters		
Parameter	**Value**	**Units**
K	-6.4	mU L $mmol^{-1}$ min^{-1}
τ	3300	min
θ	30	min
τ_c	30	min
K_c	12	mU L $mmol^{-1}$ min^{-1}
τ_I	3300	min
τ_D	40	min
K (disturbance)	1.08×10^5	mU L $mmol^{-1}$
τ (disturbance)	1.08×10^5	min
θ	0	min

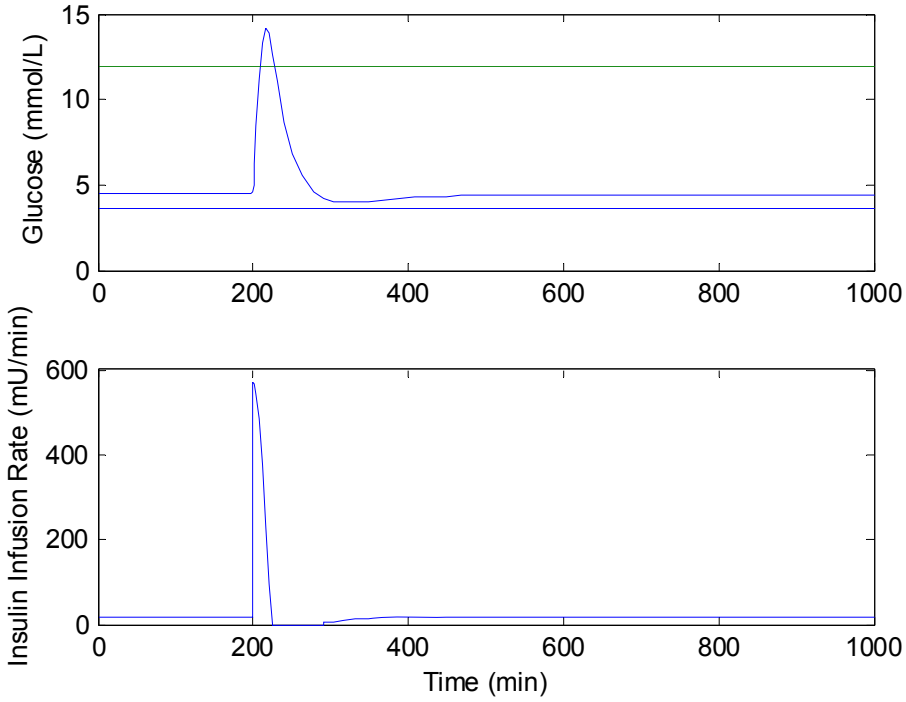

Figure 6-12: PID-controlled glucose response of the minimal model to a 50 g glucose ingestion at time 200 min. K_c = 12 (mU/min)/(mmol/L), τ_I = 3300 min, and τ_D = 40 min.

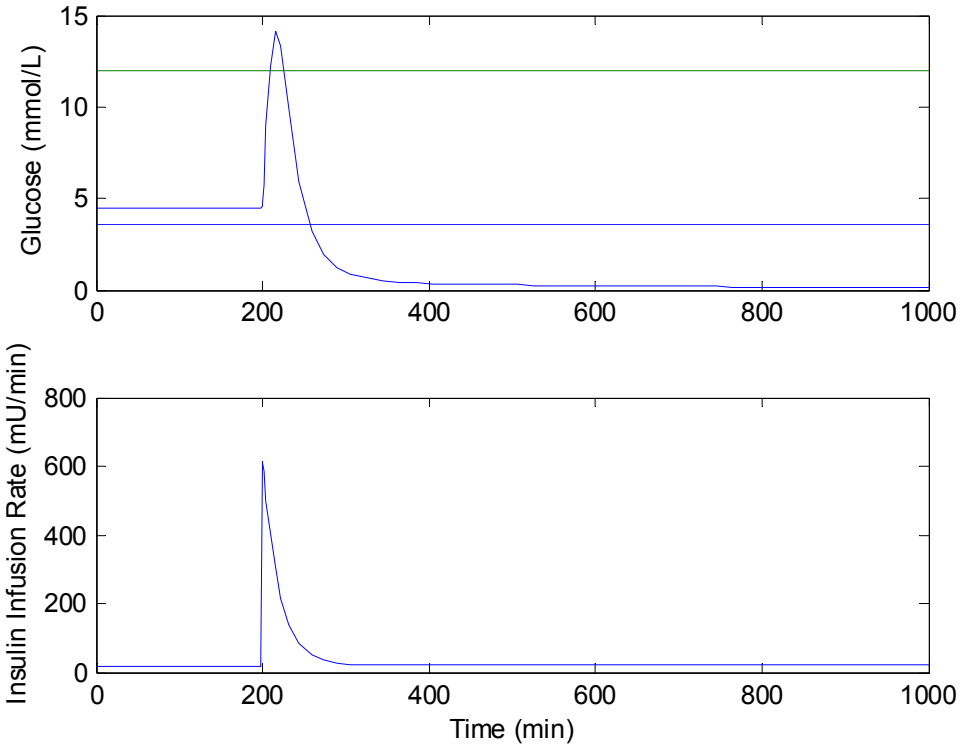

Figure 6-13: Minimal model simulation of feedforward-controlled glucose response to 50 g glucose ingestion at time 200 min.

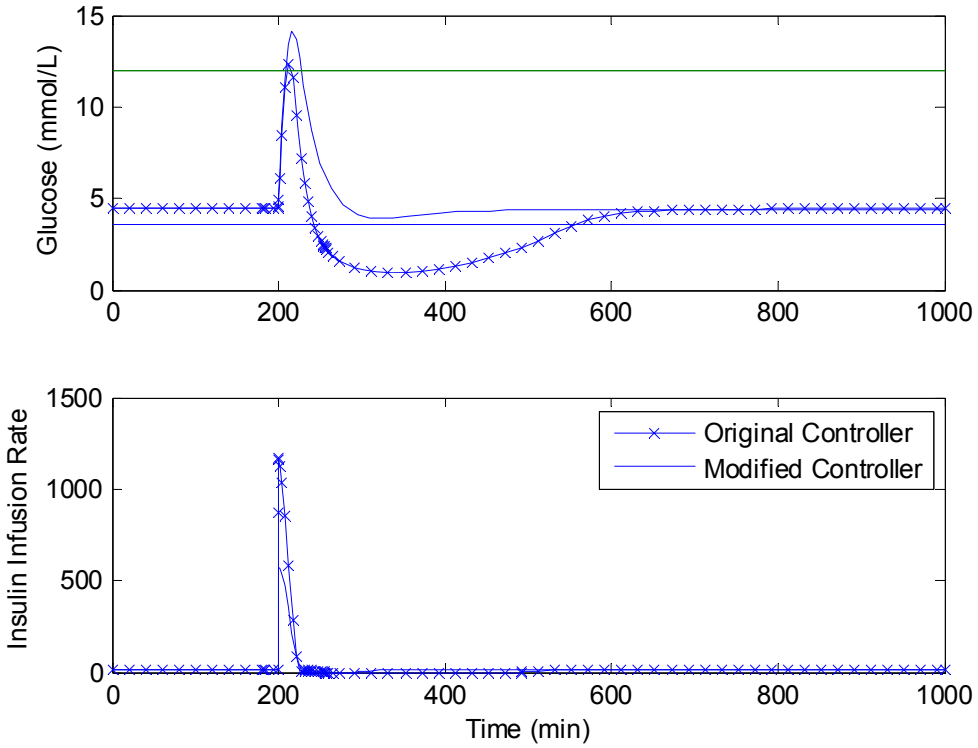

Figure 6-14: Minimal model simulation of feedforward-feedback-controlled glucose response to 50 g glucose ingestion at time 200 min. The line with x's shows the original feedforward controller, while the solid line shows the modified controller developed by reducing the controller gain to prevent hypoglycemia.

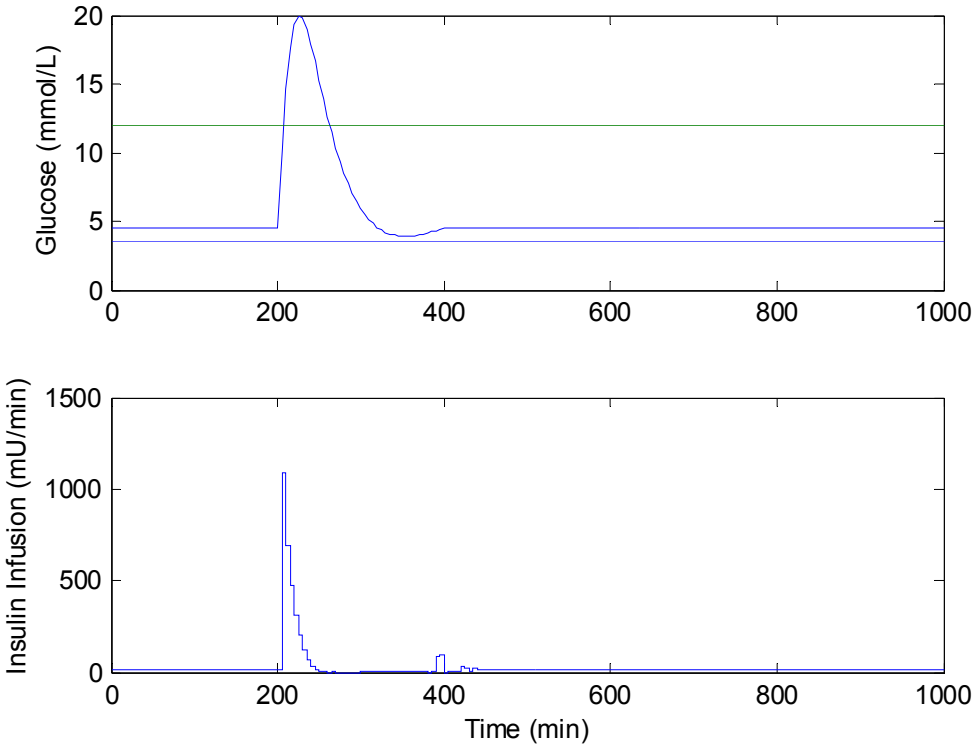

Figure 6-15: Linearized minimal model simulation of Model Predictive Control implementation for diabetic patient who consumes a 50 g of glucose at time 200 min. The lines in the top figure represent the specified upper and lower limits of glucose.

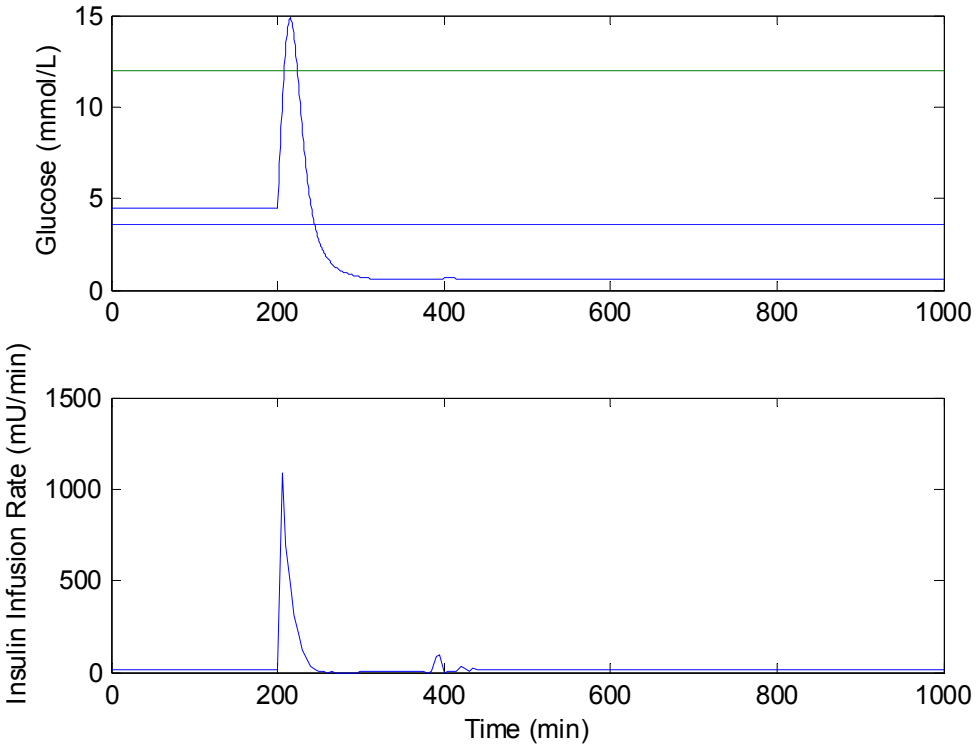

Figure 6-16: Minimal Model Simulation of glucose response to a 50 g glucose ingestion at time 200 min. Control is established by using the insulin infusion profile of the linearized minimal model MPC simulation. The solid horizontal lines on the top figure represent the upper and lower limits of glucose.

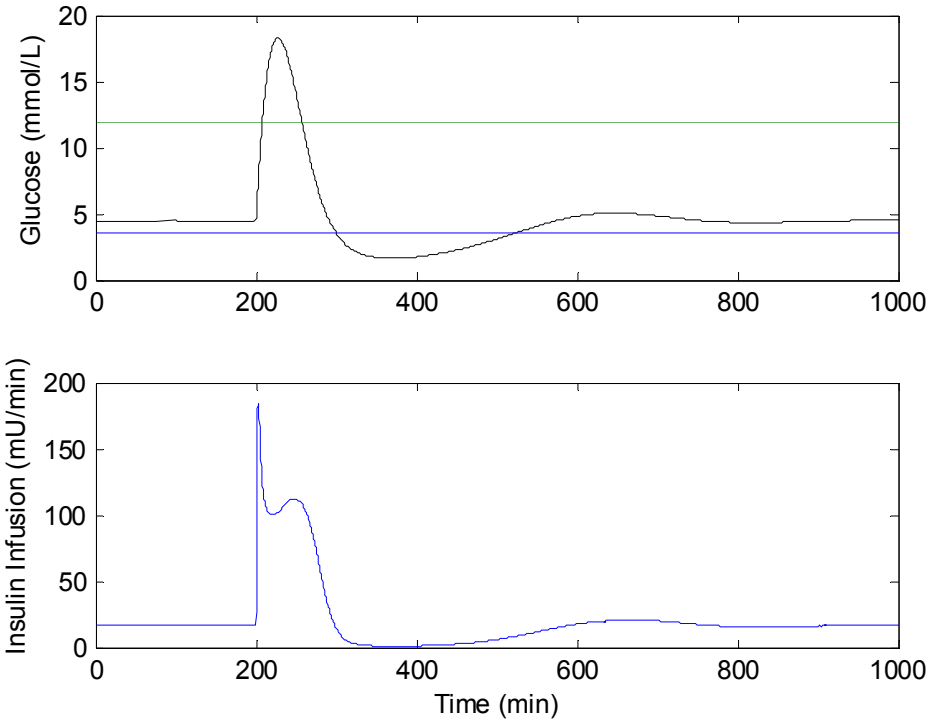

Figure 6-17: Minimal model glucose response to a 50 g glucose ingestion with pancreatic type controller. The horizontal lines on the top graph show the upper and lower glucose limits for good control.

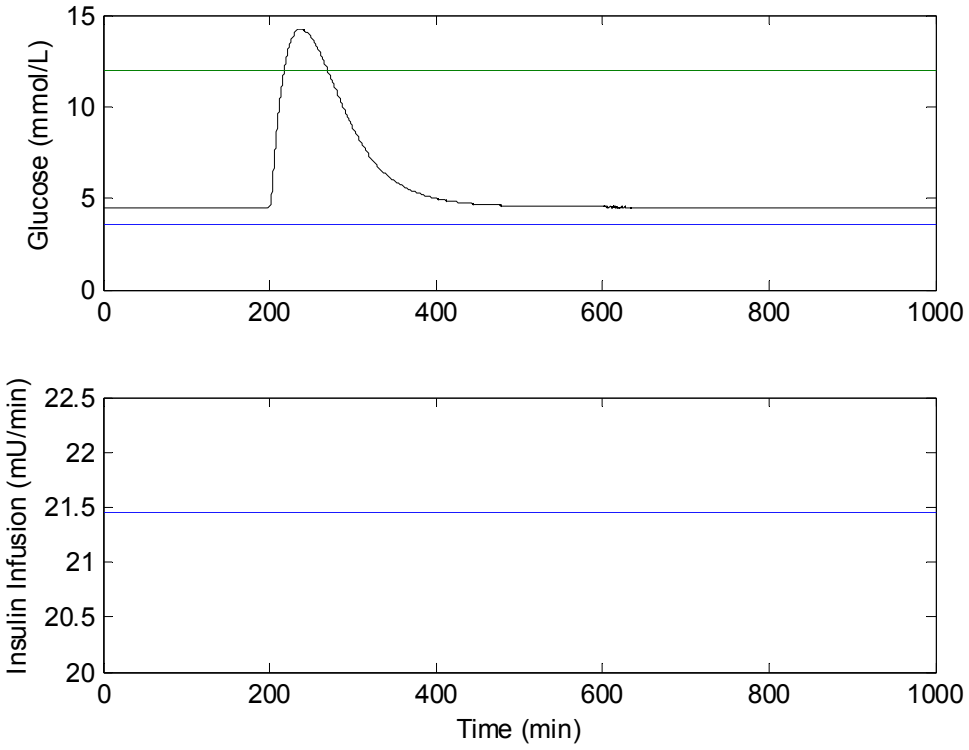

Figure 6-18: Sorensen Model glucose response to 50 g glucose ingestion at time 200 min. The horizontal lines in the top graph represent the upper and lower limits for good glucose control.

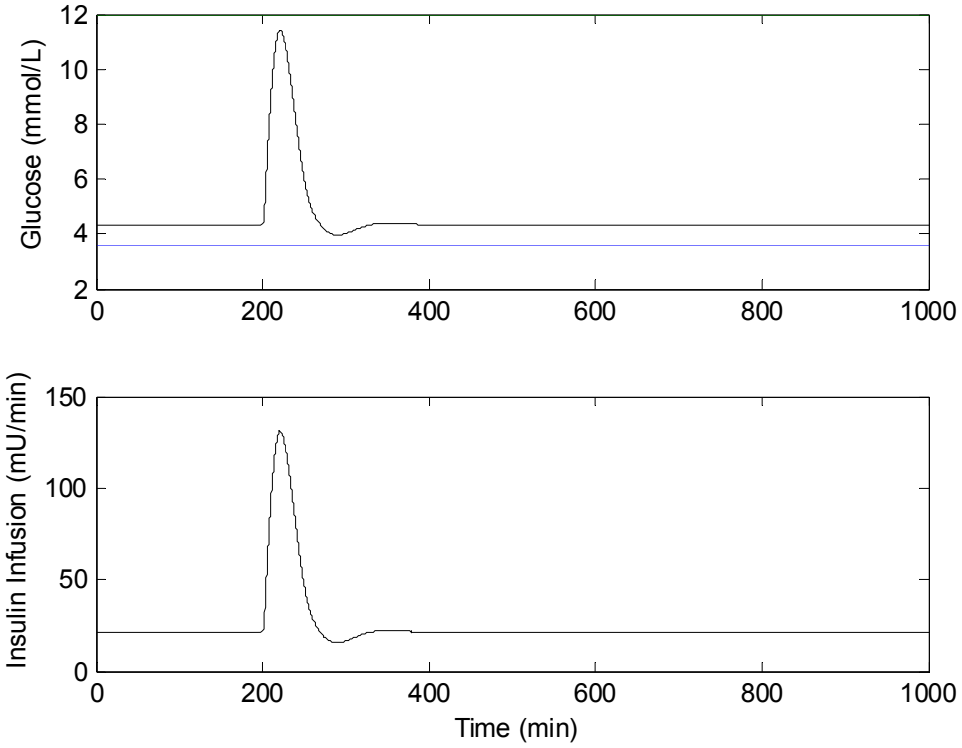

Figure 6-19: Sorensen model proportional-controlled glucose response to 50 g glucose ingestion at time 200 min. The horizontal line on the top graph represents the lower limit glucose concentration to prevent hypoglycemia. The upper limit is the top of the graph.

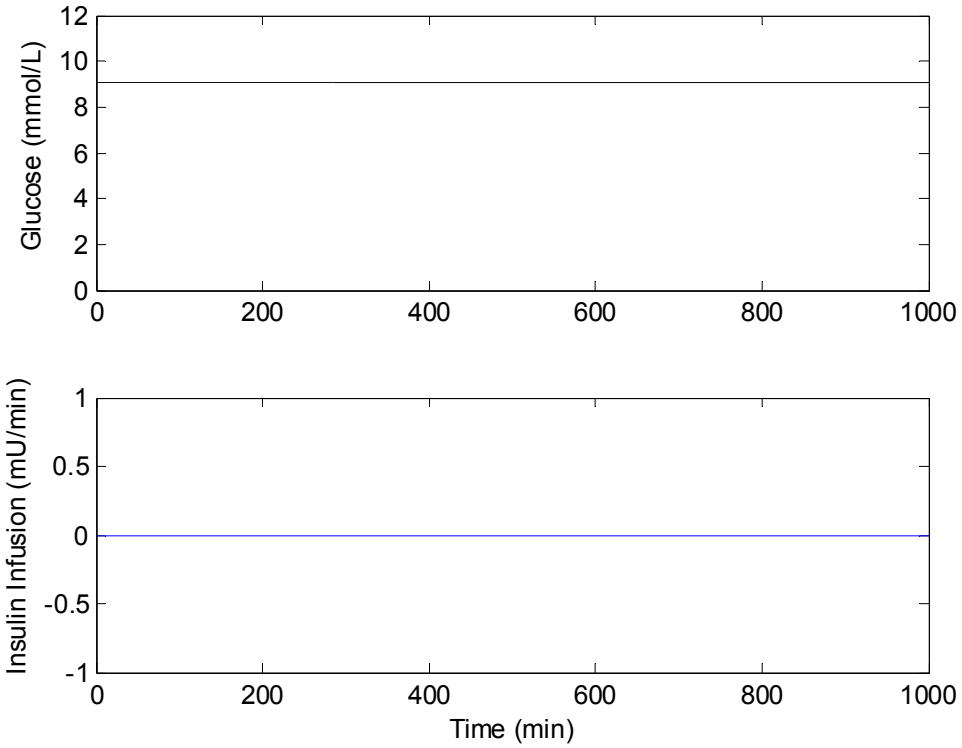

Figure 6-20: Sorensen model glucose steady-state response when there is no insulin being infused.

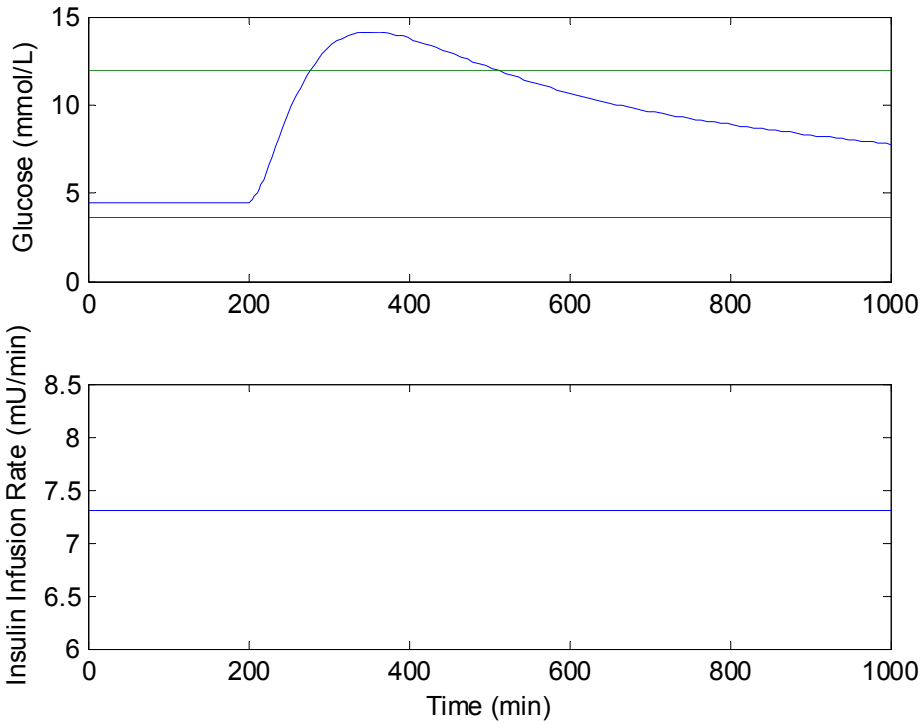

Figure 6-21. Hovorka model glucose response to 50 g glucose ingestion. Insulin is infused at a constant rate to keep the insulin concentration at the basal level. The two horizontal lines in the upper graph show the upper and lower limits of glucose to prevent hyper- and hypoglycemia.

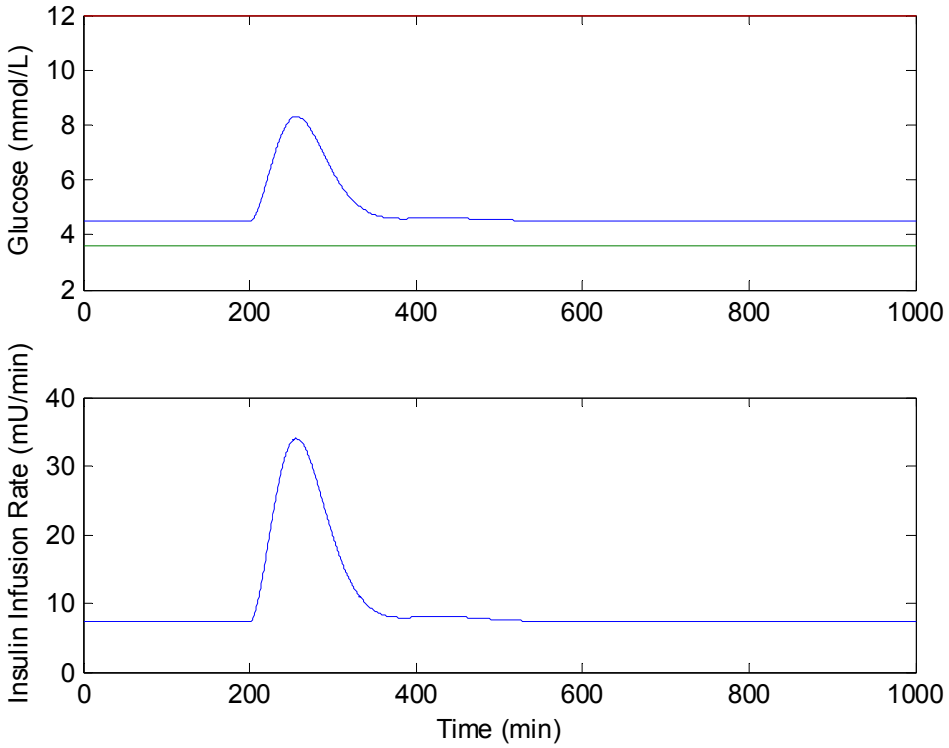

Figure 6-22: Hovorka model proportional-controlled glucose response to a 50 g glucose ingestion. The lower glucose limit for good control is given by the horizontal line on the top graph.

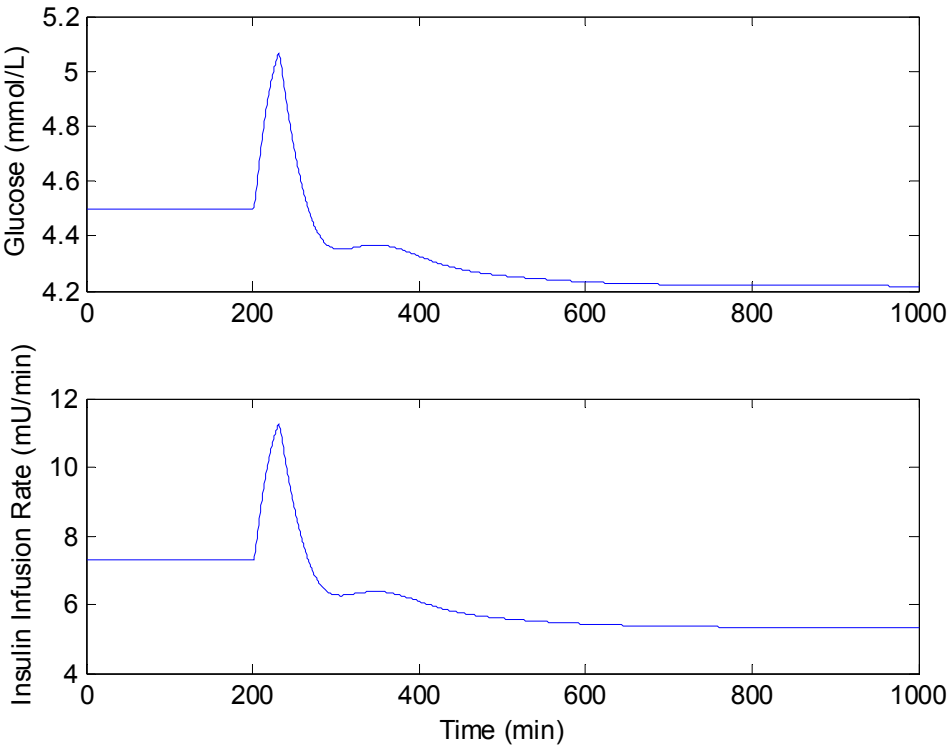

Figure 6-23: Hovorka model proportional-controlled glucose response to moderate exercise. Exercise intensity level is at 60% of VO_2^{max}, and is 30 minutes in duration. Neither the upper nor the lower glucose limits can be seen on the screen, as they are both outside the range of the data.

6.5 References

1. Bergman, R. N., Ider, Y. Z., Bowden, C. R., and Cobelli, C., "Quantitative Estimation of Insulin Sensitivity," *Am. J. Physiol.*, **236**, E667-E677, 1979.

2. Furler, S. M., Kraegen, E.W., Smallwood, R.H, and Chisolm, D.J., "Blood Glucose Control by Intermittent Loop Closure in the Basal Mode: Computer Simulation Studies with a Diabetic Model", *Diabetes Care*, **8**, 553-561, 1985.

3. Sorensen, J. T., "A Physiologic Model of Glucose Metabolism in Man and Its Use to Design and Assess Improved Insulin Therapies For Diabetes", Ph.D. thesis, Dept. Chem. Eng., Massachusetts Institute of Technology, Cambridge, 1985.

4. Hovorka, R., Canonico, V., Chassin, L. J., Haueter, U., Massi-Benedetti, M., Federici, M. O., Pieber, T. R., Schaller, H. C., Schaupp, L., Vering, T., and Wilinska, M. E., "Nonlinear Model Predictive Control of Glucose Concentration In Subjects With Type I Diabetes", *Physiol. Meas.*, **25**, 905-920, 2004.

5. Cobelli, C., Bettini, F., Caumo, A., and Quon, M. J., "Overestimation of Minimal Model Glucose Effectiveness In Presence of Insulin Response Is Due to Undermodeling," *Am. J. Physiol.*, **277**, E1031-E1036, 1998.

6. Fisher, M. E., "A Semiclosed-Loop Algorithm For the Control of Blood Glucose Levels In Diabetics," *IEEE Trans. Biomed. Eng.*, **38**, 57-61, 1991.

7. Bequette, B. W., *Process Control: Modeling, Design, and Simulation*, 1st Ed., Prentice Hall, Upper Saddle River, NJ, 2003.

8. Roy, A. and Parker, R. S., "Dynamic Modeling of Exercise Effects On Plasma Glucose and Insulin Levels," *Proc. ADCHEM 2006*, Gramado, Brazil, 2006.

9. Lenart, P. J., and Parker, R. S., "Modeling Exercise Effects in Type I Diabetic Patients," *Proc. 15th IFAC World Congress On Automatic Control*, Barcelona, Spain, 2002.

10. Seborg, D. E., Edgar, T. F., and Mellichamp, D. A., *Process Dynamics and Control, 2nd Edition*, Wiley, NY, 2004.

11. Muske, K. R., and Rawlings, J. B., "Model Predictive Control with Linear Models", *AIChE J.*, **39**, 262-287, 1993.

12. Shampine, L. F. and Reichelt, M. W., "The MATLAB ODE Suite," *SIAM J. Sci. Comput.*, **18**, 1-22, 1997.

13. Hovorka, R, Shojaee-Moradie, F., Carroll, P. V., Chassin, L. J., Gowrie, I. J., Jackson, N. C., Tudor, R. S., Umpleby, A. M., and Jones, R. H., "Partitioning Glucose Distribution/Transport, Disposal, and Endogenous Production During IVGTT", *Amer. J. Physiol.,* **282,** E992–1007, 2002.

14. Ollerton, R. L., "Application of Optimal Control Theory to Diabetes Mellitus," *Int. J. Control*, **50**, 2503-2522, 1989.

15. Guyton, A. and Hall, J., *Textbook of Medical Physiology*, 11th ed., Elsevier Saunders, Philadelphia, PA, 2006.

CHAPTER 7

IMPLICIT CLOSED-LOOP SYSTEM DESIGN

7.1 Introduction

The goal of implicit closed-loop glucose control in Type 1 diabetic patients is to be able to release a specific amount of insulin in response to the levels of glucose in the bloodstream without the need for equipment such as sensors or pumps. To this end, Peppas [1,2] has proposed the use of cationic, pH-responsive hydrogels of poly(diethyl aminoethyl methacrylate-g-ethylene glycol monomethyl ether monomethacrylate) (poly(DEAEM-g-EGMMA)) as a means to provide such control.

A cationic hydrogel system in which glucose oxidase has been immobilized would result in excess glucose in the environment being oxidized to form gluconic acid. The resulting acid would cause the local pH of the system to decrease, resulting in swelling of the hydrogel. This swelling results in an increase in the mesh size of the gel.

When insulin is incorporated into the gel, the increased mesh size results in increased mass transfer of insulin from the gel. As glucose is removed from the environment, the amount of oxidation is decreased, resulting in an increase in pH. This results in reversible swelling and deswelling as a result of the concentration of glucose in the environment. Such a system allows insulin to be released entirely as a function of the glucose levels in the bloodstream, resulting in the desired closed-loop control.

Before such a device can be implemented, testing in patients would be required to verify efficacy in release. One way to reduce the amount of testing required is through

the use of models. With models, a mathematical representation of the hydrogel dynamics can be combined with a mathematical model of a Type 1 diabetic patient's glucose and insulin dynamics to simulate the effects implementing the hydrogel system.

Such a hydrogel device model would have to describe the diffusion of glucose to within the hydrogel, the oxidation of glucose to form gluconic acid, the elimination of gluconic acid via diffusion, the effect of gluconic acid on the local pH of the system, the effect of pH on the swelling of the gel, and finally the effect of swelling on the mass transfer coefficients of the various species involved. The approach taken here is to model the simplest dynamics first and then to add complexity as the desirable characteristics are able to be simulated.

The first goal in modeling the gel dynamics is to verify that a lower limit mass transfer coefficient exists such that two primary features in insulin release result. First, in the absence of a disturbance change in glucose (i.e., a meal), the insulin should be released from the gel over a long period of time. Second, the release rate from a gel in the absence of a glucose disturbance should be at the physiologic levels of basal insulin release, either from a healthy pancreas or from a pump. *Because it is not realistic to expect a constant infusion rate from a gel device*, the more appropriate objective would that the gel should be able to demonstrate rapid oscillatory swelling and deswelling in order maintain glucose levels within a physiological basal range. This work aims to achieve such objectives.

First, a simple model is developed describing insulin and glucose dynamics within the gel in basal, high pH conditions. Second, an engineering analysis is performed using

reported literature values and basic assumptions to determine reasonable parameter values for the simple model. Finally, the model parameters are varied by orders of magnitude to determine their effects on release with the minimal model [3], as they relate to the two desired primary features.

7.2 Methods

7.2.1 Model Development

In order to describe the dynamics of the release system, it is important to understand each step in the process. A block diagram of the process is given in Figure 7-1.

When the glucose concentration in the blood is greater than normal levels, a concentration gradient exists between the glucose in the blood and the equilibrium levels within the polymer system. This results in the diffusion of glucose into the system. However, as glucose is diffusing within the gel, the presence of immobilized glucose oxidase results in the homogenous oxidation of glucose to form gluconic acid. This species will now exist in greater concentrations than that in the external environment (the gluconic acid concentration in the blood is assumed to be zero, based on the idea that blood acts as a perfect sink for foreign hydrogen ions as the pH is rapidly regulated by the buffers in the blood), resulting in passive diffusion of ionic species to the external environment.

The presence of gluconic acid results in a pH change at the local environment, resulting in a change in the size of the gel. This swelling also results in an increase in the

diffusion coefficients of species through the hydrogel system. This increase in the diffusion coefficient results in increased diffusion of insulin from the gel to the external environment. Therefore, in order to model the system, the diffusion of glucose, gluconic acid, and insulin must be modeled, along with the effect of gluconic acid on the local pH and the effect of pH on the size of the hydrogel.

Assuming no dynamics associated with metabolic glucose uptake or production, the dynamics of glucose in the external environment is described by Equation (7.1).

$$\frac{d(V_B G)}{dt} = -A(N_G) \tag{7.1}$$

In Equation (7.1) V_B is the distribution volume of the bloodstream, G is the blood glucose concentration, and the mass transfer area, A, is given by Equation (7.2).

$$A = N_g 4\pi R^2 \tag{7.2}$$

Here, N_g is the number of hydrogel spheres are in the bloodstream, and R represents the radius of a hydrogel particle. N_G is the mass transfer flux from the bloodstream to the gel interior, as given by Equation (7.3).

$$N_G = \frac{D_G}{L}(G - G_D) \tag{7.3}$$

In Equation (7.3), D_G is the diffusion coefficient of glucose within the hydrogel network, L is the diffusion length across the gel, and G_D is the glucose concentration within the hydrogel. For simplicity, spatial considerations have been eliminated and it is assumed that the internal glucose concentration beyond the characteristic diffusion length from the outside radius is uniform throughout the gel.

While a more accurate description would be one that included gradient terms, the purpose of the model is to investigate the feasibility of the hydrogel device as a control system, and a simplified model allows such feasibility to be determined. When the distribution volume of the bloodstream is assumed constant, Equations (7.1) through (7.3) can be combined to give the following dynamic equation for glucose in the bloodstream:

$$\frac{dG}{dt} = \frac{4\pi N_g D_G R^2}{L V_B}\left(G - G_D\right) \tag{7.4}$$

As with Equation (7.1), the dynamics of glucose within the hydrogel can be described by a basic material balance, as shown in Equation (7.5).

$$\frac{d\left(V_D G_D\right)}{dt} = A\left(N_G\right) - V_D r_G \tag{7.5}$$

In Equation (7.5), V_D is the volume of the particle environment. The parameter r_G is the rate of glucose oxidase-catalyzed glucose oxidation. This reaction is given in Equations (7.6) and (7.7) [4].

$$Glucose + O_2 \xrightarrow{GlucoseOxidase} GluconicAcid + H_2O_2 \qquad (7.6)$$

$$2H_2O_2 \xrightarrow{Catalase} 2H_2O + O_2 \qquad (7.7)$$

In the reaction, glucose is oxidized by glucose oxidase to form gluconic acid and hydrogen peroxide. As hydrogen peroxide is a toxic substance and must be eliminated from the body, catalase is also immobilized into the gel network. Catalase catalyzes the decomposition of hydrogen peroxide to form water and oxygen. Therefore, it is assumed that the oxygen content is enough to ensure that the glucose oxidation can occur freely, without oxygen limitations [1].

The rate of oxidation is described by Michaelis-Menten kinetics for enzyme catalyzed reactions and is given by Equation (7.8).

$$r_G = \frac{V_{\max} G_D}{K_S + G_D} \qquad (7.8)$$

Here, V_{max} describes the maximum rate of reaction and is directly proportional to the amount of enzyme immobilized into the gel system. In addition, K_s describes the concentration of glucose when the reaction is proceeding at exactly half the maximum rate. This equation is derived in Appendix H. The volume of the gel system, V_D, is described by Equation (7.9).

$$V_D = \frac{4}{3}\pi N_g R^3 \qquad (7.9)$$

Because the cationic hydrogel system will swell in response to pH, V_D cannot be removed from the derivative. Figure 7-2 shows the dynamic swelling response of two different hydrogel microspheres [2]. When the particle size is on the order of 30 μm, the swelling and deswelling are showed to occur on the order of one minute or less. Since minute to minute control is the objective, and because the particles will be an order of magnitude smaller than 30 μm, the assumption is made that the volume change will occur much quicker than the observed time scale of minutes. Therefore, a quasi steady-state volume assumption can be made, allowing for the volume to be removed from the derivative. Combining Eqs. (7.2) and (7.3) with Equations (7.5), (7.8) and (7.9) results in the following simplified description for the dynamics of glucose in the hydrogel environment:

$$\frac{dG_D}{dt} = \frac{3D_G}{RL}\left(G - G_D\right) - \frac{V_{\max} G_D}{K_S + G_D} \tag{7.10}$$

The dynamics of insulin within the gel is primarily driven by two processes. The first is the diffusion of solution insulin from the gel to the external environment. The second is the dissolution of any undissolved insulin in the hydrogel solution. If the assumption is made that the insulin concentration within the gel is below the saturation concentration of insulin (8 mg/mL), then the dynamics of insulin within the gel reduces to the following equation:

$$\frac{d}{dt}\left(V_D I_D\right) = -A\left(N_I\right) \qquad (7.11)$$

The terms V_D and A have previously been defined, I_D is the insulin concentration in the gel, and N_I is the insulin flux from the device, as described by Equation (7.12).

$$N_I = \frac{D_I}{L}\left(I_D - I\right) \qquad (7.12)$$

Using the simplifications of Equations (7.2) and (7.9), and assuming again that the time scale of importance is greater than the time scale associated with the change in the particle radius, the dynamics of insulin within the gel can be simplified to the following expression:

$$\frac{dI_D}{dt} = \frac{-3D_I}{RL}\left(I_D - I\right) \qquad (7.13)$$

The insulin infusion rate from the gel is merely the absolute value of the dynamic change in insulin mass within the gel system, as described by Equation (7.11). Combining Equations (7.2), (7.11), and (7.12) results in the expression for the insulin infusion rate from the implicit closed-loop control system.

$$U = \frac{4\pi N_g R^2 D_I}{L}\left(I_D - I\right) \qquad (7.14)$$

Finally, the dynamics of insulin in the external environment can be determined in an analogous manner to the dynamics of glucose in the external environment. Neglecting the metabolic production and elimination of insulin within the body, the accumulation of insulin within the bloodstream depends entirely the rate of insulin infusion from the device.

$$\frac{d}{dt}\left(V_B I\right) = U \tag{7.15}$$

Assuming the circulation volume is constant, Equation (7.15) is simplified to the following dynamic expression for insulin in the bloodstream:

$$\frac{dI}{dt} = \frac{U}{V_B} \tag{7.16}$$

It should be noted that the dynamics of insulin and glucose, as given by Equations (7.4) and (7.16) assume no metabolic production or elimination of either species. In reality these effects clearly exist, and in order to use the dynamic equations to simulate the in vivo response of the system, a patient model must be chosen, and the form of the model chosen will determine the form of the glucose and insulin dynamic equations.

The ability of the gel to both sense glucose and change its transport properties in response to its presence is made possible by the production of gluconic acid. Gluconic

acid dynamics was represented in a similar manner to the representation of glucose and insulin. The overall mass balance is described by Equation (7.17):

$$\frac{dGA_D}{dt} = \frac{V_{max} G_D}{K_s + G_D} + \frac{3D_{GA}}{RL}\left(GA_D - GA\right) \tag{7.18}$$

The gluconic acid production rate is equivalent to the device glucose oxidation rate. Gluconic acid is then assumed to passively diffuse down a concentration gradient into the external environment.

While the presence of gluconic acid is integral to the implicit control process, it is important to think in terms of pH for two reasons. First, the gel response, as investigated by experimentalists, is generally shown as a function of pH, and will thus be modeled as such. Second, and more importantly, the pH of the body cannot sustain significant pH changes, and therefore an analysis of the type of pH changes in the bloodstream must be performed in order to ensure safety during the device's use.

There are two primary phenomena that determine the effect of the production of gluconic acid on the pH of the local environment of the gel system. One is the existence of biological buffers that keep the pH of the system tightly controlled. The other is the concept of Donnan equilibrium.

The purpose of a buffer is to maintain a system's pH within a certain range. It is composed of a base and its conjugate acid.

$$Buffer + H^+ \leftrightarrow HBuffer \tag{7.18}$$

The buffer base usually exists as an ionic salt. When an acid or base is present in the system, the pH change is minimized by either the quenching of the foreign acid by the buffer base or by the quenching of the foreign by the buffer acid. The buffer system exists in equilibrium, as described by the Henderson-Hasselbalch equation:

$$pH = pK_a + log\frac{[BufferBase]}{[BufferAcid]} \tag{7.19}$$

In the Henderson-Hasselbalch equation, the buffer pK_a and the concentrations of acid and base in the system determine the pH of the system. When gluconic acid is produced in the gel, the gel buffer quenches the foreign acid to form more of the buffer acid. The new pH will simply be based on the new acid and base concentrations [4]:

$$pH_{new} = pK_a + log\frac{[BufferBase]_0 - GA}{[BufferAcid]_0 + GA} \tag{7.20}$$

Therefore, to determine the pH as a function of gluconic acid, only the gluconic acid concentration, the buffer pK_a, and the initial buffer and base concentrations, as designated by the subscript "0", are needed.

While the concentrations of the major buffer species in the blood are readily found in medical physiology texts [5] or clinic biochemistry texts [6], these values will

not be the same inside the gel environment. Because there are negatively charged methacrylate groups immobilized on the polymer backbone of the gel, there will inevitably be different concentrations of ionic species in the gel compared to the bloodstream. This is known as the Donnan effect [7]. When Donnan equilibrium is established, all charges are balanced at the cost of having different species concentrations across a semi-permeable membrane, which for this case is the gel device. The concentration differences for species across the membrane are described using the Donnan ratio, K [8]:

$$\frac{c_{i,gel}}{c_{i,blood}} = K^{z_i} \tag{7.21}$$

For the ith ionic species, the ratio of gel concentration to the blood concentration is simply the Donnan ratio raised to the power of the valence of the ionic species. The Donnan ratio can be found by performing an overall charge balance to develop the following relationship:

$$(1-\varphi)\sum_i z_i K^{z_i} c_{i,blood} + \frac{\sigma\varphi}{1+K^{-1}10^{pH-pK_g}} = 0 \tag{7.22}$$

Equation (7.22) has been derived in Appendix I. It is based on the assumption of ideal Donnan equilibrium.

As discussed by Siegel in reference [9], there are many assumptions made for this relationship to be valid. Among those are the assumption that ion activity is equal to its concentration, that the fixed amine groups of the polymer backbone can be assumed to have a single ionization constant, K (or pK_g), that bulk electroneutrality does indeed hold, and that the species concentrations are given with respect to the fluid solvent within the gel, not the entire gel volume. Siegel has pointed out that the possibility of positive ions in plasma associating with the amine groups, resulting in the ideal Donnan equilibrium assumption being invalid. However, provided there exists an anion in relatively high concentration, the assumptions are applicable. For the purpose of simulations, ideal Donnan equilibrium is assumed valid.

The variable pK_g represents the pK_a of the methacrylate functional group of the polymer backbone. The variable σ represents the density of functional groups in the polymer. This is a design parameter for this system. These two variables can be selected by choosing specific materials. The variable φ represents the volume fraction of the polymer in the device system. Because the gel is assumed to be swollen as a result of absorbed water, the actual volume fraction of polymer will be significantly smaller than that of the collapsed particle. The volume fraction is represented by Equation (7.23):

$$\varphi = \frac{V_{polymer}}{V_{total}} = \frac{v}{Qv} = \frac{1}{Q} \tag{7.23}$$

The volume fraction is simply the total polymer volume divided by the total volume. Given a collapsed polymer volume v, the total volume of the device is characterized by the volume swelling ratio Q. Q is defined as the volume of swollen polymer complex to the initial volume of collapsed polymer:

$$Q = \frac{R^3}{R_{collapsed}^3} \tag{7.24}$$

The product Qv denotes the total device volume, and it is easily shown that the volume fraction is merely the inverse of the swelling ratio. Given value of swelling ratio, the polymer design characteristics, and the ionic concentrations of the different species in the blood and the gel, the Donnan ratio can be determined using a nonlinear system solver and used to determine the buffer acid and base concentrations within the gel, as well as the normal pH within the gel as a result. Given the gel pH and buffer concentrations, the pH as a function of gluconic acid concentration can then easily be determined.

Peppas and co-authors [1, 2] have demonstrated a dramatic increase in the swelling ratio for poly(DEAEM-g-EGMMA) when subjected to a pH below 7.1. These results are given in Figures 7-3 and 7-4. Using the quasi steady-state assumption with respect to volume swelling, it is assumed that swelling ratio will rapidly approach its equilibrium value provided as shown in Figures 7-3 and 7-4. For the purposes of simulation, only empirical models were needed to describe the effects of pH on swelling.

Based on the form of the curve of the results shown in Figure 7-3, a hyperbolic tangent relationship was used, as indicated below:

$$Q = A + B\,tanh\left(C \cdot pH + D\right) \tag{7.25}$$

It can be seen in Figure 7-3 that a hyperbolic tangent relationship does not perfectly reflect the swelling profile, as the gel continues to swell as the pH drops. However, because the pH of the system will not deviate from the range of 7.0 in the gel to 7.4 of the blood, it was concluded that such a relationship is adequate for the interval selected.

Figure 7-4 also shows the swelling effects of pH for gels of different crosslinking ratios. Clearly, as the crosslinking ratio is increased, the gel is unable to repel as much, resulting in a much more stiff device. To quantify this effect, empirical relationships using the data of Figure 7-4 were developed. Based on the hyperbolic relationships, at maximum and minimum swelling, the hyperbolic tangent function can be approximated as unity. This allows A and B to be determined based on the asymptotic swelling values.

$$A + B = Q_{max} \tag{7.26}$$

$$A - B = Q_{min} \tag{7.27}$$

From an inspection of Figure 7-4, Q_{min} does not change significantly as a function of crosslinking ratio, and it was approximated as 3 at crosslinking ratios lower than 0.02 and 2 at crosslinking ratios of 0.02 or greater.

Clearly Q_{max} is strongly dependent on crosslinking, and the maximum swelling values were plotted as a function of crosslinking ratio, as shown in Figure 7-5. A decaying exponential was chosen to describe the data, simply because it gave the best fit. The relationship is described by Equation (7.28).

$$Q_{max} = 40\, exp\left[-49.8\left(X - 0.005\right)\right] \tag{7.28}$$

This fit was based on the data observation that a crosslinking ratio, X, of 0.005 (moles crosslinking agent/moles monomer) has a maximum swelling ratio of approximately 40. As shown in Figure 7-6, parameter *C* exhibited no crosslinking dependence, and so an average value of -10 was chosen. Finally, because the swelling transition is supposed to occur at the gel pK_g, the hyperbolic tangent functions inflection point was assumed to occur when the pH is equal to the pK_g. Taking the second derivative of the function shows that the hyperbolic tangent function goes to zero at this point. To show this mathematically, the parameter *D* is described by Equation (7.29).

$$D = -C \cdot pK_g \tag{7.29}$$

With parameters *A*, *B*, *C*, and *D* expressed as a function of crosslinking ratio, the swelling ratio for any pH can now be performed as long as the crosslinking ratio is known. Given the swelling and crosslinking ratio, the remaining transport parameters can be determined

as well. Diffusion of a species within the gel is based on the size of species relative to the size of the mesh of the network. The mesh is described by Equation (7.30) [10].

$$\xi \cong C_n^{1/2} Q^{1/3} N^{1/2} l_c \tag{7.30}$$

Equation (7.30) is based on the assumption of isotropic stretching of the polymer chains during the swelling process. The cube root of the swelling ratio represents the relative increase in size of a chain. The parameter C_n is known as the characteristic ratio and is taken to be 14.4 for poly(DEAEM-g-EGMMA) [1]. The parameter l_c is simply the length of the bond between two carbon atoms. The parameter N is taken to be the number of repeating units between two crosslinks. Combined, N and l_c give the average length of the unstretched chain. Each cross-linking agent has four functional groups, enabling to link four polymer chains together. However, each chain is shared between two crosslinking agent functional group sites. Thus, N can be approximated as shown:

$$N \cong \frac{1}{2X} \tag{7.31}$$

Given the mesh size, the swelling ratio, and the size of the particle being transported, the diffusion coefficient for a species i through the gel is given by Equation (7.32) [10].

$$D_i \cong D_{i,0}\left(1 - \frac{r_{H,i}}{\xi}\right) exp\left(\frac{-Y}{Q-1}\right) \tag{7.32}$$

Y is a constant assumed to be one for this and most other polymeric systems [1], and $r_{H,i}$ is the hydrodynamic radius of the particular species. Equation (7.32) is a scaling law based on statistical thermodynamics and the probability that both enough free volume exists for the solute to move through the gel and that the gel network conformation is such that the solute can move through it as well.

The final process associated with model development is with respect to the degradation of the polymer. At this point, the authors know of no attempts to make degradable cationic hydrogels, but it is noted that such a system must be degradable in order to prevent a gradual accumulation of polymer within the patient. The development of degradable systems is an ongoing project in the Peppas laboratory at the University of Texas at Austin.

As an approximation of degradation, the works of Langer and co-authors [11] and Anseth and co-authors [12] have been studied and adapted for crosslinked gels. Langer and co-authors showed that microparticles of 50:50 poly(D,L-lactic-co-glycolic acid) (PLGA) degrade by the cleaving of bonds on the polymer chains, resulting an increase in the porosity of the spheres. This bond cleavage was modeled as a zero order process because all bonds are equally likely to be cleaved. Anseth and co-authors investigated the bulk degradation of hydrogels of poly(lactic acid-b-ethylene glycol-b-lactic acid) (poly(LA-b-EG-b-LA)) and assumed first order kinetics with respect to the degradable units.

To develop pH-responsive hydrogels that are degradable, a degradable crosslinking agent must be used. As the system degrades, instead of the average pore

size increasing, the mesh size will increase. With respect to bond cleavage, the only degradation that occurs will be respect to the bonds between a chain and the crosslinking agent. Based on this analysis, the degradation rate was assumed to be first order in the crosslinking ratio only.

$$\frac{dX(t)}{dt} = -k_d X(t) \tag{7.33}$$

As the ratio decreases, insulin will be able to diffuse faster from the gel, until a certain threshold value is reached in which the insulin will be rapidly dumped from the device. The goal of design will then be to ensure that insulin is essentially depleted from the device before such degradation occurs.

Finally, given the model of hydrogel dynamics, implicit-closed loop control can be investigated by incorporating the model into a patient model. For this purpose, the minimal model [3,13], as described in Chapter 6, was used.

7.2.2 Parameter Determination

To perform the simulations, numerical values are needed for each parameter. Many of the parameters could not be determined from experiment, requiring other methods. Model parameters were determined in three ways. First, available values from literature were used when applicable. Second, parameters from the simulation results of references [14] and [4] were used as first approximations for some of the values. Finally,

intuitive reasoning was used to determine approximate values of the remaining parameters.

Reference [13] provided the basal concentrations of glucose and insulin, as well as the parameter values of the patient model. References [14] and [4] were used to determine both the hydrodynamic radius for the different species and their associated solvent diffusion coefficients, $D_{i,0}$. The degradation rate, k_d, was approximated as the same order of magnitude as the random scission rate given in reference [11]. The parameter values for V_{max}, K_s, pK_g, and σ were initially approximated using the parameters of reference [4]. Finally, the concentrations of buffer species were taken from references [5] and [6].

To determine the maximum loading of insulin within the gel, the saturation concentration of insulin in water was used [14]. It was then assumed that insulin is always dissolved within the gel. The average particle size was given an upper limit of 5 μm. In order to be able to circulate in the bloodstream, the particles must be able to flow through the capillaries. Given the average capillary internal diameter of 5-9 μm [5], the gel would likely have to be much smaller than this value. The nominal values of all parameters are summarized in Table 7-1.

The final parameter, N_g, was determined based on the particle size and some assumptions about the administration of the device. It was assumed that the gels would be injected into the bloodstream in a solution that does not cause them to swell initially. A patient using insulin injections will likely inject between 3/10 to 1 mL of U-100 insulin daily for basal insulin [15]. U-100 means that the insulin solution contains 100 units per

mL of solution. A device designed to provide insulin for multiple days would have inject a higher volume of solution every few days. As an initial assumption, it is assumed that 10 mL of solution will be injected into the bloodstream periodically. To be comparable to intravenous injections of other species, such glucose [16], which has previously been injected in solutions at up to 50 wt%, the particles should only represent up to 5 wt% (wt) of the injection solution. Assuming the particles have a density of approximately unity, the entire volume of particles can only equal 5 cubic centimeters. Therefore, N_g is determined by noting that the total number of particles must have a volume no greater than 5 cm^3. Table 7-2 shows the maximum number of assumed particles for different particle sizes.

It should be noted that, assuming rapid diffusion and rapid oxidation, the gluconic acid concentration within the gel would reach a maximum value equal to the glucose value in the blood stream. In the worst case, a scenario would occur in which all the gluconic acid from the gels is released into the bloodstream. Given that the total particle volume is only 5 cm^3, compared to the body's volume of more than 3 L of plasma [7], the acid concentration would likely be considerably diluted. Finally, considering the plasma carbonate buffer concentration of 25 mmol/L, it can be assumed that gluconic acid would be quenched nearly instantaneously with nearly no impact on the buffer system. Therefore, the gluconic acid concentration in the bloodstream is considered to be zero at all times.

Finally, the model neglects any immune response effects on the delivery system. The presence of ethylene glycol grafts has been assumed to provide stealth

characteristics, although the duration of the system in blood has not been determined. The small size of the particles also means that they could be eliminated via opsonization [17], in which the particles are enveloped and ultimately eliminated by the body. While these concepts are extremely important with respect to the system design, it is assumed here, for the sake of investigating feasibility with respect to insulin release and glucose control effectiveness, that immune response effects are not present.

7.2.3 Simulation Objectives

There were two primary objectives associated with model simulations. First was to investigate the effects of each parameter on the systems ability to perform. These simulations were performed by choosing up to five different values for each parameter, each increasing by an order of magnitude. The second objective was to design a gel that is able to effectively provide adequate glucose control. To achieve satisfactory control, three criteria were used. First, insulin release from the gel should be sustainable for at least two to three days. If a patient is injecting daily, there has been no improvement over the currently used regimen. Second, the device should be able to provide a basal level of insulin throughout the day. As a specified basal value cannot be expected from a polymeric device, this criterion establishes that glucose should stay within a normal range of 70 to 100 mg/dL (3.9 to 5.6 mmol/L) during the day. Finally, the response of the device to a glucose infusion should result in a rapid increase in insulin diffusion, in order to provide adequate control of the disturbance. Using the simulation results and the

control criteria, the parameters were adjusted in order to select the optimal gel design that results in effective control.

7.2.4 Computational Methods

All simulations were performed in MATLAB. To solve the differential equations, the MATLAB function ode23s was used, which is based on a modified Rosenbrock function to solve stiff systems [18]. To solve the system for the Donnan ratio, the function fsolve in the MATLAB Optimization Toolbox was used.

An investigation of the system equations shows that swelling is a function of pH. However, the pH is a function of the buffer concentration in the gel, and the buffer concentration is a function of the Donnan ratio. Because the Donnan ratio is a function of the swelling ratio, the system had to be solved iteratively in order to simultaneously determine the gel pH and the swelling ratio.

Finally, the system was initialized by providing the design characteristics and the basal values of the patient model. The initial values of the device insulin and cross-linking ratio were provided. The initial concentrations of device glucose and gluconic acid were determined using iterations. Because transport was pH dependent, the initial pH, gel swelling, diffusion coefficients, Donnan ratio, and state values had to be determined simultaneously. The source code used to perform the simulations is provided in Appendix J.

7.3 Results

7.3.1 Parameter Effects on Device Insulin Release

Before the gel's ability to control glucose levels is investigated, the system must be designed such that insulin is able to be infused at realistic levels for a period of multiple days. Thus, the transport of insulin was investigated initially to ensure that sufficient release can be achieved. The primary design characteristics important to release are the duration of the release from the device and the magnitude of the insulin infusion rates. All investigations were performed at basal conditions.

Figures 7-7 and 7-8 show the effects of insulin loading on the device behavior. The upper limit on insulin loading was established to be the saturation concentration of insulin in water. Figure 7-7 shows that insulin loading had no effect on the duration of release. As shown in Figure 7-8, insulin loading did affect the flow rates that were achievable. Mathematically, this is easily seen in Equation (7.14), where the concentration driving force is directly dependent on the insulin concentration within the gel. Increasing or decreasing the insulin loading causes a directly proportional increase or decrease in the release rates.

Figures 7-9 and 7-10 show the effects of the number of particles assumed to be circulating at any time. Because the total number of particles possible is size dependent, these results were all determined for a gel with an average collapsed radius of 1.5 μm. As with insulin loading, the number of gels circulating played no role in the duration of release. This can be explained simply by investigating Equation (7.13). Assuming uniform insulin concentrations, each gel will have the same insulin profile, dependent

only upon the mass transfer coefficient and the concentration gradient of insulin. Also like insulin loading, the number of gels has a directly proportional effect with respect to changing the infusion rate from the polymeric device. This can also be seen in Equation (7.14), in which insulin infusion is directly proportional to the number of circulating particles.

Figures 7-11 and 7-12 show the effects of the collapsed particle radius on the gel release characteristics. For each simulation, the number of gel particles in circulation was set at 3.54×10^{7}. The maximum N_g for a particle of radius 1.5 μm is 3.54×10^{10}, and the number was decreased by 3 orders of magnitude in order to ensure the number was feasible for bigger particles, in accordance with Table 7-2. Both figures show a strong dependence on particle size. As the particle size was increases, the duration of insulin release increased. This was a result of the increased diffusion path from gel to the circulation. Mathematically, it is seen in Equation (7.13) that the gel insulin concentration change is inversely proportional to the particle size. The infusion rate, however, will depend on the flux and the gel surface area, resulting in a directly proportional relationship between insulin infusion and the collapsed size of the particle.

Figures 7-13 and 7-14 show the effects of the diffusion coefficient on the gel characteristics. The duration of release was a strong function of the order of magnitude of the diffusion coefficient. An order of magnitude decrease in the diffusion coefficient resulted in an increase in the duration of release from the microparticle. As shown in Figure 7-14, decreasing the diffusivity also resulted in a decrease in the insulin infusion rate, although the device was able to infuse this level of insulin for a longer period of

time. Mathematically, this can be analyzed by an investigation of the model equations. As insulin flux is proportional to the diffusion coefficient, a higher coefficient will result in a higher insulin release rate. The higher infusion rate, when the particle size, the number of gels, and the insulin loading are maintained constant, means the gels are losing their insulin at a faster rate, thus leading to a shorter duration of release.

While the diffusion coefficient of glucose could also have been investigated, it was assumed here that it will likely always be approximately an order of magnitude larger than the insulin coefficient, as a result of the much smaller hydrodynamic radius and its known diffusion coefficient in water relative to that of insulin. Thus, a change in the glucose coefficient was implied when the change was made in the insulin coefficient.

Figures 7-15 and 7-16 show the effects of the gel crosslinking ratio on the gel insulin release characteristics. As the figures show, decreasing the initial crosslinking ratio resulted in an increase in the insulin infusion rate and a decrease in the duration of the gel release, as more was released at a time. Mathematically, this can be explained by observation of Equations (7.30) and (7.31). Physically, as the crosslinking ratio decreases, the average gel mesh size will be larger, as there will be more repeat units between crosslinks. In addition, as previously mentioned, the lower crosslinking ratio will also lead to higher swelling ratios for the same pH environment. Because the swelling ratio also contributes to the mesh size, the crosslinking ratio affects the mesh size in both fashions. An investigation of Equation (7.32) shows that both a larger mesh size and a higher swelling ratio lead to an increase in the diffusion coefficient.

7.3.2 Parameter Effects on Glucose-Induced Swelling

The parameters investigated were those primarily responsible for the insulin release magnitude and duration. In addition, to provide minute-to-minute control of glucose, the gel must be able to rapidly swell and de-swell in response to changing glucose conditions. While the diffusion of glucose is important, this transport will be related to the transport of insulin, and the gel will have to be designed based on the glucose diffusion rate that allows insulin to diffuse at a reasonable level. Of more importance are the effects of glucose on swelling and release. Given that release will be based on the previously mentioned parameters for a given swelling ratio, glucose sensitivity is primarily based on swelling. While realistically, glucose sensitivity would also depend on thermodynamic interactions with other components of the system, the model neglects these interactions. Thus, the important design characteristics are the rate of glucose oxidation to form gluconic acid and the resulting pH from the formation.

Figures 7-17 and 7-18 show the effect of glucose oxidase immobilization with respect to gluconic acid formation and pH. As the figures show, gels with enzyme loadings greater than 0.1 μM did not display different glucose sensitive characteristics by increasing the enzyme loading. At this loading upper limit, all glucose was oxidized very rapidly. As Figure 7-17 shows, high loading resulted in a high gluconic acid concentration, whereas low loading resulted in a low acid concentration. As shown by Figure 7-18, this resulted in a low pH at basal conditions for high loading, and a high pH at basal conditions for low loading. *For low loading, the high pH resulted in low insulin release, which caused glucose levels to rise. However, the low loading resulted in only a*

small amount of gluconic acid produced for the glucose rise, and the pH decrease was very slow. For high loading, the insulin infusion rate was initially high, causing glucose to fall. The drop in glucose caused an equal drop in gluconic acid, raising the pH rapidly. This rise causes insulin release to decrease, resulting in a rise in glucose. This process cycles between high and low release rates, with the goal being to keep glucose oscillating in a physiologically acceptable range.

Figures 7-19 and 7-20 show the effects of varying the pK_g of the monomer used in the hydrogel. As can be seen, the pH in the device was below the transition pH of all three devices at basal conditions. This resulted in a large insulin infusion rate, causing glucose, and ultimately gluconic acid, to decrease at a rapid rate. This decrease caused the pH to increase. As the transition pH was reached, the system collapsed, and gluconic acid ultimately began to increase. As Figure 7-19 shows, however, when the pK_g of the monomer increased, it became more difficult to ever approach the transition pH. Given the conditions, the monomers of pK_g 7.5 and 8 were not able to approach their transition pH values before gluconic acid was completely depleted. Therefore, no transition would ever occur, and these systems would not be able to collapse.

Figures 7-21 and 7-22 show the effects of the functional group loading on the glucose response. Given the same initial gluconic acid concentrations, an increase in the functional group loading resulted in an increase in the basal state pH of the system. This allowed the state of the gel to be controlled such that the device was in the collapsed state at basal conditions. Mathematically, this is because the functional group loading directly

affects the Donnan ratio, which is used to determine the buffer species concentrations within the gel.

An interesting phenomenon was the sharp rise and fall of the pH in Figure 7-22. This occurred because of the recursive relationship between the pH and the swelling ratio. The pH determined the swelling ratio of the species. However, because the swelling ratio also contributed to the Donnan ratio, the swelling ratio affected the internal pH of the system. Thus, as the pH change caused the sharp rise in the device swelling ratio, the sharp rise resulted in a sharp drop of the pH.

7.3.3 Optimization of the Hydrogel Device for Insulin Release

The optimal design of the device occurs in three phases. The first phase is to ensure that release can happen for a long enough duration. The second phase is to then make sure that the steady release is occurring at a high enough delivery rate to be physiologically beneficial. Finally, the system must be optimized in order to ensure glucose response occurs rapidly and effectively enough to maintain normal levels during basal conditions.

The duration of insulin release was shown to depend only upon the diffusion coefficient and the particle size. For an intravenous device, the particle size is limited by the size of the capillaries. Given an average capillary diameter of between 5 and 9 μm, the gels have to be able to flow through the capillaries without getting stuck. Realistically, the particles should then be designed on the submicron level. Using 5 μm as the upper limit for the swollen device diameter results in the maximum collapsed

particle radius of 1.35 μm. However, such a device would only be able to pass through capillaries one gel at a time, and as such the gels would likely not be circulating at a uniform number concentration, as assumed for a pharmacokinetic model.

Based on the development of Equation (7.32), $D_{i,0}$ is actually the diffusion coefficient in the pure solvent. As shown in Table 7-2, this value is on the order of 10^{-7} cm^2/s. As shown in Figure 7-13, this is 4 orders of magnitude greater than a coefficient value that causes a larger particle to be depleted within two hours of circulation. Insulin release will not be at the desired duration for diffusion coefficients on the order of 10^{-15} cm^2/s, a value that is not feasible for a mesh particle system. On the other side, assuming the diffusion coefficient in pure solvent was used, the particles would have to be on the order of one mm in diameter. Such a system would not be able to circulate. In addition, the quasi steady-state assumption would no longer be valid, and the time constants and delays associated with viscoelastic swelling and relaxation would have to be considered. Thus, based on the transport requirements, such a device is not feasible for use as an intravenous delivery system.

While the previous paragraph essentially renders the hydrogel system infeasible as an intravenous insulin delivery device, optimization continued with the assumption that a gel could be developed with the necessary diffusion coefficient-particle size combination that results in release for a duration of three days or longer. Given the release duration, the necessary insulin infusion rate could be achieved simply by increasing or decreasing the insulin loading or number of particles accordingly. For the case in which large particles and fast diffusion is assumed, insulin loading and the

number of particles will have to be reduced by several orders of magnitude to achieve desired levels, as infusion rates will be very high. In contrast, the slow diffusion and small particle assumption will require maximum insulin loading and the maximum number of gels that can feasibly be in circulation.

To optimize the gel for glucose response, two primary objectives must be achieved. First, the gel must be collapsed at basal levels of glucose and lower, and it must expand upon achieving high glucose levels. Second, this response must be fast. To achieve the second objective requires a high enough enzyme loading to result in a gluconic acid concentration within the gel that is able to cause pH changes in the presence of buffers. The first objective can be achieved by careful selection of the type and amount of monomer used in the device. For this optimization, the desired swelling ratio of 3 in the basal state was specified.

Based on this value, different combinations of pK_g and functional group loading were used in the determination of the Donnan ratio and ultimately the pH. This pH was then used to determine the swelling ratio of the system. If this value did not match the original value, the process was used again until the swelling ratios converged. As was often the case, this iterative process diverged to a large swelling ratio, resulting in the low pH values seen in section 6.3.2. Figure 7-23 shows a plot of the specified swelling ratio vs. the actual ratio for a monomer loading of 1 M. The large slopes usually resulted in divergence to the flatter regions of the graph.

Figure 7-24 shows the same iterative routine used with a monomer loading of 4 M. At the low swelling ratio region, the curves became flatter, indicating that the higher

monomer loading allows the collapsed state to be achieved at the basal condition. Based on the figure, the first glucose response objective was achieved by using a monomer with pK_g of 7.0-7.1, at a loading of 4 M or greater. Based on this optimization sequence, and the assumption that size and diffusion limitations are neglected, the gel insulin infusion and glucose response are shown in Figure 7-25 for basal conditions.

The change in glucose resulted in an order of magnitude change in the insulin infusion rate. In this way, the control system was most similar to a simple switching mechanism as opposed to a real controller. Thus, the implicit closed-loop control system was quite inferior to a controller developed using process control principles. Furthermore, the oscillations that occurred resulted in alternating conditions of hyperglycemia and hypoglycemia, although this behavior may have been a consequence of using the minimal model, given its shortcomings from Chapter 6.

7.4 Conclusions

A model has been developed describing the processes associated with implicit closed-loop control, including glucose diffusion into the gel, the oxidation of glucose to form gluconic acid, the effect of gluconic acid on the gel pH, the gel pH effect on gel swelling, and swelling effects on transport. Each model parameter was varied by several orders of magnitude in order to show parametric effects on release duration, insulin delivery rates, and glucose responsiveness. Given the fundamental parametric understanding, the gel was then optimized for glucose control in Type I diabetic patients. Based on physiological considerations, the requirement of small particles and the

inherently fast diffusion times associated with a mesh network result in the conclusion that the use of pH-responsive hydrogels as an intravenous implicit closed-loop glucose control system is likely infeasible, as delivery cannot be sustained for a long enough duration to offer any advantage to current treatment methods.

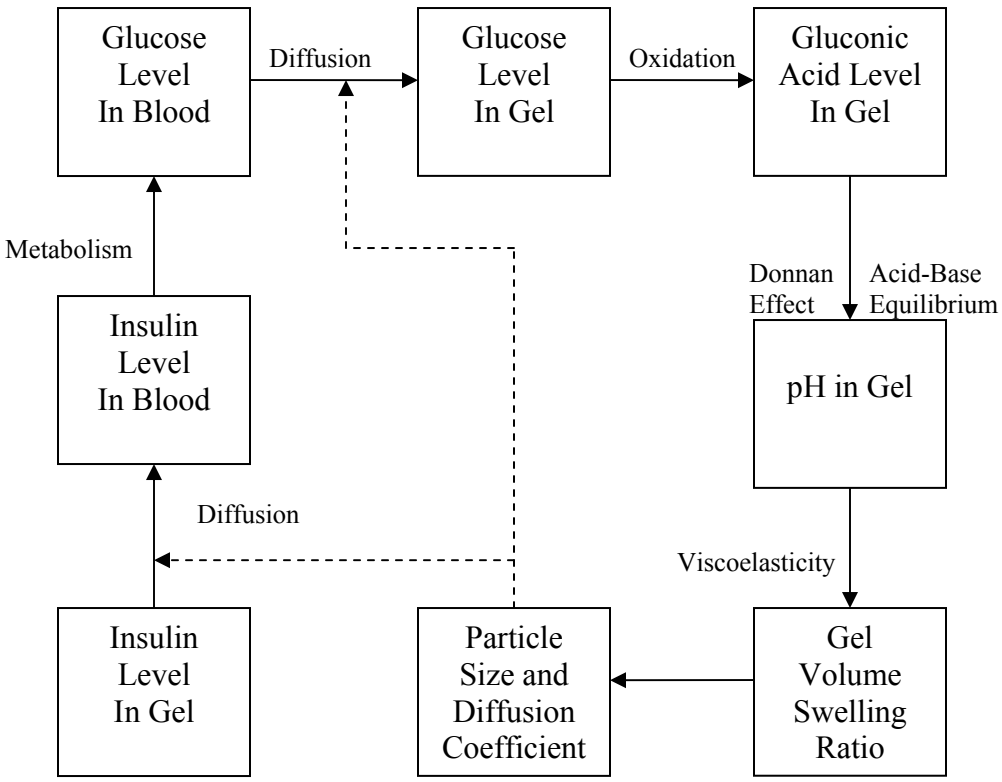

Figure 7-1: Block diagram of the implicit closed-loop control process. Glucose diffuses into the hydrogel along a concentration gradient. Within the gel, glucose is oxidized to form gluconic acid, which causes the pH to decrease within the gel. The pH change results in swelling of the gel network, resulting in an increase in both the particle size and the diffusion coefficients of solutes through the gel. This causes an increase in insulin infusion, which increases glucose uptake. As the glucose production rate decreases, diffusion will decrease, causing less oxidation, an increase in pH, a decrease in volume swelling and diffusion, and a decrease in insulin release.

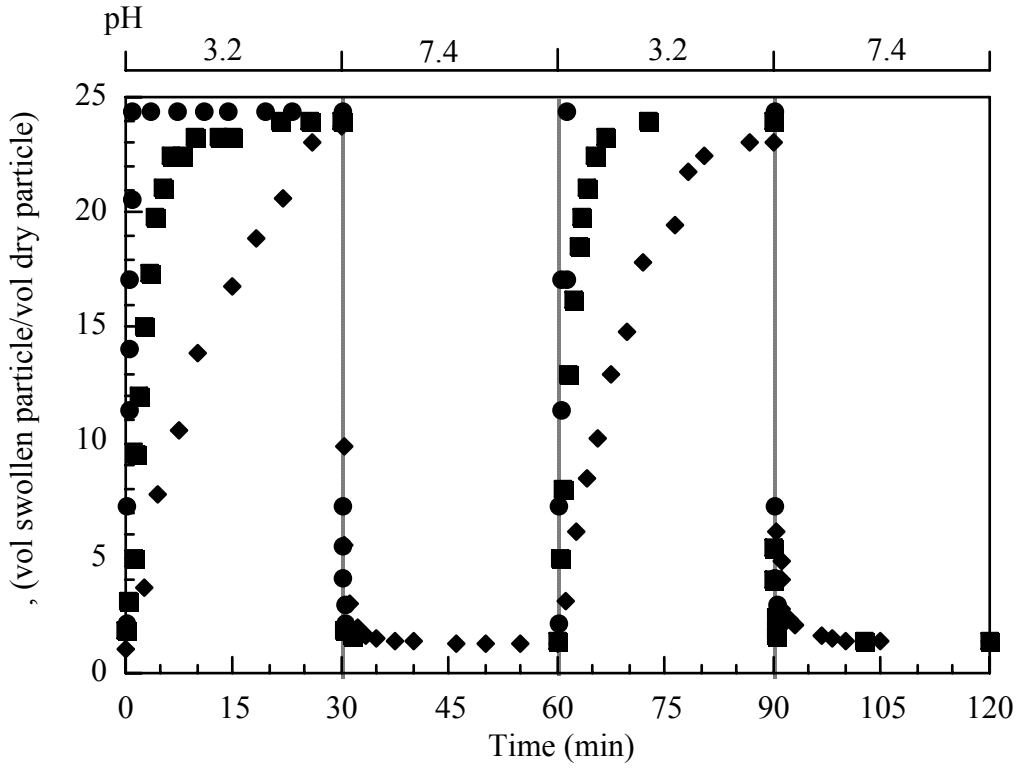

Figure 7-2: Dynamic swelling response of pH-sensitive hydrogel spherical particles to step changes in pH [2]. The circles represent a particle radius of 30 μm, squares represent a particle radius of 170 μm, and the diamonds represent a particle radius of 300 μm.

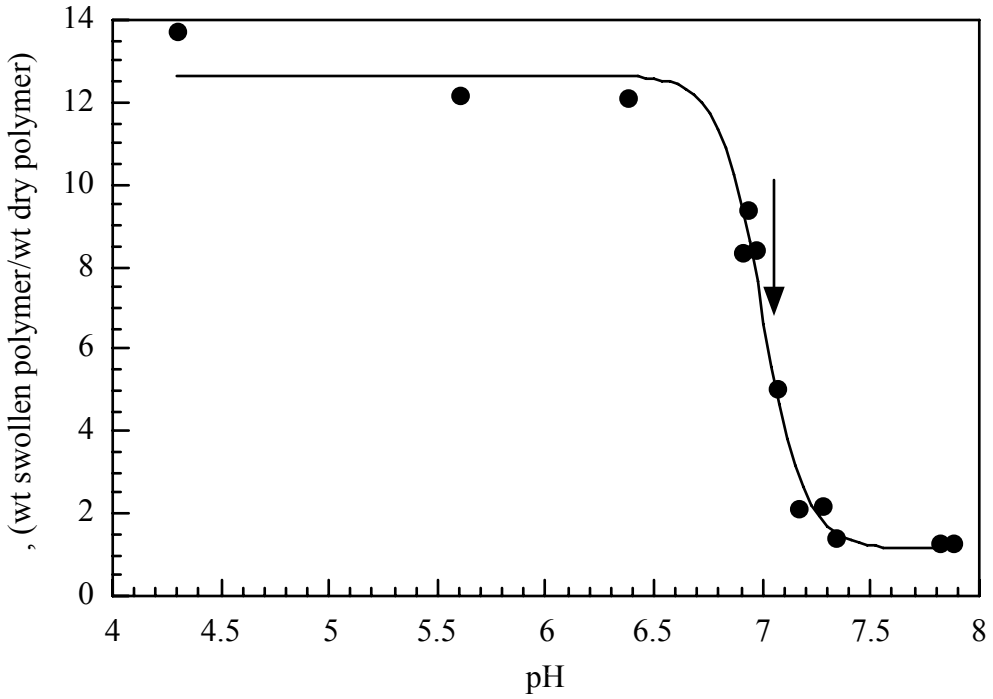

Figure 7-3: Typical equilibrium swelling curve for pH-sensitive cationic hydrogel.

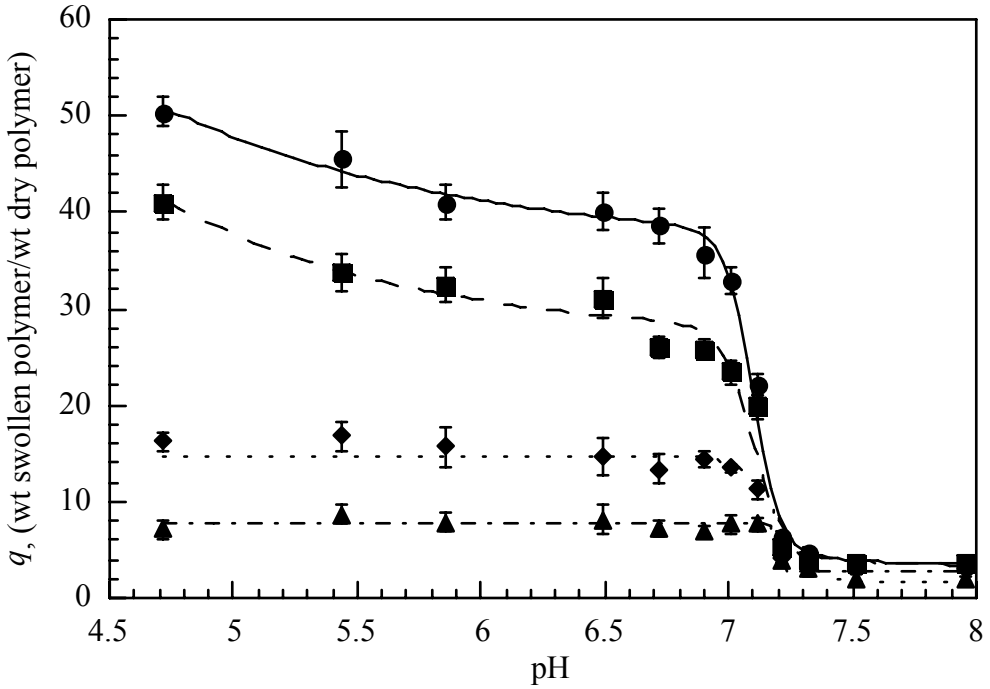

Figure 7-4: Equilibrium swelling response of pH-sensitive cationic hydrogels as a function of pH and crosslinking ratio [1]. Circles represent a crosslinking ratio of 0.005, squares represent 0.01, diamonds represent 0.02, and triangles represent a ratio of 0.04.

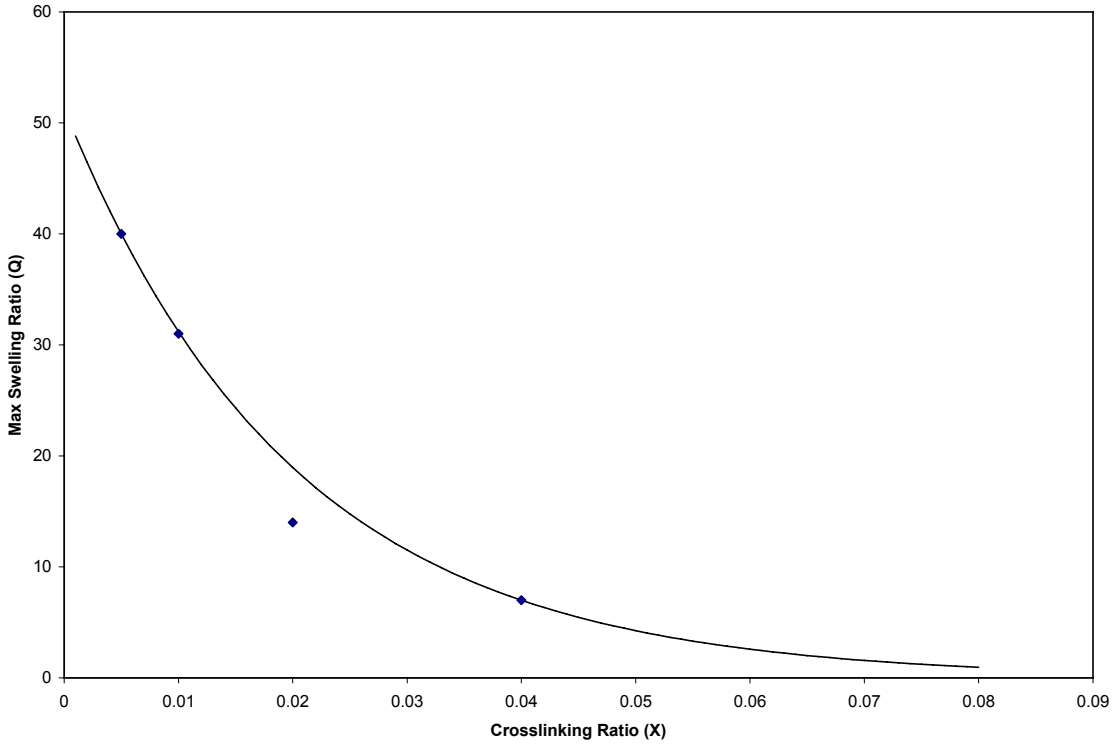

Figure 7-5: Maximum swelling ratio of pH-sensitive cationic hydrogel as a function of the crosslinking ratio. The line represents an exponential function used to fit the data.

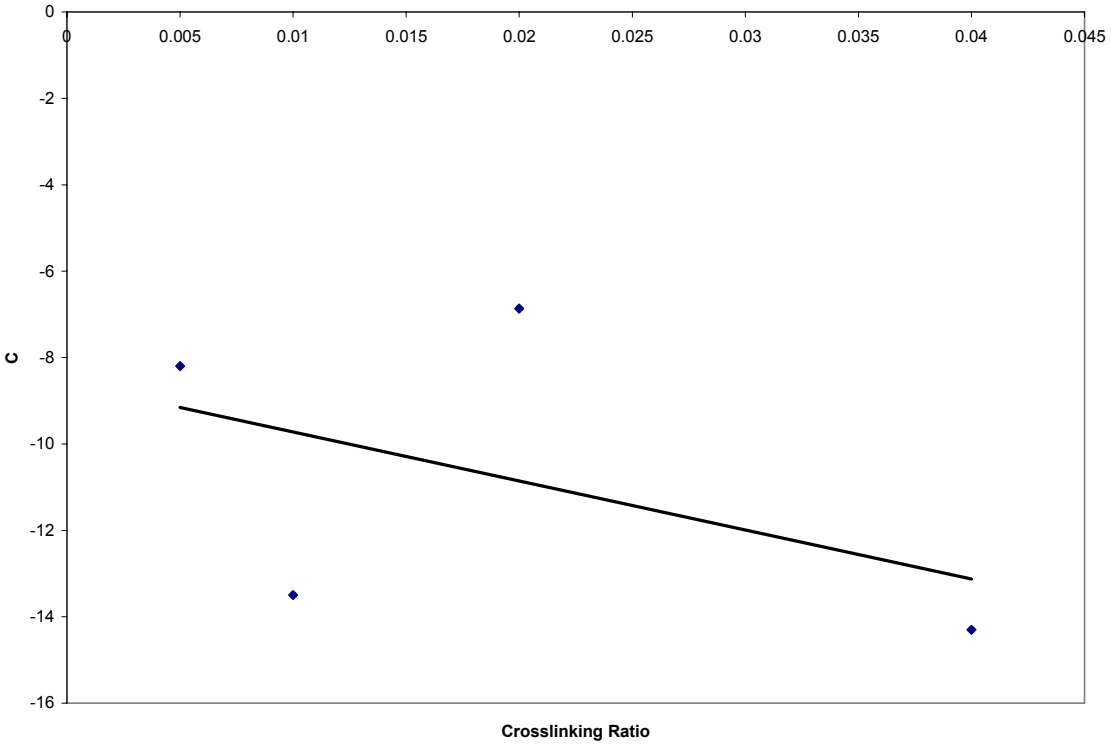

Figure 7-6: Change of hyperbolic tangent parameter C with respect to crosslinking ratio.

Table 7-1: Nominal Parameter Values Used For Hydrogel Device Simulations		
Parameter	**Value**	**Units**
$I_{D,0}$	$1x10^{8}$	mU L^{-1}
$R_{collapsed}$	5	μm
$D_{I,0}$	$1.41x10^{-13}$	cm^2 s^{-1}
$D_{G,0}$	$6.9x10^{-12}$	cm^2 s^{-1}
l_c	1.54	Å
L	0.5	μm
pK_g	7.1	dimensionless
σ	1.0	M
pH_{blood}	7.4	dimensionless
X_0	0.004	dimensionless
k_d	0.001	min^{-1}
C_{enz}	1	μM
V_{max}	$51.6C_{enz}$	mmol L^{-1} min^{-1}
K_S	0.6187	mmol L^{-1}
r_I	16	Å
r_G	2.5	Å
$[H^+]_{blood}$	$3.98x10^{-8}$	M
$[Na^+]_{blood}$	142	mM
$[K^+]_{blood}$	4.2	mM
$[Ca^{2+}]_{blood}$	1.2	mM
$[Cl^-]_{blood}$	108	mM
$[HCO_3^-]_{blood}$	25	mM
$[CO_2]_{blood}$	1.224	mM
Carbonate Buffer pK_a	6.33	dimensionless

Table 7-2: Particle Size Effects on Maximum Number of Circulating Particles	
$R_{collapsed}$ (μm)	N_G (dimensionless)
1	1.19E+11
5	9.55E+08
10	1.19E+08
25	7.64E+06
50	9.55E+05

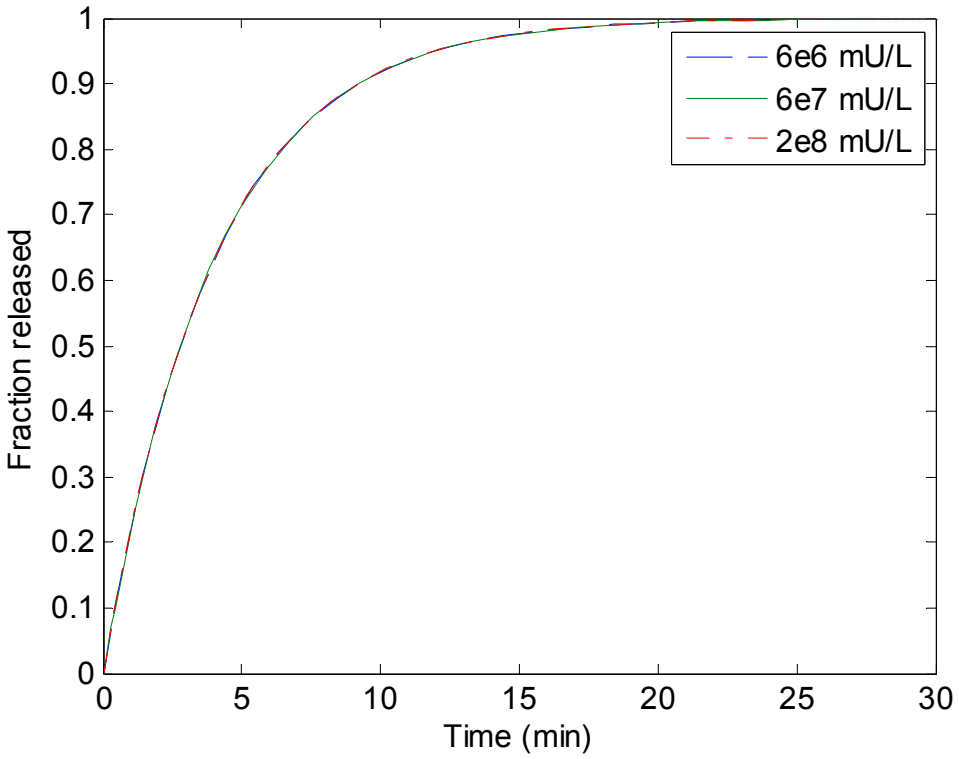

Figure 7-7: Fraction of insulin released as a function of time and the initial gel insulin concentration.

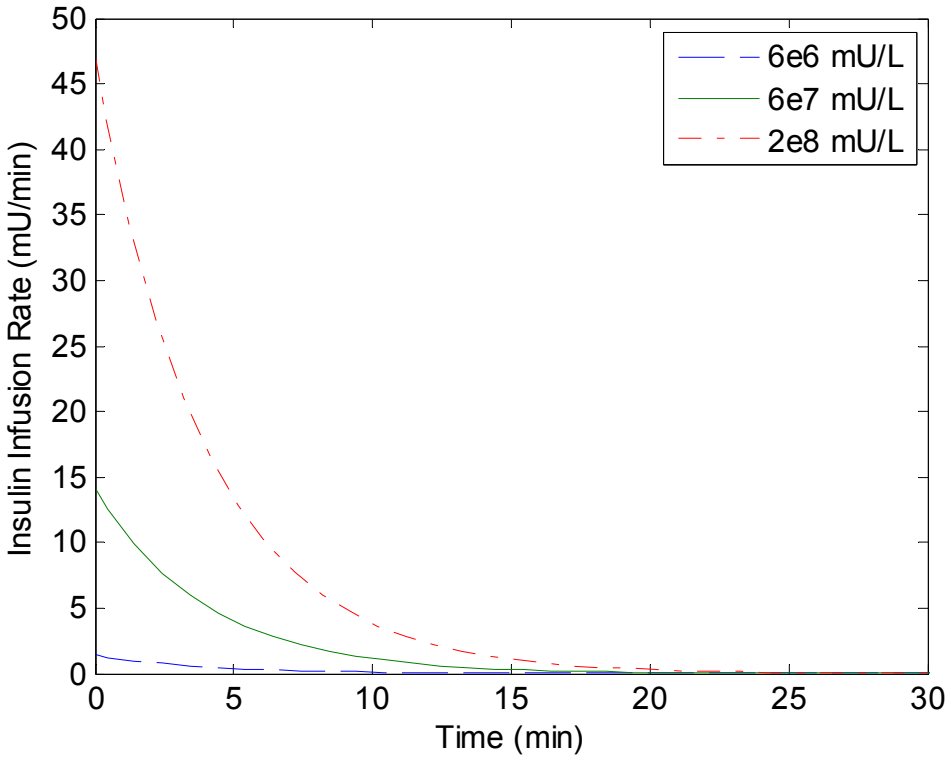

Figure 7-8: Insulin infusion rate as a function of time and initial gel insulin concentration.

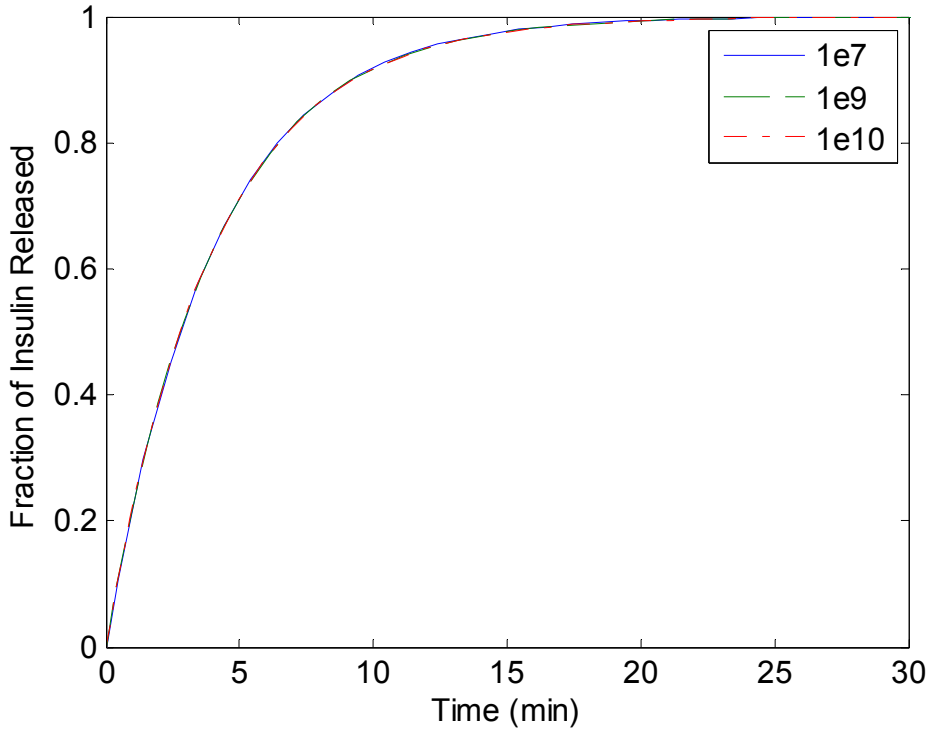

Figure 7-9: Fraction of insulin released as a function of time and the number of circulating gels. The particle is assumed to have a collapsed state radius of 1.5 μm.

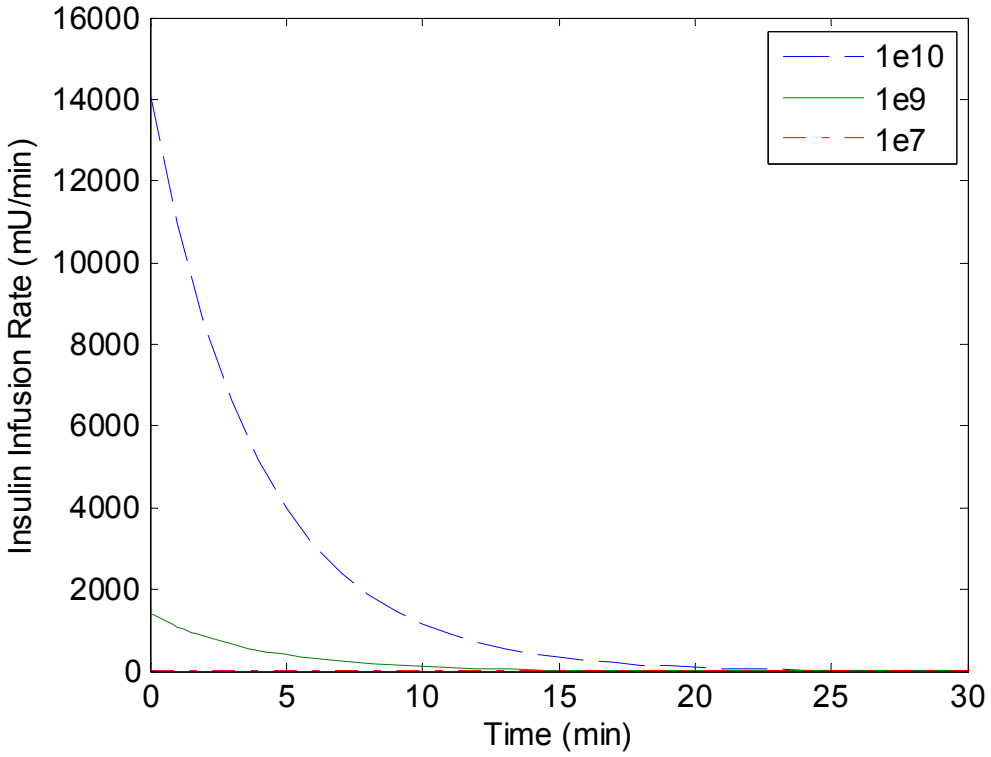

Figure 7-10: Insulin infusion rate as a function of time and the number of circulating hydrogel particles. Particles are assumed to be 1.5 μm in radius in the collapsed state.

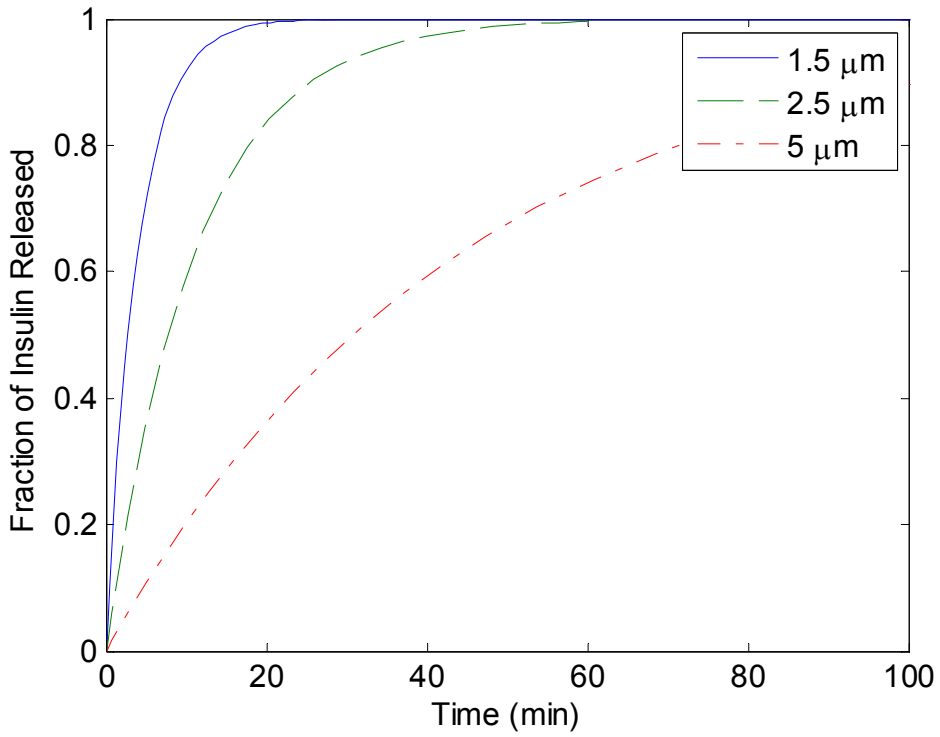

Figure 7-11: Fraction of insulin released as a function of time and collapsed particle size. For all sizes, it is assumed that 3.54×10^7 gels are in circulation.

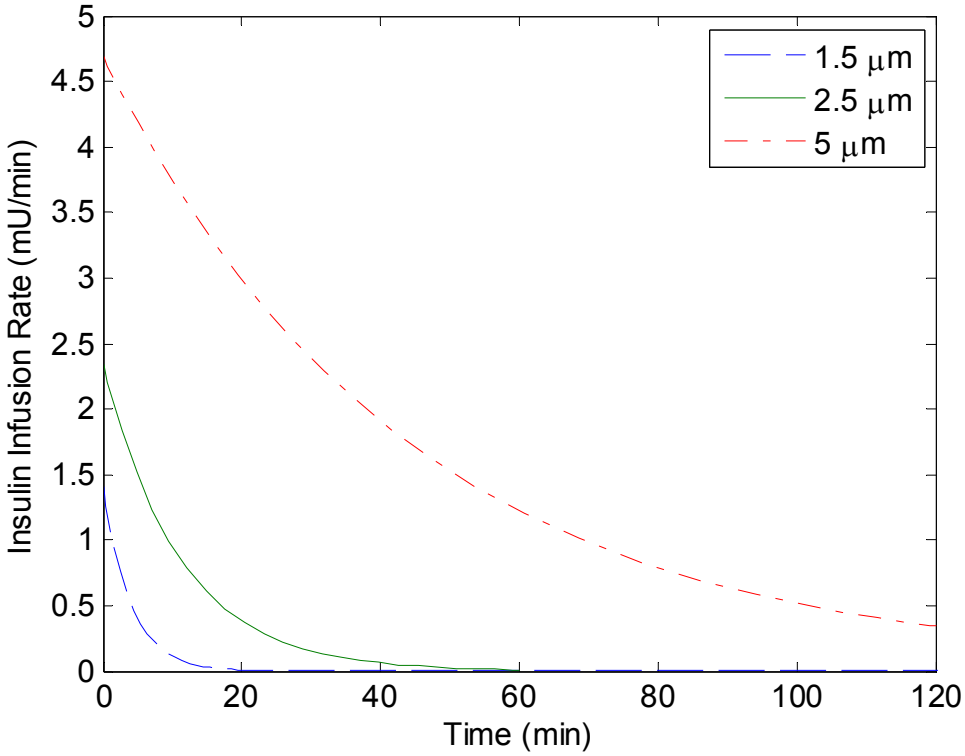

Figure 7-12: Insulin infusion rate as a function of time and the collapsed particle size. For the simulations, there are 3.54×10^7 particles in circulation.

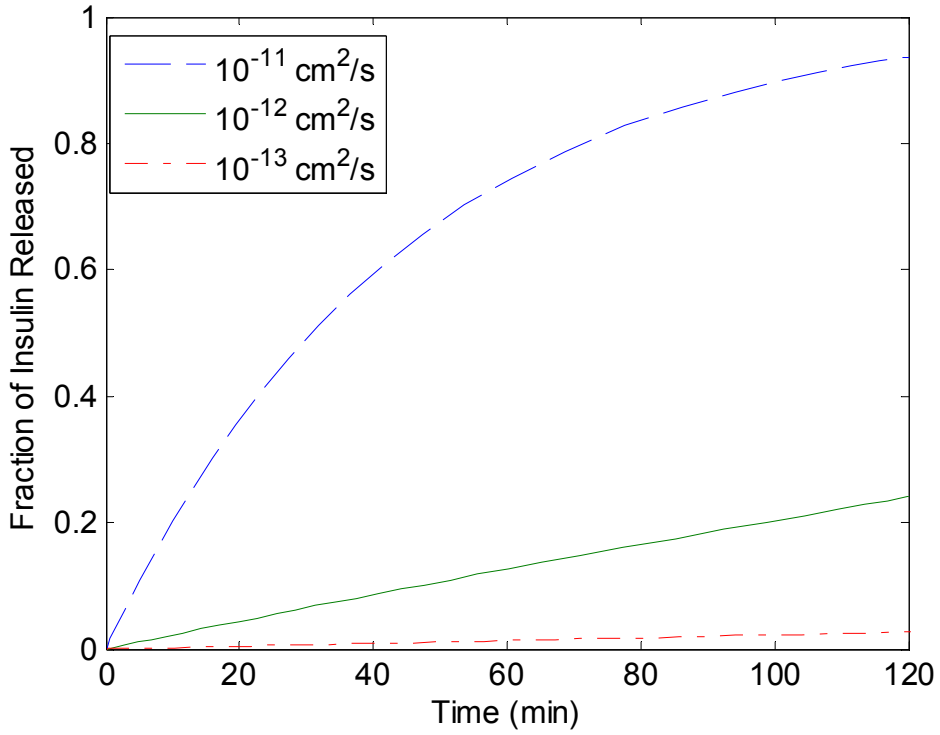

Figure 7-13: Fraction of insulin released as a function of time and the diffusion coefficient of insulin, $D_{i,0}$.

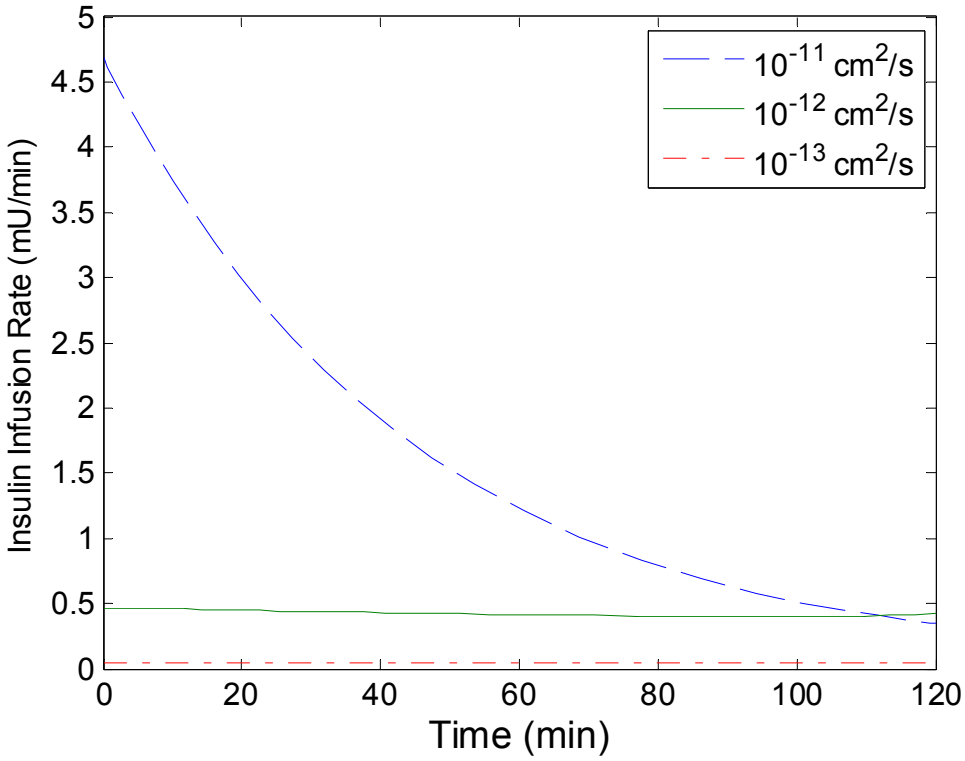

Figure 7-14: Insulin infusion rate as a function of time and the insulin diffusion coefficient, $D_{i,0}$.

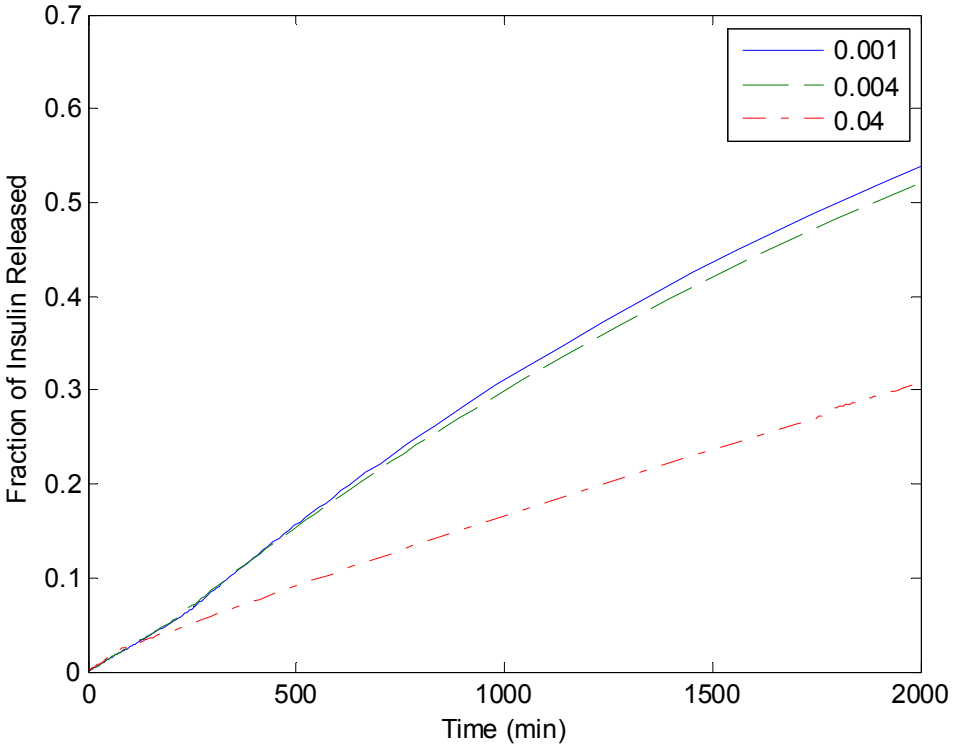

Figure 7-15: Fraction of insulin released as a function of time and the initial crosslinking ratio of the hydrogel network.

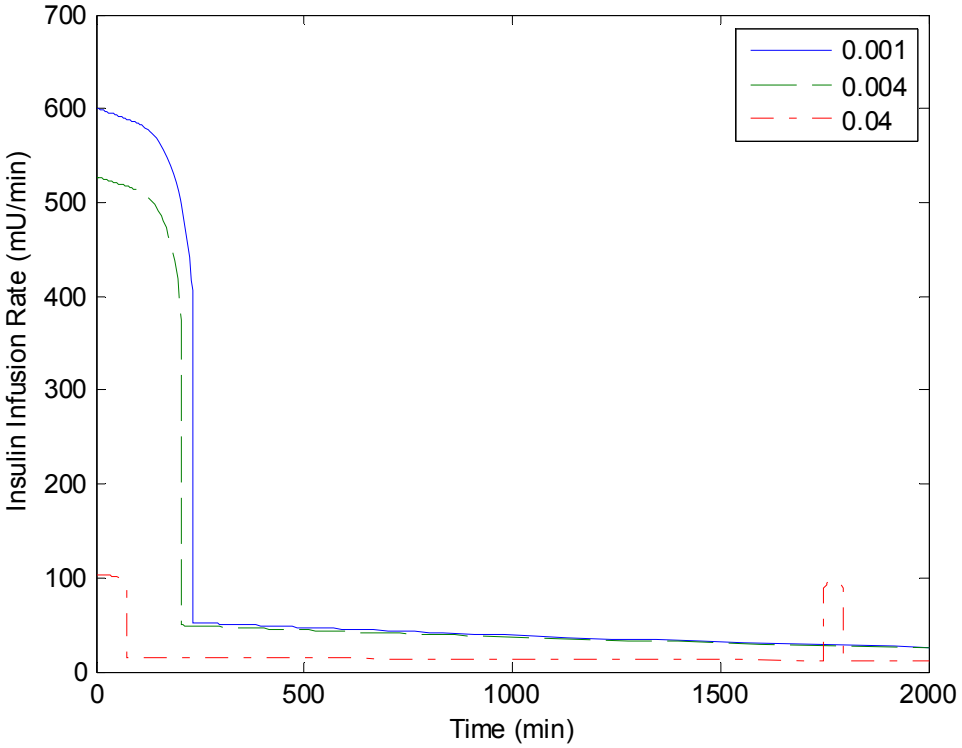

Figure 7-16: Insulin infusion rate as a function of time and crosslinking ratio. The rapid fall is a result of the high infusion rates causing the particle to collapse and, thereby decreasing the infusion rate. The rapid rise of the rate for X = 0.04 is a result of a rapid swelling as the glucose concentration increases.

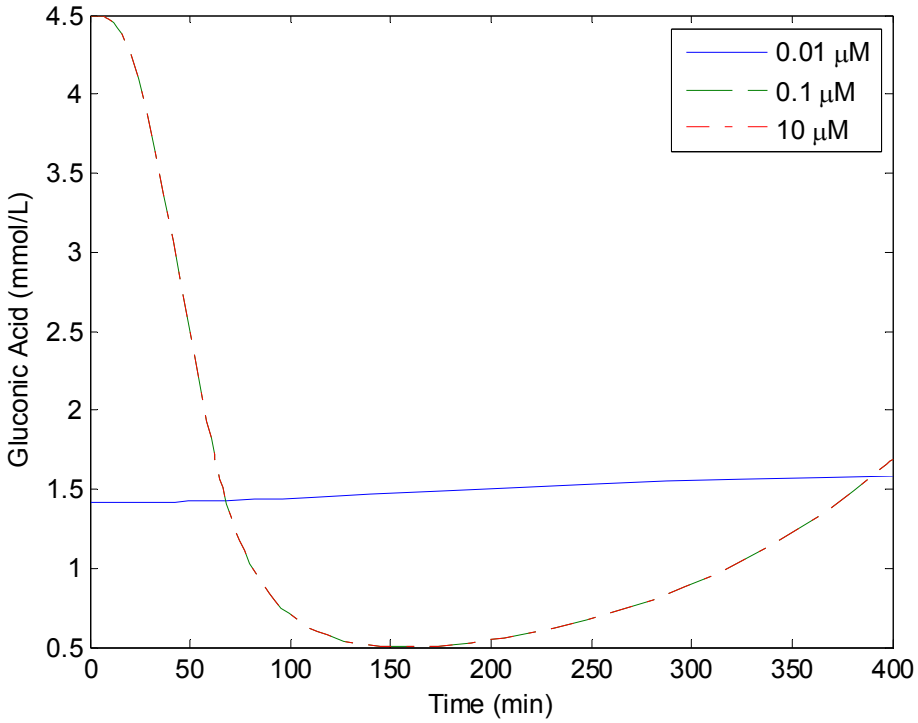

Figure 7-17: Gluconic acid concentration as a function of time and enzyme loading. The initial value is the gluconic acid concentration at basal conditions. For low loading, low gluconic acid levels result in low infusion rates, causing a rise in glucose levels. The high loading results in all glucose being oxidized rapidly, leading to very high infusion rates. This causes glucose to drop until the insulin infusion drops to a level that causes a glucose rise again. For glucose oxidase loading above 0.1 μM, the response does not change with increasing loading.

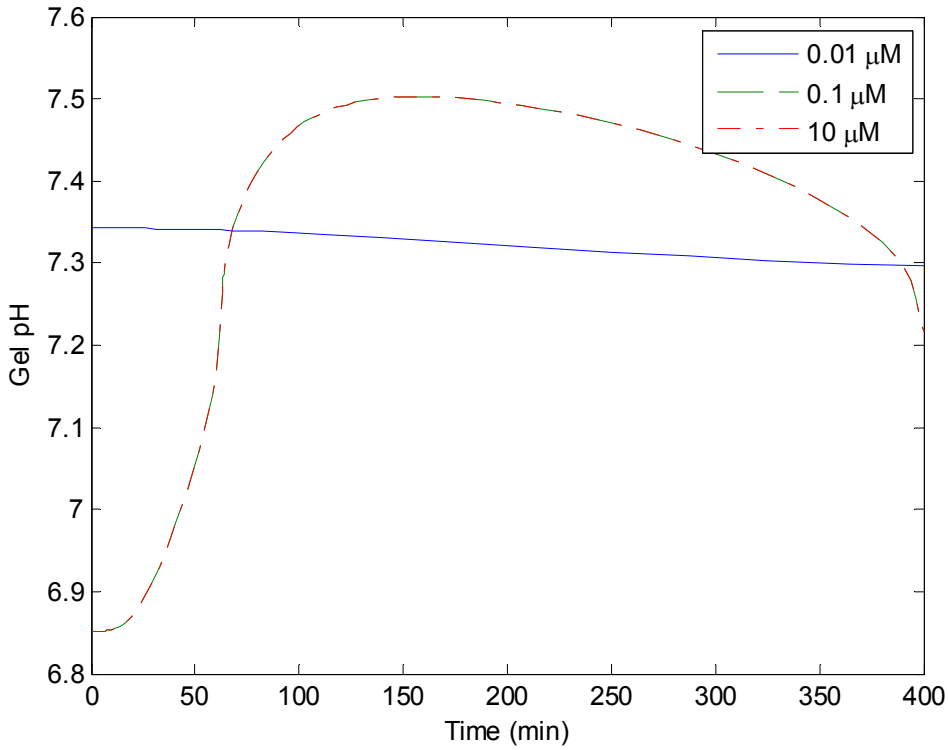

Figure 7-18: Gel pH as a function of time and enzyme loading. When there is insufficient enzyme to oxidize glucose, the gel exists in the collapsed state for basal glucose levels, and the pH level changes slowly. As glucose oxidase is increased, the gel is at a lower pH for the given glucose concentration, and pH changes are more rapid for changing glucose levels. Above 0.1 μM, the enzyme response does not change, indicating enzyme saturation for the particular level of glucose.

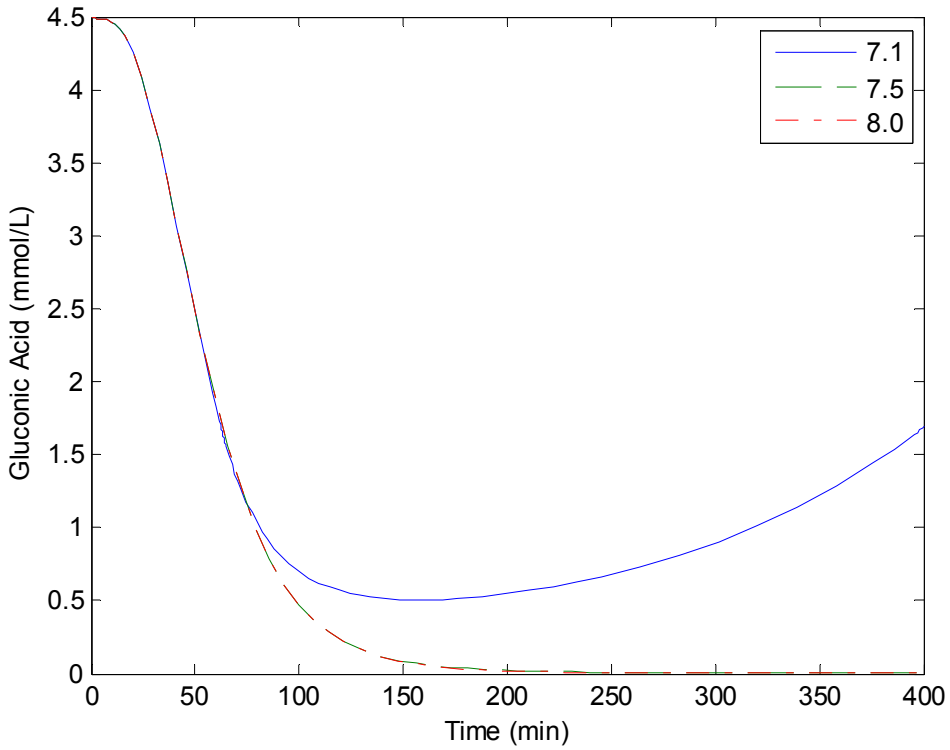

Figure 7-19: Gluconic acid concentration as a function of time and the pK of the monomer used in the hydrogel device. Identical behavior is seen for systems with monomer pKs of 7.5 and 8.0.

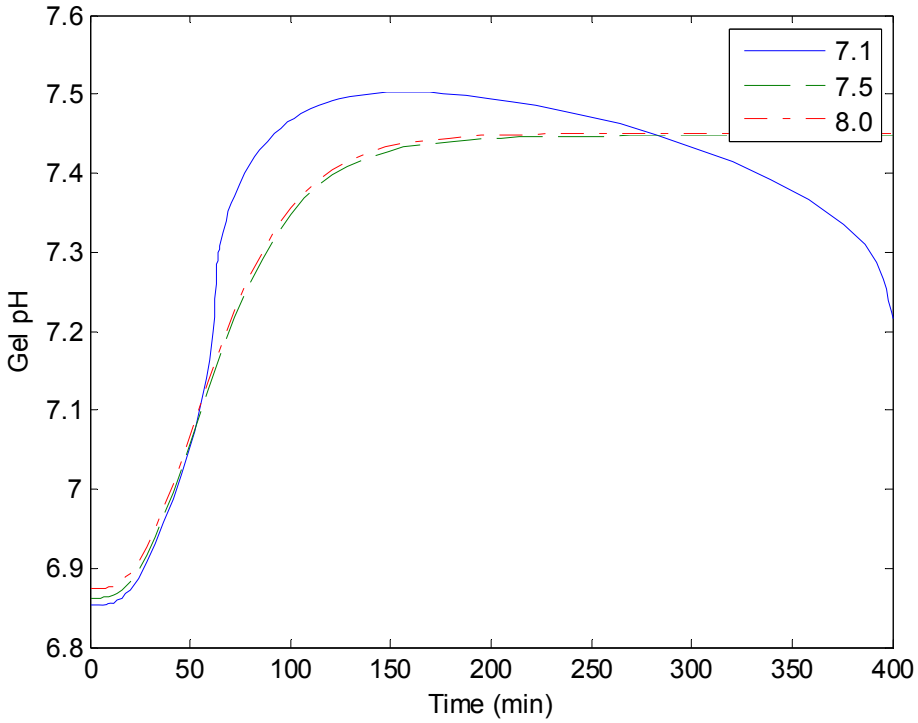

Figure 7-20: Gel pH as a function of time and the pK of the monomer used in the hydrogel.

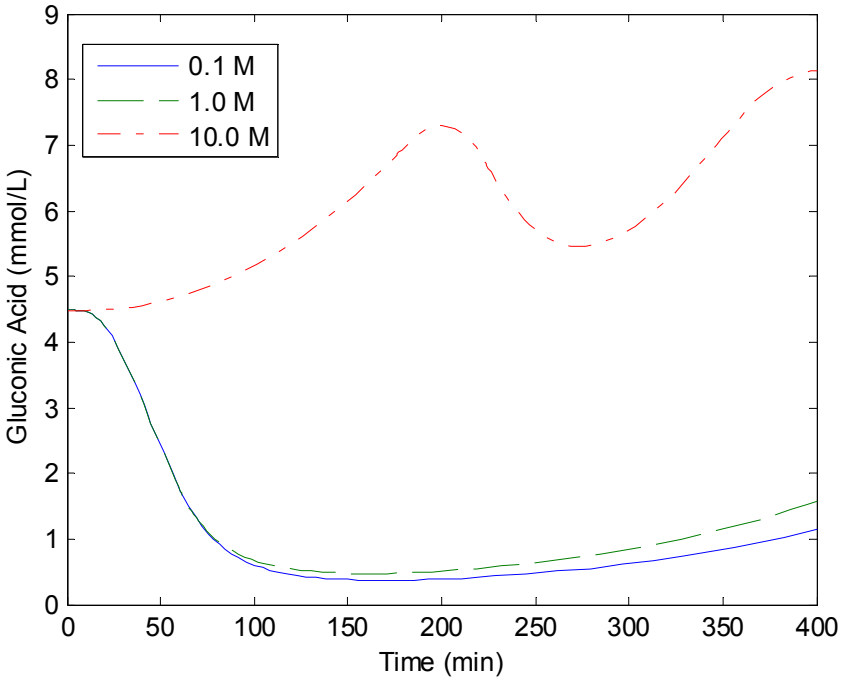

Figure 7-21: Gluconic acid as a function of time and the functional group loading in the hydrogel device.

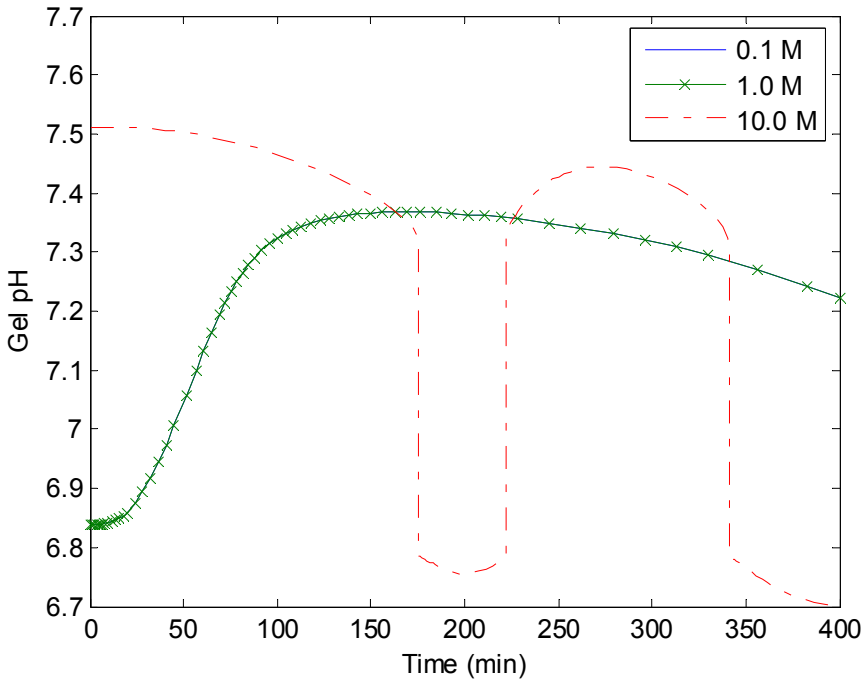

Figure 7-22: Gel pH as a function of time and function group loading in the hydrogel device.

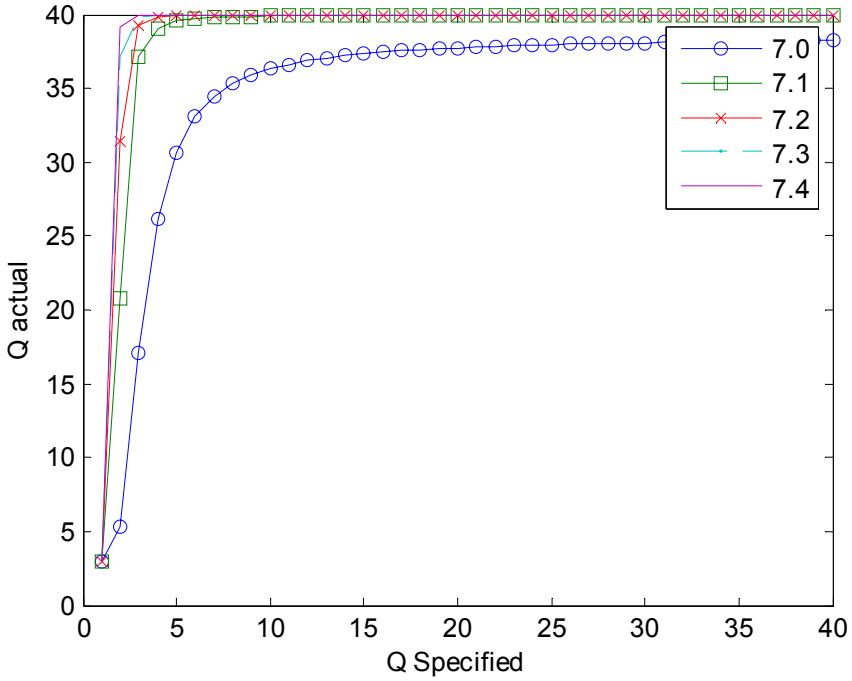

Figure 7-23: Results of device optimization for optimal pK_g and monomer loading. For each pK_g value, a Q is specified and used with a monomer loading of 1 M to determine the Donnan ratio. The Donnan ratio is then used to calculate pH and the actual Q. If Q actual does not match Q specified, the process is performed again until the two swelling ratios converge.

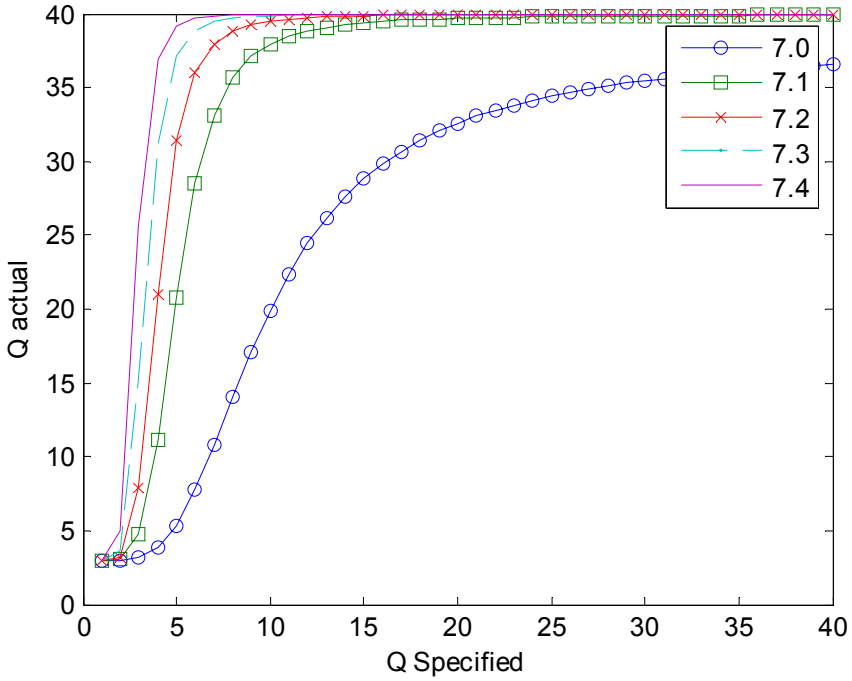

Figure 7-24: Results of device optimization for optimal pK_g and monomer loading. For each pK_g value, a Q is specified and used with a monomer loading of 4 M to determine the Donnan ratio. The Donnan ratio is then used to calculate pH and the actual Q. If Q actual does not match Q specified, the process is performed again until the two swelling ratios converge.

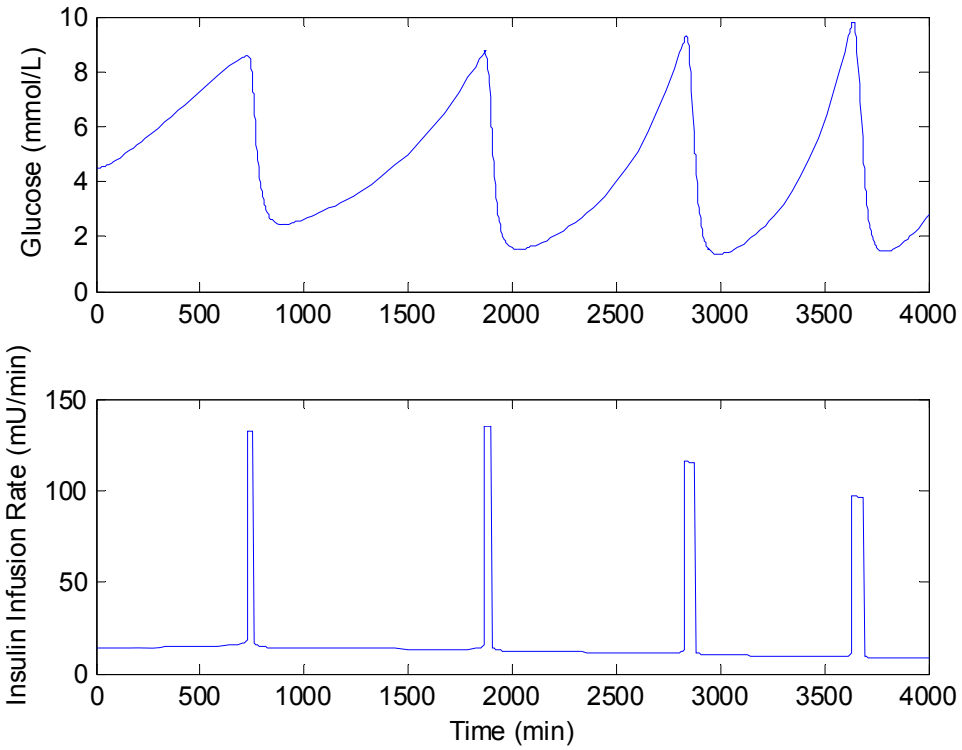

Figure 7-25: Minimal model implicit closed-loop controlled glucose response at basal conditions, over a period of 2.8 days. $N_G = 5x10^{10}$, $D_{I,0} = 1.41x10\text{-}15$ cm^2/s, $R_{collapsed} = 1.35$ μm, $\sigma = 1$ M, enzyme loading = 0.1 μM, and $pK_g = 7.0$.

7.5 References

1. Podual, K., Doyle, F. J., III, and Peppas, N. A., "Preparation and Dynamic Response of Cationic Copolymer Hydrogels Containing Glucose Oxidase," *Polymer*, **41**, 3975-3983, 2000.

2. Podual, K., Doyle, F. J., III, and Peppas, N. A., "Dynamic Behavior of Glucose Oxidase-Containing Microparticles of Poly(Ethylene Glycol)-Grafted Cationic Hydrogels In an Environment of Changing pH," *Biomaterials*, **21**, 1439-1450, 2000.

3. Bergman, R. N., Ider, Y. Z., Bowden, C. R., and Cobelli, C., "Quantitative Estimation of Insulin Sensitivity," *Am. J. Physiol.*, **236**, E667-E677, 1979.

4. Abdekhodaie, M. J., and Wu, X. Y., "Modeling of a Cationic Glucose-Sensitive Membrane With Consideration of Oxygen Limitation," *J. Membrane Sci.*, **254**, 119-127, 2005.

5. Guyton, A. and Hall, J., *Textbook of Medical Physiology*, 11th ed., Elsevier Saunders, Philadelphia, PA, 2006.

6. Kaplan, L. A., Pesce, J. A., and Kazmierczak, S. C., Eds., *Clinical Chemistry: Theory, Analysis, Correlation, 3rd Ed.*, Mosby, St. Louis, MO, 1996.

7. Cooney, D. O., *Biomedical Engineering Principles: An Introduction To Fluid, Heat, and Mass Transport Processes*, Dekker, NY, 1976.

8. Ricka, J. and Tanaka, T., "Swelling of Ionic Gels: Quantitative Performance of the Donnan Theory," *Macromolecules*, **17**, 2916-2921, 1984.

9. Siegel, R. A., "Hydrophobic Weak Polyelectrolyte Gels: Studies of Swelling Equilibria and Kinetics," in *Advances in Polymer Science 109*, *Responsive Gels: Volume Transitions I*, K. Dusek, Ed., Springer-Verlag, NY, 233-267, 1993.

10. Lustig, S. R., and Peppas, N. A., "Solute Diffusion in Swollen Membranes. IX. Scaling Laws For Solute Diffusion In Gels," *J. App. Polymer Sc.*, **36**, 735-747, 1988.

11. Batycky, R. P., Hanes, J., Langer, R., and Edwards, D. A., "A Theoretical Model of Erosion and Macromolecular Drug Release From Biodegrading Microspheres," *J. Pharm. Sci.*, **86** (12), 1464-1477, 1997.

12. Martens, P., Metters, A. T., Anseth, K. S., and Bowman, C. N., "A Generalized Bulk-Degradation Model For Hydrogel Networks Formed From Multivinyl Cross-linking Molecules," *J. Phys. Chem. B*, **105**, 5131-5138, 2001.

13. Furler, S. M., Kraegen, E.W., Smallwood, R.H, and Chisolm, D.J., "Blood Glucose Control by Intermittent Loop Closure in the Basal Mode: Computer Simulation Studies with a Diabetic Model", *Diabetes Care*, **8**, 553-561, 1985.

14. Podual, K., Doyle, F. III, and Peppas, N. A., "Modeling of Water Transport In and Release From Glucose-Sensitive Swelling-Controlled Release Systems Based On Poly(Diethylaminoethyl Methacrylate-g-Ethylene Glycol)," *Ind. Eng. Chem. Res.*, **43**, 7500-7512, 2004.

15. Becton-Dickinson, "Diabetes Education", available http://www.bddiabetes.com, Sept. 2006.

16. Lozner, E. L., Winkler, E. W., Taylor, F. H. L., and Peters, J. P., "The Intravenous Glucose Tolerance Test," J. Clin. Invest., **20**, 507-515, 1941.

17. Owens, D. E. III and Peppas, N. A., "Opsonization, Biodistribution, and Pharmacokinetics of Polymeric Nanoparticles," *Intern. J. Pharm.*, **307**, 93-102, 2006.

18. Shampine, L. F. and Reichelt, M. W., "The MATLAB ODE Suite," *SIAM J. Sci. Comput.*, **18**, 1-22, 1997.

CHAPTER 8

CONCLUSIONS

As the role of chemical engineering in the development of solutions of today's medical and biological problems continues to grow, the application of systems engineering toward the development of optimal materials and optimal drug delivery regimens will increase. By considering the body to be a complex chemical process and medical problems as behaviors of the process, the systems engineer can develop solutions to today's medical problems in the same way that solutions are developed in a chemical plant. The treatment of Type I diabetes mellitus is a problem that can be investigated by treating glucose homeostasis as the process, and controlling glucose levels to prevent hyperglycemia and hypoglycemia as the control objective.

The goal of this research was to investigate diabetes treatment from a systems engineering standpoint. Specifically, the goal was to perform simulations that demonstrate the efficacy of both explicit and implicit closed-loop control methods with respect to controlling glucose levels for basal conditions, during a meal, and during exercise. To perform the simulations, three objectives had to be met. First, an identified patient model was either to be developed or retrieved from literature. Second, insulin pump algorithms were to be developed using principles of process control, and the ability of these algorithms to control glucose was to be investigated. Finally, a process model describing the implicit closed-loop control process utilizing pH-responsive cationic

hydrogel microspheres was to be developed and used in simulations to optimize the delivery of insulin to control glucose levels.

Two different model frameworks were developed to describe the significant features of the glucose homeostasis process. Included in the models were the primary fuels, glucose, fatty acids, and amino acids. Also included in the models were the primary hormones involved in the process, including insulin, glucagon, epinephrine, and glucagon-like peptide-1. Both a simple pharmacokinetic model framework and a physiological model were developed. The model parameters have not been identified, because appropriate data to perform the parameter estimation were not easily acquired. The subject of parameter estimation was investigated to determine how well parameters can be estimated using nonlinear least squares algorithms. It was determined that typical estimates have large confidence intervals and are highly dependent on an initial guess of the parameter values. Estimation can be improved by utilizing the dynamic sensitivity equations in the estimation routine and by using a stiff differential equation solver. It was also shown that different parameter sets can result in satisfactory fits to data, thus making is possible that multiple parameter sets may be able to both fit the data and predict future results.

Insulin infusion algorithms were investigated by implementing them in the minimal model [1], the Sorensen model [2], and the Hovorka model [3], using a range of model parameters. Using the minimal model, it was observed that no method of control was able to reduce the glucose excursion resulting from a 50 g oral glucose ingestion without also resulting in severe hypoglycemia. This was attributed to the model's

possible underprediction of the role of glucose in glucose uptake. Both the Sorensen model and Hovorka model simulations showed that simple proportional control can be used to control glucose in response to oral ingestion. An investigation of the Sorensen model shows that the role of glucose in glucose uptake is likely overstated, making simulation results with the Sorensen diabetic model questionable with respect to accuracy. The Hovorka model, while able to control glucose during both a glucose ingestion and exercise, may overestimate the role of insulin in glucose uptake, as predicted infusion rates are much lower than those rates seen in literature [4].

To perform simulations of implicit closed-loop control, a model describing the dynamics of glucose diffusion and oxidation, gluconic acid production and diffusion, and the changes in the gel pH, device swelling, and device transport properties was developed using the quasi steady-state assumption with respect to the particle size. It was shown that the particle size is limited for intravenous use by the diameter of the capillaries, and that at the maximum particle size, the diffusion coefficient of insulin in the gel system would have to be several orders of magnitude lower than what is realistically possible. It was concluded that microspheres of pH-responsive cationic hydrogels are infeasible for use in intravenous insulin delivery.

In conclusion, the developed models have the potential to be more descriptive than existing models describing the glucose homeostasis system, if patient data of sufficient richness becomes available. Ideally, the data would describe the individual effects of each metabolic species on each metabolic rate associated with glucose metabolism. Second, implicit closed-loop control via the intravenous route is not

feasible, as release would occur too quickly to be useful. Finally, the effectiveness of intravenous explicit closed-loop control is model dependent, but given its superiority relative to the hydrogel in the ability to give a precisely determined insulin dose, the use of implanted pumps shows more promise than the use of a polymeric system at utilizing the intravenous route to control glucose in diabetic patients.

8.1 References

1. Bergman, R. N., Ider, Y. Z., Bowden, C. R., and Cobelli, C., "Quantitative Estimation of Insulin Sensitivity," *Am. J. Physiol.*, **236**, E667-E677, 1979.

2. Sorensen, J. T., "A Physiologic Model of Glucose Metabolism in Man and Its Use to Design and Assess Improved Insulin Therapies For Diabetes", Ph.D. thesis, Dept. Chem. Eng., Massachusetts Institute of Technology, Cambridge, 1985.

3. Hovorka, R., Canonico, V., Chassin, L. J., Haueter, U., Massi-Benedetti, M., Federici, M. O., Pieber, T. R., Schaller, H. C., Schaupp, L., Vering, T., and Wilinska, M. E., "Nonlinear Model Predictive Control of Glucose Concentration In Subjects With Type I Diabetes", *Physiol. Meas.*, **25**, 905-920, 2004.

4. Guyton, A. and Hall, J., *Textbook of Medical Physiology*, 11th ed., Elsevier Saunders, Philadelphia, PA, 2006.

APPENDIX A

MINIMAL MODEL DERIVATION

To derive minimal model, the pharmacokinetics of the system must be known or assumed. Bergman and Cobelli [1] assumed that glucose metabolism occurred in a single well-mixed compartment, that insulin metabolism occurred in one compartment, and that any insulin action that affects glucose metabolism occurs only after insulin is bound to cells, representing this bound insulin in a "remote" compartment. They considered three primary glucose reactions, excluding the removal of glucose from the kidneys at or above a threshold glucose value. The three reactions were glucose uptake into liver, glucose production by the liver, and glucose uptake by the periphery, defined as all other tissue systems in the body. These kinetics are described by Equation (A.1).

$$\frac{dG(t)}{dt} = R_{prod,L} - R_{up,L} - R_{up,P} \tag{A.1}$$

Where the subscripts L and P represent the liver and periphery, respectively. Because the liver is both producing and consuming glucose, the two terms were combined to form the net hepatic glucose production rate, NHGP. Based on physiologic knowledge, NHGP was known to have a dependence on both glucose and insulin. There is also a base level of glucose produced independently of concentration. Based on these assessments, NHGP was expressed mathematically by Equation (A.2).

$$NHGP(t) = R_{prod,0} - [k_1 + k_2 I'(t)]G(t) \qquad \text{(A.2)}$$

The variable I'(t) represents the insulin concentration in the remote compartment, and by inspection it can be seen that the elimination rates are modeled as simple reaction kinetics. NHGP is assumed to be first order with respect to glucose and first order with respect to remote compartment insulin.

Glucose uptake into the periphery is also known to have a glucose dependence and an insulin dependence. To account for the fact that glucose uptake is linear with glucose concentration, but not necessarily proportional, the authors introduced a constant into the relationship to describe peripheral uptake by Equation (A.3).

$$R_{up,P} = [k_3 + k_4 I'(t)]G(t) + R_{up,P,0} \qquad \text{(A.3)}$$

Combining Equations (A.2) and (A.3), results in the equation of glucose pharmacokinetics, as shown by (A.4).

$$\frac{dG(t)}{dt} = \left(R_{prod} - R_{up,P}\right)_0 - [(k_1 + k_3) + (k_2 + k_4)I'(t)]G(t) \qquad \text{(A.4)}$$

Insulin is assumed to be produced by the pancreas and eliminated by either uptake or degradation.

$$\frac{dI(t)}{dt} = R_{prod} - R_{elim} \tag{A.5}$$

For diabetic patients, insulin is production is taken to be zero. All insulin elimination is assumed to occur via first order kinetics in insulin. The rate coefficient of each first order process is combined to form the elimination coefficient, n. Using these assumptions, Insulin kinetics, assuming insulin infusion from a source at a rate U(t), is given by Equation (A.6).

$$\frac{dI(t)}{dt} = \frac{U(t)}{V} - nI(t) \tag{A.6}$$

The parameter V is the total insulin distribution volume.

A portion of the insulin in the body is used to increase glucose uptake into liver and muscle cells. The rest is degraded and eliminated. The pharmacokinetics of insulin bound to these cells was assumed to have first order rates of appearance and elimination upon being used to enhance uptake.

$$\frac{dI'(t)}{dt} = k_5 I(t) - k_6 I'(t) \tag{A.7}$$

Equations (A.4), (A.6), and (A.7) form the primary equations of the minimal model. Because the estimation of up to 8 model parameters (V, k_i, and $(R_{prod}\text{-}R_{up})_0$), the

authors simplified the model by first defining a variable to replace bound insulin, as shown by Equation (A.8).

$$X(t) = (k_2 + k_4)I'(t) \tag{A.8}$$

With this new proportional variable defined, the authors defined the collective parameters given by Equations (A.9-A.12).

$$P_1 = k_1 + k_3 \tag{A.9}$$

$$P_2 = k_5 \tag{A.10}$$

$$P_3 = k_6(k_2 + k_4) \tag{A.11}$$

$$\left(R_{prod} - R_{up}\right)_0 = P_1 G_0 \tag{A.12}$$

As a final modification, Furler and co-authors [2] noted that the bound insulin term should not increase above its basal value unless insulin is above its basal value. The authors also defined the reference glucose value, G_0, as the basal glucose value. When all these modifications are combined, the result is the minimal model as it is used today:

$$\frac{dG(t)}{dt} = -P_1(G(t) - G_b) - G(t)X(t) + D(t) \tag{A.13}$$

$$\frac{dX(t)}{dt} = -P_2(X(t) - X_b) + P_3(I(t) - I_b) \tag{A.14}$$

$$\frac{dI(t)}{dt} = -nI(t) + \frac{U(t)}{V} \tag{A.15}$$

APPENDIX B

HOVORKA MODEL EQUATIONS

Unlike the minimal model, Hovorka et al.[3] did not develop collective terms. This makes the model straightforward to understand by simply following the process diagram given in Figure 2.2.

Mass Balances:

Glucose

$$\frac{dQ_1(t)}{dt} = -\left[F_{01}^{C}(t) + x_1(t)Q_1(t)\right] + k_{12}Q_2(t) - F_R(t) + U_G(t) + EGP_0\left[1 - x_3(t)\right] \tag{B.1}$$

$$\frac{dQ_2(t)}{dt} = x_1(t)Q_1(t) - \left[k_{12} + x_2(t)\right]Q_2(t) \tag{B.2}$$

$$G(t) = \frac{Q_1(t)}{V_G} \tag{B.3}$$

Insulin

$$\frac{dI(t)}{dt} = \frac{U(t)}{V_I} - k_e I(t) \tag{B.4}$$

Insulin Action

$$\frac{dx_1(t)}{dt} = -k_{a1}x_1(t) + k_{b1}I(t) \tag{B.5}$$

$$\frac{dx_2(t)}{dt} = k_{b1}x_2(t) + k_{b2}I(t) \tag{B.6}$$

$$\frac{dx_3}{dt} = k_{c1}x_3(t) + k_{c2}I(t) \tag{B.7}$$

Metabolic Sources and Sinks

$$F_{01}^{C}(t) = \begin{cases} F_{01} & G \geq 4.5\frac{mmol}{L} \\ \frac{F_{01}G(t)}{4.5} & G < 4.5\frac{mmol}{L} \end{cases} \tag{B.8}$$

$$F_R(t) = \begin{cases} 0.003(G(t) - 9) & G \geq 9\frac{mmol}{L} \\ 0 & G < 9\frac{mmol}{L} \end{cases} \tag{B.9}$$

$$U_G(t) = \frac{M_{meal}A_G t\, exp\left(-\frac{t}{t_{max}}\right)}{t_{max}^2} \tag{B.10}$$

Table B-1: Hovorka Model Variable Definition		
Variable	**Definition**	**Units**
G	Plasma Glucose Concentration	$mmolL^{-1}$
Q_1	Glucose Mass In Compartment 1	mmol
Q_2	Glucose Mass In compartment 2	mmol
F_{01}	Insulin-indep. Glucose Flux	$mmol\ (Lmin)^{-1}$
F_R	Renal Glucose Clearance	$mmol\ (Lmin)^{-1}$
U_G	Glucose Absorption Rate	$mmol\ (Lmin)^{-1}$
I	Plasma Insulin Concentration	$mU\ L^{-1}$
x_1	Insulin Action On Glucose Transport	min^{-1}
x_2	Insulin Action on Glucose Uptake	min^{-1}
x_3	Insulin Action on Glucose Production	min^{-1}

Table B-2: Hovorka Model Parameter Definitions and Values			
Parameter	**Definition**	**Value**	**Units**
k_{12}	Transfer Rate	0.066	min^{-1}
k_{a1}	Deactivation Rate	0.006	min^{-1}
k_{a2}	Deactivation Rate	0.06	min^{-1}
k_{a3}	Deactivation Rate	0.03	min^{-1}
k_{b1}	Activation Rate	3.07e-5	min^{-1}
k_{b2}	Activation Rate	4.92e-5	min^{-1}
k_{b3}	Activation Rate	1.56e-4	min^{-1}
k_e	Insulin Elimination From Plasma	0.138	min^{-1}
V_I	Insulin Distribution Kinetics	0.12	$L\ kg^{-1}$
V_G	Glucose Distribution Volume	0.16	$L\ kg^{-1}$
A_G	Carbohydrate Bioavailability	0.8	unitless
t_{maxG}	Time to Maximum Absorption	40	min
EGP_0	Insulin Independent Glucose Prod.	0.0161	$mmol\ kg^{-1}\ min^{-1}$
F_{01}	Insulin-Independent Glucose Flux	0.0097	$mmol\ kg^{-1}\ min^{-1}$

APPENDIX C

SORENSEN MODEL EQUATIONS

Like the Hovorka Model, the Sorensen model [4] mass balances can derived simply by writing mass balances for each species at each compartment. Figures 6-2 through 6-4 are the diagrams showing the compartment diagrams for each species. Sorensen assumed all kinetics can be described by non-dimensional multiplicative factors for each species, and that each factor is in the form of a hyperbolic tangent function. He used a least squares technique to estimate the parameter values from various sources of data.

Glucose Model

Mass Balances:

Brain:

$$V_{BV}^{G}\frac{dG_{BV}}{dt}=Q_{B}^{G}\left(G_{H}-G_{BV}\right)-\frac{V_{BI}}{T_{B}}\left(G_{BV}-G_{BI}\right) \tag{C.1}$$

$$V_{BI}\frac{dG_{BI}}{dt}=\frac{V_{BI}}{T_{B}}\left(G_{BV}-G_{BI}\right)-r_{BGU} \tag{C.2}$$

Heart and Lungs:

$$V_{H}^{G}\frac{dG_{H}}{dt}=Q_{B}^{G}G_{BV}+Q_{L}^{G}G_{L}+Q_{K}^{G}G_{K}+Q_{P}^{G}G_{PV}-Q_{H}^{G}G_{H}-r_{RBCU} \tag{C.3}$$

Gut:

$$V_G^G \frac{dG_G}{dt} = Q_G^G\left(G_H - G_G\right) - r_{GGU} \tag{C.4}$$

Liver:

$$V_L^G \frac{dG_L}{dt} = Q_A^G G_H + Q_G^G G_G - Q_L^G G_L + r_{HGP} - r_{HGU} \tag{C.5}$$

Kidney:

$$V_K^G \frac{dG_K}{dt} = Q_K^G\left(G_H - G_K\right) - r_{KGE} \tag{C.6}$$

Periphery:

$$V_{PV}^G \frac{dG_{PV}}{dt} = Q_P^G\left(G_H - G_{PV}\right) - \frac{V_{PI}}{T_P^G}\left(G_{PV} - G_{PI}\right) \tag{C.7}$$

$$V_{PI} \frac{dG_{PI}}{dt} = \frac{V_{PI}}{T_P^G}\left(G_{PV} - G_{PI}\right) - r_{PGU} \tag{C.8}$$

Metabolic Sources and Sinks:

$$r_{PGU} = M_{PGU}^I M_{PGU}^G r_{PGU}^B \tag{C.9}$$

$$M_{PGU}^I = 7.03 + 6.52\, tanh\left[0.338\left(\frac{I_{PI}}{I_{PI}^B} - 5.82\right)\right] \tag{C.10}$$

$$M_{PGU}^G = \frac{G_{PI}}{G_{PI}^B} \tag{C.11}$$

$$r_{HGP} = M_{HGP}^I M_{HGP}^\Gamma M_{HGP}^G r_{HGP}^B \tag{C.12}$$

$$\frac{d}{dt}\left(M_{HGP}^{I}\right)=\frac{1}{\tau_I}\left(M_{HGP}^{I\infty}-M_{HGP}^{I}\right) \tag{C.13}$$

$$M_{HGP}^{I\infty}=1.21-1.14\,tanh\left[1.66\left(\frac{I_L}{I_L^B}-0.89\right)\right] \tag{C.14}$$

$$M_{HGP}^{\Gamma}=M_{HGP}^{\Gamma_0}-f_2 \tag{C.15}$$

$$M_{HGP}^{\Gamma_0}=2.7\,tanh\left(0.39\frac{\Gamma}{\Gamma^B}\right) \tag{C.16}$$

$$\frac{df_2}{dt}=\frac{1}{\tau_\Gamma}\left[\left(\frac{M_{HGP}^{\Gamma_0}-1}{2}\right)-f_2\right] \tag{C.17}$$

$$M_{HGP}^{G}=1.42-1.41\,tanh\left[0.62\left(\frac{G_L}{G_L^B}-0.497\right)\right] \tag{C.18}$$

$$r_{HGU}=M_{HGU}^{I}M_{HGU}^{G}r_{HGU}^{B} \tag{C.19}$$

$$\frac{d}{dt}\left(M_{HGU}^{I}\right)=\frac{1}{\tau_I}\left(M_{HGU}^{I_\infty}-M_{HGU}^{I}\right) \tag{C.20}$$

$$M_{HGU}^{I_\infty}=2.0\,tanh\left(0.55\frac{I_L}{I_L^B}\right) \tag{C.21}$$

$$M_{HGU}^{G}=5.66+5.66\,tanh\left[2.44\left(\frac{G_L}{G_L^B}-1.48\right)\right] \tag{C.22}$$

$$r_{KGE}=71+71\,tanh\left[0.11\left(G_K-460\right)\right] \tag{C.23}$$

$$r_{KGE}=-330+0.872G_K \tag{C.24}$$

Parameter values:

V^G_{BV}	= 3.5 dL	G^G_B	= 5.9 dL/min	T_B	= 2.1 min
V_{BI}	= 4.5 dL	Q^G_H	= 43.7 dL/min	T^G_P	= 5.0 min
V^G_H	= 13.8 dL	Q^G_A	= 2.5 dL/min	r_{BGU}	= 70 mg/min
V^G_L	= 25.1 dL	Q^G_L	= 12.6 dL/min	r_{RBCU}	= 10 mg/min
V^G_G	= 11.2 dL	Q^G_G	= 10.1 dL/min	r_{GGU}	= 20 mg/min
V^G_K	= 6.6 dL	Q^G_K	= 10.1 dL/min	r^B_{PGU}	= 35 mg/min
V^G_{PV}	= 10.4 dL	Q^G_P	= 15.1 dL/min	r^B_{HGP}	= 155 mg/min
V_{PI}	= 67.4 dL	τ_I	= 25 min	r^B_{HGU}	= 20 mg/min
τ_Γ	= 65 min				

Nomenclature :

Variables :

G	=	glucose concentration (mg/dL)
I	=	insulin concentration (mU/L)
M	=	multiplier of basal metabolic rate (dimensionless)
Q	=	vascular blood water flow rate (dL/min)
r	=	metabolic source or sink rate (mg/min)
T	=	transcapillary diffusion time constant (min)
V	=	volume (dL)
τ	=	time constant (min)
t	=	time (min)

First subscript : Physiologic Compartment

B = brain

G = gut

H = heart and lungs

L = liver

P = periphery

A = hepatic artery

Second subscript: Physiologic Subcompartment

I = interstitial fluid space

V = vascular blood water space

Metabolic Rate Subscripts:

BGU = brain glucose uptake

GGU = gut glucose utilization

HGP = hepatic glucose production

HGU = hepatic glucose uptake

KGE = kidney glucose excretion

PGU = peripheral glucose uptake

RBCU = red blood cell glucose uptake

First Superscript:

G = glucose model

I = insulin model

Γ = glucagon

B = basal value

Second Superscript

0 = initial value (normalized)

∞ = final steady state value (normalized)

Insulin Model:

Mass Balances:

Brain:

$$V_B^I \frac{dI_B}{dt} = Q_B^I \left(I_H - I_B \right) \tag{C.25}$$

Heart and Lungs:

$$V_H^I \frac{dI_H}{dt} = Q_B^I I_B + Q_L^I I_L + Q_K^I I_K + Q_P^I I_{PV} - Q_H^I I_H \tag{C.26}$$

Gut:

$$V_G^I \frac{dI_G}{dt} = Q_G^I \left(I_H - I_G \right) \tag{C.27}$$

Liver:

$$V_L^I \frac{dI_L}{dt} = Q_A^I I_H + Q_G^I I_G - Q_L^I I_L + r_{PIR} - r_{LIC} \tag{C.28}$$

Kidney:

$$V_K^I \frac{dI_K}{dt} = Q_K^I \left(I_H - I_K\right) - r_{KIC} \tag{C.29}$$

Periphery:

$$V_{PV}^I \frac{dI_{PV}}{dt} = Q_P^I \left(I_H - I_{PV}\right) - \frac{V_{PI}}{T_P^I} \left(I_{PV} - I_{PI}\right) \tag{C.30}$$

$$V_{PI}^I \frac{dI_{PI}}{dt} = \frac{V_{PI}}{T_P^I} \left(I_{PV} - I_{PI}\right) - r_{PIC} \tag{C.31}$$

Metabolic Sources and Sinks:

$$r_{LIC} = F_{LIC} \left(Q_A^I I_H + Q_G^I I_G + r_{PIR}\right) \tag{C.32}$$

$$r_{KIC} = F_{KIC} Q_K^I I_K \tag{C.33}$$

$$r_{PIC} = \frac{I_{PI}}{\left[\left(\frac{1 - F_{PIC}}{F_{PIC}}\right)\left(\frac{1}{Q_P^I}\right) - \left(\frac{T_P^I}{V_{PI}}\right)\right]} \tag{C.34}$$

Parameter values:

V^I_B	= 0.26 L	Q^I_B	= 0.45 L/min	T^I_P	= 20 min
V^I_H	= 0.99 L	Q^I_H	= 3.12 L/min	F_{LIC}	= 0.40
V^I_G	= 0.94 L	Q^I_A	= 0.18 L/min	F_{KIC}	= 0.30
V^I_L	= 1.14 L	Q^I_K	= 0.72 L/min	F_{PIC}	= 0.15
V^I_K	= 0.51 L	Q^I_P	= 1.05 L/min		
VI_{PV}	= 0.74 L	QI_G	= 0.72 L/min		
VI_{PI}	= 6.74 L	QI_L	= 0.90 L/min		

Nomenclature:

Variables:

I	=	insulin concentration
Q	=	vascular plasma flow rate (L/min)
r	=	metabolic source or sink rate (mU/min)
F	=	fractional clearance (dimensionless)
T	=	transcapillary diffusion time constant
V	=	volume (L)
t	=	time (min)

First Subscript: Physiologic Compartment

B = brain

G = gut

H = heart and lungs

L = liver

P = periphery

A = hepatic artery

Second Subscript: Physiologic Subcompartment

I = interstitial fluid space

V = vascular plasma space

Metabolic Rate Subscripts:

KIC = kidney insulin clearance

LIC = liver insulin clearance

PIC = peripheral insulin clearance

First Superscript:

I = insulin model

B = basal value

Glucagon Model:

Mass Balances:

$$V^{\Gamma}\frac{d\Gamma}{dt} = r_{P\Gamma R} - r_{P\Gamma C} \tag{C.35}$$

$$r_{P\Gamma C} = r_{M\Gamma C}\Gamma \tag{C.36}$$

$$r_{P\Gamma R} = M^{G}_{P\Gamma R} M^{I}_{P\Gamma R} r^{B}_{P\Gamma R} \tag{C.37}$$

$$M^{G}_{P\Gamma R} = 2.93 - 2.10\,tanh\left[4.18\left(\frac{G_H}{G^B_H} - 0.61\right)\right] \tag{C.38}$$

$$M^{I}_{P\Gamma R} = 1.31 - 0.61\,tanh\left[1.06\left(\frac{I_H}{I^B_H} - 0.47\right)\right] \tag{C.39}$$

Parameter Values:

V^{Γ} = 11310 mL

Nomenclature:

Variables:

G	=	glucose concentration (mg/dL)
I	=	insulin concentration (mU/L)
Γ	=	glucagon concentration (pg/mL)
V	=	glucagon distribution volume (mL)
r	=	metabolic source or sink rate (pg/min)
M	=	multiplier of basal metabolic rate (dimensionless)
t	=	time (min)

Metabolic Rate Subscripts:

PΓC	=	plasma glucagon clearance
MΓC	=	metabolic glucagon clearance
PΓR	=	pancreatic glucagon release

First Superscript

G	=	glucose
I	=	insulin
Γ	=	glucagon
B	=	basal value

Pancreas Model For Healthy Patient:

$$r_{PIR} = \frac{S(G_H)}{S(G_H^B)} r_{PIR}^B \tag{C.39}$$

$$S = \begin{cases} [M_1 Y + M_2 (X - I)]Q & X > I \\ M_1 Y Q & X \le I \end{cases} \tag{C.40}$$

$$Y = (X)^{1.11} \tag{C.41}$$

$$X = \frac{(G_H)^{3.27}}{(132)^{3.27} + 5.93(G_H)^{3.02}} \tag{C.42}$$

$$\frac{dI}{dt} = \beta(X - I) \tag{C.43}$$

$$\frac{dQ}{dt} = K(Q - Q_0) + \gamma P - S \tag{C.44}$$

$$\frac{dP}{dt} = \alpha(Y - P) \tag{C.45}$$

Parameter Values

α = 0.0482 min^{-1}

β = 0.932 min^{-1}

γ = 0.575 U/min

K = 0.00747 min^{-1}

Q_0 = 6.33 U

M_1 = 0.00747 min^{-1}

M_2 = 0.0958 min^{-1}

Nomenclature :

P	=	Potentiator (dimensionless)
I	=	Inhibitor (dimensionless)
Q	=	labile insulin (U)
S	=	Secretion Rate (U/min)
X,Y	=	Intermediate Variables (dimensionless)

APPENDIX D

TEST DATA FOR PARAMETER ESTIMATION

Table D-1: One-Compartment Data Generated with Stiff Solver		
Time (min)	**U (mU/min)**	**y (mU/L)**
0	20	0
1	20	1.2565
2	20	2.3709
3	20	3.3594
4	20	4.2361
5	20	5.0138
6	20	5.7036
7	20	6.3156
8	20	6.8587
9	20	7.3398
10	20	7.7672
11	20	8.1459
12	20	8.4825
13	20	8.7797
14	20	9.0454
15	20	9.2797
16	20	9.4871
17	20	9.6728
18	20	9.8368
19	20	9.9804
20	20	10.1097
21	20	10.2248
22	20	10.3254
23	20	10.4141
24	20	10.4941
25	20	10.5655
26	20	10.6282
27	20	10.6824
28	20	10.7313
29	20	10.7753
30	20	10.8143
31	20	10.8485
32	20	10.878
33	20	10.9045
34	20	10.9285

35	20	10.9499
36	20	10.9686
37	20	10.9846
38	20	10.9989
39	20	11.0119
40	20	11.0235
41	20	11.0339
42	20	11.0429
43	20	11.0506
44	20	11.0574
45	20	11.0636
46	20	11.0692
47	20	11.0742
48	20	11.0786
49	20	11.0825
50	20	11.0857
51	20	11.0885
52	20	11.0911
53	20	11.0935
54	20	11.0956
55	20	11.0975
56	20	11.0992
57	20	11.1007
58	20	11.1019
59	20	11.1029
60	20	11.1038
61	20	11.1046
62	20	11.1054
63	20	11.1061
64	20	11.1068
65	20	11.1073
66	20	11.1078
67	20	11.1083
68	20	11.1086
69	20	11.1089
70	20	11.1092
71	20	11.1094
72	20	11.1096
73	20	11.1097
74	20	11.1099
75	20	11.1101
76	20	11.1102

77	20	11.1103
78	20	11.1105
79	20	11.1106
80	20	11.1107
81	20	11.1107
82	20	11.1108
83	20	11.1109
84	20	11.1109
85	20	11.1109
86	20	11.1109
87	20	11.111
88	20	11.111
89	20	11.111
90	20	11.111
91	20	11.111
92	20	11.111
93	20	11.111
94	20	11.111
95	20	11.1111
96	20	11.1111
97	20	11.1111
98	20	11.1111
99	20	11.1111
100	20	11.1111
101	20	11.1111
102	20	11.1111
103	20	11.1111
104	20	11.1111
105	20	11.1111
106	20	11.1111
107	20	11.1111
108	20	11.1111
109	20	11.1111
110	20	11.1111
111	20	11.1111
112	20	11.1111
113	20	11.1111
114	20	11.1111
115	20	11.1111
116	20	11.1111
117	20	11.1111
118	20	11.1111

119	20	11.1111
120	20	11.1111
121	20	11.1111
122	20	11.1111
123	20	11.1111
124	20	11.1111
125	20	11.1111
126	20	11.1111
127	20	11.1111
128	20	11.1111
129	20	11.1111
130	20	11.1111
131	20	11.1111
132	20	11.1111
133	20	11.1111
134	20	11.1111
135	20	11.1111
136	20	11.1111
137	20	11.1111
138	20	11.1111
139	20	11.1111
140	20	11.1111
141	20	11.1111
142	20	11.1111
143	20	11.1111
144	20	11.1111
145	20	11.1111
146	20	11.1111
147	20	11.1111
148	20	11.1111
149	20	11.1111
150	20	11.1007
151	40	12.3911
152	40	13.5032
153	40	14.4918
154	40	15.3665
155	40	16.1442
156	40	16.8321
157	40	17.4445
158	40	17.9845
159	40	18.467
160	40	18.8924

161	40	19.2698
162	40	19.6074
163	40	19.9054
164	40	20.1665
165	40	20.4017
166	40	20.6112
167	40	20.7946
168	40	20.9553
169	40	21.1006
170	40	21.2305
171	40	21.345
172	40	21.4437
173	40	21.5318
174	40	21.6116
175	40	21.6831
176	40	21.7462
177	40	21.801
178	40	21.8478
179	40	21.8905
180	40	21.9292
181	40	21.964
182	40	21.9947
183	40	22.0214
184	40	22.044
185	40	22.064
186	40	22.0822
187	40	22.0988
188	40	22.1136
189	40	22.1266
190	40	22.138
191	40	22.1475
192	40	22.1558
193	40	22.1634
194	40	22.1703
195	40	22.1766
196	40	22.1822
197	40	22.1872
198	40	22.1914
199	40	22.195
200	40	22.198
201	40	22.2007
202	40	22.2032

203	40	22.2055
204	40	22.2075
205	40	22.2094
206	40	22.2111
207	40	22.2126
208	40	22.2138
209	40	22.2149
210	40	22.2157
211	40	22.2164
212	40	22.217
213	40	22.2176
214	40	22.2182
215	40	22.2187
216	40	22.2192
217	40	22.2196
218	40	22.22
219	40	22.2203
220	40	22.2206
221	40	22.2209
222	40	22.2211
223	40	22.2212
224	40	22.2214
225	40	22.2215
226	40	22.2215
227	40	22.2216
228	40	22.2217
229	40	22.2217
230	40	22.2218
231	40	22.2219
232	40	22.2219
233	40	22.222
234	40	22.222
235	40	22.222
236	40	22.2221
237	40	22.2221
238	40	22.2221
239	40	22.2222
240	40	22.2222
241	40	22.2222
242	40	22.2222
243	40	22.2222
244	40	22.2223

245	40	22.2223
246	40	22.2223
247	40	22.2223
248	40	22.2223
249	40	22.2223
250	40	22.2222
251	40	22.2222
252	40	22.2222
253	40	22.2222
254	40	22.2222
255	40	22.2222
256	40	22.2222
257	40	22.2222
258	40	22.2222
259	40	22.2222
260	40	22.2222
261	40	22.2222
262	40	22.2222
263	40	22.2222
264	40	22.2222
265	40	22.2222
266	40	22.2222
267	40	22.2222
268	40	22.2222
269	40	22.2222
270	40	22.2222
271	40	22.2222
272	40	22.2222
273	40	22.2222
274	40	22.2222
275	40	22.2222
276	40	22.2222
277	40	22.2222
278	40	22.2222
279	40	22.2222
280	40	22.2222
281	40	22.2222
282	40	22.2222
283	40	22.2222
284	40	22.2222
285	40	22.2222
286	40	22.2222

287	40	22.2222
288	40	22.2222
289	40	22.2222
290	40	22.2222
291	40	22.2222
292	40	22.2222
293	40	22.2222
294	40	22.2222
295	40	22.2222
296	40	22.2222
297	40	22.2222
298	40	22.2222
299	40	22.2222
300	40	22.2222

Table D-2: One-Compartment Data Generated with Nonstiff Solver		
Time (min)	**U (mU/min)**	**y (mU/L)**
0	20	0
1	20	1.2564
2	20	2.3708
3	20	3.3592
4	20	4.2357
5	20	5.0132
6	20	5.7028
7	20	6.3144
8	20	6.8567
9	20	7.3379
10	20	7.7646
11	20	8.143
12	20	8.4786
13	20	8.7762
14	20	9.0404
15	20	9.2747
16	20	9.4823
17	20	9.6664
18	20	9.8296
19	20	9.9746
20	20	10.1033
21	20	10.2175
22	20	10.3185
23	20	10.408
24	20	10.4873
25	20	10.5577
26	20	10.6205
27	20	10.6762
28	20	10.7256
29	20	10.7693
30	20	10.8079
31	20	10.842
32	20	10.8721
33	20	10.899
34	20	10.923
35	20	10.9446

36	20	10.9637
37	20	10.9807
38	20	10.9957
39	20	11.0088
40	20	11.0202
41	20	11.0302
42	20	11.039
43	20	11.0469
44	20	11.0539
45	20	11.0605
46	20	11.0664
47	20	11.0718
48	20	11.0766
49	20	11.0808
50	20	11.0845
51	20	11.0876
52	20	11.0902
53	20	11.0924
54	20	11.0943
55	20	11.0958
56	20	11.0972
57	20	11.0985
58	20	11.0997
59	20	11.101
60	20	11.1023
61	20	11.1035
62	20	11.1046
63	20	11.1055
64	20	11.1064
65	20	11.1071
66	20	11.1077
67	20	11.1081
68	20	11.1085
69	20	11.1087
70	20	11.1088
71	20	11.1089
72	20	11.1089
73	20	11.1089
74	20	11.1089
75	20	11.109
76	20	11.1092

77	20	11.1094
78	20	11.1097
79	20	11.1099
80	20	11.1101
81	20	11.1104
82	20	11.1105
83	20	11.1107
84	20	11.1108
85	20	11.1109
86	20	11.111
87	20	11.111
88	20	11.111
89	20	11.111
90	20	11.111
91	20	11.1109
92	20	11.1108
93	20	11.1107
94	20	11.1106
95	20	11.1106
96	20	11.1106
97	20	11.1106
98	20	11.1106
99	20	11.1108
100	20	11.1109
101	20	11.111
102	20	11.1112
103	20	11.1113
104	20	11.1115
105	20	11.1116
106	20	11.1118
107	20	11.1119
108	20	11.1119
109	20	11.112
110	20	11.112
111	20	11.112
112	20	11.112
113	20	11.1119
114	20	11.1118
115	20	11.1117
116	20	11.1115
117	20	11.1114

118	20	11.1112
119	20	11.111
120	20	11.1109
121	20	11.1107
122	20	11.1105
123	20	11.1104
124	20	11.1103
125	20	11.1102
126	20	11.1102
127	20	11.1102
128	20	11.1103
129	20	11.1104
130	20	11.1105
131	20	11.1106
132	20	11.1106
133	20	11.1107
134	20	11.1107
135	20	11.1108
136	20	11.1108
137	20	11.1108
138	20	11.1109
139	20	11.1109
140	20	11.1109
141	20	11.1109
142	20	11.111
143	20	11.111
144	20	11.111
145	20	11.111
146	20	11.0073
147	20	10.8805
148	20	11.0814
149	20	11.754
150	20	12.8278
151	40	14.0177
152	40	14.9647
153	40	15.7863
154	40	16.5146
155	40	17.1599
156	40	17.7316
157	40	18.2386
158	40	18.689

159	40	19.0888
160	40	19.4433
161	40	19.7575
162	40	20.036
163	40	20.283
164	40	20.5025
165	40	20.6974
166	40	20.8701
167	40	21.023
168	40	21.1584
169	40	21.2783
170	40	21.3847
171	40	21.4796
172	40	21.564
173	40	21.6388
174	40	21.705
175	40	21.7635
176	40	21.8151
177	40	21.8607
178	40	21.9012
179	40	21.9374
180	40	21.9699
181	40	21.9989
182	40	22.0247
183	40	22.0474
184	40	22.0674
185	40	22.0849
186	40	22.1001
187	40	22.1135
188	40	22.1252
189	40	22.1357
190	40	22.1454
191	40	22.1543
192	40	22.1625
193	40	22.1699
194	40	22.1765
195	40	22.1823
196	40	22.1872
197	40	22.1914
198	40	22.1949
199	40	22.1978

200	40	22.2001
201	40	22.202
202	40	22.2036
203	40	22.205
204	40	22.2064
205	40	22.208
206	40	22.2097
207	40	22.2114
208	40	22.213
209	40	22.2144
210	40	22.2157
211	40	22.2168
212	40	22.2178
213	40	22.2185
214	40	22.2191
215	40	22.2195
216	40	22.2197
217	40	22.2198
218	40	22.2197
219	40	22.2196
220	40	22.2195
221	40	22.2193
222	40	22.2192
223	40	22.2193
224	40	22.2195
225	40	22.2199
226	40	22.2204
227	40	22.2208
228	40	22.2213
229	40	22.2217
230	40	22.2221
231	40	22.2225
232	40	22.2228
233	40	22.223
234	40	22.2232
235	40	22.2233
236	40	22.2233
237	40	22.2232
238	40	22.2231
239	40	22.2229
240	40	22.2226

241	40	22.2223
242	40	22.222
243	40	22.2216
244	40	22.2213
245	40	22.221
246	40	22.2207
247	40	22.2206
248	40	22.2205
249	40	22.2207
250	40	22.2209
251	40	22.2213
252	40	22.2217
253	40	22.2222
254	40	22.2226
255	40	22.2231
256	40	22.2236
257	40	22.224
258	40	22.2243
259	40	22.2246
260	40	22.2248
261	40	22.2249
262	40	22.225
263	40	22.2249
264	40	22.2248
265	40	22.2245
266	40	22.2242
267	40	22.2238
268	40	22.2234
269	40	22.2229
270	40	22.2223
271	40	22.2218
272	40	22.2212
273	40	22.2207
274	40	22.2202
275	40	22.2198
276	40	22.2195
277	40	22.2193
278	40	22.2193
279	40	22.2196
280	40	22.2199
281	40	22.2202

282	40	22.2206
283	40	22.2209
284	40	22.2212
285	40	22.2214
286	40	22.2216
287	40	22.2218
288	40	22.2219
289	40	22.222
290	40	22.2221
291	40	22.2221
292	40	22.222
293	40	22.222
294	40	22.2219
295	40	22.2218
296	40	22.2217
297	40	22.2216
298	40	22.2215
299	40	22.2215
300	40	22.2215

Table D-3: Test Data with 5% Noise		
Time (min)	**U (mU/min)**	**y (mU/L)**
0	20	0
1	20	1.1936
2	20	2.4895
3	20	3.1914
4	20	4.4479
5	20	4.7631
6	20	5.9888
7	20	5.9998
8	20	7.2016
9	20	6.9728
10	20	8.1555
11	20	7.7386
12	20	8.9066
13	20	8.3407
14	20	9.4977
15	20	8.8157
16	20	9.9615
17	20	9.1892
18	20	10.3286
19	20	9.4814
20	20	10.6152
21	20	9.7136
22	20	10.8417
23	20	9.8934
24	20	11.0188
25	20	10.0372
26	20	11.1596
27	20	10.1483
28	20	11.2678
29	20	10.2365
30	20	11.3551
31	20	10.3061
32	20	11.4219

33	20	10.3593
34	20	11.4749
35	20	10.4024
36	20	11.517
37	20	10.4354
38	20	11.5489
39	20	10.4613
40	20	11.5747
41	20	10.4822
42	20	11.595
43	20	10.498
44	20	11.6102
45	20	10.5104
46	20	11.6226
47	20	10.5205
48	20	11.6326
49	20	10.5283
50	20	11.64
51	20	10.5341
52	20	11.6456
53	20	10.5388
54	20	11.6504
55	20	10.5426
56	20	11.6542
57	20	10.5456
58	20	11.657
59	20	10.5477
60	20	11.659
61	20	10.5494
62	20	11.6607
63	20	10.5508
64	20	11.6621
65	20	10.552
66	20	11.6632
67	20	10.5529
68	20	11.6641
69	20	10.5535

70	20	11.6646
71	20	10.5539
72	20	11.665
73	20	10.5543
74	20	11.6654
75	20	10.5546
76	20	11.6657
77	20	10.5548
78	20	11.666
79	20	10.555
80	20	11.6662
81	20	10.5552
82	20	11.6663
83	20	10.5553
84	20	11.6664
85	20	10.5554
86	20	11.6665
87	20	10.5554
88	20	11.6665
89	20	10.5554
90	20	11.6665
91	20	10.5555
92	20	11.6666
93	20	10.5555
94	20	11.6666
95	20	10.5555
96	20	11.6666
97	20	10.5555
98	20	11.6666
99	20	10.5555
100	20	11.6667
101	20	10.5556
102	20	11.6667
103	20	10.5556
104	20	11.6667
105	20	10.5556
106	20	11.6667

107	20	10.5556
108	20	11.6667
109	20	10.5556
110	20	11.6667
111	20	10.5556
112	20	11.6667
113	20	10.5556
114	20	11.6667
115	20	10.5556
116	20	11.6667
117	20	10.5556
118	20	11.6667
119	20	10.5556
120	20	11.6667
121	20	10.5556
122	20	11.6667
123	20	10.5556
124	20	11.6667
125	20	10.5556
126	20	11.6667
127	20	10.5556
128	20	11.6667
129	20	10.5556
130	20	11.6667
131	20	10.5556
132	20	11.6667
133	20	10.5556
134	20	11.6667
135	20	10.5556
136	20	11.6667
137	20	10.5556
138	20	11.6667
139	20	10.5556
140	20	11.6667
141	20	10.5556
142	20	11.6667
143	20	10.5556

144	20	11.6667
145	20	10.5556
146	20	11.6667
147	20	10.5556
148	20	11.6667
149	20	10.5556
150	20	11.6558
151	40	11.7716
152	40	14.1784
153	40	13.7672
154	40	16.1349
155	40	15.337
156	40	17.6737
157	40	16.5722
158	40	18.8838
159	40	17.5437
160	40	19.837
161	40	18.3063
162	40	20.5878
163	40	18.9101
164	40	21.1748
165	40	19.3816
166	40	21.6417
167	40	19.7548
168	40	22.0031
169	40	20.0456
170	40	22.2921
171	40	20.2778
172	40	22.5158
173	40	20.4552
174	40	22.6922
175	40	20.5989
176	40	22.8335
177	40	20.7109
178	40	22.9402
179	40	20.796
180	40	23.0257

181	40	20.8658
182	40	23.0944
183	40	20.9203
184	40	23.1462
185	40	20.9608
186	40	23.1863
187	40	20.9938
188	40	23.2192
189	40	21.0203
190	40	23.2449
191	40	21.0401
192	40	23.2635
193	40	21.0552
194	40	23.2788
195	40	21.0678
196	40	23.2913
197	40	21.0778
198	40	23.301
199	40	21.0853
200	40	23.3079
201	40	21.0906
202	40	23.3133
203	40	21.0952
204	40	23.3179
205	40	21.0989
206	40	23.3216
207	40	21.1019
208	40	23.3245
209	40	21.1041
210	40	23.3265
211	40	21.1055
212	40	23.3279
213	40	21.1067
214	40	23.3291
215	40	21.1077
216	40	23.3301
217	40	21.1086

218	40	23.331
219	40	21.1093
220	40	23.3316
221	40	21.1098
222	40	23.3321
223	40	21.1102
224	40	23.3324
225	40	21.1104
226	40	23.3326
227	40	21.1105
228	40	23.3328
229	40	21.1106
230	40	23.3329
231	40	21.1108
232	40	23.333
233	40	21.1109
234	40	23.3331
235	40	21.1109
236	40	23.3332
237	40	21.111
238	40	23.3333
239	40	21.1111
240	40	23.3333
241	40	21.1111
242	40	23.3333
243	40	21.1111
244	40	23.3334
245	40	21.1111
246	40	23.3334
247	40	21.1111
248	40	23.3334
249	40	21.1111
250	40	23.3334
251	40	21.1111
252	40	23.3334
253	40	21.1111
254	40	23.3333

255	40	21.1111
256	40	23.3333
257	40	21.1111
258	40	23.3333
259	40	21.1111
260	40	23.3333
261	40	21.1111
262	40	23.3333
263	40	21.1111
264	40	23.3333
265	40	21.1111
266	40	23.3333
267	40	21.1111
268	40	23.3333
269	40	21.1111
270	40	23.3333
271	40	21.1111
272	40	23.3333
273	40	21.1111
274	40	23.3333
275	40	21.1111
276	40	23.3333
277	40	21.1111
278	40	23.3333
279	40	21.1111
280	40	23.3333
281	40	21.1111
282	40	23.3333
283	40	21.1111
284	40	23.3333
285	40	21.1111
286	40	23.3333
287	40	21.1111
288	40	23.3333
289	40	21.1111
290	40	23.3333
291	40	21.1111

292	40	23.3333
293	40	21.1111
294	40	23.3333
295	40	21.1111
296	40	23.3333
297	40	21.1111
298	40	23.3333
299	40	21.1111
300	40	23.3333

Table D-4: Test Data with Random Noise		
Time (min)	**U (mU/min)**	**y (mU/L)**
0	20	0.9501
1	20	1.4876
2	20	2.9778
3	20	3.8454
4	20	5.1274
5	20	5.7759
6	20	6.1601
7	20	6.3341
8	20	7.6801
9	20	7.7845
10	20	8.3826
11	20	8.9378
12	20	9.4043
13	20	9.5179
14	20	9.2217
15	20	9.6854
16	20	10.4226
17	20	10.5897
18	20	10.2471
19	20	10.8741
20	20	10.1676
21	20	10.5777
22	20	11.1386
23	20	10.424
24	20	10.633
25	20	10.7683
26	20	10.8269
27	20	11.2862
28	20	11.0035
29	20	10.9741
30	20	10.8296
31	20	11.5953
32	20	11.3231
33	20	11.8363
34	20	11.3945

35	20	11.3685
36	20	11.8148
37	20	11.5098
38	20	11.2016
39	20	11.684
40	20	11.8616
41	20	11.0535
42	20	11.7242
43	20	11.43
44	20	11.8891
45	20	11.5664
46	20	11.7786
47	20	11.5031
48	20	11.3832
49	20	11.2721
50	20	11.2791
51	20	11.7707
52	20	11.3939
53	20	11.6351
54	20	11.2465
55	20	11.7954
56	20	11.4776
57	20	11.9607
58	20	11.9556
59	20	11.6964
60	20	11.6003
61	20	12.0044
62	20	11.927
63	20	11.751
64	20	11.9247
65	20	11.7676
66	20	11.4498
67	20	11.398
68	20	11.4498
69	20	11.643
70	20	11.8363
71	20	11.4187
72	20	11.9481

73	20	11.6778
74	20	11.4803
75	20	11.8128
76	20	11.6568
77	20	11.5552
78	20	11.805
79	20	11.7319
80	20	11.9055
81	20	12.0676
82	20	11.6334
83	20	11.991
84	20	11.2838
85	20	12.0907
86	20	11.3824
87	20	11.3633
88	20	11.9867
89	20	11.8483
90	20	11.2475
91	20	11.1228
92	20	12.0049
93	20	11.3102
94	20	11.4098
95	20	11.7725
96	20	11.3955
97	20	11.5803
98	20	11.1759
99	20	12.0994
100	20	11.6939
101	20	11.5346
102	20	11.6266
103	20	11.4451
104	20	11.544
105	20	11.3371
106	20	11.6909
107	20	11.8715
108	20	11.641
109	20	11.7517
110	20	11.3202

111	20	11.4909
112	20	11.8945
113	20	11.792
114	20	11.5722
115	20	11.6789
116	20	11.9053
117	20	11.1703
118	20	11.714
119	20	11.1614
120	20	11.5265
121	20	11.4161
122	20	11.9855
123	20	11.1261
124	20	11.8791
125	20	12.082
126	20	12.1012
127	20	11.9
128	20	11.5498
129	20	11.6094
130	20	11.3251
131	20	11.7546
132	20	11.4311
133	20	12.0712
134	20	11.8377
135	20	11.5231
136	20	11.8557
137	20	11.3791
138	20	11.551
139	20	12.0445
140	20	11.7944
141	20	11.3237
142	20	11.9503
143	20	11.7399
144	20	11.2449
145	20	11.3182
146	20	11.7183
147	20	11.741
148	20	11.4816

149	20	11.6863
150	20	11.5522
151	40	12.435
152	40	13.5304
153	40	14.8045
154	40	15.3794
155	40	16.5282
156	40	17.5152
157	40	17.5373
158	40	18.0199
159	40	19.0794
160	40	19.5009
161	40	19.2855
162	40	19.6238
163	40	20.0955
164	40	20.7534
165	40	20.4593
166	40	20.9787
167	40	21.426
168	40	21.6729
169	40	21.7933
170	40	21.3146
171	40	21.7994
172	40	21.8855
173	40	21.885
174	40	21.7652
175	40	22.3587
176	40	22.4454
177	40	22.5285
178	40	22.3262
179	40	22.4454
180	40	22.0503
181	40	22.4147
182	40	22.7106
183	40	22.9143
184	40	22.3171
185	40	22.3187
186	40	22.9478

187	40	22.3311
188	40	22.9184
189	40	23.035
190	40	22.3699
191	40	22.3868
192	40	22.2055
193	40	22.2418
194	40	22.8111
195	40	22.3675
196	40	23.0261
197	40	22.3611
198	40	22.3622
199	40	23.1893
200	40	22.6378
201	40	22.5407
202	40	22.5174
203	40	22.5705
204	40	22.6008
205	40	22.8009
206	40	22.3308
207	40	22.2507
208	40	22.6724
209	40	23.0847
210	40	23.1499
211	40	22.4808
212	40	22.3773
213	40	23.0905
214	40	22.456
215	40	22.8645
216	40	23.186
217	40	22.8845
218	40	23.0903
219	40	22.2302
220	40	22.3576
221	40	23.0396
222	40	22.6512
223	40	23.1116
224	40	22.9563

225	40	22.9088
226	40	22.5676
227	40	22.3876
228	40	22.3773
229	40	22.4129
230	40	22.6442
231	40	23.0778
232	40	22.7122
233	40	23.0379
234	40	22.6828
235	40	22.6794
236	40	22.6728
237	40	22.6343
238	40	23.1238
239	40	22.2278
240	40	22.5196
241	40	22.2714
242	40	22.9154
243	40	22.8724
244	40	23.2052
245	40	22.7749
246	40	22.6223
247	40	22.421
248	40	22.8475
249	40	22.9556
250	40	22.5981
251	40	22.2321
252	40	22.6421
253	40	22.9759
254	40	23.0161
255	40	23.1422
256	40	23.067
257	40	22.59
258	40	22.843
259	40	22.9535
260	40	22.4161
261	40	23.127
262	40	22.7914

263	40	22.854
264	40	22.4566
265	40	22.771
266	40	23.1538
267	40	22.5574
268	40	22.8777
269	40	22.6141
270	40	22.8495
271	40	22.9213
272	40	22.6194
273	40	22.6358
274	40	22.8774
275	40	23.0598
276	40	22.5938
277	40	22.6475
278	40	22.8169
279	40	22.788
280	40	22.9388
281	40	22.7335
282	40	22.9986
283	40	22.7116
284	40	22.4081
285	40	22.9229
286	40	23.2049
287	40	23.0289
288	40	22.9258
289	40	22.7072
290	40	22.3368
291	40	22.8871
292	40	22.5876
293	40	22.3623
294	40	22.789
295	40	23.0452
296	40	22.8962
297	40	23.2217
298	40	23.1839
299	40	22.2811
300	40	22.5825

Table D-5: Two-Compartment Test Data with Stiff Solver		
Time (min)	**U (mU/min)**	**y (mU/L)**
0	20	0
1	20	2.9367
2	20	5.2088
3	20	6.9742
4	20	8.3524
5	20	9.4356
6	20	10.2923
7	20	10.9751
8	20	11.5246
9	20	11.9716
10	20	12.3404
11	20	12.648
12	20	12.9072
13	20	13.131
14	20	13.324
15	20	13.4955
16	20	13.6473
17	20	13.7854
18	20	13.9107
19	20	14.0266
20	20	14.1344
21	20	14.2347
22	20	14.3296
23	20	14.4192
24	20	14.5039
25	20	14.5849
26	20	14.6623
27	20	14.736
28	20	14.8066
29	20	14.8746
30	20	14.94
31	20	15.0027
32	20	15.0628
33	20	15.1207
34	20	15.1766

35	20	15.2305
36	20	15.2823
37	20	15.332
38	20	15.3801
39	20	15.4264
40	20	15.4711
41	20	15.5142
42	20	15.5556
43	20	15.5955
44	20	15.6341
45	20	15.6713
46	20	15.7071
47	20	15.7415
48	20	15.7748
49	20	15.8069
50	20	15.8378
51	20	15.8676
52	20	15.8963
53	20	15.924
54	20	15.9507
55	20	15.9765
56	20	16.0014
57	20	16.0252
58	20	16.0482
59	20	16.0705
60	20	16.092
61	20	16.1128
62	20	16.1328
63	20	16.152
64	20	16.1705
65	20	16.1883
66	20	16.2055
67	20	16.2221
68	20	16.2382
69	20	16.2537
70	20	16.2686
71	20	16.283
72	20	16.2968

73	20	16.31
74	20	16.3228
75	20	16.3352
76	20	16.3472
77	20	16.3588
78	20	16.37
79	20	16.3807
80	20	16.391
81	20	16.401
82	20	16.4105
83	20	16.4197
84	20	16.4286
85	20	16.4372
86	20	16.4455
87	20	16.4535
88	20	16.4612
89	20	16.4686
90	20	16.4758
91	20	16.4826
92	20	16.4892
93	20	16.4956
94	20	16.5018
95	20	16.5078
96	20	16.5135
97	20	16.5191
98	20	16.5244
99	20	16.5295
100	20	16.5344
101	20	16.5392
102	20	16.5438
103	20	16.5482
104	20	16.5525
105	20	16.5566
106	20	16.5606
107	20	16.5644
108	20	16.5681
109	20	16.5716
110	20	16.5751

111	20	16.5784
112	20	16.5816
113	20	16.5846
114	20	16.5876
115	20	16.5905
116	20	16.5932
117	20	16.5958
118	20	16.5984
119	20	16.6008
120	20	16.6032
121	20	16.6055
122	20	16.6077
123	20	16.6099
124	20	16.6119
125	20	16.6139
126	20	16.6158
127	20	16.6176
128	20	16.6194
129	20	16.6211
130	20	16.6227
131	20	16.6243
132	20	16.6258
133	20	16.6273
134	20	16.6287
135	20	16.6301
136	20	16.6314
137	20	16.6327
138	20	16.6339
139	20	16.6351
140	20	16.6362
141	20	16.6373
142	20	16.6384
143	20	16.6394
144	20	16.6404
145	20	16.6413
146	20	16.6422
147	20	16.6431
148	20	16.644

149	20	16.6448
150	20	16.6297
151	40	19.6076
152	40	21.8752
153	40	23.6371
154	40	25.0135
155	40	26.0948
156	40	26.9508
157	40	27.6328
158	40	28.1814
159	40	28.6282
160	40	28.9973
161	40	29.3038
162	40	29.5637
163	40	29.7868
164	40	29.9807
165	40	30.1516
166	40	30.3044
167	40	30.4419
168	40	30.5682
169	40	30.6838
170	40	30.7919
171	40	30.8929
172	40	30.9876
173	40	31.0776
174	40	31.1629
175	40	31.2438
176	40	31.3214
177	40	31.3956
178	40	31.4667
179	40	31.5346
180	40	31.6
181	40	31.6631
182	40	31.7236
183	40	31.7817
184	40	31.8377
185	40	31.8917
186	40	31.9437

187	40	31.9937
188	40	32.0418
189	40	32.0883
190	40	32.1332
191	40	32.1765
192	40	32.2181
193	40	32.2582
194	40	32.2968
195	40	32.3341
196	40	32.3701
197	40	32.4047
198	40	32.438
199	40	32.4702
200	40	32.5013
201	40	32.5314
202	40	32.5602
203	40	32.588
204	40	32.6147
205	40	32.6406
206	40	32.6656
207	40	32.6897
208	40	32.7129
209	40	32.7353
210	40	32.7567
211	40	32.7774
212	40	32.7974
213	40	32.8167
214	40	32.8354
215	40	32.8534
216	40	32.8707
217	40	32.8874
218	40	32.9034
219	40	32.9188
220	40	32.9337
221	40	32.9482
222	40	32.9621
223	40	32.9755
224	40	32.9884

225	40	33.0007
226	40	33.0126
227	40	33.0242
228	40	33.0354
229	40	33.0461
230	40	33.0565
231	40	33.0666
232	40	33.0762
233	40	33.0854
234	40	33.0943
235	40	33.1029
236	40	33.1112
237	40	33.1192
238	40	33.127
239	40	33.1345
240	40	33.1417
241	40	33.1486
242	40	33.1552
243	40	33.1616
244	40	33.1678
245	40	33.1737
246	40	33.1795
247	40	33.1851
248	40	33.1904
249	40	33.1956
250	40	33.2006
251	40	33.2054
252	40	33.2099
253	40	33.2144
254	40	33.2187
255	40	33.2228
256	40	33.2268
257	40	33.2307
258	40	33.2344
259	40	33.2379
260	40	33.2414
261	40	33.2447
262	40	33.2479

263	40	33.2509
264	40	33.2539
265	40	33.2568
266	40	33.2596
267	40	33.2622
268	40	33.2648
269	40	33.2672
270	40	33.2696
271	40	33.2719
272	40	33.2741
273	40	33.2763
274	40	33.2783
275	40	33.2803
276	40	33.2822
277	40	33.2841
278	40	33.2858
279	40	33.2875
280	40	33.2892
281	40	33.2908
282	40	33.2923
283	40	33.2938
284	40	33.2952
285	40	33.2966
286	40	33.2979
287	40	33.2992
288	40	33.3004
289	40	33.3016
290	40	33.3028
291	40	33.3039
292	40	33.3049
293	40	33.306
294	40	33.3069
295	40	33.3079
296	40	33.3088
297	40	33.3097
298	40	33.3105
299	40	33.3114
300	40	33.3122

Table D-6: Two-Compartment Test Data with Nonstiff Solver		
Time (min)	**U (mU/min)**	**y (mU/L)**
0	20	0
1	20	2.9367
2	20	5.2085
3	20	6.9733
4	20	8.3509
5	20	9.4328
6	20	10.2884
7	20	10.9709
8	20	11.5204
9	20	11.9672
10	20	12.3359
11	20	12.6433
12	20	12.9029
13	20	13.1263
14	20	13.3206
15	20	13.4912
16	20	13.6435
17	20	13.7821
18	20	13.9087
19	20	14.0247
20	20	14.1318
21	20	14.2321
22	20	14.3275
23	20	14.418
24	20	14.5037
25	20	14.5845
26	20	14.6611
27	20	14.7341
28	20	14.8045
29	20	14.8728
30	20	14.9385
31	20	15.0014
32	20	15.0618
33	20	15.1197
34	20	15.1753
35	20	15.2289
36	20	15.2808
37	20	15.3308

38	20	15.3791
39	20	15.4255
40	20	15.4702
41	20	15.5132
42	20	15.5545
43	20	15.5943
44	20	15.6328
45	20	15.6699
46	20	15.7058
47	20	15.7405
48	20	15.7739
49	20	15.8061
50	20	15.8371
51	20	15.8669
52	20	15.8956
53	20	15.9232
54	20	15.9497
55	20	15.9752
56	20	15.9999
57	20	16.0237
58	20	16.0468
59	20	16.0692
60	20	16.0908
61	20	16.1115
62	20	16.1315
63	20	16.1507
64	20	16.1692
65	20	16.1871
66	20	16.2043
67	20	16.2209
68	20	16.2369
69	20	16.2524
70	20	16.2673
71	20	16.2816
72	20	16.2954
73	20	16.3088
74	20	16.3216
75	20	16.334
76	20	16.3459
77	20	16.3575

78	20	16.3686
79	20	16.3793
80	20	16.3896
81	20	16.3996
82	20	16.4092
83	20	16.4184
84	20	16.4273
85	20	16.4359
86	20	16.4442
87	20	16.4522
88	20	16.4599
89	20	16.4673
90	20	16.4745
91	20	16.4814
92	20	16.4881
93	20	16.4945
94	20	16.5007
95	20	16.5066
96	20	16.5124
97	20	16.5179
98	20	16.5232
99	20	16.5284
100	20	16.5333
101	20	16.5381
102	20	16.5427
103	20	16.5472
104	20	16.5515
105	20	16.5556
106	20	16.5596
107	20	16.5635
108	20	16.5672
109	20	16.5707
110	20	16.5742
111	20	16.5775
112	20	16.5807
113	20	16.5838
114	20	16.5868
115	20	16.5896
116	20	16.5924
117	20	16.5951

118	20	16.5976
119	20	16.6001
120	20	16.6025
121	20	16.6048
122	20	16.607
123	20	16.6092
124	20	16.6112
125	20	16.6132
126	20	16.6152
127	20	16.617
128	20	16.6188
129	20	16.6205
130	20	16.6222
131	20	16.6238
132	20	16.6253
133	20	16.6268
134	20	16.6282
135	20	16.6296
136	20	16.6309
137	20	16.6322
138	20	16.6335
139	20	16.6346
140	20	16.6358
141	20	16.6369
142	20	16.638
143	20	16.639
144	20	16.64
145	20	16.6409
146	20	16.6419
147	20	16.6428
148	20	16.6436
149	20	16.6445
150	20	16.6428
151	40	19.5506
152	40	21.8304
153	40	23.6014
154	40	24.9839
155	40	26.0697
156	40	26.9283
157	40	27.6134

158	40	28.1646
159	40	28.6136
160	40	28.9836
161	40	29.2918
162	40	29.5529
163	40	29.7773
164	40	29.9718
165	40	30.1431
166	40	30.297
167	40	30.4361
168	40	30.5625
169	40	30.6784
170	40	30.7864
171	40	30.8886
172	40	30.9852
173	40	31.0758
174	40	31.1608
175	40	31.2409
176	40	31.3171
177	40	31.391
178	40	31.4627
179	40	31.5315
180	40	31.5974
181	40	31.6605
182	40	31.7209
183	40	31.7789
184	40	31.8348
185	40	31.8889
186	40	31.9412
187	40	31.9915
188	40	32.04
189	40	32.0865
190	40	32.1313
191	40	32.1744
192	40	32.2159
193	40	32.2559
194	40	32.2946
195	40	32.3321
196	40	32.3683
197	40	32.4032

198	40	32.4368
199	40	32.4691
200	40	32.5002
201	40	32.53
202	40	32.5586
203	40	32.5862
204	40	32.6127
205	40	32.6384
206	40	32.6632
207	40	32.6873
208	40	32.7107
209	40	32.7331
210	40	32.7548
211	40	32.7756
212	40	32.7957
213	40	32.8149
214	40	32.8335
215	40	32.8515
216	40	32.8688
217	40	32.8855
218	40	32.9016
219	40	32.9171
220	40	32.9321
221	40	32.9465
222	40	32.9604
223	40	32.9738
224	40	32.9867
225	40	32.9991
226	40	33.0112
227	40	33.0227
228	40	33.0339
229	40	33.0447
230	40	33.055
231	40	33.065
232	40	33.0746
233	40	33.0839
234	40	33.0929
235	40	33.1015
236	40	33.1098
237	40	33.1179

238	40	33.1256
239	40	33.1331
240	40	33.1403
241	40	33.1472
242	40	33.1539
243	40	33.1604
244	40	33.1666
245	40	33.1725
246	40	33.1783
247	40	33.1838
248	40	33.1892
249	40	33.1944
250	40	33.1994
251	40	33.2042
252	40	33.2088
253	40	33.2133
254	40	33.2176
255	40	33.2218
256	40	33.2258
257	40	33.2296
258	40	33.2334
259	40	33.237
260	40	33.2404
261	40	33.2438
262	40	33.247
263	40	33.2501
264	40	33.2531
265	40	33.256
266	40	33.2587
267	40	33.2614
268	40	33.264
269	40	33.2665
270	40	33.2689
271	40	33.2712
272	40	33.2734
273	40	33.2756
274	40	33.2777
275	40	33.2797
276	40	33.2816
277	40	33.2834

278	40	33.2852
279	40	33.287
280	40	33.2886
281	40	33.2902
282	40	33.2918
283	40	33.2933
284	40	33.2947
285	40	33.2961
286	40	33.2974
287	40	33.2987
288	40	33.3
289	40	33.3012
290	40	33.3023
291	40	33.3034
292	40	33.3045
293	40	33.3055
294	40	33.3065
295	40	33.3075
296	40	33.3084
297	40	33.3093
298	40	33.3102
299	40	33.311
300	40	33.3118

APPENDIX E

SOURCE CODE FOR PARAMETER ESTIMATION

```
% Solver

% Created by Terry Farmer, 7/26/06

% Purpose- To use parameter estimation to determination the optimal
% parameters of the one compartment Joseph Model with confidence limits

clc
clear

% First, get parameters
A01 = .2; %min^-1
A12 = 0.4; %min^-1
A13 = 0.04; %min^-1
A21 = .1; %min^-1
A31 = .02; %min^-1
V = 4; %L
global tdata yode1

tdata = [0:1:300];
y0 = 0; %mU/L
x20 = 0; %mU
x30 = 0; % mU

[tode1,xode1] =
ode23s(@state,tdata,[y0;x20;x30;zeros(18,1)],[],A01,A12,A13,A21,A31,V);
yode1 = xode1(:,1);

%Initial Guess for parameters
    P01 = [.2;.4;.04;.1;.02;2];
LB = [0;0;0;0;0;.001]; % Lower Bounds
UB = [.6;.6;.6; .6;.6;inf]; % Upper Bounds

options =
optimset('MaxFunEvals',8000,'MaxIter',2000,'GradObj','on','Hessian','on
','LevenbergMarquardt','on');

[P,sse] =fmincon(@resid,P01,[],[],[],[],LB,UB,[],options);


% Compare to original
[tpost1,Xpost1] =
ode23s(@state,tdata,[y0;x20;x30;zeros(18,1)],[],P(1),P(2),P(3),P(4),P(5
),P(6));
```

```
ypost1 = Xpost1(:,1);
S11 = Xpost1(:,4);
S12 = Xpost1(:,5);
S13 = Xpost1(:,6);
S14 = Xpost1(:,7);
S15 = Xpost1(:,8);
S16 = Xpost1(:,9);

% Confidence Interval Calculations
S = [S11 S12 S13 S14 S15 S16]; % Sensitivity Matrix
H = 2*S'*S;
np = length(P); % Number of parameters
nd = length(tdata); % Number of data points
s2 = (1/(nd-np))*postsse; % Sample variance
b = 2*s2*np*finv(.95,np,nd-np);

Htild = inv(H);
P

% Size of confidence interval
L1 = sqrt(b*Htild(1,1));
L2 = sqrt(b*Htild(2,2));
L3 = sqrt(b*Htild(3,3));
L4 = sqrt(b*Htild(4,4));
L5 = sqrt(b*Htild(5,5));
L6 = sqrt(b*Htild(6,6));

% Percent size of confidence interval (relative to average parameter
value)
P1 = 100*L1/P(1)
P2 = 100*L2/P(2)
P3 = 100*L3/P(3)
P4 = 100*L4/P(4)
P5 = 100*L5/P(5)
P6 = 100*L6/P(6)

% Confidence window
C1 = [P(1)-L1 P(1)+L1]
C2 = [P(2)-L2 P(2)+L2]
C3 = [P(3)-L3 P(3)+L3]
C4 = [P(4)-L4 P(4)+L4]
C5 = [P(5)-L5 P(5)+L5]
C6 = [P(6)-L6 P(6)+L6]
```

```
function [res,grad,hess] = resid(X)

% Written by Terry Farmer, 7/27/06
% Purpose: To produce y, based on a determined model.  Also produce
% gradient and hessian for y with respect to each model parameter. To
be
% used with fmincon to determine optimal parameter values, given data.

global yode1 tdata

% Differential Equation
A01 = X(1);
A12 = X(2);
A13 = X(3);
A21 = X(4);
A31 = X(5);
V = X(6);



% Get Initial Values
y0 = 0;
x20 = 0;
x30 = 0;

% Now calculate y values with model
[tmodel,y] =
ode23s(@state,tdata,[y0;x20;x30;zeros(18,1)],[],A01,A12,A13,A21,A31,V);

ymodel = y(:,1);
S = y(:,4:9);
% Now get quantities for optimization
% First, calculate objective function
res = sum((yode1 - ymodel).^2);
grad = (-2*S'*(yode1-ymodel))';
hess = 2*S'*S;
```

```
function Xdot = state(t,X,A01,A12,A13,A21,A31,V)

% Written by Terry Farmer 6/21/06
% Purpose- To solve ODE's from Joseph's 3 compartment model, along with
sensitivities

y = X(1);
x2 = X(2);
x3 = X(3);
S11 = X(4);
S12 = X(5);
S13 = X(6);
S14 = X(7);
S15 = X(8);
S16 = X(9);
S21 = X(10);
S22 = X(11);
S23 = X(12);
S24 = X(13);
S25 = X(14);
S26 = X(15);
S31 = X(16);
S32 = X(17);
S33 = X(18);
S34 = X(19);
S35 = X(20);
S36 = X(21);


if t <=150
U = 20;
else
    U = 40;
end

xdot = -(A01+A21+A31)*y + (A13/V)*x3 + (A12/V)*x2 +U/V; % Actual ode
for dependent variable
x2dot = A21*y*V - A12*x2;
x3dot = A31*y*V - A13*x3;

S = [S11 S12 S13 S14 S15 S16;S21 S22 S23 S24 S25 S26; S31 S32 S33 S34
S35 S36];

% Create fx matrix
f1x1 = -(A01+A21+A31);
f1x2 = (A12/V);
f1x3 = (A13/V);
f2x1 = A21*V;
f2x2 = -A12;
f2x3 = 0;
f3x1 = A31*V;
f3x2 = 0;
```

```
f3x3 = -A13;

fx = [f1x1 f1x2 f1x3; f2x1 f2x2 f2x3; f3x1 f3x2 f3x3];

% Create ftheta matrix
f1th1 = -y;
f1th2 = x2/V;
f1th3 = x3/V;
f1th4 = -y;
f1th5 = -y;
f1th6 = -(1/V^2)*(A12*x2 + A13*x3 + U);
f2th1 = 0;
f2th2 = -x2;
f2th3 = 0;
f2th4 = V*y;
f2th5 = 0;
f2th6 = A21*y;
f3th1 = 0;
f3th2 = 0;
f3th3 = -x3;
f3th4 = 0;
f3th5 = V*y;
f3th6 = A31*y;

fth = [f1th1 f1th2 f1th3 f1th4 f1th5 f1th6; f2th1 f2th2 f2th3 f2th4
f2th5 f2th6;f3th1 f3th2 f3th3 f3th4 f3th5 f3th6];

% Get Sdot
Sdot = fx*S + fth;

% Get components
S11dot = Sdot(1,1);
S12dot = Sdot(1,2);
S13dot = Sdot(1,3);
S14dot = Sdot(1,4);
S15dot = Sdot(1,5);
S16dot = Sdot(1,6);
S21dot = Sdot(2,1);
S22dot = Sdot(2,2);
S23dot = Sdot(2,3);
S24dot = Sdot(2,4);
S25dot = Sdot(2,5);
S26dot = Sdot(2,6);
S31dot = Sdot(3,1);
S32dot = Sdot(3,2);
S33dot = Sdot(3,3);
S34dot = Sdot(3,4);
S35dot = Sdot(3,5);
S36dot = Sdot(3,6);
```

```
Xdot =
[xdot;x2dot;x3dot;S11dot;S12dot;S13dot;S14dot;S15dot;S16dot;S21dot;S22d
ot;S23dot;S24dot;...
    S25dot;S26dot;S31dot;S32dot;S33dot;S34dot;S35dot;S36dot];
```

APPENDIX F

HOVORKA MEAL MODEL DERIVATION

Hovorka and co-authors [3] assumed that oral ingestion of glucose is described by two compartments in series. Each compartment has a kinetic elimination rate of the inverse of the time to maximum absorption, t_{maxG}. For the first compartment, assume there is no glucose flow. In this way, the first compartment is modeled as a semi-batch reactor, in which there is only outflow, and the initial loading of the reactor is accounted for in the initial conditions. This is shown in Equation (F.1) with the initial condition described by Equation (F.2).

$$\frac{dm_1}{dt} = -\frac{m_1}{t_{max\,G}} \tag{F.1}$$

$$m_1(0) = m_{meal} \tag{F.2}$$

The variable m_1 represents the mass of glucose in the first compartment. This is a simple linear ODE that can easily be solved using separation of variables, as given by (F.3).

$$m_1 = m_{meal}\, exp\left(-\frac{t}{t_{max\,G}}\right) \tag{F.3}$$

The second compartment will have the outlet of the first compartment as its input, and the absorption of the glucose into the blood as its output. Both are described by the same kinetic rate, as shown in Equation (F.4).

$$\frac{dm_2}{dt} = \frac{1}{t_{max\,G}}\left(m_1 - m_2\right) = \frac{1}{t_{max\,G}}\left[m_{meal} A_G \, exp\left(-\frac{t}{t_{max\,G}} \right) - m_2 \right] \qquad \text{(F.4)}$$

This is also a simple linear ODE, which can be solved by determining and integrating factor. Bringing m_2 to the left side of the equation, and multiplying both sides by $\exp(t/t_{maxG})$ results in (F.5):

$$\frac{d}{dt}\left[m_2 \, exp\left(\frac{t}{t_{max\,G}} \right) \right] = \frac{m_{meal} A_G}{t_{max\,G}} \qquad \text{(F.5)}$$

Initially, there is no glucose in the second compartment, so $m_2(0)$ is zero. Multiplying through by dt and integrating both sides gives (F.6)

$$m_2 \, exp\left(\frac{t}{t_{max\,G}} \right) = K + \frac{m_{meal} A_G t}{t_{max\,G}} \qquad \text{(F.6)}$$

K can be shown to be zero by using the initial condition. By isolating m_2 and noting that the absorption rate is simply the kinetic elimination of glucose from the second compartment, U_G is shown to be given by (F.7).

$$U_G = \frac{m_2}{t_{max\,G}} = \frac{m_{meal} A_G t \, exp\left(-\frac{t}{t_{max\,G}}\right)}{t_{max\,G}^2} \tag{F.7}$$

This is the glucose absorption rate expression used in the Hovorka model.

APPENDIX G

SORENSEN DIABETIC MODEL INITIALIZATION ITERATIONS

```
%Program Solver.m
%I.  Documentation

% Created for Sorensen Model Solution
% by Terry G. Farmer
% 1/25/05


%Tasks:  Uses ODE45 to solve the Sorensen model for glucose, insulin,
and
%glucagon.  The model
%dependent variables are given by an output vector x, which is
determined
%by inputing the models and the initial x conditions, x_ss, into the
%ODE45 solver.



% Description of inputs needed for the program
%   x0 vector consisting of initial steady state conditions for the
%   model.  Used as initial values vector for ODE45
%   tf, the duration of time for which the model will be solved
%

% Description of outputs returned by the program
%   x, the vector of G's, I's and Tau.
%   t, all time values at the model was evaluated
%   Plots graphing various outputs as functions of time.


%II.  Variable declaration/initialization
clc                         %  Clears the command window
clear all                   %  Deletes all variables from memory
close all                   %  Closes all open figure windows

global GPIb GLb GHb IPIb ILb IHb rIVIb tmeal rIVI

%Parameter Values
%Volumes
VGBV = 3.5; % dL
VBI = 4.5; % dL
```

```
VGH= 13.8; % dL
VGL = 25.1; % dL
VGG = 11.2; % dL
VGK = 6.6; % dL
VGPV = 10.4; % dL
VPI = 63; % dL
VIB = 0.265; %L
VIH = 0.985; %L
VIG = 0.945; %L
VIL = 1.14; %L
VIK = 0.505; %L
VIPV = 0.735; %L
VIPI = 0.1*VPI; %L
VTau = VIB + VIH + VIPV + VIK + VIL +(VIPI); %L

%Flow Rates
QGB = 5.9; % dL/min
QGH = 43.7; % dL/min
QGA = 2.5; % dL/min
QGL = 12.6; % dL/min
QGG = 10.1; % dL/min
QGK = 10.1; % dL/min
QGP = 15.1; % dL/min
QIB = 0.45; %L/min
QIH = 3.12; %L/min
QIA = 0.18; %L/min
QIK = 0.72; %L/min
QIP = 1.05; %L/min
QIG = 0.72; %L/min
QIL = 0.90; %L/min

%Times
TB = 2.1; % min Transcapillary diffusion time constant
TGP = 5.0; % min Transcapillary diffusion time constant
TIP = 20; %min Transcapillary diffusion time constant

%Source and Sink Terms
rBGU = 70; % mg/min (constant)
rRBCU = 10; % mg/min (constant)
rGGU = 20; % mg/min (constant)
rBPGU = 35; % mg/min
rBHGP = 155; % mg/min
rBHGU = 20; % mg/min
TI = 25; % min
TT = 65; % min
FLIC = 0.40; %fractional clearance
FKIC = 0.3; %fractional clearance
FPIC = 0.15; %fractional clearance
rMTauC = .910; % L/min

% Basal values for diabetic model
GLb = 101.0; % mg/dL
GPIb = 86.81;
```

```
GHb = 91.89;
ILb = 21.43; % mU/L
IPIb = 5.304;
IHb = 15.15;


% Initializations for diabetic model
% Initial values of glucose and insulin conc.
rIVIb     = 20; % mU/min
IHi       = rIVIb/(QIH - QIL*(1-FLIC) - QIK*(1-FKIC) - QIP*(1-FPIC) -
QIB); % mU/L
IPVi      = IHi * (1-FPIC); % mU/L
IBi       = IHi;
IGi       = IHi;
IKi       = IHi*(1-FKIC);
ILi       = IHi*(1-FLIC);
IPIi      = IPVi - (QIP*(TIP/VIPI))*(IHi - IPVi);

% Determine Glucose and glucose concentrations
% Iterate to find arterial glucose concentration
j = 1;
GHi = GHb; % Initial guess for GH is GH basal.

while j < 1000

%Initialize Glucagon Model

MGPTauR = (1+2.095*tanh(4.18*(1-.6191))) - 2.095 * tanh( 4.18 *
((GHi/GHb) - 0.6191 ));
MIPTauR = (1+.61016*tanh(1.0571*(1-.46981))) - 0.61016 * tanh( 1.0571 *
((IHi/IHb) - 0.46981));
TauNi = MIPTauR * MGPTauR;

GBVi = GHi - rBGU/QGB;
GGi = GHi - rGGU/QGG;

MIPGU = (1-6.51623*tanh(.33827*-4.82113)) + 6.51623 * tanh ((0.33827 *
((IPIi/IPIb) - 5.82113)));
GPVi = GHi/(1 + ((VPI*MIPGU*rBPGU)/((QGP*VPI*GPIb) +
(TGP*QGP*MIPGU*rBPGU))));

%Iterate to find Kidney glucose concentration
GKi = GHb; % Initial guess is GHb
k = 1;
while k < 1000
if GKi < 460
    rKGE = 71 + 71 * tanh ( 0.11 * (GKi - 460)); % mg/min if GK <= 460
mg/dL
else
    rKGE = -330 + 0.872 * GKi; % mg/min if GK >= 460 mg/dL
end
```

```
GKc = GKi;
GKi = GHi - (rKGE / QGK);
if (abs(GKi - GKc))<1.0e-18
    k = 1000;
else
    k = k + 1;
end
end

% Iterate to find liver glucose concentration.
GLi = GLb; % Initial liver glucose concentration guess
i = 1;
while i < 1000
% rHGP calculation
MIinfHGP = (1+1.138*tanh(1.669*(1-.8885))) - 1.138 *tanh ((1.669 *
((ILi/ILb) - 0.8885)));
MIHGPi = MIinfHGP;
MTau0HGP = (1/(tanh(.388)))*tanh (0.388 * TauNi);
f2i = (MTau0HGP - 1)/2;
MTauHGP = MTau0HGP - f2i;
MGHGP = (1+1.406*tanh(.6199*(1-.4969))) - 1.406 * tanh (0.6199 *
((GLi/GLb) - 0.4969));
rHGP = MIHGPi * MTauHGP * MGHGP * rBHGP;
% rHGU calculation
MIinfHGU = (1/(tanh(.549))) * tanh (0.549 * (ILi/ILb));
MIHGUi = MIinfHGU;
MGHGU = (1-5.6589*tanh(2.4375*(-0.48))) + 5.6589 * tanh (2.4375 *
((GLi/GLb) - 1.48));
rHGU = MIHGUi * MGHGU * rBHGU;
GLc = GLi;
GLi = (1/QGL)*(QGA*GHi + QGG*GGi + rHGP - rHGU) ;%Checking liver
glucose
if (abs(GLi - GLc))<1.0e-18
    i = 1000;
else
    i = i + 1;
end
end

GHc = GHi;
GHi = (1/QGH)*(QGB*GBVi + QGL*GLi +QGK*GKi +QGP*GPVi - rRBCU);
%Checking arterial glucose
if (abs(GHi - GHc)) < 1.0e-18
    j = 1000;
else j = j +1;
end

end

GPIi = GPVi /(1 + ((MIPGU*rBPGU*TGP)/(VPI*GPIb)));
GBIi = GBVi - (TB*(rBGU/VBI));
```

```
x0 = [GBVi; GBIi; GHi; GGi; GLi; GKi; GPVi; GPIi; MIHGPi; f2i;
    MIHGUi; IBi; IHi; IGi; ILi; IKi; IPVi; IPIi; TauNi];   % Initial
conditions are the results of the iterations
```

APPENDIX H

DERIVATION OF MICHAELIS-MENTEN KINETICS

The Michaelis-Menten equation is routinely used to describe kinetics involving an enzyme. Its derivation begins by assuming the enzyme catalyzed reaction proceeds by the following mechanism [5]:

$$Enzyme(E) + Substrate(S) \underset{k_{-1}}{\overset{k_1}{\rightleftarrows}} Complex(ES) \xrightarrow{k_2} E + Product(P) \qquad \text{(H.1)}$$

The second step in the reaction, in which the complex dissociates to form the product, is first order in the complex. The Michaelis-Menten equation makes the quasi-steady state assumption with respect to the complex, assuming that complex formation and dissociation are occurring at the same rate. It is also assumed that there is a total maximum enzyme concentration, and that the complex concentration is less than or equal to this concentration. Complex formation is assumed to be first order in the concentration of available enzyme, which is simply the total enzyme minus the complexes formed, and first order in the substrate concentration. Complex formation is also considered reversible, meaning that the complex may dissociate back to the substrate and the enzyme. The reverse reaction is first order in complex concentration. All of this is combined to show the following steady state relation:

$$k_1\left(E_{Total} - ES\right)S = ES\left(k_{-1} + k_2\right) \tag{H.2}$$

where subscript 1 represents complex formation, -1 represents the complex reverse reaction, and 2 represents product formation. For ease of derivation, the rate constants are collected to form K_s, as shown in Equation (H.3).

$$\frac{k_{-1} + k_2}{k_1} = K_s = \frac{\left(E_{Total} - ES\right)S}{ES} \tag{H.3}$$

The complex concentration, ES, is then isolated, and the product formation rate is written in terms of the rates, E_{Total}, and S.

$$v_0 = k_2 ES = \frac{k_2 E_{Total} S}{K_S + S} \tag{H.4}$$

The rate v_0 represents the initial reaction rate, which is often measured in enzymatic reactions that can reach equilibrium fairly quickly. The parameter V_{max} is defined as the product of k_2 and E_{Total}. When this substitution is made, the result is the Michaelis-Menten Equation.

$$v_0 = \frac{V_{max} S}{K_S + S} \tag{H.5}$$

APPENDIX I

DERIVATION OF DONNAN RATIO EQUATION

The purpose of this derivation is to use the concept of equilibrium with respect to swellable hydrogel polymer network to determine the Donnan ratio, K, of the system, for a particular set of conditions. Given the Donnan ratio and the concentrations of ionic species in the external solution, the gel concentrations of the various species can be determined.

At equilibrium, the following ideal assumptions are made [6]. First, only hydrogen ions are interacting with the amine groups on the polymer chain. Second, at equilibrium, the gel is assumed to be electrically neutral. Third, because of the first assumption, any interactions between ions and the gel surface are neglected. Fourth, the electric potential is assumed to be uniformly distributed throughout the gel, meaning that spatial considerations are neglected as well. Finally, the amine groups are assumed to not interact with each other.

Because the gel is considered electrically neutral, the total charge is zero. This is represented by Equation (I.1).

$$0 = \sum_i n_i z_i + n_{aH} z_a \qquad \text{(I.1)}$$

This says that the total charge is equal to the total charge associated with each species including the amine groups in the gel network. The variable n_{aH} represents the number of

protonated amine groups in the network. The number of moles of each species is best represented by the concentration of each species and the volume at which that concentration exists. The mobile species exist in the gel solvent, while the amine groups are present on the polymer itself. Neglecting volume effects of the mobile ionic species, it can be assumed that the volume of each species is simply the solvent volume, V_s. as shown by Equation (I.2).

$$0 = \sum_i V_s c_i z_i + V_p c_{aH}(+1) \tag{I.2}$$

In order to relate this equation to known quantities, a few definitions will be given. First, the concentration of ionic species i in the gel, c_i, is related to concentration of the species in the external environment through the Donnan ratio:

$$K^{z_i} = \frac{c_i}{c_i'} \tag{I.3}$$

where c'_i is the concentration in the external environment. Next, the two volumes used in (I.2) can be simplified when expressed as volume fractions of the total gel volume:

$$V_p = V_g \varphi \tag{I.4}$$

$$V_s = V_g(1-\varphi) \tag{I.5}$$

where V_g is the total gel volume and φ is the polymer volume fraction. Finally, While the concentration of protonated amine groups cannot be determine experimentally, it can be calculated if the original amine loading, the amine pK_g, and the system pH are known by accounting for acid dissociation equilibrium:

$$K_g = \frac{c_a c_H}{c_{aH}} \tag{I.6}$$

Solving for c_{aH} results in (I.6):

$$c_{aH} = \frac{c_H c_a}{K_g} \tag{I.7}$$

where c_a represents the amine concentration that has not been protonated. Based on the functional group loading, this term can be found to eliminate an unknown term:

$$c_{aH} + c_a = \sigma \tag{I.8}$$

in which σ is the functional group density of the polymer, and (I.8) is simply a mass balance of the functional groups. Using (I.8) to eliminate c_a in (I.7) and noting that the gel hydrogen ion concentration is related to the external hydrogen ion concentration through Donnan equilibrium results in the following equation in terms of only external environment variables:

$$c_{aH} = \frac{\sigma}{1 + K_g K^{-1} c_H'^{-1}} \tag{I.9}$$

Substituting (I.4), (I.5), and (I.9) into (I.2), and using the definition of pK_g and pH, the final equation for Donnan equilibrium is given in (I.10).

$$0 = (1 - \varphi)\sum_i z_i K^{z_i} c_i' + \frac{\sigma\varphi}{1 + K^{-1} 10^{pH - pK_g}} \tag{I.10}$$

APPENDIX J

MATLAB SOURCE CODE FOR IMPLICIT CLOSED-LOOP CONTROL

```
      function xdot =
device_degrade(t,x,Ng,tmeal,DI0,DG0,DGA0,Rcoll,G_b,I_b,Vmax,sigma,pKg,k
1,thick)

% Device gives the insulin output from the injectible polymer
% nanoparticles.  Given the material parameters, the function
determines
% the insulin output of the system.

% Written by Terry Farmer, 6/14/06


G = x(1); % glucose concentration in medium (mmol/L)
X = x(2); % Proportional to bound insulin (remote compartment) (min^-1)
I = x(3); % Insulin Level
Gd = x(4);  % Glucose concentration in device (mmol/L)
GA = x(5);  % gluconic acid concentration  (mmol/L)
Id = x(6);  % insulin concentration in device (mU/L)
XL = x(7); % crosslinking ratio


% Get parameter values for model equations
Ks = 6.187e-1; % Glucose concentration at 50% of max rate (mmol/L)
Cn = 14.4;
L = 1.54; % Angstroms
rI = 16; % Insulin radius (Angstroms)
rG = 4.2; % Glucose radius (Angstroms)
rGA = .012; % Gluconic acid radius; Either taken as same as glucose or
as hydrogen ion (Angstroms)

% Equations
pH0 = 7.4; % Initial pH guess
Qmax = 40*exp(-49.8*(XL-0.005));
if XL >0.02
    Qmin = 2;
else
    Qmin = 3;
end

A = 0.5*(Qmax+Qmin);
B = Qmax-A;
dPH = 1;
Iter = 0;
```

```
% Use iteration to determine pH and swelling

while abs(dPH) > 1.0e-6 & Iter < 1001
q = A + B * tanh(-10*(pH0-pKg));
phi = 1/q;
% First get necessary model parameters
pH = 7.4; % Blood pH
pK = 6.33; % pK of bicarbonate buffer
phi0 = 1/q; % Initial volume fraction

% Assume bicarbonate buffer conditions
H1 = 3.98e-8; % mol/L
Na1 = 142/1000; % mol/L Sodium concentration
K1 = 4.2/1000; % mol/L Potassium concentration
Ca1 = 1.2/1000; % mol/L Calcium concentration
Cl1 = 108/1000; % mol/L Chloride ion concentration
HCO3 = 25/1000; % bicarbonate concentration (mol/L)
CO2 = 1.224/1000; % carbon dioxide concentration (mol/L)

% use fsolve to find donnan ratio for cationic gel
options = optimset('Display','off');
lambda = fsolve(@don,10,options,q,sigma,pKg);

pH1 = pH - log10(lambda); % Device pH without gluconic acid

% Determine device concentrations of buffer molecules
H = lambda*H1; % Device H concentration (mol/L)
Na = lambda*Na1; % Device Na concentration (mol/L)
HCO3 = HCO31*(lambda^(-1)); % Device HCO3 concentration (mol/L)

buffer = HCO3 + CO2; % buffer concentration

% Given gluconic acid concentration, determine pH

pH2 = pK + log10(((10^(pH1-pK))-((GA*.001/buffer)*(1+(10^(pH1-
pK)))))/(1+((GA*.001/buffer)*(1+(10^(pH1-pK))))));
dPH = pH2 - pH0;
pH0 = pH2;
Iter = Iter + 1;
end

R = Rcoll*(q^(1/3));
mesh = (Cn^.5)*(q^(1/3))*((XL*2)^(-.5))*(L); % Mesh size for
diffusivity (Angstroms)
DI = DI0*(1 - (rI/mesh))*exp(-1/(q-1)); % Initial insulin diffusivity
(Cm^2/s)
DG = DG0*(1 - (rG/mesh))*exp(-1/(q-1)); % Initial glucose diffusivity
(cm^2/s)
DGA = DG;% Initial gluconic acid diffusivity (cm^2/s)
V = 12*1000; % Volume of tank (cm^3)

if t < tmeal
```

```
    D = 0;
else
D = 1.157*exp(-0.05*(t - tmeal));
end
D = 0;
% Bergman model parameters
P1 = 0.00001; % min^-1
P2 = 0.025; %min ^-1
P3 = .000013; %L/(mU*min^2)
n = 5/54; % min^-1

U = (4*pi*Ng*DI*60*(Id-I)*(R^2/(thick)))/1000;

Gdot = real(-4*pi*Ng*DG*60*(R^2/(thick*V))*(G-Gd) - P1*(G-G_b) - G*X +
D);
Xdot = (-P2*X + P3*(I - I_b));
Idot = (U/(V/1000)) - n*I;
Gddot = (3*60*DG*(G - Gd)/(R*thick) - (Vmax*Gd)/(Ks+Gd));
GAdot = ((Vmax*Gd/(Ks+Gd)) - (3*60*DGA/(R*thick))*GA);
Iddot = (-3*DI*60*(Id - I)/(R*thick));
XLdot = (-k1*XL);


% Results
xdot = [Gdot;Xdot;Idot;Gddot;GAdot;Iddot;XLdot];
xdot;
```

```
function char = don(lambda,q,sigma,pKg);


% Function don determines the value of the nonlinear Donnan equilibrium
to use in a solver program to solve for the Donnan ratio.  The equation
is set to zero, and given other parameters, is solved for lambda.

% Written by Terry Farmer, 10/11/06

% First get necessary model parameters
pH = 7.4; % Blood pH
phi0 = 1/q; % Initial volume fraction

% Assume phosphate buffer conditions
H1 = 3.98e-8; % mol/L
Na1 = 142/1000; % mol/L Sodium concentration
K1 = 4.2/1000; % mol/L Potassium concentration
Ca1 = 1.2/1000; % mol/L Calcium concentration
Cl1 = 108/1000; % mol/L Chloride ion concentration
HCO3 = 25/1000; % bicarbonate concentration (mol/L)


char = (1 - phi0)*((-1*(lambda^(-1))*(HCO3+Cl1)...
    +(lambda*(H1+Na1+K1))+((lambda^2)*2*Ca1))) + ((sigma*phi0)/(1 +
(lambda^(-1))*(10^(pH-pKg))));
```

```
% Program Solver
% Written by Terry Farmer, 6/29/06

% Purpose: To simulate the response of injected hydrogels that release
% insulin in response to a change in plasma glucose levels.  The model
uses
% the Bergman minimal model to simulate the diabetic patient, and the
% Hydrogel model to describe the dynamics of an injected nanoscale
device.


% Get parameter values for model equations
% System design parameters
Cenz = 1; % glucose oxidase concentration (uM)
Ng = 3.54e7; % Number of injected particles
xx = .004; % Crosslinking ratio
DI0 = (1.41e-13); % Initial insulin diffusivity (Cm^2/s)
DG0 = (6.9e-12);% Initial glucose diffusivity (cm^2/s)
sigma = 4; % Charged group density (mol/L)
pKg = 7.1; % pK of functional group
kd = 0.001; %min^-1 (Degradation rate constant)
Id_b = 1e8; % mU/L (Insulin Loading)
thickness = 0.1; % Fraction of collapsed gel size
% Simulation Time
t0 = 0; % minutes
tmeal = 60; % minutes
tfinal = 400; % minutes

% Characteristic values
Vmax = 860*60*Cenz*(1e-3); % Maximum oxidation rate (mmol/L*min)
Ks = (6.187e-7)*1000*1000; % Glucose concentration at 50% of max rate
(mmol/L)
Cn = 14.4;
L = 1.54; % Angstroms
rI = 16; % Insulin radius (Angstroms)
rG = 2.5; % Glucose radius (Angstroms)
rGA = 2.5; % Gluconic acid radius; Either taken as same as glucose or
as hydrogen ion (Angstroms)
DGA0 = DG0; % Initial gluconic acid diffusivity (cm^2/s)


% Getting initial values
G_b = 4.5; % Basal glucose (mmol/L)
X_b = 0; % Basal proportional term (min^-1)
I_b = 15; % Basal insulin level (mU/L)

% Guess pH
pHb = 7.4;
dPH = 1;
Iter = 0;
```

```
Qmax = 40*exp(-49.8*(xx-0.005)); % From curve fitting
Rcoll = (4.5/(Qmax^(1/3)))*(1e-6)*100; % Maximum collapsed particle
size (cm)
thick = thickness*Rcoll; % assumes 10% thickness

if xx >0.02
    Qmin = 2;
else
    Qmin = 3;
end
A = (Qmax + Qmin)/2;
B = Qmax - A;
C = -10;
while abs(dPH) > 1.0e-6 & Iter < 1001

Q_b = A + B * tanh(C*(pHb-pKg));
phi = 1/Q_b;
% First get necessary model parameters
pH = 7.4; % Blood pH
pK = 6.33; % pK of phosphate buffer
phib = 1/Q_b; % Initial volume fraction

% Assume bicarbonate buffer conditions
H1 = 3.98e-8; % mol/L
Na1 = 142/1000; % mol/L Sodium concentration
K1 = 4.2/1000; % mol/L Potassium concentration
Ca1 = 1.2/1000; % mol/L Calcium concentration
Cl1 = 108/1000; % mol/L Chloride ion concentration
HCO3 = 25/1000; % bicarbonate concentration (mol/L)
CO2 = 1.224/1000; % carbon dioxide concentration (mol/L) (PC02 = 40 mm
Hg; K = 0.03 mmol/L/mm Hg

% use fsolve to find donnan ratio for cationic gel
options = optimset('Display','off');
lambda = fsolve(@don,10,options,Q_b,sigma,pKg);

pH1 = pH - log10(lambda); % Device pH without gluconic acid

% Determine device concentrations of buffer molecules
H = lambda*H1; % Device H concentration (mol/L)
Na = lambda*Na1; % Device Na concentration (mol/L)
HCO3 = HCO31*(lambda^(-1)); % Device HCO3 concentration (mol/L)

buffer = HCO3 + CO2;

% Swelling based parameters to find GA_b (for pH calculation)
mesh = (Cn^.5)*(Q_b^(1/3))*((xx*2)^(-.5))*(L); % Mesh size for
diffusivity
DI_b = (DI0)*(1 - (rI/mesh))*exp(-1/(Q_b-1)); % Initial insulin
diffusivity (Cm^2/s)
DG_b = (DG0)*(1 - (rG/mesh))*exp(-1/(Q_b-1)); % Initial glucose
diffusivity (cm^2/s)
```

```
DGA_b = DG_b; % Initial gluconic acid diffusivity (cm^2/s)
R_b = Rcoll*(Q_b^(1/3)); % Initial particle radius


% Now solve for initial device concentrations
% Gd_b is determined via a quadratic equation
Aqd = 1;
Bqd = (((Vmax*(R_b*thick))/(3*DG_b*60)) + Ks - G_b);
Cqd = -Ks*G_b;

y1 = (-Bqd + sqrt((Bqd^2) - 4*Aqd*Cqd))/(2*Aqd); % Solution 1 to
quadratic
y2 =(-Bqd - sqrt((Bqd^2) - 4*Aqd*Cqd))/(2*Aqd); % Solution 2 to
quadratic

% Now get Gd_b
if y1 < 0
    Gd_b = y2;
else
    Gd_b = y1;
end

% Now solve for GA_b
GA_b = ((R_b*thick)*Vmax*Gd_b)/(3*60*DGA_b*(Ks+Gd_b));
% Given gluconic acid concentration, determine pH

pH2 = pK + log10(((10^(pH1-pK))-((GA_b*.001/buffer)*(1+(10^(pH1-
pK)))))/(1+((GA_b*.001/buffer)*(1+(10^(pH1-pK))))));
dPH = pH2 - pHb;
pHb = pH2;
Iter = Iter + 1;
end

% Create Initial vector
x0 = [G_b;X_b;I_b;Gd_b;GA_b;Id_b;xx];



% Create sensitivity matrix
np = 15; % number of adjustable parameters in model\
if(0)
S0 = zeros(length(x0),np);
% Convert matrix to column vector, with sequentially
for i = 1:length(x0)
    for j = 1:np
        Sp0(np*(i-1)+j,1) = S0(i,j);
    end
end
```

```
xnew0 = [x0;Sp0];
end
% Simulation
[t,x] = ode15s(@device_degrade,[t0
tfinal],x0,[],Ng,tmeal,DI0,DG0,DGA0,Rcoll,G_b,I_b,Vmax,sigma,pKg,kd,thi
ck);

% Extract values
G = x(:,1);
XC = x(:,2);
I = x(:,3);
Gd = x(:,4);
GA = x(:,5);
Id = x(:,6);
X = x(:,7);

% Remaining values are sensitivities



% First get necessary model parameters
pH = 7.4; % Blood pH
pK = 6.33; % pK of phosphate buffer

% Assume bicarbonate buffer conditions
H1 = 3.98e-8; % mol/L
Na1 = 142/1000; % mol/L Sodium concentration
K1 = 4.2/1000; % mol/L Potassium concentration
Ca1 = 1.2/1000; % mol/L Calcium concentration
Cl1 = 108/1000; % mol/L Chloride ion concentration
CO2 = 1.224/1000; % CO2 concentration (mol/L)
HCO31 = 25/1000; % bicarbonate concentration (mol/L)

% Matrix Pre-allocation
pH0 = zeros(1,length(t));
A = pH0;
B = A;
q = B;
lambda = q;
pH1 = pH0;
pH2 = pH1;
H = pH1;
Na = pH1;
buffer = pH1;
HCO3 = pH1;


for i = 1:length(GA)
    % Equations
    Qmax(i) = 40*exp(-49.8*(X(i)-0.005));
    if X(i) > 0.02
        Qmin(i) = 2;
```

```
    else
        Qmin(i) = 3;
    end

A(i) = 0.5*(Qmin(i)+Qmax(i));
B(i) = Qmax(i) - A(i);
pH0(i) = 7.4; % Initial pH guess

dPH(i) = 1;
Iter = 0;
% Use iteration to determine pH and swelling
while abs(dPH(i)) > 1.0e-6 & Iter < 1001
% Parameters for pH evaluation

q(i) = A(i) + (B(i) * tanh((-10*(pH0(i) -pKg))));

% use fsolve to find donnan ratio for cationic gel
options = optimset('Display','off');
lambda(i)= fsolve(@don,1,options,q(i),sigma,pKg);

pH1(i) = pH - log10(lambda(i)); % Device pH without gluconic acid

% Determine device concentrations of buffer molecules
H(i) = lambda(i)*H1; % Device H concentration (mol/L)
Na(i) = lambda(i)*Na1; % Device Na concentration (mol/L)
HCO3(i) = HCO31*(lambda(i)^(-1)); % Device HCO3 concentration (mol/L)

buffer(i)= HCO3(i) + CO2;

% Given gluconic acid concentration, determine pH

pH2(i) = pK + log10(((10^(pH1(i)-pK))-
((GA(i)*.001/buffer(i))*(1+(10^(pH1(i)-
pK)))))/(1+((GA(i)*.001/buffer(i))*(1+(10^(pH1(i)-pK))))));
dPH(i) = pH2(i) - pH0(i);
pH0(i) = pH2(i);
Iter = Iter + 1;
end

R(i) = Rcoll*(q(i)^(1/3)); % Vector of R's
mesh(i) = (Cn^.5)*((X(i)*2)^(-.5))*(q(i)^(1/3))*(L);
DI(i) = DI0*(1 - (rI/mesh(i)))*exp(-1/(q(i)-1)); % Vector of
Diffusivities
U(i) = (4*60*pi*R(i)^2*Ng*DI(i)*(Id(i)-I(i))/(thick*1000));
Idot(i) = -3*60*DI(i)*(Id(i)-I(i))/(R(i)*thick);
end

% Fraction of Insulin released
fr = (Id_b-Id)/(Id_b);
```

Appendix References

1. Bergman, R. N., Ider, Y. Z., Bowden, C. R., and Cobelli, C., "Quantitative Estimation of Insulin Sensitivity," *Am. J. Physiol.*, **236**, E667-E677, 1979.

2. Furler, S. M., Kraegen, E.W., Smallwood, R.H, and Chisolm, D.J., "Blood Glucose Control by Intermittent Loop Closure in the Basal Mode: Computer Simulation Studies with a Diabetic Model", *Diabetes Care*, **8**, 553-561, 1985.

3. Hovorka, R., Canonico, V., Chassin, L. J., Haueter, U., Massi-Benedetti, M., Federici, M. O., Pieber, T. R., Schaller, H. C., Schaupp, L., Vering, T., and Wilinska, M. E., "Nonlinear Model Predictive Control of Glucose Concentration In Subjects With Type I Diabetes", *Physiol. Meas.*, **25**, 905-920, 2004.

4. Sorensen, J. T., "A Physiologic Model of Glucose Metabolism in Man and Its Use to Design and Assess Improved Insulin Therapies For Diabetes", Ph.D. thesis, Dept. Chem. Eng., Massachusetts Institute of Technology, Cambridge, 1985.

5. Horton, H. R., Moran, L. A., Scrimgeour, K. G., Perry, M. D., and Rawn, J. D., Eds., *Principles of Biochemistry, 4th Ed.*, Prentice Hall, Upper Saddle River, NJ, 2006.

6. Ricka, J. and Tanaka, T., "Swelling of Ionic Gels: Quantitative Performance of the Donnan Theory," *Macromolecules*, **17**, 2916-2921, 1984.

REFERENCES

Abdekhodaie, M. J., and Wu, X. Y., "Modeling of a Cationic Glucose-Sensitive Membrane With Consideration of Oxygen Limitation," *J. Membrane Sci.*, **254**, 119-127, 2005.

Ackerman, E., Gatewood, L. C., Rosevear, J. W., and Molnar, G. D., "Model Studies of Blood-Glucose Regulation," *B. Math. Biophys.*, **27**, 21-37, 1965.

Agar, B., Birol, G., and Cinar, A., "Virtual Experiments For Controlling Blood Gulcose Level In Type I Diabetes," in *Proc. 2nd Joint EMBS-BMES Conference*, Houston, TX, 2002.

Albin, G. W., Horbett, T. A., Miller, S. R., and Ricker, N. L., "Theoretical and Experimental Studies of Glucose Sensitive Membranes," *J. Control. Release*, **6**, 267-291, 1987.

Albisser, A. M., Leibel, B. S., Ewart, T. G., Davidovac, Z., Botz, C. K., and Zingg, W., "An Artificial Endocrine Pancreas," *Diabetes*, **23**, 389-396, 1974.

Batycky, R. P., Hanes, J., Langer, R., and Edwards, D. A., "A Theoretical Model of Erosion and Macromolecular Drug Release From Biodegrading Microspheres," *J. Pharm. Sci.*, **86**, 1464-1477, 1997.

Becton-Dickinson, "Diabetes Education", available http://www.bddiabetes.com, Sept. 2006.

Bequette, B. W., *Process Control: Modeling, Design, and Simulation*, 1st Ed., Prentice Hall, Upper Saddle River, NJ, 2003.

Bequette, B. W., "A Critical Assessment of Algorithms and Challenges In the Development of a Closed-Loop Artificial Pancreas," *Diabetes Technology and Therapeutics*, **7**, 28-47, 2005.

Bergman, R. N., Ider, Y. Z., Bowden, C. R., and Cobelli, C., "Quantitative Estimation of Insulin Sensitivity," *Am. J. Physiol.*, **236**, E667-E677, 1979.

Bergman, R. N., Bowden, C. R., and Cobelli, C., "The Minimal Model Approach to Quantification of Factors Controlling Glucose in Man," in *Carbohydrate Metabolism*, C. Cobelli and R. N. Bergman, Eds., Wylie, London, 269-296, 1981.

Bergman, R. N., Phillips, L. S., and Cobelli, C., "Physiologic Evaluation of Factors Controlling Glucose Tolerance in Man," *J. Clin. Invest.*, **68**, 1456-1467, 1981.

Bergman, R. N., Finegood, D. T., and Ader, M., "Assessment of Insulin Sensitivity in Vivo," *Endocr. Rev.*, **6**, 45-86, 1985.

Bischoff, K. B., and Brown, R. G., "Drug Distribution in Mammals," *Chem. Eng. Prog. Symp. Ser.*, **66**, 33-45, 1966.

Bischoff, K. B., "Applications of a Mathematical Model For Drug Distribution in Mammals," in *Chemical Engineering in Medicine and Biology*, D. Hershey, Ed., Plenum, NY, 417-446, 1967.

Bischoff, K. B., "Some Fundamental Considerations of the Applications of Pharmacokinetics to Cancer Chemotherapy," *Cancer Chemoth. Rep. 1*, **59**, 777-793, 1975.

Bischoff, K. B., "Physiologically Based Pharmacokinetic Modeling," in *Pharmacokinetics in Risk Assessment: Drinking Water and Health, Volume 8*, NAS Press, Washington, 36-61, 1987.

Bolie, V. W., "Coefficients of Normal Blood Glucose Regulation," *J. Clin. Invest.*, **39**, 783-788, 1960.

Bouwens, L., and Rooman, I., "Regulation of Pancreatic Beta Cell Mass," *Physiol. Rev.*, **85**, 1255-1270, 2005.

Caumo. A, Vicini, P., Zachwieja, J., Avogaro, A., Yarasheski, K., Bier, D., M., and Cobelli, C., "Undermodeling Affects Minimal Model Indexes: Insights From a Two-Compartment Model," *Am. J. Physiol.*, **276**, E1171-E1193, 1999.

Caumo, A., Bergman, R. N., and Cobelli, C., "Insulin Sensitivity From Meal Tolerance Tests In Normal Subjects: A Minimal Model Index," *J. Clin. Endocr. Metab.*, **85**, 4396-4402, 2000.

Cerasi, E., Fick, G., and Rudemo, M., "A Mathematical Model For the Glucose Induced Insulin Release In Man," *Europ. J. Clin. Invest.*, **4**, 267-278, 1974.

Clemens, A. H., "Feedback Control Dynamics For Glucose Controlled Insulin Infusion Systems," *Med. Prog. Technol.*, **6**, 91-98, 1979.

Cobelli, C., Federspil, G., Pacini, G., Salvan, A., and Scandellari, C., "An Integrated Mathematical Model of the Dynamics of Blood Glucose and Its Hormonal Control," *Math. Biosci.*, **58**, 27-60, 1981.

Cobelli, C., Bettini, F., Caumo, A., and Quon, M. J., "Overestimation of Minimal Model Glucose Effectiveness In Presence of Insulin Response Is Due to Undermodeling," *Am. J. Physiol.*, **277**, E1031-E1036, 1998.

Cobelli, C., Caumo, A., and Omenetto, M., "Minimal Model S_G Overestimation and S_I Underestimation: Improved Accuracy By a Bayesian Two-Compartment Model," *Am. J. Physiol.*, **277**, E481-E488, 1999.

Colberg, S. R., "Glucose Monitoring and Physical Activity: The Present and Future Challenges," Diabetes Technology & Therapeutics, 7, 681-683, 2005.

Constantinides, A. and Mostoufi N., *Numerical Methods For Chemical Engineers With MATLAB Applications*, Prentice Hall, Upper Saddle River, NJ, 1999.

Cooney, D. O., *Biomedical Engineering Principles: An Introduction To Fluid, Heat, and Mass Transport Processes*, Dekker, NY, 1976.

Cornejo-Bravo, J. M. and Siegel, R. A., "Water Vapor Sorption Behavior of Copolymers of N,N-Diethylaminoethyl Methacrylate and Methyl Methacrylate," *Biomaterials*, **17**, 1187-1196, 1993.

Cornejo-Bravo, J. M. and Siegel, R. A., "Kinetics of Drug Release From Hydrophobic Polybasic Gels: Effect of Buffer Acidity," *J. Control. Release*, **33**, 223-229, 1995.

Cryer, P. E., "Glucose Homeostasis and Hypoglycemia," in Larsen, P.R., Kronenberg, H.M., Melmed,S., and Kenneth S. Polonsky, eds., *Williams Textbook of Endocrinology*, 10th ed., Saunders, Philadelphia, PA, 1585-1618, 2003.

Dalla Man, C., Campioni, M., Polonsky, K. S., Basu, R., Rizza, R. A., Toffolo, G., and Cobelli, C., "Two-Hour Seven-Sample Oral Glucose Tolerance Test and Meal Protocol: Minimal Model Assessment of β-Cell Responsitivity and Insulin Sensitivity In Nondiabetic Individuals," *Diabetes*, **54**, 3265-3273, 2005.

Dhanarajan, A. P., Misra, G. P., and Siegle, R. A., "Autonomous Chemomechanical Oscillations In a Hydrogel/Enzyme System Driven By Glucose," *J. Phys. Chem. A*, **106**, 8835-8838, 2002.

Diaz, R. G., Roldan, G., and Basualdo, M., "A Decision Support System Based On a Closed Loop PFC Applied For Type I Diabetes," in *Proceedings of the 16th IFAC World Congress*, Prague, Czech Republic, 2005.

Doyle, F. J. III, Dorski, C., Harting, J. E., and Peppas, N. A., "Control and Modeling of Drug Delivery Devices For the Treatment of Diabetes," in *Proc. American Control Conf.*, Seattle, WA, 776-780, 1995.

Edgar, T. F. and Himmelblau, D. M., *Optimization of Chemical Processes*, McGraw-Hill, NY, 1988.

El-Khatib, F. H., Jiang, J., and Damiano, E. R., "Adaptive Closed-Loop Control Provides Blood-Glucose Regulation Using Dual Subcutaneous Insulin and Glucagon Infusion In Diabetic Swine," *J. Diabetes Sci. Tech.*, **1**, 181-192, 2007.

Ende, M. T., Hariharan, D., and Peppas, N. A., "Factors Influencing Drug and Protein Transport and Release From Ionic Hydrogels," *React. Polym.*, **25**, 127-137, 1995.

Finegood, D. T., and Tzur, D., "Reduced Glucose Effectiveness Associated With Reduced Insulin Release: An Artifact of the Minimal-Model Method," *Am. J. Physiol.*, **271**, E485-E495, 1996.

Firestone, B. A. and Siegel, R. A., "Dynamic pH-Dependent Swelling Properties of a Hydrophobic Polyelectrolyte Gel," *Polym. Commun.,* **29**, 204-208, 1988.

Firestone, B. A., and Siegel, R. A., "Kinetics and Mechanisms of Water Sorption In Hydrophobic, Ionizable Copolymer Networks," *J. Appl. Polymer Sci.*, **43**, 901-914, 1991.

Fisher, M. E., "A Semiclosed-Loop Algorithm For the Control of Blood Glucose Levels In Diabetics," *IEEE Trans. Biomed. Eng.*, **38**, 57-61, 1991.

Foster, R. O., Soeldner, J. S., Tan, M. H., and Guyton, J. R., "Short Term Glucose Homeostasis In Man: A System's Dynamics Model," *J. Dyn. Syst. Meas. Control,* **95**, 308-314, 1973.

Freeland, A. C. and Bonnecaze, R. T., "Inference of Blood Glucose Concentrations From Subcutaneous Glucose Concentrations: Applications to Glucose Biosensors," *Ann. Biomed. Eng.*, **27**, 525-537, 1999.

Frost, D. P., Srivastava, M. C., Jones, R. H., Nabarro, J. D. N., and Sonksen, P. H., "The Kinetics of Insulin Metabolism In Diabetes Mellitus," *Postgrad. Med. J.*, **49**, 949-954, 1973.

Furler, S. M., Kraegen, E.W., Smallwood, R.H, and Chisolm, D.J., "Blood Glucose Control by Intermittent Loop Closure in the Basal Mode: Computer Simulation Studies with a Diabetic Model", *Diabetes Care*, **8**, 553-561, 1985.

Ginsberg, B. H., "How Accurate Are Accuracy Measurements of Continuous Glucose Sensing," *Diabetes Technology & Therapeutics*, **7**, 673-674, 2005.

Greenspan, F. S., and David G. Gardner, eds., *Basic and Clinical Endocrinology*, 7th ed., McGraw-Hill, United States, 2004.

Guyton, A. and Hall, J., *Textbook of Medical Physiology*, 11th ed., Elsevier Saunders, Philadelphia, PA, 2006.

Guyton, J. R., Foster, R. O., Soeldner, J. S., Tan, M. H., Kahn, C. B., Koncz, L., and Gleason, R. E., "Model of Glucose-Insulin Homeostasis In Man That Incorporates the Heterogeneous Fast Pool Theory of Pancreatic Insulin Release," *Diabetes*, **27**, 1027-1042, 1978.

Habener, J. F., "Insulinotropic Glucagon-Like Peptides," in LeRoith, D., Taylor, S. I., and Jerrold M. Olefsky, Eds., *Diabetes Mellitus: A Fundamental and Clinical Text*, 2nd ed., Lippincott, Williams, and Wilkins, Philadelphia, PA, 94-105, 2000.

Hariharan, D. and Peppas, N. A., "Modelling of Water Transport and Solute Release In Physiologically Sensitive Gels," *J. Contr. Rel.*, **23**, 123-136, 1993.

Hariharan, D. and Peppas, N. A., "Characterization, Dynamic Swelling Behavior and Solute Transport In Cationic Networks With Applications To the Development of Swelling-Controlled Release Systems," *Polymer*, **37**, 149-161, 1996.

Harland, R. S., Dubernet, C., Benoit, J., and Peppas, N. A., "A Model of Dissolution-Controlled, Diffusional Drug Release From Non-Swellable Polymeric Microspheres," *J. Control. Release*, **7**, 207-215, 1988.

Heller, A., "Integrated Medical Feedback Systems For Drug Delivery", *AIChE J.*, **51**, 1054-1066, 2005.

Himmelstein, K. J., and Lutz, R. J., "A Review of the Applications of Physiologically Based Pharmacokinetic Modeling," *J. Pharmacokinet. Biopharm.*, **7**, 127-145, 1979.

Hipszer, B., Joseph, J., and Kam, M., "Pharmacokinetics of Intravenous Insulin Delivery in Humans With Type I Diabetes," *Diabetes Technology & Therapeutics*, **7**, 83-93, 2005.

Holz, M., and Fahr, A., "Compartmental Modeling," *Adv. Drug Deliver. Rev.*, **48**, 249-264, 2001.

Home, P. D., Massi-Benedetti, M., Shepard, G. A., Hanning, I., Alberti, K. G., and Owens, D. R., "A Comparison of the Activity and Disposal of Semi-Synthetic Human Insulin and Porcine Insulin In Normal Man By the Glucose Clamp Technique," *Diabetologia*, **22**, 41-45, 1982.

Horton, H. R., Moran, L. A., Scrimgeour, K. G., Perry, M. D., and Rawn, J. D., Eds., *Principles of Biochemistry, 4th Ed.*, Prentice Hall, Upper Saddle River, NJ, 2006.

Hovorka, R, Shojaee-Moradie, F., Carroll, P. V., Chassin, L. J., Gowrie, I. J., Jackson, N. C., Tudor, R. S., Umpleby, A. M., and Jones, R. H., "Partitioning Glucose Distribution/Transport, Disposal, and Endogenous Production During IVGTT", *Amer. J. Physiol.,* **282,** E992–1007, 2002.

Hovorka, R., Canonico, V., Chassin, L. J., Haueter, U., Massi-Benedetti, M., Federici, M. O., Pieber, T. R., Schaller, H. C., Schaupp, L., Vering, T., and Wilinska, M. E., "Nonlinear Model Predictive Control of Glucose Concentration In Subjects With Type I Diabetes", *Physiol. Meas.*, **25**, 905-920, 2004.

Insel, P. A., Liljenquist, J. E., Tobin, J. D., Sherwin, R. S., Watkins, P., Andres, R., and Berman, M., "Insulin Control of Glucose Metabolism In Man," *J. Clin. Invest.*, **55**, 1057-1066, 1975.

Johnson, R. A., Ed., *Miller & Freund's Probability and Statistics For Engineers, Sixth Edition*, Prentice Hall, Upper Saddle River, NJ, 2000.

Joseph, J. I., and Torjman, M. J., "Glucose Sensors," in *Encyclopedia of Biomaterials and Biomedical Engineering*, G. Wnek and G. Bowlin, eds., Dekker, NY, 683-692, 2004.

Kaplan, L. A., Pesce, J. A., and Kazmierczak, S. C., Eds., *Clinical Chemistry: Theory, Analysis, Correlation, 3rd Ed.*, Mosby, St. Louis, MO, 1996.

Kobayashi, T., Sawano, S., Itoh, T., Kosaka, K., Hirayama, H., and Kasuya, Y., "The Pharmacokinetics of Insulin After Continuous Subcutaneous Infusion or Bolus Subcutaneous Injection In Diabetic Patients," *Diabetes*, **32**, 331-336, 1983.

Krudys, K. M., Dodds, M. G., Nissan, S. M., and Vicini, P., "Integrated Model of Hepatic and Peripheral Glucose Regulation For Estimation of Endogenous Glucose Production During the Hot IVGTT," *Am. J. Physiol.*, **288**, E1038-E1046, 2005.

Larsen, P.R., Kronenberg, H.M., Melmed,S., and Kenneth S. Polonsky, eds., *Williams Textbook of Endocrinology*, 10th ed., Saunders, Philadelphia, PA, 2003.

Lenart, P. J., and Parker, R. S., "Modeling Exercise Effects in Type I Diabetic Patients," *Proc. 15th IFAC World Congress On Automatic Control*, Barcelona, Spain, 2002.

LeRoith, D., Taylor, S. I., and Jerrold M. Olefsky, eds., *Diabetes Mellitus: A Fundamental and Clinical Text*, 2nd ed., Lippincott, Williams, and Wilkins, Philadelphia, PA, 2000.

Leroux, J. and Siegel, R. A., "Autonomous Gel/Enzyme Oscillator Fueled By Glucose: Preliminary Evidence For Oscillations," *Chaos*, **9**, 267-275, 1999.

Lozner, E. L., Winkler, E. W., Taylor, F. H. L., and Peters, J. P., "The Intravenous Glucose Tolerance Test," J. Clin. Invest., **20**, 507-515, 1941.

Lustig, S. R., and Peppas, N. A., "Solute Diffusion in Swollen Membranes. IX. Scaling Laws For Solute Diffusion In Gels," *J. App. Polymer Sc.*, **36**, 735-747, 1988.

Lynch, S. M., and Bequette, B. W., "Estimation-Based Model Predictive Control of Blood Glucose In Type I Diabetics: A Simulation Study," in *Proceedings of the IEEE 27th Annual Northeastern Bioengineering Conference,* Storrs, CT, 79-80, 2001.

Lynch, S. M., and Bequette, B. W., "Model Predictive Control of Blood Glucose In Type I Diabetics Using Subcutaneous Glucose Measurements," in *Proceedings of the 2002 American Control Conference*, Anchorage, AK, 4039-4043, 2002.

Martens, P., Metters, A. T., Anseth, K. S., and Bowman, C. N., "A Generalized Bulk-Degradation Model For Hydrogel Networks Formed From Multivinyl Cross-linking Molecules," *J. Phys. Chem. B*, **105**, 5131-5138, 2001.

McMahon, G. T. and Arky, R. A., "Inhaled Insulin For Diabetes Mellitus", *New Engl. J. Med.*, **356**, 497-502, 2007.

Medtronic Minimed, "Bolus Wizard Calculator," available http://www.minimed.com/products/insulinpumps/features/boluswizard.html, March 2007.

Medtronic Minimed, "Minimed Paradigm 522 or 722 Insulin Pump," available http://www.minimed.com/products/insulinpumps/components/insulinpump.html, March 2007.

Medtronic Minimed, "REAL-Time Glucose Monitoring," available http://www.minimed.com/products/insulinpumps/components/cgm.html, March 2007.

Morishita, M., and Peppas, N. A., "Is The Oral Route Possible For Peptide and Protein Drug Delivery," *Drug Discov. Today*, **11**, 905-910, 2006.

Muske, K. R., and Rawlings, J. B., "Model Predictive Control with Linear Models", *AIChE J.*, **39**, 262-287, 1993.

Nomura, M., Shichiri, M., Kawamori, R., Yamasaki, Y., Iwama, N., and Abe, H., "A Mathematical Insulin-Secretion Model and Its Validation In Isolated Rat Pancreatic Islets Perfusion," *Comput. Biomed. Res.*, **17**, 570-579, 1984.

Ollerton, R. L., "Application of Optimal Control Theory to Diabetes Mellitus," *Int. J. Control*, **50**, 2503-2522, 1989.

Owens, D. E. III and Peppas, N. A., "Opsonization, Biodistribution, and Pharmacokinetics of Polymeric Nanoparticles," *Intern. J. Pharm.*, **307**, 93-102, 2006.

Parker, R. S., Doyle, F. J., III, and Peppas, N. A., "A Model-Based Algorithm For Blood Glucose Control In Type I Diabetic Patients," *IEEE Trans. Biomed. Eng.*, **46**, 148-157, 1999.

Parker, R. S., Doyle, F. J. III, Ward, J. H., and Peppas, N. A., "Robust H_∞ Glucose Control In Diabetes Using a Physiological Model," *AIChE J.*, **46**, 2537-2549, 2000.

Parker, R. S., and Doyle, F. J. III, "Control-Relevant Modeling in Drug Delivery," *Adv. Drug Deliver. Rev.*, **48**, 211-228, 2001.

Parker, R. S., Doyle, F. J. III, and Peppas, N. A., "The Intravenous Route To Blood Glucose Control," IEEE Eng. Med. Biol., **20**, 65-73, 2001.

Parker, R. S., "Insulin Delivery", in *Encyclopedia of Biomaterials and Biomedical Engineering*, G. Wnek and G. Bowlin, eds., Dekker, NY, 857-866, 2004.

Peppas, N. A., "Hydrogels," in *Biomaterials Science*, B. D. Ratner, A. S. Hoffman, F. J., Schoen, and J. E. Lemons, Eds., Academic Press, NY, 100-107, 2004.

Peppas, N. A., "Devices Based on Intelligent Biopolymers for Oral Protein Delivery", *Int.. J. Pharm.*., **277**, 11-17, 2004.

Peppas, N. A., "Is There a Future in Glucose-Sensitive, Responsive Insulin Delivery Systems?", *J. Drug. Del. Sci. Tech.*, **14**, 247-256, 2004.

Podual, K., "Glucose-Sensitive Cationic Hydrogels For Insulin Release," PhD Dissertation, Department of Chemical Engineering, Purdue University, West Lafayette, IN, 1998.

Podual, K., Doyle, F. J. III, and Peppas, N. A., "Insulin Release From pH-Sensitive Cationic Hydrogels," *Proceed. Intern. Symp. Control. Rel. Bioact. Mater.*, **25**, 56-57, 1998.

Podual, K., Doyle, F. J., III, and Peppas, N. A., "Preparation and Dynamic Response of Cationic Copolymer Hydrogels Containing Glucose Oxidase," *Polymer*, **41**, 3975-3983, 2000.

Podual, K., Doyle, F. J. III, and Peppas, N. A., "Glucose-Sensitivity of Glucose Oxidase-Containing Cationic Polymer Hydrogels Having Poly(Ethylene Glycol) Grafts," *J. Control. Release*, **67**, 9-17, 2000.

Podual, K., Doyle, F. J., III, and Peppas, N. A., "Dynamic Behavior of Glucose Oxidase-Containing Microparticles of Poly(Ethylene Glycol)-Grafted Cationic Hydrogels In an Environment of Changing pH," *Biomaterials*, **21**, 1439-1450, 2000.

Podual, K., Doyle, F. III, and Peppas, N. A., "Modeling of Water Transport In and Release From Glucose-Sensitive Swelling-Controlled Release Systems Based On Poly(Diethylaminoethyl Methacrylate-g-Ethylene Glycol)," *Ind. Eng. Chem. Res.*, **43**, 7500-7512, 2004.

Podual, K. and Peppas, N. A., "Relaxational Behavior and Swelling-pH Master Curves of Poly[(Diethylaminoethyl Methacrylate)-Graft-(Ethylene Glycol)] Hydrogels," *Polym. Int.*, **54**, 581-593, 2005.

Puckett, W.R., *Dynamic Modelling of Diabetes Mellitus*, PhD Dissertation, Department of Chemical Engineering, The University of Wisconsin-Madision, 1992.

Renard, E., "Implantable Closed-Loop Glucose-Sensing and Insulin Delivery: The Future of Insulin Pump Therapy," *Curr. Opin. Pharmacol.*, **2**, 708-716, 2002.

Ricka, J. and Tanaka, T., "Swelling of Ionic Gels: Quantitative Performance of the Donnan Theory," *Macromolecules*, **17**, 2916-2921, 1984.

Quon, M. J., Cochran, C., Taylor, S. I., and Eastman, R. C., "Non-Insulin-Mediated Glucose Disappearance In Subjects With IDDM. Discordance Between Experimental Results and Minimal Model Analysis," *Diabetes*, **43**, 890-896, 1994.

Rawlings, J. B., Miller, S. M., and Witkowski, W. R., "Model Identification and Control of Solution Crystallization Processes: A Review," *Ind. Eng. Chem. Res.*, **32**, 1275-1296, 1993.

Rawlings, J. B. and Ekerdt, J. G., *Chemical Reactor Analysis and Design Fundamentals*, Nob Hill, Madison, WI, 2002.

Roy, A. and Parker, R. S., "Dynamic Modeling of Exercise Effects On Plasma Glucose and Insulin Levels," *Proc. ADCHEM 2006*, Gramado, Brazil, 2006.

Roy, A., and Parker, R. S., "Dynamic Modeling of Free Fatty Acid, Glucose, and Insulin: An Extended 'Minimal Model'," *Diabetes Technology & Therapeutics*, **8**, 617-626, 2006.

Salzsieder, E., Albrecht, G., Fischer, U., and Freyse, E. J., "Kinetic Modeling of the Glucoregulatory System to Improve Insulin Therapy," *IEEE T. Bio.-Med. Eng.*, **32**, 846-855, 1985.

Schmidtke, D. W., Freeland, A. C., Heller, A., and Bonnecaze, R. T., "Measurement and Modeling of the Transient Difference Between Blood and Subcutaneous Glucose Concentrations In the Rat After Injection of Insulin," *Proc. Natl. Acad. Sci.*, **95**, 294-299, 1998.

Schwarte, L. M., Podual, K., and Peppas, N. A., "Cationic Hydrogels For Controlled Release of Proteins and Other Macromolecules," in I. McCullogh and S. W. Shalaby, Eds., *Tailored Polymeric Materials For Controlled Drug Delivery Systems*, ACS Symposium Series, Vol. 709, 56-66, 1998.

Seborg, D. E., Edgar, T. F., and Mellichamp, D. A., *Process Dynamics and Control, 2nd Edition*, Wiley, NY, 2004.

Shampine, L. F. and Reichelt, M. W., "The MATLAB ODE Suite," *SIAM J. Sci. Comput.*, **18**, 1-22, 1997.

Sherwin, R. S., Kramer, K. J., Tobin, J. D., Insel, P. A., Liljenquist, J. E., Berman, M., and Andres, R., "A Model of the Kinetics of Insulin In Man," *J. Clin. Invest.*, **53**, 1481-1492, 1974.

Siegel, R. A., Falamarzian, M., Firestone, B. A., and Moxley, B. C., "pH-Controlled Release From Hydrophobic/Polyelectrolyte Copolymer Hydrogels," *J. Control. Release*, **8**, 179-182, 1988.

Siegel, R. A., Johannes, I., Hunt, C. A., and Firestone, B. A., "Buffer Effects On Swelling Kinetics In Polybasic Gels," *Pharm. Res.*, **9**, 76-81, 1992.

Siegel, R. A., "Hydrophobic Weak Polyelectrolyte Gels: Studies of Swelling Equilibria and Kinetics," in *Advances in Polymer Science 109*, *Responsive Gels: Volume Transitions I*, K. Dusek, Ed., Springer-Verlag, NY, 233-267, 1993.

Sorensen, J. T., "A Physiologic Model of Glucose Metabolism in Man and Its Use to Design and Assess Improved Insulin Therapies For Diabetes", Ph.D. thesis, Dept. Chem. Eng., Massachusetts Institute of Technology, Cambridge, 1985.

Steil, G. M., Panteleon, A. E., and Rebrin, K., "Closed-Loop Insulin Delivery—the Path to Physiological Glucose Control," *Adv. Drug Deliver Rev.*, **56**, 125-144, 2004.

Steil, G. M., Clark, B., Kanderian, S., and Rebrin, K., "Modeling Insulin Action For Development of a Closed-Loop Artificial Pancreas," *Diabetes Technology & Therapeutics*, **7**, 94-108, 2005.

Tiran, J. and Galle K. R., "A Simulation Model of Extracellular Glucose Distribution In the Human Body," *Ann. Biomed. Eng.*, **3**, 34-46, 1975.

Tiran, J., Avruch, L. I., and Albisser, A. M., "A Circulation and Organs Model For Insulin Dynamics," *Am. J. Physiol.*, **237**, E331-E339, 1979.

Toffolo, G., and Cobelli, C., "The Hot IVGTT Two-Compartment Minimal Model: An Improved Version," *Am. J. Physiol.*, **284**, E317-E321, 2003.

Tranberg, K. G., and Dencker, H., "Modeling of Plasma Disappearance of Unlabeled Insulin In Man," *Am. J. Physiol.*, **235**, E577-E585, 1978.

Wilinska, M. E., Chassin, L. J., Schaller, H. C., Schaupp, L., Pieber, T. R., and Hovorka, R., "Insulin Kinetics In Type-1 Diabetes: Continuous and Bolus Delivery of Rapid Acting Insulin," *IEEE Trans. Biomed. Eng.*, **52**, 3-12, 2005.

VITA

Terry Glen Farmer Jr. was born in Fort Hood, Texas on November 6, 1979. He is the son of Terry Glen Farmer and Lori Ann Smith. After graduating from Lampasas High School in Lampasas, Texas in 1998, Terry enrolled in the University of Texas at Austin, where he studied chemical engineering. Terry worked as a co-op engineer at Ondeo Nalco Energy Services from 2001-2002. He received the degree of Bachelors of Science in May 2003 and entered the Graduate School at The University of Texas at Austin in August 2003. He currently lives with his wife, Kate Melynda Farmer, and his daughter, Leah Michelle Farmer.

Permanent Address: 3563 Lake Austin Blvd, Apt D, Austin, TX, 78703

This dissertation was typed by the author.